



**Politecnico di Torino**

Master of Science in Civil Engineering

*Master Thesis*

Supervisors:

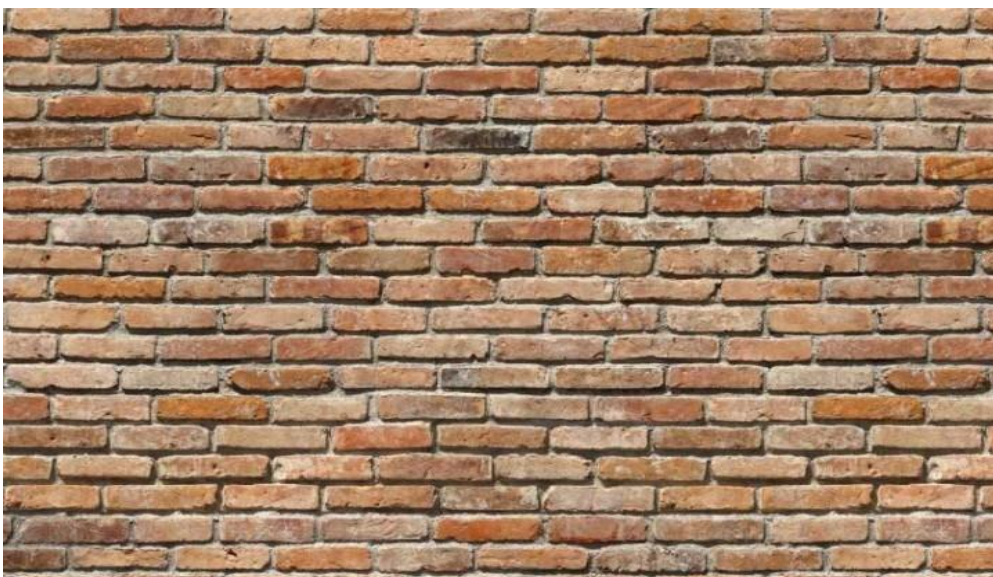
**René Mazur M.Sc.**

**Ing. Grazzini Alessandro**

Student:

**Edoardo Murgia**

**Numerical investigation of the load bearing capacity of exterior  
wall-ceiling-nodes**



**Torino 2017**



**To my family**



---

## **Abstract**

The object of this thesis is to understand the structural behaviour of brick masonry walls taking into account the interaction between the brick supporting walls and reinforced concrete floors.

Chapter 1 introduces the problem of brickwork in compression describing the general behaviour of the masonry structures under eccentric compression.

The theoretical models used for the determination of the capacity reduction factors and accordingly the load bearing capacities for walls vertically loaded is discussed in Chapter 2.

In Chapter 3, the materials and the modeling strategies properties were analysed.

Chapter 4 presents a description of the test programme carried out by the Technische Universität Dresden, and the analyses of the test results are presented.

Chapter 5 describes the numerical investigation carried out in order to calibrate the FEM model used for the next evaluations.

In Chapter 6 the load bearing capacity of the structure is estimate by using two different theoretical formulations.

In Chapter 7, 8, 9, 10 the influence of the slab position, the wall thickness, the wall elastic modulus and the slab elastic modulus respectively were evaluated.

Finally, in Chapter 11, the general conclusions arising from this research are listed together.

---

## **Ringraziamenti**

Vorrei ringraziare tutti coloro che mi hanno aiutato nella realizzazione della mia tesi.

Ringrazio René Mazur M.Sc. della Università Tecnica di Darmstadt, per avermi dato la opportunità di lavorare con lui. Mi è stato sempre accanto durante lo sviluppo di questa tesi, con i suoi utili consigli e con la disponibilità offerta. Sviluppare questa indagine in un altro paese mi ha dato la opportunità di crescere non solo professionalmente, ma anche a livello umano. E' stata una esperienza che porterò per sempre con me.

Ringrazio Ing. Alessandro Grazzini del Politecnico di Torino, per aver accettato di seguire, anche se a distanza, il lavoro svolto nei mesi che ho trascorso in Germania.

Il ringraziamento più grande va ai miei genitori, per avermi dato il loro supporto durante questi anni di studi. Senza di loro tutto ciò non sarebbe stato possibile. In questa tesi sono racchiusi i miei sacrifici, ma specialmente i loro.

Ringrazio mio fratello e mia sorella, per avermi supportato e compreso anche nei momenti più difficili. Ci sono sempre stati, e so che ci saranno per sempre. Spero di poter ricambiare tutto quello che hanno fatto per me.

Ringrazio tutti i miei amici e colleghi, con i quali ho condiviso gioie e dolori durante questi anni di studio. Il loro supporto è stato essenziale per superare le difficoltà incontrate.

## **Acknowledgement**

I would like to thank all those who helped me in the realization of my thesis.

I want to thank René Mazur M.Sc. from Technische Universität Darmstadt, for giving me the opportunity to work with him. He having been continuously alongside me during the development of this thesis, with his helpful advice and with the availability he has offered. Developing this survey in another country has given me the opportunity to grow up not only professionally, but also at a human level. It was a life experience that I will always carry with me.

I thank Ing. Alessandro Grazzini from Polytechnic of Turin, for having agreed to follow, though at a distance, the work done during the months which I spent in Germany.

The greatest thanks go to my parents, for giving me their support during these years of studies. The completion of my studies and the achievement of this first professional goal, is certainly a source of pride for me. Without them, all this would not have been possible. In this thesis I enclose my sacrifices, but especially theirs.

I thank my brother and sister, for always supporting and understanding me even in the most difficult moments. There have always been, and I know there will always be. I hope I can return all that they has done for me.

I thank all my friends and colleagues, with whom I have shared joys and sorrows during these years of study. Their support was essential to overcome all the difficulties encountered.

---

# Index

<b>LIST OF FIGURES</b> .....	<b>IV</b>
<b>LIST OF ABBREVIATIONS</b> .....	<b>VIII</b>
<b>1 INTRODUCTION</b> .....	<b>1</b>
1.1 General considerations .....	1
1.2 Aims.....	2
<b>2 THEORETICAL MODELS</b> .....	<b>3</b>
2.1 Awni, A.W. Hendry Model.....	4
2.1.1 Stress failure equations .....	6
2.1.1.1 Uncracked wall .....	6
2.1.1.2 Cracked wall .....	8
2.2 DIN EN 1996 1-1/NA.....	8
2.2.1 Simplified method for moment calculation .....	9
<b>3 MATERIALS AND MODELING STRATEGIES</b> .....	<b>11</b>
3.1 Micro- and macro- modeling .....	11
3.2 Softening behaviour .....	13
3.3 Properties of unit and mortar .....	14
3.4 Properties of the unit-mortar interface .....	15
3.4.1 Tensile failure .....	15
3.4.2 Shear failure .....	16
3.5 Properties of the composite material.....	18
<b>4 EXPERIMENTAL INVESTIGATION</b> .....	<b>19</b>
4.1 Materials .....	20
4.1.1 Bricks Thermopor P14 .....	20
4.1.2 Mortar .....	21
4.1.3 Masonry .....	21
4.1.4 Concrete .....	22
4.2 Load program .....	22

4.3	Measurements.....	23
<b>5</b>	<b>NUMERICAL INVESTIGATION .....</b>	<b>24</b>
5.1	Atena 3D .....	24
5.2	FEM model .....	25
5.2.1	Material properties.....	26
5.2.2	Load cases .....	27
5.3	Results evaluation.....	28
<b>6</b>	<b>LOAD BEARING CAPACITY EVALUATION .....</b>	<b>33</b>
<b>7</b>	<b>INFLUENCE OF SLAB POSITION.....</b>	<b>38</b>
7.1	a= 50 mm .....	39
7.2	a= 100 mm .....	41
7.3	a= 150 mm .....	45
7.4	a= 200 mm .....	45
7.5	a= 250 mm .....	49
<b>8</b>	<b>INFLUENCE OF WALL THICKNESS.....</b>	<b>50</b>
8.1	t= 365 mm .....	50
8.2	t= 315 mm .....	51
8.3	t= 265 mm .....	52
8.4	t= 215 mm .....	54
8.5	t= 175 mm .....	56
<b>9</b>	<b>INFLUENCE OF WALL ELASTIC MODULUS.....</b>	<b>60</b>
9.1	E= 2314 N/mm <sup>2</sup> .....	60
9.2	E= 2629 N/mm <sup>2</sup> .....	62
9.3	E= 2928 N/mm <sup>2</sup> .....	64
9.4	E= 3215 N/mm <sup>2</sup> .....	65
9.5	E= 3492 N/mm <sup>2</sup> .....	67

---

<b>10</b>	<b>INFLUENCE OF SLAB ELASTIC MODULUS .....</b>	<b>71</b>
10.1	C25/30 (E= 31000 N/mm <sup>2</sup> ) .....	73
10.2	C30/37 (E= 33000 N/mm <sup>2</sup> ).....	74
10.3	C40/50 (E=35000 N/mm <sup>2</sup> ) .....	76
10.4	C45/55 (E= 36000 N/mm <sup>2</sup> ) .....	78
<b>11</b>	<b>CONCLUSIONS .....</b>	<b>82</b>
<b>12</b>	<b>REFERENCES .....</b>	<b>84</b>
	<b>ANNEX A – LOAD CASES .....</b>	<b>86</b>
	<b>ANNEX B – FEM RESULT FOR DIFFERENT SLAB POSITIONS.....</b>	<b>96</b>
	<b>ANNEX C – EXPERIMENTAL AND FEM RESULTS COMPARISON .....</b>	<b>100</b>
	<b>ANNEX D – FEM SIMULATION RESULTS .....</b>	<b>101</b>
	<b>ANNEX E – GEOMETRICAL PARAMETERS OF EXPERIMENTAL AND FEM STRUCTURE.....</b>	<b>128</b>

**List of Figures**

Figure 1.1 Eccentric axial load .....	1
Figure 2.1 Failure stress curve .....	3
Figure 2.2 Frame system (Awni & Hendry, 1981) .....	4
Figure 2.3 Wall curvatures (Awni & Hendry, 1981) .....	5
Figure 2.4 Simplified frame system .....	10
Figure 2.5 Stress block .....	10
Figure 3.1 Modeling strategies for masonry structures: (a) masonry sample; (b) detailed micro-modeling; (c) simplified micro-modeling; (d) macro-modeling ....	12
Figure 3.2 Stress displacement diagrams: a) Uniaxial tension ( $f_t$ is the tensile strength); b) Uniaxial compression ( $f_c$ is the compressive strength) .....	13
Figure 3.3 Shear behaviour ( $c$ is the cohesion) .....	14
Figure 3.4 Tensile bond behaviour of masonry. (a) test specimen; (b) stress-crack displacement results .....	15
Figure 3.5 Tensile bond surface. (a) bond surface for tensile specimens; (b) net bond surface .....	16
Figure 3.6 Shear bond behaviour of the joint. (a) stress-displacement diagram for different normal stress levels; (b) fracture energy as a function of the normal stress level .....	16
Figure 3.7 Friction and dilatancy angles. (a) Coulomb friction law with initial and residual friction angle; (b) dilatancy angle .....	17
Figure 3.8 Shear bond behaviour of the joint. (a) tangent of the dilatancy angle $\Psi$ as a function of the normal stress level; (b) relation between the normal and the shear displacement upon loading .....	17
Figure 3.9 Relation between the different components .....	18
Figure 4.1 Experimental structure .....	19
Figure 4.2 Wall/Slab node .....	20
Figure 4.3 Frame system and binding reactions .....	20
Figure 4.4 Brick Thermopor P14 .....	20
Figure 4.5 Masonry test specimen .....	21
Figure 4.6 Proof's execution .....	21
Figure 4.7 Concrete specimen .....	22
Figure 4.8 Frame system .....	22
Figure 5.1 FEM model used for the numerical investigation .....	25
Figure 5.2 Binding reactions on the frame system .....	27
Figure 5.3 Slab vertical displacement from Measuring Point MP 13 .....	28

---

Figure 5.4 Horizontal binding reaction comparison.....	28
Figure 5.5 Horizontal binding reaction comparison.....	29
Figure 5.6 Bending moment comparison above the slab.....	29
Figure 5.7 Bending moment comparison below the slab .....	30
Figure 5.8 Eccentricity comparison above the slab .....	30
Figure 5.9 Eccentricity comparison below the slab .....	31
Figure 6.1 Model used for the load bearing capacity evaluation .....	33
Figure 6.2 Bending moment comparison above the slab.....	34
Figure 6.3 Bending moment comparison below the slab .....	34
Figure 6.4 Eccentricity comparison above the slab .....	34
Figure 6.5 Eccentricity comparison below the slab .....	35
Figure 6.6 Load bearing capacity above the slab comparison.....	36
Figure 6.7 Load bearing capacity below the slab comparison .....	36
Figure 7.1 Wall/Slab connection detail.....	38
Figure 7.2 Structure geometry $a= 50$ mm.....	39
Figure 7.3 Bending moment comparison above the slab.....	39
Figure 7.4 Bending moment comparison below the slab .....	39
Figure 7.5 Eccentricity comparison above the slab .....	40
Figure 7.6 Eccentricity comparison below the slab .....	40
Figure 7.7 Structure geometry $a=100$ mm.....	41
Figure 7.8 Bending moment comparison above the slab.....	41
Figure 7.9 Bending moment comparison below the slab .....	42
Figure 7.10 Eccentricity comparison above the slab .....	42
Figure 7.11 Eccentricity comparison below the slab.....	42
Figure 7.12 Structure geometry $a= 150$ mm .....	45
Figure 7.13 Structure geometry $a=200$ mm .....	45
Figure 7.14 Bending moment comparison above the slab .....	46
Figure 7.15 Bending moment comparison below the slab.....	46
Figure 7.16 Eccentricity comparison above the slab .....	46
Figure 7.17 Eccentricity comparison below the slab.....	46
Figure 7.18 Structure geometry $a=250$ mm .....	49
Figure 8.1 Bending moment comparison above the slab.....	51
Figure 8.2 Bending moment comparison below the slab .....	51
Figure 8.3 Eccentricity comparison above the slab .....	51
Figure 8.4 Eccentricity comparison below the slab.....	52

Figure 8.5 Bending moment comparison above the slab.....	52
Figure 8.6 Bending moment comparison below the slab .....	53
Figure 8.7 Eccentricity comparison above the slab .....	53
Figure 8.8 Eccentricity comparison below the slab.....	53
Figure 8.9 Bending moment comparison above the slab.....	54
Figure 8.10 Bending moment comparison below the slab.....	54
Figure 8.11 Eccentricity comparison above the slab .....	55
Figure 8.12 Eccentricity comparison below the slab.....	55
Figure 8.13 Bending moment comparison above the slab .....	56
Figure 8.14 Bending moment comparison below the slab.....	56
Figure 8.15 Eccentricity comparison above the slab .....	56
Figure 8.16 Eccentricity comparison below the slab.....	57
Figure 8.17 Relation between bending moment and wall slenderness .....	58
Figure 8.18 Relation between eccentricity and wall slenderness.....	58
Figure 8.19 Relation between eccentricity ratio and slenderness .....	59
Figure 8.20 Relation between Load Bearing Capacity and Slenderness ratio .....	59
Figure 9.1 Bending moment comparison above the slab.....	60
Figure 9.2 Bending moment comparison below the slab .....	61
Figure 9.3 Eccentricity comparison above the slab .....	61
Figure 9.4 Eccentricity comparison below the slab.....	61
Figure 9.5 Bending moment comparison above the slab.....	62
Figure 9.6 Bending moment comparison below the slab .....	62
Figure 9.7 Eccentricity comparison above the slab .....	63
Figure 9.8 Eccentricity comparison below the slab.....	63
Figure 9.9 Bending moment comparison above the slab.....	64
Figure 9.10 Bending moment comparison below the slab.....	64
Figure 9.11 Eccentricity comparison above the slab .....	64
Figure 9.12 Eccentricity comparison below the slab.....	65
Figure 9.13 Bending moment comparison above the slab .....	65
Figure 9.14 Bending moment comparison below the slab.....	66
Figure 9.15 Eccentricity comparison above the slab .....	66
Figure 9.16 Eccentricity comparison below the slab.....	66
Figure 9.17 Bending moment comparison above the slab .....	67
Figure 9.18 Bending moment comparison below the slab.....	67
Figure 9.19 Eccentricity comparison above the slab .....	68

---

Figure 9.20 Eccentricity comparison below the slab.....	68
Figure 9.21 Relation between bending moment and wall elastic modulus .....	69
Figure 9.22 Relation between eccentricity and wall elastic modulus .....	69
Figure 9.23 Relation between Wall Elastic Modulus and Load Bearing Capacity .....	70
Figure 10.1 Stress strain curve for concrete .....	71
Figure 10.2 Bending moment comparison above the slab .....	73
Figure 10.3 Bending moment comparison below the slab.....	73
Figure 10.4 Eccentricity comparison above the slab .....	73
Figure 10.5 Eccentricity comparison below the slab.....	74
Figure 10.6 Bending moment comparison above the slab .....	74
Figure 10.7 Bending moment comparison below the slab.....	75
Figure 10.8 Eccentricity comparison above the slab .....	75
Figure 10.9 Eccentricity comparison below the slab.....	75
Figure 10.10 Bending moment comparison above the slab .....	76
Figure 10.11 Bending moment comparison below the slab.....	76
Figure 10.12 Eccentricity comparison above the slab .....	77
Figure 10.13 Eccentricity comparison below the slab .....	77
Figure 10.14 Bending moment comparison above the slab .....	78
Figure 10.15 Bending moment comparison below the slab.....	78
Figure 10.16 Eccentricity comparison above the slab .....	78
Figure 10.17 Eccentricity comparison below the slab .....	79
Figure 10.18 Relation between bending moment and slab elastic modulus.....	79
Figure 10.19 Relation between eccentricity and slab elastic modulus .....	80
Figure 10.20 Relation between Slab Elastic Modulus and Load Bearing Capacity.	81
Figure B12.1 Bending moment comparison above the slab.....	96
Figure B.2 Bending moment comparison below the slab.....	96
Figure B.3 Eccentricity comparison above the slab .....	96
Figure B.4 Eccentricity comparison below the slab .....	97
Figure B.5 Bending moment comparison above the slab .....	97
Figure B.6 Bending moment comparison below the slab.....	98
Figure B.7 Eccentricity comparison above the slab .....	98
Figure B.8 Eccentricity comparison below the slab .....	98

## List of abbreviations

i.e.	that is
DIN	DIN EN 1996 1-1/NA
EC6	EN 1996 1-1
FEM	Finite Element Method

# 1 Introduction

## 1.1 General considerations

Investigations into the load bearing strength of brickwork has come today into use on the basis of engineering principles. The interest in loadbearing brickwork was prompted by the realization that structural brickwork, unlike other materials, could be an economic solution for constructions.

Theoretical solutions which could describe the behavior of brickwork in compression are still under development.

From observations of the failure mode of centrally compressed walls, it has been noted that failure is usually initiated by vertical cracking of the bricks (Hilsdorf, 1969). Furthermore, in order to maximize the load bearing capacity, the vertical load applied to the masonry should be as concentrically as possible because of the low tensile strength of the mortar between the masonry blocks. However, the axial load situation is virtually impossible to reach because of different factors, like the bending moment applied by the slab to the joint and the consequent rotation which causes the displacement of the vertical reaction from the axis of the wall.

For this reason the eccentricity and the slenderness must both be taken in account, and by knowing this two factors is possible to estimate the load bearing capacity by using a capacity reduction factor.

Since the bearing strength of masonry decreases rapidly with increasing eccentricity because the low tensile strength (Hailer, 1969), it is important to estimate the correct value of the bending moment acting to the wall/slab joint.

The calculation of the bending moment acting on the wall/slab joint is actually difficult, because it is influenced by the degree of fixity at the joint, the method of construction, the external loads and on the relative rigidity of the slab and wall.

There are different problems to consider in modeling a structure composed of load bearing masonry walls and reinforced concrete floors with a frame structure. These problems are mainly related to the rigidity of the wall slab connections. The determination of the distribution of moment throughout the frame, for a given loading, is complicated by the fact that the wall stiffness may be dependent on the wall loading. Thus, if the eccentricities of the wall loadings cause tension cracking, the rigidity of the frame is reduced and a redistribution of moment takes place.

Due to the nonlinearity of the structural behavior a complete nonlinear analysis is therefore required for each load case. Also the secondary effects of wall bending deformations on the extent of cracking should be considered.

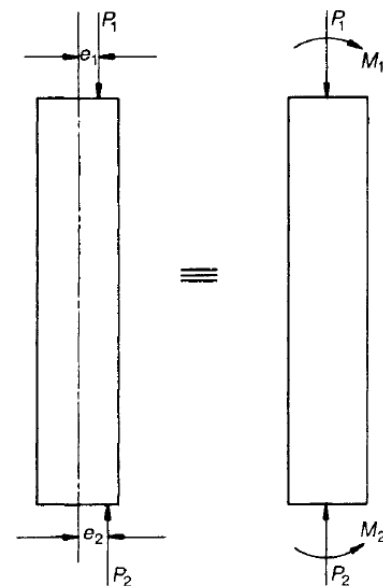


Figure 1.1 Eccentric axial load

At the other extreme, there are not clear theoretical models which define the magnitude of the eccentricity of the slab reaction. A common assumption is that the pressure distribution under the bearing area is triangular (Recommended Practice for Engineered Brick Masonry, 1969), although if the floor slab span is reduced, a uniform pressure distribution may be assumed but there is little information to indicate that the errors involved are on the safe side.

For a semi-rigid wall slab connection, the moment rotation behavior of the joint must be accurately known, and a nonlinear iterative solution procedure will be required. In this case also, details of the joint construction, properties of the concrete floor slab, masonry and mortar, and the pre compression in the joint will influence the moment rotation behavior.

Next chapter shows two possible theoretical ways to analyze the problem of the determination of the load bearing capacity with reference to the wall slab connection.

### **1.2 Aims**

The ultimate capacity of masonry walls under vertical loading strongly depends by the effective eccentricity of the vertical loads. Geometrical parameters, such as the slenderness ratio, or material parameters such as the compressive strength and the elastic modulus of masonry and slab are significant. The use of sophisticated numerical tools, such as nonlinear approaches framed within the macro- or micro-modeling strategies, offers interesting possibilities for the study of this kind of problem.

The aim of this master thesis is to analyze the behavior of exterior wall-ceiling-nodes using a numerical model. After a theoretical introduction to the problem, a 3D-model is developed and calibrated by using existing experimental data. Following, the influence of different parameters on the structural behavior (material and geometry) will be examined. The results of these analysis will be compared to the results according to DIN EN 1996 1-1/NA.

## 2 Theoretical models

One of the aspect which causes the nonlinear behaviour of the masonry wall is, among other aspects, the low tensile strength of the mortar joints. For practical use it seems reasonable to consider the masonry structures with no tensile strength but, when buckling failure is involved, the collapse load may be very dependent on the tensile strength of the material. For this reason, any realistic theoretical or numerical analysis aimed at producing accurate predictions needs to consider the impact of the tensile strength on the ultimate response of the wall. (Sandoval, 2011)

Masonry members under compression may fail either because of material over-stressing or because of stability failure of slender members. For squat masonry members, the failure takes place if the compressive strain at any cross-section reached the ultimate compressive strain of the material. Nevertheless, for slender masonry elements the failure occurs before reaching the ultimate compressive strain of the material at any cross-section.

The slenderness of the structure is important for the determination of the structure's failure behaviour. A typical failure stress curve is shown in Fig.2.1. For short columns, where the slenderness ratio is low, failure would result from compression of the material, whereas for long thin columns and higher values of slenderness ratio, failure would occurs from lateral instability.

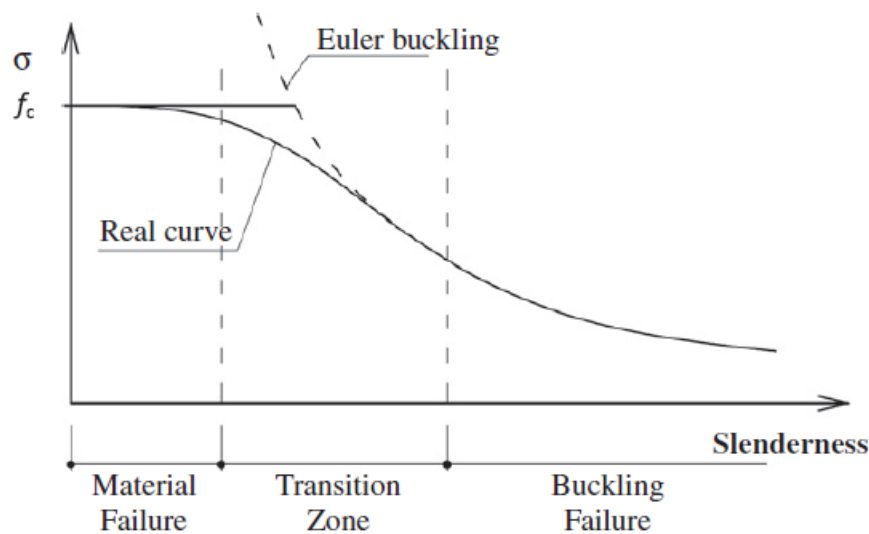


Figure 2.1 Failure stress curve

The failure stress at zero slenderness ratio is dependent on the compressive strength of masonry units and mortar used in the construction.

If it were possible to apply pure axial loading to walls or columns then the type of failure which would occur would be independent on the slenderness ratio, i.e. the ratio of the effective height to the effective thickness.

However, it is virtually impossible to apply an axial load to a wall or column since this would require a perfect unit with no fabrication errors. The vertical load will, in general, be eccentric to the central axis and this will produce a bending moment into the joint.

The stresses due to the equivalent axial loads and bending moments can be added using the formula:

$$\text{Total Stress} = P/A \pm M/Z$$

where  $A$  and  $Z$  are the area and section modulus of the cross-section,  $P$  is the axial vertical load and  $M$  is the bending moment.

The interaction between the bending moment and the applied load can be considered by reducing the axial load bearing capacity of the wall by a suitable factor. The resistance of walls to vertical loading is obviously related to the characteristic strength of the material used for construction.

Real walls in multi-storey buildings are usually compressed between reinforced concrete slabs through joints which are capable of transmitting bending moments. The transmitted moments on the one hand influence the deflected form of the wall and, on the other one, control the end rotation of the wall. It follows that a satisfactory method for the design of masonry walls in compression must take in consideration the effects between walls and floor slabs.

### 2.1 Awni, A.W. Hendry Model

Awni and A.W. Hendry have developed a theoretical approach for estimating the compressive strength of brick masonry walls taking into account the interaction between the brick supporting walls and reinforced concrete slab floors. The theory presented is a development of other solutions, produced by Sahlin, Risager and Colville.

In this method, the basic idea is to calculate the magnitude of the bending moment introduced into the walls on a frame system with bend-resistant corners in a linearly elastic way and, subsequently, to reduce this moment by means of a reduction factor. The calculation of the reduction factor depends, in addition to other aspects, on the eccentricities of the axial load applied on the wall and can be calculated assuming that the point of inflection of the wall is known, or can be estimated, and that the portions of the equivalent column between the points of zero moment have a parabolic deflection curve.

The wall curvature is one of the aspect taken in account into the Awni's model to determine the bearing capacity of the wall. The types of wall curvatures are governed by the wall end eccentricities which in turn are related to the type and condition of floor loading.

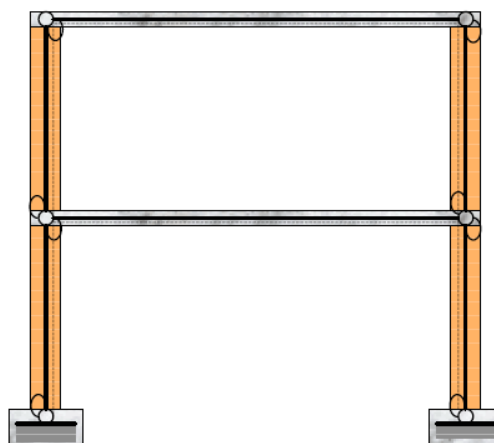


Figure 2.2 Frame system (Awni & Hendry, 1981)

Thus, three types of wall bending are considered in this study:

- Walls bent in double curvature with equal and opposite end eccentricities, as shown in Fig 2.3a
- Walls bent in single curvature with equal end eccentricities, Fig. 2.3b
- Walls bent in single curvature with zero eccentricity at one end, Fig. 2.3c

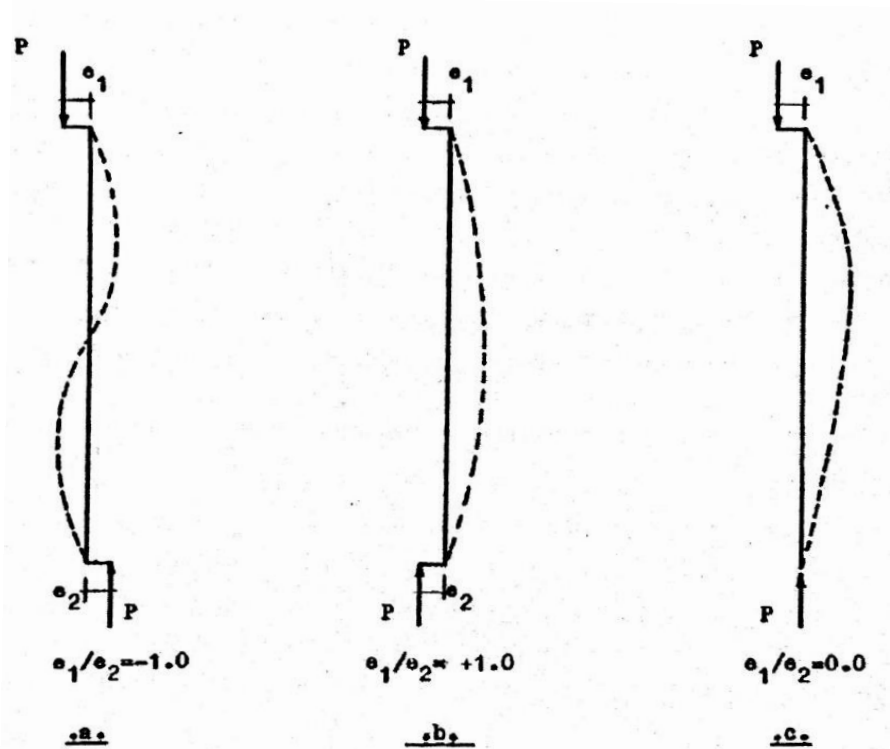


Figure 2.3 Wall curvatures (Awni & Hendry, 1981)

In relation to the wall curvature type, there are different ways to calculate the capacity reduction factor, and for every case there are distinctions between slender or short walls, and for cracked or uncracked state.

The solution taken in account in this work investigates the behaviour of a short wall with no eccentricity to one end.

The principal problem which has to be solved in order to calculate the load bearing capacity is to determine the section where the eccentricity is maximum and, secondly, the reduction factor resulting from eccentricity and wall slenderness. For different curvatures, the maximum eccentricity section changes position. It is noted that the distance of the section where the maximum eccentricity is located depends on the slenderness of the wall, and it increases with the increasing of the slenderness.

As noted by (Colville, 1978), if the maximum eccentricity lies at the ends of the actual wall (i.e. at floor levels), the wall slenderness does not affect the wall bearing capacity computed from the ultimate compressive strength. This is the case of short walls with zero eccentricity to one end. Of course, if the bearing strength is based on stability of the wall, then the variations in wall slenderness ratio will, in all cases, influence the wall load bearing capacity.

The aim is to estimate the load bearing capacity when the eccentricity is maximum on the wall slab joint.

The eccentricity at joint level depends on the ratio of stiffness of walls and floors and on the characteristics of the joint between them as well as on the wall curvature type. The load bearing capacity of a wall is influenced by the same factors, for this reason both problems are considered in the analytics method.

In the case of reinforced concrete slabs supported by masonry walls, the actual joint moment that could develop depends primarily on two factors. Firstly, on the ratio of the flexural rigidity of the wall slab joint, secondly, on the magnitude of the wall pre-compression above the slab under consideration. It is assumed that uniform wall pre-compression acts as a restraining force in clamping the floor slab. Hence, the higher the wall pre-compression is, the smaller the slab end rotation is.

If, on the other hand, the magnitude of this wall pre-compression is small, a crack will develop at the wall slab joint due to loading on the slab. Hence, in this case the slab restraining moment will be smaller.

Experiments show that the fixity of the joint in a masonry structure depends, primarily, on the ratio of the flexural rigidity of the floor slab compared to the supporting wall. Since full joint fixity may never be achieved in actual structures, the full end moment may never be developed.

### 2.1.1 Stress failure equations

The following formulations allow to calculate the load bearing reduction factor for wall bent in double curvature or single curvature with no eccentricity to one end, when the slenderness ratio is less than 10 and assuming that the maximum value of the eccentricity is located in the wall/slab connection. The slenderness ratio is defined by the ratio between the wall height  $h$  and the wall thickness  $t$ .

The load bearing capacity can be estimated in this way by knowing the value of the eccentricity to the wall slab connection, where the maximum eccentricity is located. This value can be computed experimentally or with nonlinear analysis using FEM programs.

#### 2.1.1.1 Uncracked wall

For a rectangular wall of width,  $b$ , and thickness,  $t$ , composed of a linearly elastic material, and loaded by an eccentric load  $P$ , the maximum compressive stress is given by the following equation (Sahlin, Structural Masonry, 1971):

$$\sigma_{max} = \frac{P}{bt} \left( 1 + \frac{6e_{max}}{t} \right) \quad 2.1$$

The stress-strain relationship for masonry is nonlinear. However, it is noted that for eccentrically loaded walls, good agreement is obtained between tests and theory using a linear stress-strain curve if failure is assumed to occur when the maximum stress equals 1.5 times the compressive strength (Recommended Practice for Engineered Brick Masonry, 1969).

Thus, it is assumed that stress failure will occur when the maximum compressive stress in the wall is 1.5 times the compressive wall strength:

$$\sigma_{max} = 1.5\sigma_b \quad 2.2$$

Where  $\sigma_b$  is the prism maximum compressive strength.

Substituting eq. (2.2) into eq. (2.1) and introducing the notation:

$$\beta = \frac{P}{\sigma_b b t} \quad 2.3$$

Where,  $P$ , is the compressive force in the wall, and  $\sigma_b b t$ , is the compressive force of the same concentrically loaded wall, gives:

$$\beta = \frac{3}{2\left(1 + \frac{6e_{max}}{t}\right)} \leq 1 \quad 2.4$$

This term may be considered to be a capacity reduction factor whose value depends on the maximum eccentricity of the load,  $e_{max}$ . By definition, it is the ratio of the compressive (eccentric or concentric) force in the wall, to the compressive force of the same concentrically loaded wall. It follows that it must always be less than or equal to unity.

The magnitude of  $e_{max}$  that has to be used in eq. (2.4) depends on the slenderness of the wall. Thus, when the height of the equivalent column becomes equal to or greater than the actual wall height, the maximum eccentricity will occur at the wall end (at floor level). Conversely, if the height of the equivalent column is less than the actual wall height, then the maximum eccentricity will occur between the wall ends and  $e_{max} = e$  is substituted in eq. (2.4). Considering this case we obtain from eq. (2.4):

$$\beta = \frac{3}{2(1+6\varepsilon)} \leq 1 \quad 2.5$$

Where:

$$\varepsilon = \frac{e}{t} \quad 2.6$$

Equation (2.5) is based on a compressive stress failure occurring at a floor level. As indicated in reference (Sahlin, 1959), however, the stress condition at a wall/floor joint is much more complex than indicated by eq. (2.1). As a result, eq. (2.5) is too conservative and it is assumed that compression failures cannot occur within a distance equal to 1.5 times the wall thickness from the joint (Colville, 1978). Thus, equation (2.5) is modified by the factor  $\gamma$ , given as:

$$\gamma = \frac{\left(\frac{H}{2}\right)}{\left(\frac{H}{2} - 1.5t\right)} \quad 2.7$$

Applying eq. (2.7) into eq. (2.6) we finally get:

$$\beta = \frac{1.5\left(\frac{H}{2}\right)}{\left(\frac{H}{2} - 1.5t\right)(1+6\varepsilon)} \leq 1 \quad 2.8$$

Based on information given in (Colville, 1978), to distinguish between short and slender walls, it is suggested that for walls having a slenderness ratio  $h/t$  less than 10 be regarded as a short wall and hence, the maximum eccentricity will always occur at the floor level.

### 2.1.1.2 Cracked wall

For a rectangular cross-section of a linear elastic material without tensile strength, the width of the compressed zone after tensile cracking will be  $3(t/2 - e)$ , and the magnitude of the maximum compressive strength is (Sahlin, Structural Masonry, 1971):

$$\sigma_{max} = \frac{2P}{3b\left(\frac{t}{2} - e_{max}\right)} \quad 2.9$$

Considering walls with slenderness ratio less than 10, the maximum eccentricity is assumed to occur at the floor level, and by applying the assumption of failure at a distance of 1.5 times the wall thickness away from the joint, the following eq. is derived from equations (2.2 and 2.3). After substituting into eq. (2.9):

$$\beta = \frac{9}{8}(1 - 2\varepsilon) \frac{\left(\frac{H}{2}\right)}{\left(\frac{H}{2} - 1.5t\right)} \leq 1 \quad 2.10$$

This equation replace the eq. (2.8) when the wall is cracked.

## 2.2 DIN EN 1996 1-1/NA

Eurocode 6 is one of a group of standards for structural design being issued by the Commission of the European Communities.

EC6 Part 1–1 is laid out in the following six sections:

- *Section 1.* General
- *Section 2.* Basis of design
- *Section 3.* Materials
- *Section 4.* Design of masonry
- *Section 5.* Structural detailing
- *Section 6.* Construction

The design vertical load resistance per unit length,  $N_{Rd}$ , of an unreinforced masonry wall is calculated using the National Annex DIN EN 1996 1-1/NA, with the following expression:

$$N_{Rd} = \Phi_i t f_d \quad 2.11$$

where  $\Phi_i$  is a capacity reduction factor allowing for the effects of slenderness and eccentricity,  $t$  is the thickness of the wall,  $f_d$  is the design value of the compressive strength of the wall.

In DIN, the capacity reduction factor has been approximated by a linear formula, but the formula gives rise to negative capacity reduction factors at high values of slenderness.

The capacity reduction factor  $\phi_i$  is given by:

$$\phi_i = 1 - 2 \frac{e_i}{t} \quad 2.12$$

where  $e_i$  is the eccentricity at the top or bottom of the wall calculated from:

$$e_i = \frac{M_i}{N_i} + e_{hi} > 0.05t \quad 2.13$$

$M_i$  and  $N_i$  are respectively the design bending moment and vertical load at the top or bottom of the wall and  $e_{hi}$  is eccentricity resulting from lateral loads.

The basis of the capacity reduction factor is not stated but is known to derive from a complex theoretical solution originally developed for plain concrete sections (Kukulski, 1966).

The *effective height* is related to the degree of restraint imposed by the floors and beams which frame into the wall. Rules are given for the assessment of the effective height of a wall. In general, walls restrained top and bottom by reinforced concrete slabs are assumed to have an effective height of  $0.75 \times$  actual height. If similarly restrained by timber floors the effective height is equal to the actual height. Formulae are given for making allowance for restraint on vertical edges where this is known to be effective.

In the DIN the effective height is taken as:

$$h_{ef} = \rho_n h \quad 2.14$$

where  $h$  is the clear storey height and  $\rho_n$  is a reduction factor where  $n=2, 3$  or  $4$  depending on the edge restraint or stiffening of the wall. Suggested values of  $\rho_n$  are given in the code for walls restrained at the top and bottom. In this case the value of the reduction factor is taken equal to 1.

The *effective thickness* of single leaf walls is usually taken as the actual thickness.

The *slenderness* is the ratio of the effective height to the effective thickness, and therefore both of these quantities must be determined for design purposes.

### 2.2.1 Simplified method for moment calculation

In order to calculate the eccentricity  $e_i$ , it is necessary to determine the value of  $M_i$ . A simplified method of calculating these moments is described in Annex C of DIN. Using the simplified frame diagram illustrated in Fig. 2.4 in which the remote ends of each member framing into a joint are assumed to be fixed (unless known to be free), the bending moment  $M_i$  can be calculated using:

$$M_i = \frac{n \frac{E_1 I_1}{h_1}}{n \frac{E_1 I_1}{h_1} + n \frac{E_2 I_2}{h_2} + n \frac{E_3 I_3}{h_3} + n \frac{E_4 I_4}{h_4}} \left( \frac{\omega_3 L_3^2}{12} - \frac{\omega_4 L_4^2}{12} \right) \quad 2.15$$

where  $n$  is taken as 4 if the remote end is fixed and 3 if free. Here  $E$  and  $I$  represent the appropriate elastic modulus and second moment of area respectively, and  $\omega_3$  and  $\omega_4$  are the uniformly distributed loads. While  $L$  and  $h$  indicate the height of the wall and the length of the slab respectively.

The load bearing capacity depends on the value of the moment acting in the different part of the wall. The higher values of the moment are above and beside the slab.

If less than four members frame into a joint, then the equation is modified by ignoring the terms related to the missing members.

The results of such calculations will usually be conservative because the true fixity, i.e. the ratio of the actual moment transmitted by a joint to that which would exist if the joint was fully rigid, of the wall slab joint cannot be achieved. It will be permissible for use in design to reduce the bending moment, obtained from the calculations in accordance with equation (2.15) above, by multiplying it by a factor:

$$\eta = 1 - \frac{k}{4} \tag{2.16}$$

The value of  $k$  is given by:

$$k = \frac{n \frac{E_3 I_3}{h_3} + n \frac{E_4 I_4}{h_4}}{n \frac{E_1 I_1}{h_1} + n \frac{E_2 I_2}{h_2}} \leq 2 \tag{2.17}$$

If the wall bending moment and axial load are calculated for any joint in a multi-storey framed structure, then the eccentricity can be determined by dividing the moment by the axial load. The required moment and axial load can be determined using a normal rigid frame analysis. This approach is reasonable when the wall compression is high enough to contribute to the rigidity of the joints, but it could lead to inaccuracies when the compression is small.

When the eccentricity overcome the value equal to 0.33 times the wall thickness, then the DIN suggest to consider the minimal value of the thickness to calculate the load bearing capacity.

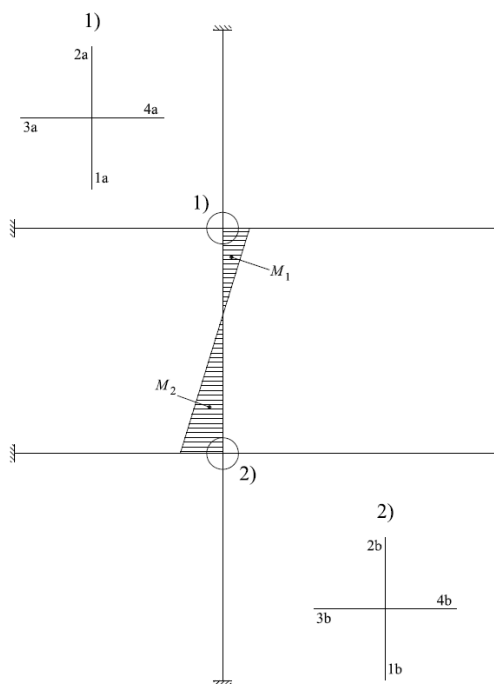


Figure 2.4 Simplified frame system

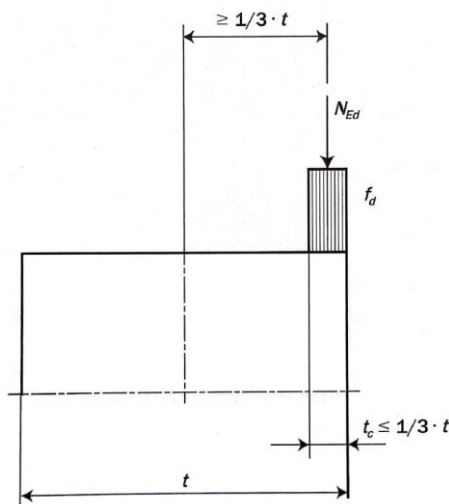


Figure 2.5 Stress block

### 3 Materials and modeling strategies

Numerical simulations are necessary to provide information about the structural behaviour and support the derivation of rational design rules. Nevertheless, the development of reliable and accurate numerical models cannot be achieved without a careful material description and a validation by comparison with a significant number of experimental results. This means that experiments in large-scale masonry tests, small masonry samples and masonry components are necessary.

Nonlinear finite element analyses will always be helpful for the validation of the design of complex masonry structures under complex loading conditions.

#### 3.1 Micro- and macro- modeling

Masonry is a composite material that consists of units and mortar joints. A detailed analysis of masonry, must then include a representation of units, mortar and the unit/mortar interface. The primary aim of micro-modeling is to carefully represent masonry starting from the knowledge of the properties of each constituent and the interface. The necessary experimental data must be obtained from laboratory tests in the constituents and small masonry samples.

Due to the mortar joints, which act as a planes of weakness, and to the anisotropy of the blocks, the masonry mechanical properties change as a function of the direction taken in consideration. Generally, its numerical representation can be made using an approach based on the micro-modeling of the individual components (brick, block, etc.) and mortar, or the macro-modeling of masonry as a composite. Depending on the level of accuracy and the simplicity desired, it is possible to use the following modeling strategies, see Figure 3.1:

- *Detailed micro-modeling* - units and mortar in the joints are represented by continuum elements whereas the unit-mortar interface is represented by discontinuous elements;
- *Simplified micro-modeling* - expanded units are represented by continuum elements whereas the behaviour of the mortar joints and unit-mortar interface is lumped in discontinuous elements;
- *Macro-modeling* - units, mortar and unit-mortar interface are smeared out in the continuum.

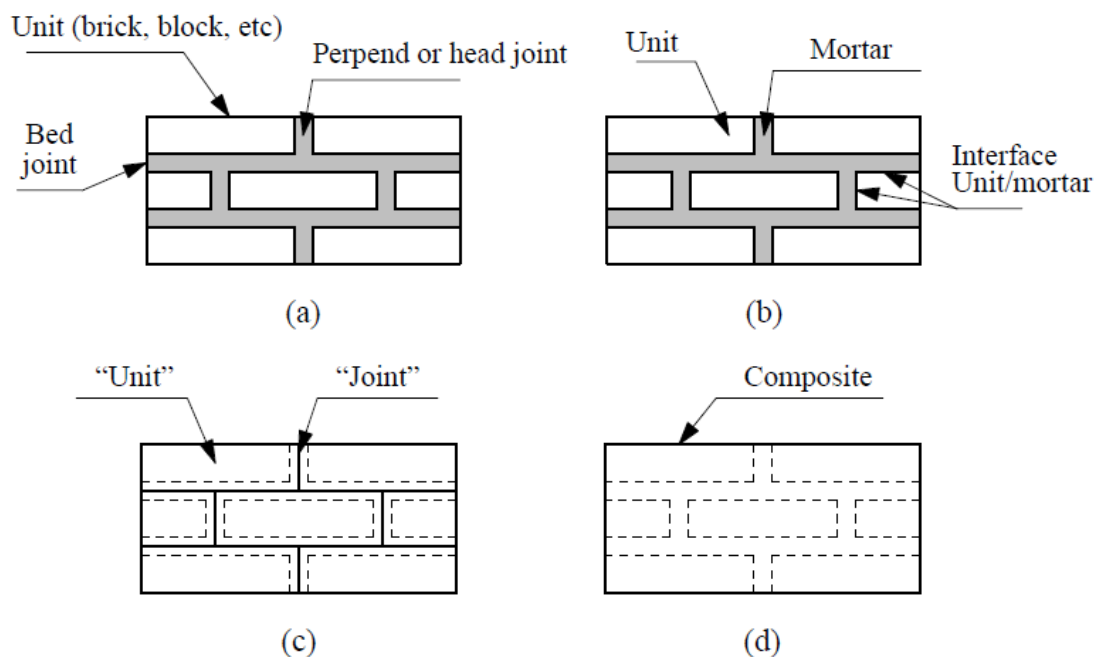


**Figure 3.1 Modeling strategies for masonry structures: (a) masonry sample; (b) detailed micro-modeling; (c) simplified micro-modeling; (d) macro-modeling**

In the *first approach*, Young's modulus, Poisson's ratio and, optionally, inelastic properties of both unit and mortar are taken into consideration. The interface represents a potential crack/slip plane provided with stiffness to avoid interpenetration of the continuum. This enables the combined action of unit, mortar and interface.

In the *second approach*, each joint, consisting of mortar and the two units mortar interfaces, is assumed into an "average" interface, while the units are expanded in order to keep the geometry unchanged. Masonry is thus considered as a set of elastic blocks bonded by potential fracture/slip lines at the joints. Accuracy is lost since Poisson's effect of the mortar is not included.

The *third approach* does not make a distinction between individual units and joints but treats masonry as a homogeneous anisotropic continuum.

One modeling strategy cannot be preferred over the other because different application fields exist for micro- and macro-models. Micro-modeling studies are necessary to give a better understanding about the local behaviour of masonry structures. This type of modeling is particularly used to structural details. Macro-models are applicable when the structure is composed of solid walls with sufficiently large dimensions so that the stresses across or along a macro-length will be essentially uniform. Clearly, macro-modeling is more practice oriented due to the reduced time and memory requirements as well as a user-friendly mesh generation. This type of modeling is most valuable when a compromise between accuracy and efficiency is needed.

Accurate micro- or macro- modeling of masonry structures requires a careful experimental description of the material. However, the properties of masonry are influenced by many different factors, such as material properties of the units and mortar, arrangement of bed and head joints, anisotropy of units, dimension of units, joint width, quality of workmanship, degree of curing, environment and age.

### 3.2 Softening behaviour

Softening is a gradual decrease of mechanical resistance under a continuous increase of deformation forced upon a sample or structure. It is an important characteristic of quasi-brittle materials like clay brick, mortar, ceramics, rock or concrete, which fail due to a process of internal crack formation. Such mechanical behaviour is usually attributed to the heterogeneity of the material, due to the presence of different phases and material defects even prior to loading (micro- and macro- defects).

The initial stresses and cracks as well as variations of internal stiffness and strength cause progressive crack development when the material is subjected to progressive deformation. Initially, the microcracks are stable which means that they grow only when the load is increased. Around peak load, an acceleration of crack formation takes place and the formation of macrocracks starts. The macrocracks are unstable, which means that the load has to decrease to avoid an uncontrolled growth. In a deformation controlled test the macrocrack growth results in softening and localization of cracking in a small zone while the rest of the sample remains uncracked.

For shear failure, a softening process is also observed as degradation of the cohesion in Coulomb friction models. For compressive failure, softening behaviour is highly dependent upon the boundary conditions in the experiments and the size of the specimen, (Mier, 1984) and (Vonk, 1992). Experimental concrete data provided by (Vonk, 1992) indicated that the behaviour in uniaxial compression is governed by both local and continuum fracturing processes.

Fig. (3.2) shows characteristic stress-displacement diagrams for *quasi-brittle materials* in uniaxial tension and compression. It is assumed that the inelastic behaviour both in tension and compression can be described by the diagram's integral. These quantities, denoted respectively as fracture energy  $G_f$  and compressive fracture energy  $G_c$ , are assumed to be material properties. With this energy-based approach, tensile and compressive softening can be described within the same context.

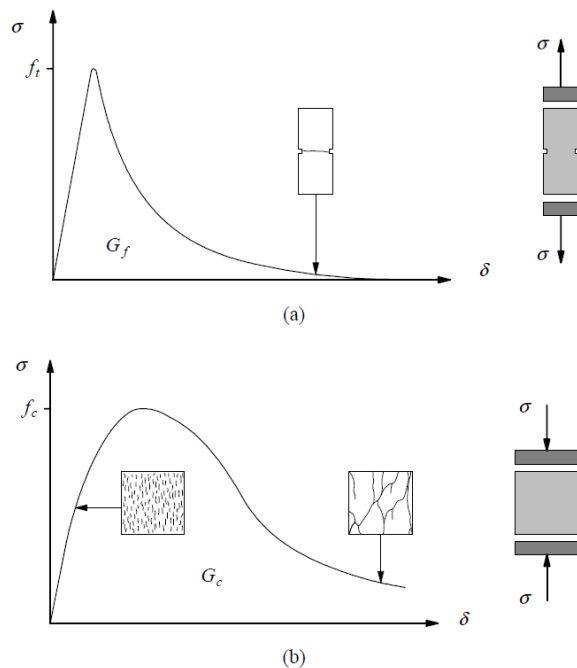


**Figure 3.2** Stress displacement diagrams: a) Uniaxial tension ( $f_t$  is the tensile strength); b) Uniaxial compression ( $f_c$  is the compressive strength)

It is noted that masonry presents other type of failure mechanism, which consists of unit-mortar interface slip under shear loading, see Fig.3.3. Again, it is assumed that the inelastic shear behaviour can be described by the fracture energy  $G_f^II$ , defined by the integral of the diagram in the absence of normal confining load.

Shear failure is an important feature of masonry behaviour which must be considered in a micro-modeling strategy. However, for continuum models, this failure cannot be directly included because the unit and mortar geometries are not discretized. Failure is, then, associated with tension and compression modes in a principal stress space.

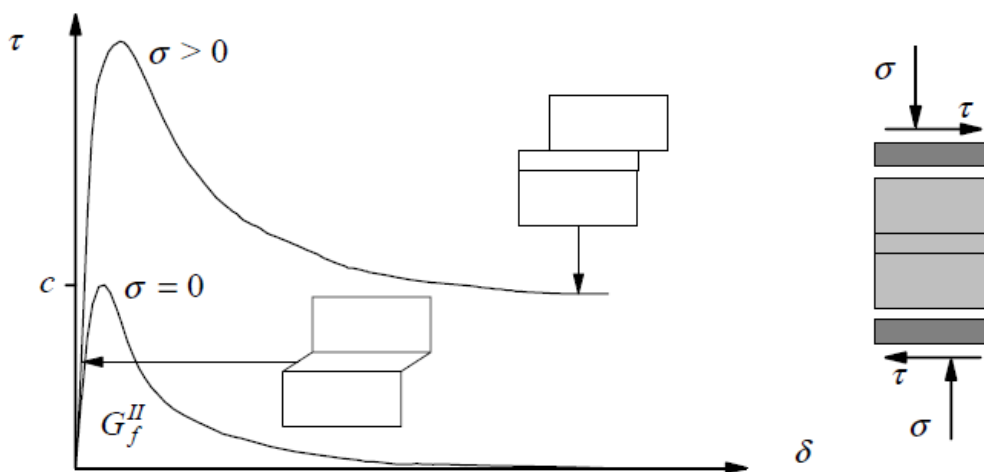


Figure 3.3 Shear behaviour ( $c$  is the cohesion)

### 3.3 Properties of unit and mortar

The properties of masonry are strongly dependent upon the properties of its constituents. The EC6 uses the compressive strength of the components to determine the strength of masonry even if a real indication of those values is not simple. For the masonry units, standard tests with solid plates result in an artificial compressive strength due to the restraint effect of the plates. The EC6 minimizes this effect by considering a normalized compressive strength  $f_b$ , which results from the standard compressive strength, in the relevant direction of loading, multiplied by an appropriate shape/size factor.

Experiments in the uniaxial post-peak behaviour of compressed bricks and blocks are virtually non-existent and no recommendations about the compressive fracture energy  $G_c$  can be made. It is difficult to relate the tensile strength of the masonry unit to its compressive strength due to the different shapes, materials, manufacture processes and volume of perforations. For the longitudinal tensile strength of clay, calcium-silicate and concrete units, (Schubert, 1994) carried out an extensive testing program and obtained a ratio between the tensile and compressive strength that ranges from 0.03 to 0.10. For the fracture energy  $G_f$  of solid clay and calcium-silicate units, both in the longitudinal and normal directions, (Pluijm, 1992) found values ranging from 0.06 to 0.13 [Nmm/mm<sup>2</sup>], for tensile strength values ranging from 1.5 to 3.5 [N/mm<sup>2</sup>].

Experiments on the biaxial behaviour of bricks and blocks are also lacking in the literature. This aspect gains relevance due to the usual orthotropy of the units due to perforations. As a consequence, the biaxial behaviour of a brick or block with a given shape is likely to be unknown, even if the behaviour of the material from which the unit is made is known.

For the mortar, the compressive strength  $f_m$  is obtained from standard tests. Nevertheless, there is still a lack of knowledge about the complete mortar uniaxial behaviour, both in compression and tension.

### 3.4 Properties of the unit-mortar interface

The unit-mortar joint is often the weakest part in masonry structure. The nonlinear response of the joints, which is then controlled by the unit-mortar interface, is one of the most relevant features of masonry behaviour. Two different phenomena occur in the unit-mortar interface, one associated with tensile failure and the other associated with shear failure.

#### 3.4.1 Tensile failure

(Pluijm, 1992) carried out deformation controlled tests in small masonry specimens of solid clay and calcium-silicate units, see Figure 3.4. These tests resulted in an exponential tension softening curve with a fracture energy  $G_f^I$  ranging from 0.005 to 0.02 [Nmm/mm<sup>2</sup>] for a tensile bond strength ranging from 0.3 to 0.9 [N/mm<sup>2</sup>], according to the unit-mortar combination. The fracture energy is defined as the amount of energy to create a unitary area of a crack along the unit-mortar interface. A close observation of the cracked specimens revealed that the bond area was smaller than the cross sectional area of the specimen, see Figure 3.5. This so-called net bond surface seems to concentrate in the inner part of the specimen, which can be a combined result from shrinkage of the mortar and the process of laying units in the mortar bed. The values given above refer to the real cross section of a wall and result from an extrapolation of the measured net bond surface of the specimen to the assumed net bond surface of the wall, neglecting any influence of the vertical joints.

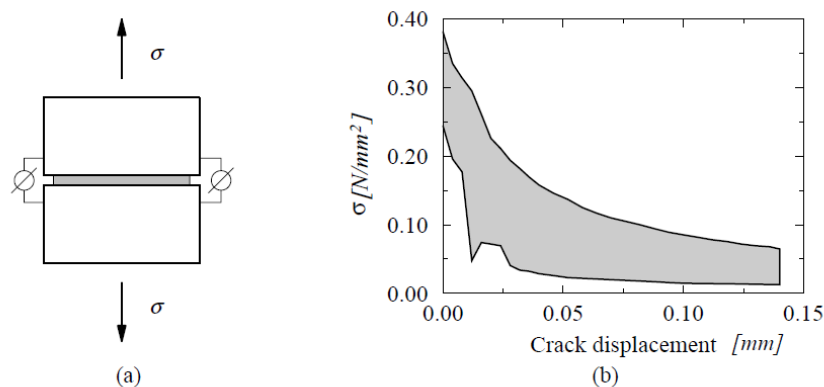


Figure 3.4 Tensile bond behaviour of masonry. (a) test specimen; (b) stress-crack displacement results

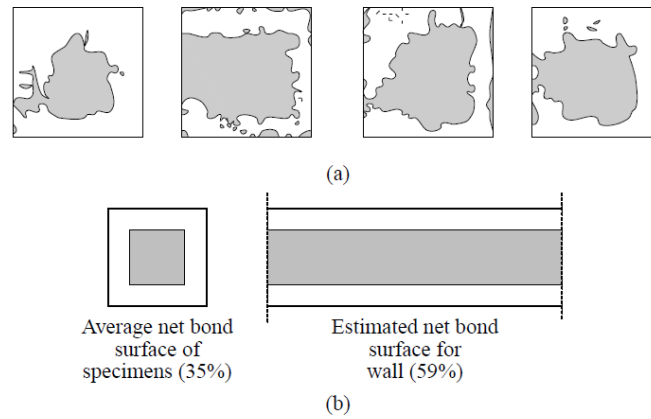


Figure 3.5 Tensile bond surface. (a) bond surface for tensile specimens; (b) net bond surface

### 3.4.2 Shear failure

An important aspect in the determination of the shear response of masonry joints is the ability of the test set-up to generate a uniform state of stress in the joints. This objective is difficult because the equilibrium constraints introduce non-uniform normal stresses in the joint.

(Pluijm, 1993) presents a characterization of the masonry shear behaviour, for solid clay and calcium-silicate units. Confining (compressive) stresses were applied with three different levels: 0.1, 0.5 and 1.0  $[N/mm^2]$ . The test apparatus did not allow for application of tensile stresses and even for low confining stresses extremely brittle results are found with potential instability of the test set-up. For several specimens with higher confining stresses shearing of the unit-mortar interface was accompanied by diagonal cracking in the unit.

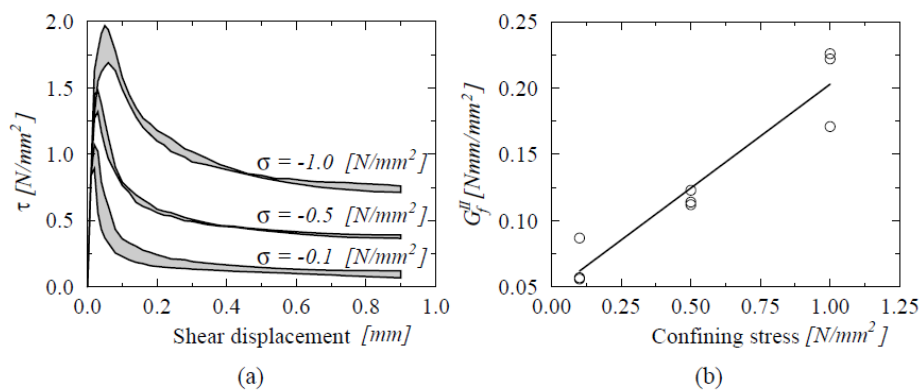
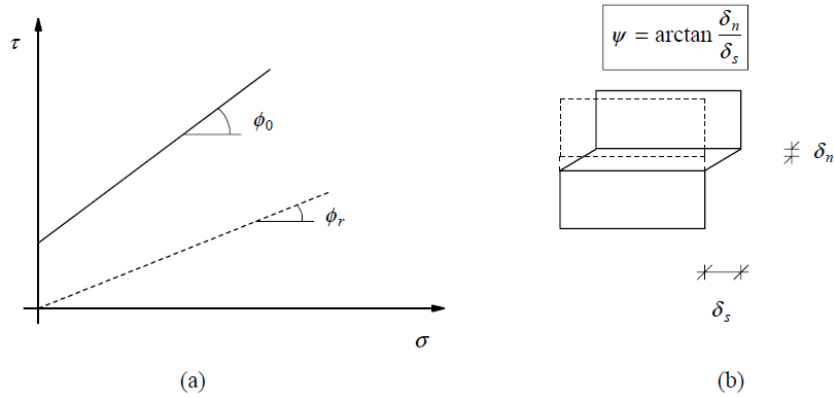


Figure 3.6 Shear bond behaviour of the joint. (a) stress-displacement diagram for different normal stress levels; (b) fracture energy as a function of the normal stress level

The experimental results yield an exponential shear softening diagram with a residual dry friction level, see Figure 3.6a. The area defined by the stress-displacement diagram and the residual dry friction shear level is named fracture energy  $G_f^{II}$ , with values ranging from 0.01 to 0.25  $[Nmm/mm^2]$ , for initial cohesion  $c$  values ranging from 0.1 to 1.8  $[N/mm^2]$ . The value for the fracture energy depends also on the level of the confining stress, see Figure 3.6b. Evaluation of the net bond surface of the specimens is no longer possible but the values measured for tensile bond strength can be assumed to hold.



**Figure 3.7 Friction and dilatancy angles. (a) Coulomb friction law with initial and residual friction angle; (b) dilatancy angle**

Additional material parameters can be obtained from such an experiment, see Figure 3.7. The initial internal friction angle  $\Phi_0$ , associated with a Coulomb friction model, is measured by  $\tan \Phi_0$ , which ranges from 0.7 to 1.2, for different unit-mortar combinations. The residual internal friction angle  $\Phi_r$  is measured by  $\tan \Phi_r$ , which seems to be approximately constant and to equal 0.75. The dilatancy angle  $\Psi$  measures the uplift of one unit over the other upon shearing, see Figure 3.7b. Note that the dilatancy angle depends on the level of the confining stress, see Figure 3.8a. For low confining pressures, the average value of  $\tan \Psi$  falls in the range from 0.2 to 0.7, depending on the roughness of the unit surface. For high confining pressures,  $\tan \Psi$  decreases to zero. With increasing slip,  $\tan \Psi$  also decreases to zero due to the smoothing of the sheared surfaces, see Figure 3.8b.

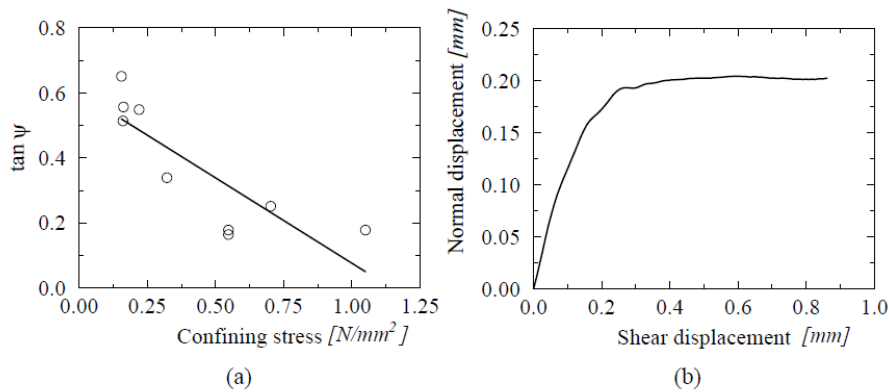


**Figure 3.8 Shear bond behaviour of the joint. (a) tangent of the dilatancy angle  $\Psi$  as a function of the normal stress level; (b) relation between the normal and the shear displacement upon loading**

### 3.5 Properties of the composite material

Masonry is a composite material which consists of units and mortar. The failure mechanism of the components loaded in tension and compression is essentially the same, with a crack growth at the microlevel of the material. In this process inelastic strains result from a dissipative process in which fracture energy is released during the process of internal fracture. The composite material shows, however, another type of failure, sliding, which results in a dry friction process between the components once softening is completed.

If a micro-modeling strategy is used all these phenomena can be incorporated in the model because joints and units are represented separately. In a macro-modeling strategy joints are considered like an anisotropic homogeneous material and the interaction between the components cannot be incorporated in the model. Instead, a relation between average stresses and strains is established.

The principal problem to realize an accurate masonry model is to know a complete materials description. This is generally difficult because experimental data suitable for numerical purpose are scarce. The principal relations between the different components of brickwork can be derived by standard test on materials. It's known that masonry loaded in uniform compression will fail by the development of tension cracks parallel to the axis of loading or by a shear failure along lines of weakness, the mode of failure depends on whether the mortar is weak or strong relative to the units.

Moreover, it is observed that the strength of masonry in compression is smaller than the nominal compressive strength of the units as given by a standard compressive test. On the other hand, the masonry strength may greatly exceed the cube crushing strength of the mortar used in it.

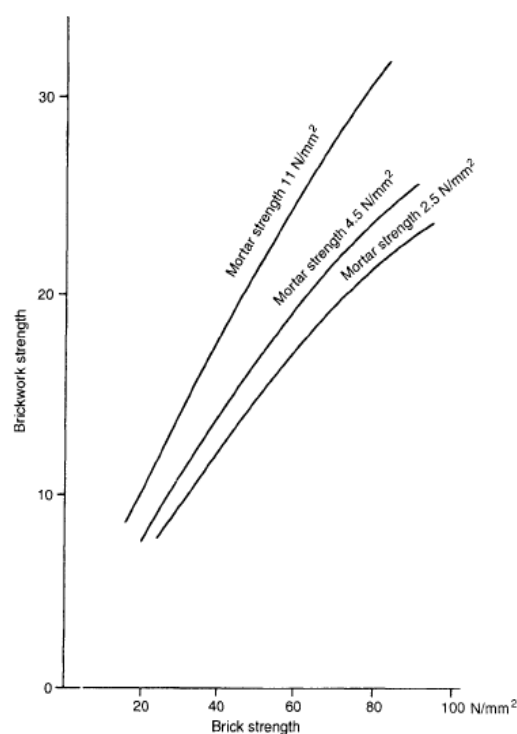


Figure 3.9 Relation between the different components

## 4 Experimental investigation

The experimental investigations are made by the Technische Universität Dresden and described in (Jäger & Baier, 2007).

The development of reliable and accurate numerical models cannot be achieved without a careful material description and a validation by comparison with a significant number of experimental results. This means that experiments in large-scale masonry tests, small masonry samples and masonry components are necessary.

For this reason, a wall-ceiling node model has been selected, which is composed from 2 outer walls, each half-storey height and a reinforced concrete slab.

### Wall

Width:	$b = 1.0 \text{ m}$
Height:	$h_{1,2} = 1.25 \text{ m}$
Thickness:	$t = 0.365 \text{ m}$
Moment of inertia:	$I = 4052260417 \text{ mm}^4$
Brick:	Thermopor P014
Mortar:	Thin-bed mortar

### Slab

Width:	$b = 1.0 \text{ m}$
Height:	$h = 5.0 \text{ m}$
Thickness:	$d = 0.2 \text{ m}$
Concrete:	B25
Steel reinforcement:	BST 500M/S
Support Depth:	$t_s = 0.19 \text{ m}$
Moment of inertia:	$I = 667000000 \text{ mm}^4$



Figure 4.1 Experimental structure

The stress is added at the head of the upper wall and to the slab in order to investigate the influence of different vertical loads. The primary aim is the experimental determination of the transferred bending moments in the node for different load combinations.

In addition, the investigations are necessary for the calibration of the FEM model used for the simulation of structural behaviour of the wall-ceiling node.

The moment of inertia of the wall is calculated by the following formulation:

$$I = \frac{t^3 b}{12} \quad \text{Equation 4.1}$$

The moment of inertia of the slab is calculated with:

$$I = \frac{d^3 b}{12} \quad \text{Equation 4.2}$$



Figure 4.2 Wall/Slab node

The static system considered is shown in Fig.4.3

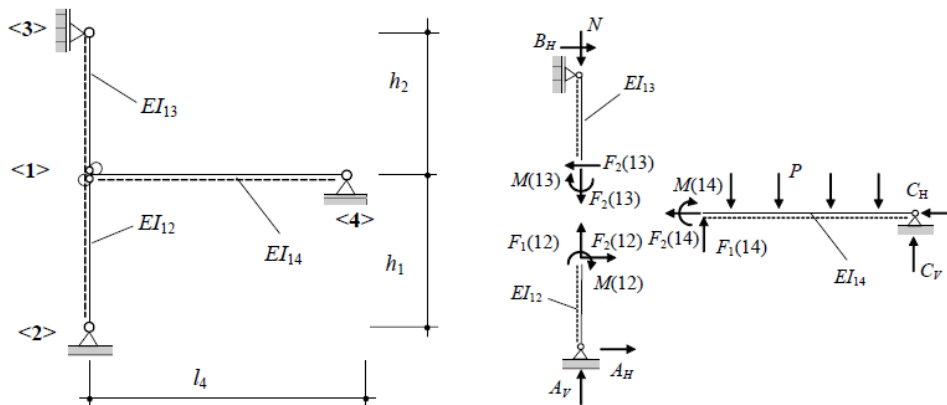


Figure 4.3 Frame system and binding reactions

## 4.1 Materials

The material parameters are obtained from experimental proofs execute according to (DIN EN 772-1, 2000) and to (DIN EN 1052-1, 1998).

### 4.1.1 Bricks Thermopor P14

The compressive strength of the bricks was tested according to (DIN EN 772-1, 2000). There were summarized the characteristics following:

#### Geometrical features:

Length in x direction:  $s_x = 247 \text{ mm}$

Length in y direction:  $s_y = 365 \text{ mm}$

Length in z direction:  $s_z = 249 \text{ mm}$

#### Mechanical parameters:

Compressive strength:  $f_b = 9.1 \text{ N/mm}^2$

Elastic modulus:  $E = 3000 \text{ N/mm}^2$

Density:  $\rho = 0.7 \text{ kg/dm}^3$

Poisson ratio:  $\nu = 0.17$



Figure 4.4 Brick Thermopor P14

### 4.1.2 Mortar

To determine the mortar properties standard tests were carried out. One compilation of relevant results is shown below.

#### Mechanical parameters:

Density:	$\rho = 1.56 \text{ kg/dm}^3$
Compressive strength:	$f_b = 19,64 \text{ N/mm}^2$
Elastic modulus:	$E = 5900 \text{ N/mm}^2$

### 4.1.3 Masonry

The determination of Young's modulus and the strength of masonry is carried out using DIN EN 1052-1.

#### Geometrical features:

Wall width:	$l_s = 500 \text{ mm}$
Wall height:	$h_s = 1250 \text{ mm}$
Wall thickness:	$t_s = 365 \text{ mm}$
Measurement tools distance:	$L_1 = 500 \text{ mm}$

#### Mechanical Parameters:

Medium compressive strength:	$f = 6.47 \text{ N/mm}^2$
Characteristic compressive strength:	$f_k = 5.39 \text{ N/mm}^2$
Elastic modulus:	$E = 4700 \text{ N/mm}^2$

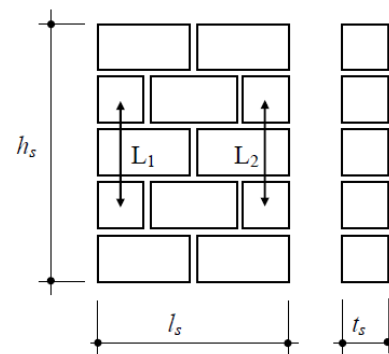


Figure 4.5 Masonry test specimen



Figure 4.6 Proof's execution

### 4.1.4 Concrete

The determination of the elastic modulus, compressive strength and the stress-strain curve are necessary in order to evaluate the concrete properties. The results of the tests are summarised following.

**Mechanical Parameters:**

- Density:  $\rho = 2.33 \text{ kg/dm}^3$
- Compressive strength:  $f_c = 47.03 \text{ N/mm}^2$
- Tensile strength:  $f_t = 3.43 \text{ N/mm}^2$
- Elastic modulus:  $E = 32000 \text{ N/mm}^2$



Figure 4.7 Concrete specimen

### 4.2 Load program

The load at the top of the upper wall is applied by two hydraulic presses to the axis of the wall. To load the ceiling plate 4 steel load plates were used. Each plate is extended over the entire width of the ceiling strip. The plates are situated at the quarter points of the slab. The vertical load  $N$  decreases during the experiment, starting from a value of about 100 kN to until 0 kN. The vertical load  $P$  increases starting from 0 kN until to about 10 kN for every load stages.

The following load cases were considered in order to calibrate the FEM model.

Load case	N [kN]	P [kN]
A4	103,33	6,26
A7	102,82	10,01
B4	52,9	6,26
B7	52,43	10,01
C4	13,79	6,27
C7	13,46	10,02

Table 4-1 Load cases

The value of  $\omega_4$  used in the DIN formulation is equal to 10.1 kN/m when the vertical load  $P$  is equal to 6.25 kN, on the contrary it is equal to 13.16 kN/m when  $P$  is equal to 10 kN. The value of the distributed load takes in consideration the death load of the concrete slab. The vertical load acting to the wall/slab connection takes in consideration the death load of the upper wall.

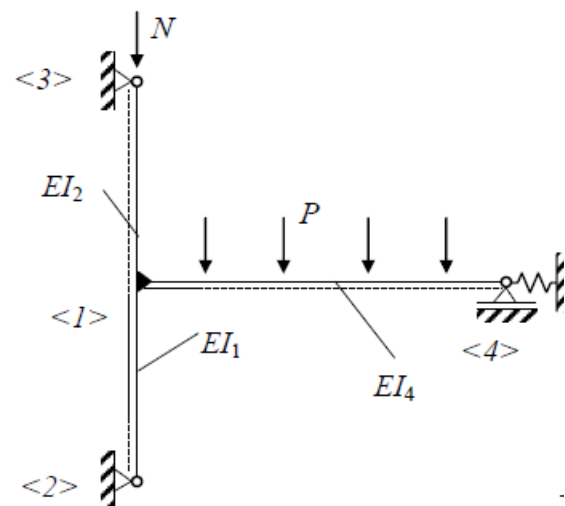


Figure 4.8 Frame system

### 4.3 Measurements

The mean values of the deformations and distortions were registered for each load stage.

The horizontal deformations of the wall are generally relatively low (<1 mm). The vertical displacement of the slab are show on the table 4-2. The measurement point 13 measures the vertical displacement of the middle of the slab and was selected to calibrate the FEM model.

Load case	Measuring point 13 [mm]
A4	2,3
A7	4,87
B4	3,64
B7	5,88
C4	4,45
C7	6,66

Table 4-2 Experimental vertical displacement

Load cells were used during the experiment in order to measure the binding reaction of the structure. In particular, the horizontal reactions  $B_H$  and  $A_H$  were considered.

Load case	$A_H$ [kN]	$B_H$ [kN]
A4	4,45	-4,25
A7	6,09	-4,53
B4	3,63	-2,31
B7	4,78	-2,53
C4	2,78	-0,78
C7	3,79	-0,99

Table 4-3 Experimental horizontal binding reactions

The other results analysed are shown on Annex C.

## 5 Numerical investigation

Numerical simulations are necessary to provide information into the structural behaviour and to support the derivation of rational design rules. Nonlinear finite element analyses will always be helpful for the validation of the design for masonry structures under complex loading conditions.

For these reasons a structural numerical model was calibrated according to the requirements of the considered problem, or the realistic determination of nodes bending moments under different structural load cases.

Masonry is a multi-component construction material which is essentially characterized by anisotropic properties. The FEM model used herein is to be construed as three-dimensional micro-model, in which the stones and the mortar joints are modelled discretely. This makes it possible to assign separate properties of the stone and the mortar. The bond between the two components is simulated by contact elements, which in turn very specific properties can be assigned

In Atena 3D program the different material properties can be detected.

A general analysis of a structure usually consists of application of many small load increments. At each of those increments an iterative solution procedure has to be executed to obtain a structural response at the end of the increment. The Atena 3D program, which is determined for nonlinear finite element analysis of structures, offers tools specially designed for computer simulation of concrete and reinforced concrete structural behavior.

### 5.1 Atena 3D

Atena 3D program is designed for 3D nonlinear analysis of solids with special tools for reinforced concrete structures. However, structures from other materials, such as soils, metals etc. can be treated as well. The program has three main functions:

1. *Pre-processing*. Input of geometrical objects (concrete, reinforcement, interfaces, etc.), loading and boundary conditions, meshing and solution parameters.
2. *Analysis*. It makes possible a real time monitoring of results during calculations.
3. *Post-processing*. Access to a wide range of graphical and numerical results.

Atena 3D recognizes two models, geometrical and numerical. Data of these models are treated strictly separately.

**Geometrical model** represents dimensions, properties and loading. It consists of an assembly of macro-elements (solids). They are connected by contacts, as a matter of fact each macro-element is an independent object defined by joints lines and surfaces. Thus, on a contact of neighboring macro-elements there are double surfaces (consequently also double lines and double joints). This provision assures that each object is independent of the others. If we add or remove a macro-element all its entities are added or removed without interference with other objects.

Reinforcement can be modeled by a discrete bar, which is defined as a geometrical multi-linear object. It is embedded in solid objects. Its geometry is defined independently of macro-element. Thus, one reinforcing bar can be embedded in any number of macro-elements.

Geometrical model is completed by defining loading (load cases and load history) and construction cases.

**Numerical model** is generated according to the geometrical model and represents a numerical approximation of the structural analysis problem. Numerical model is a result of discretization made by the finite element method. The mesh generator in ATENA makes possible to generate automatically meshes for solid and reinforcing objects. As a consequence of independent macro-elements, the finite element meshes are made for each microelement independently. Thus, when two macro-elements are connected as neighbouring objects, there are two surfaces belonging to each object on the contact. There are two sets of nodes on the contact, which may, but need not to coincide. The connection between the nodes of neighbouring objects can be perfect, or there may be a contact element to model other types of interaction.

## 5.2 FEM model

The traditional way of modeling walls, shear walls and similar structural parts, build from masonry, i.e., from bricks (or stones) connected with mortar, is to determine the material properties of the masonry. For smaller structures, it may be possible to model all bricks discretely, i.e. represent each brick with a separate macro-element or volume, and each gap with an interface.

Modeling mortar with volume elements usually does not make sense and it is also not very feasible, because the very thin layer requires mesh refinement and results in a mesh with too many finite elements. It is used maybe for some special studies of just a small region between 2 bricks.

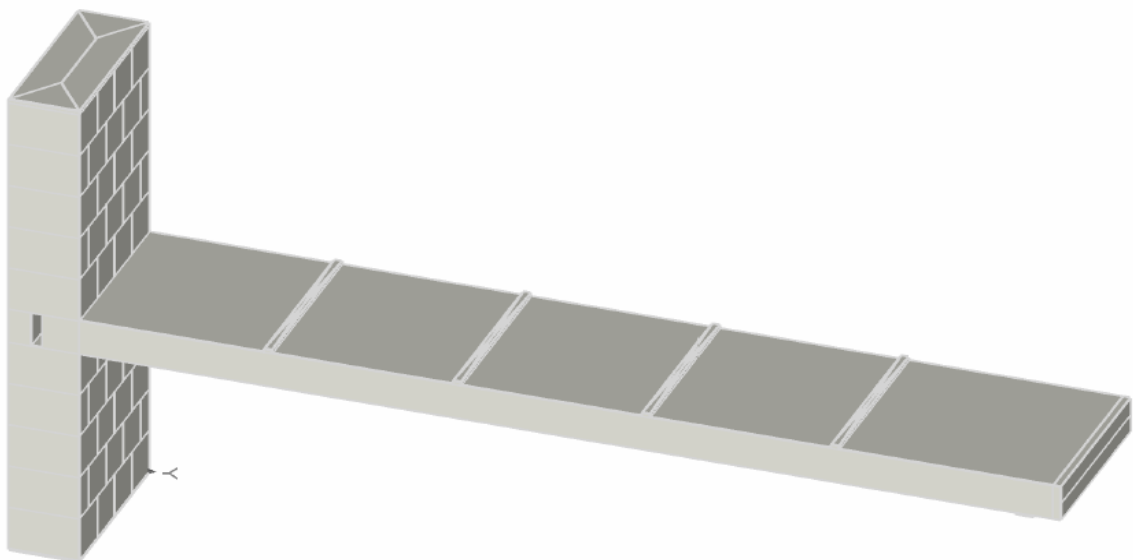


Figure 5.1 FEM model used for the numerical investigation

The FEM calibration was carried out by trying to reproduce the structure behaviour as accurately as possible. This was done through a micro-modeling of the structure, defining the parameters and the geometry of the materials used in the experimental phase. Some parameters, such as the *tensile strength* of mortar and brick, have not been provided through experimental tests. For this reason, an iterative analysis was carried out in such a way as to derive these values. For example, starting from a value of the tensile strength equal to about 0.4 times the compressive strength of the mortar, the value was changed until acceptable results, compared with the experimental results, have been achieved. Masonry brick's tensile strength is supposed to be greater than the mortar interface's one. The characteristics of the steel reinforcement used to model the slab are the same used for the experimental investigation. These are shown in Annex E.

In addition to the mechanical parameters, also the load cases are important on the structural behavior. Specifically, the vertical force applied on the top of the wall influences the structural behavior near the wall/slab joint. It seems that the higher the value of the vertical force is applied, the higher the stiffness of the node is.

### 5.2.1 Material properties

The mechanical properties are shown below:

Macro element parameters		Concrete	Brick
E	[N/mm <sup>2</sup> ]	32000	3000
v	[-]	0,17	0,17
f <sub>cu</sub>	[N/mm <sup>2</sup> ]	-55,33	-10,71
f <sub>c</sub>	[N/mm <sup>2</sup> ]	-47,03	-9,10
f <sub>t</sub>	[N/mm <sup>2</sup> ]	3,43	2,00
ρ	[kg/m <sup>3</sup> ]	2330	700

Table 5-1 Mechanical parameters of macro-elements

Interface parameters		Brick-Brick	Slab-Brick
E	[N/mm <sup>2</sup> ]	5900	5900
f <sub>m</sub>	[N/mm <sup>2</sup> ]	-19,64	-19,64
f <sub>t</sub>	[N/mm <sup>2</sup> ]	0,8	1
μ	[-]	0,6	1

Table 5-2 Mechanical parameters of interface

Where:

E= Young modulus

v= Poisson ratio

f<sub>cu</sub>= Cubic compressive strength

f<sub>c</sub>= Cylindrical compressive strength

f<sub>t</sub>=Tensile strength

ρ= Density

μ= Friction coefficient

f<sub>m</sub>= Mortar compressive strength

### 5.2.2 Load cases

After the definition of the mechanical parameters the load cases are set. The simulation is carried out by applying a vertical load on the top of the wall and four vertical loads to the slab. The load values were summarized on the table below:

Load case	N [kN]	P [kN]
A4	106	6,25
A7	106	10
B4	56	6,25
B7	56	10
C4	17	6,25
C7	17	10

Table 5-3 Load cases

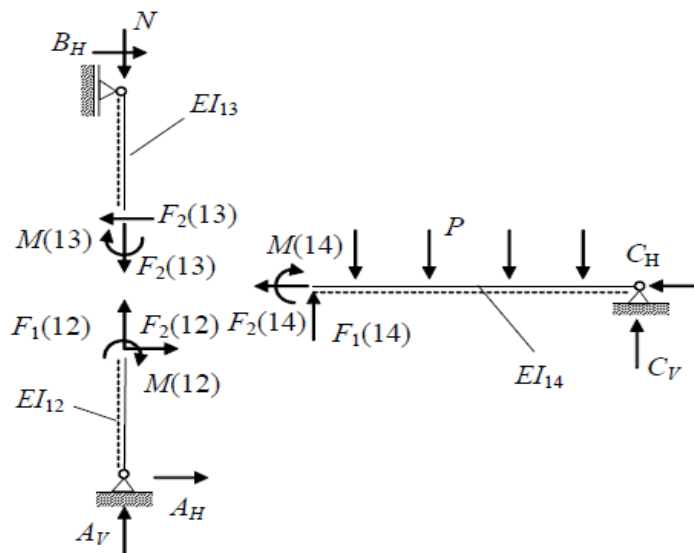


Figure 5.2 Binding reactions on the frame system

For each load case the vertical displacement on the middle point of the slab and the binding reactions are compared with the experimental measurements. The bending moment considered are:

$$M(13) = -B_H h_2 \quad 5.1$$

$$M(12) = A_H h_1 \quad 5.2$$

Where  $M(13)$  and  $M(12)$  are the bending moments acting above and below the slab respectively, while  $h_1$  and  $h_2$  are the height of the lower and upper wall respectively.

By knowing the bending moments it is possible to calculate the eccentricities:

$$e_o = \frac{M(13)}{N} \quad 5.3$$

$$e_u = \frac{M(12)}{A_V} \quad 5.4$$

Where  $e_o$  and  $e_u$  are the upper and the lower load eccentricity, on the wall/slab connection.

### 5.3 Results evaluation

To calibrate the FEM model the numerical results are compared with the experimental results. The diagram below shows the vertical displacement of the middle point of the slab. Next, the error of the FEM model is calculated. This process is repeated also for the horizontal binding reactions  $B_H$  and  $A_H$ , with which is possible to calculate the bending moments acting to the wall slab connection, above and below the slab respectively.

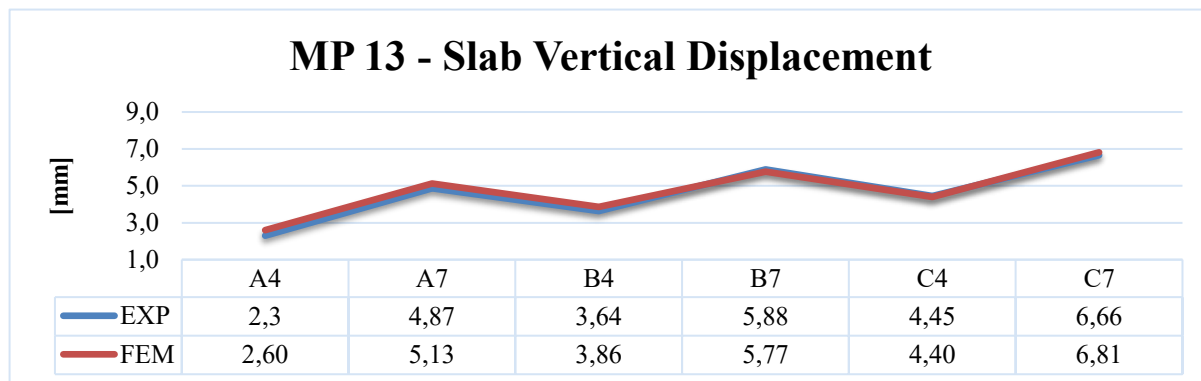


Figure 5.3 Slab vertical displacement from Measuring Point MP 13

Load case	Error [%]
A4	13,0
A7	5,3
B4	6,0
B7	1,9
C4	1,1
C7	2,3

Table 5-4 MP 13 Error evaluation

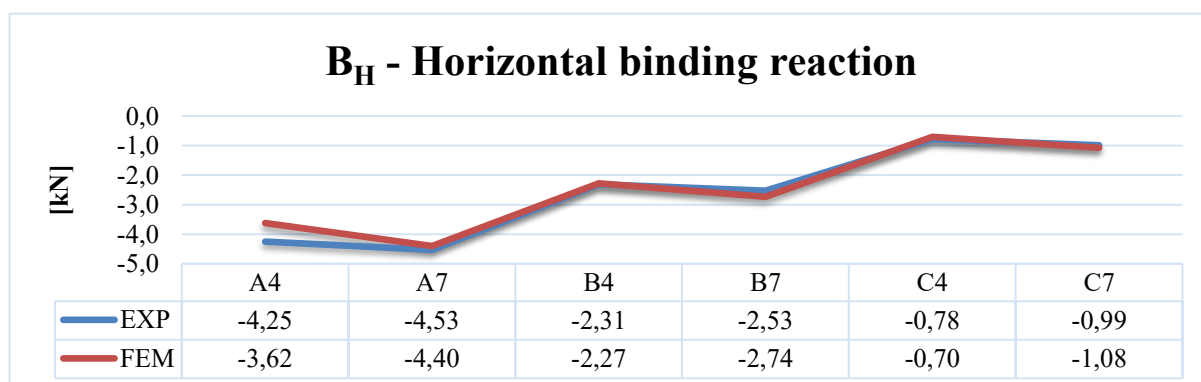


Figure 5.4 Horizontal binding reaction comparison

Load case	Error [%]
A4	14,8
A7	2,8
B4	1,6
B7	8,1
C4	9,7
C7	9,0

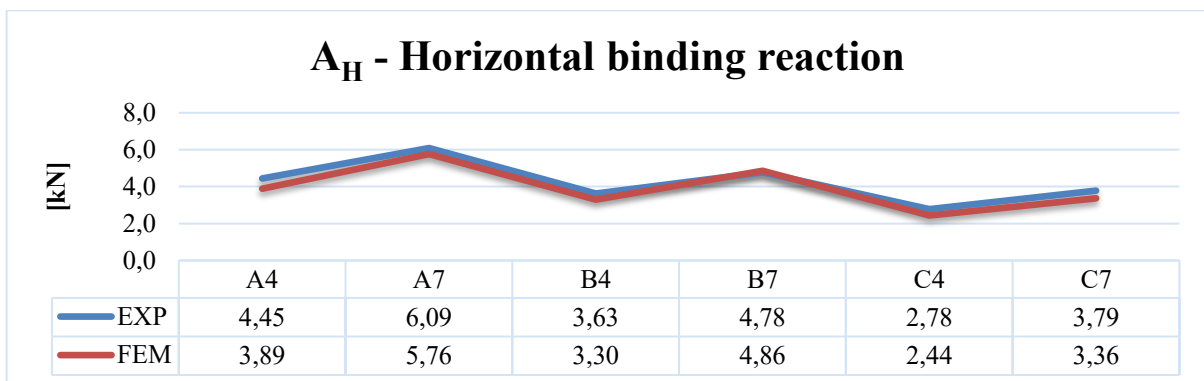
Table 5-5 B<sub>H</sub> Error evaluation

Figure 5.5 Horizontal binding reaction comparison

Load case	Error [%]
A4	12,6
A7	5,3
B4	9,0
B7	1,7
C4	12,3
C7	11,2

Table 5-6 A<sub>H</sub> Error evaluation

Once the model was calibrated, the bending moments and the eccentricities on the node at the top and bottom of the slab were calculated.

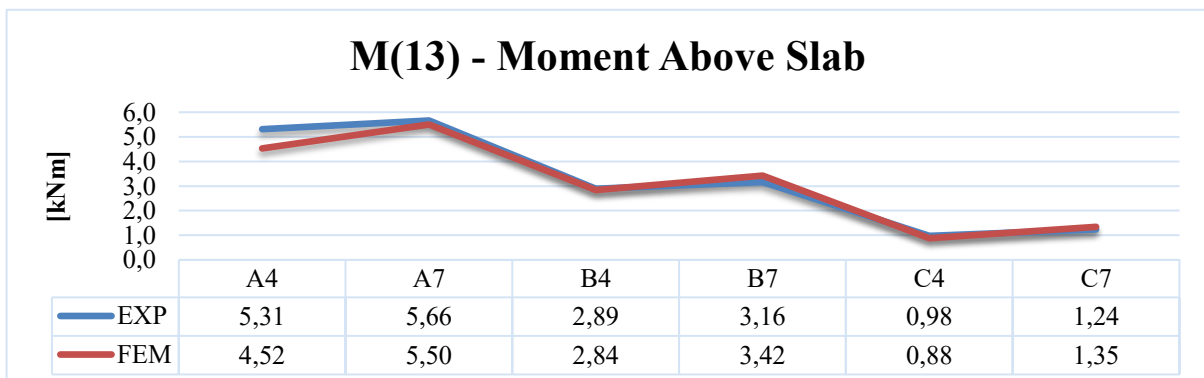


Figure 5.6 Bending moment comparison above the slab

Load case	Error [%]
A4	14,8
A7	2,8
B4	1,6
B7	8,1
C4	9,7
C7	9,0

Table 5-7 M(13) Error evaluation

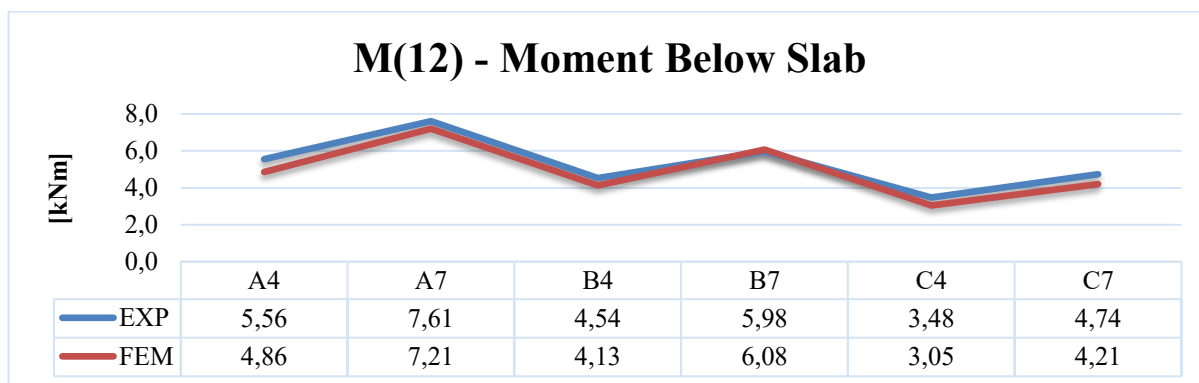


Figure 5.7 Bending moment comparison below the slab

Load case	Error [%]
A4	12,6
A7	5,3
B4	9,0
B7	1,7
C4	12,3
C7	11,2

Table 5-8 M(12) Error evaluation

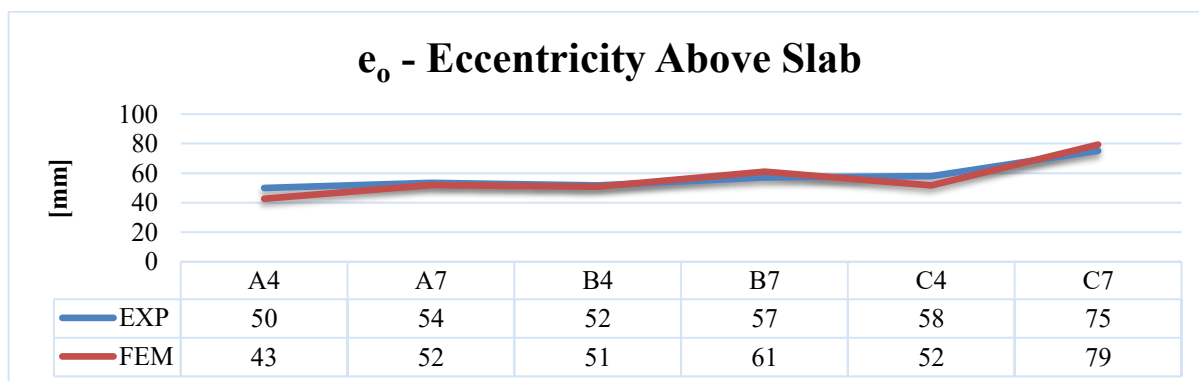


Figure 5.8 Eccentricity comparison above the slab

Load case	Error [%]
A4	14,6
A7	3,0
B4	1,8
B7	7,0
C4	10,9
C7	5,5

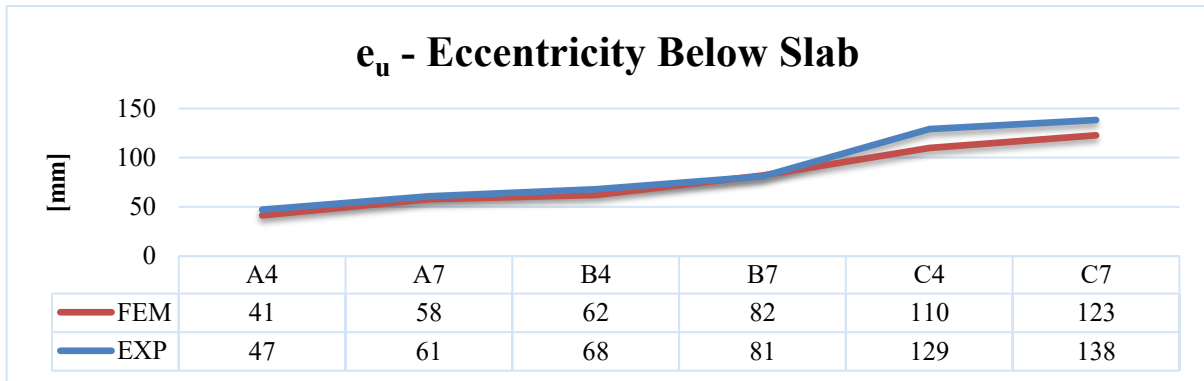
Table 5-9  $e_o$  Error evaluation

Figure 5.9 Eccentricity comparison below the slab

Load case	Error [%]
A4	12,2
A7	5,1
B4	8,6
B7	1,3
C4	14,7
C7	11,2

Table 5-10  $e_u$  Error evaluation

The bending moment and the eccentricities values are influenced by the vertical force acting above the wall. It is clear that the lower the vertical force is, the lower the bending moment is and the higher the eccentricity is.

The following pictures show the vertical stress  $\sigma_{zz}$  acting to the node. The yellow area indicates the tensile stress, while the green area indicates the compressive stress.

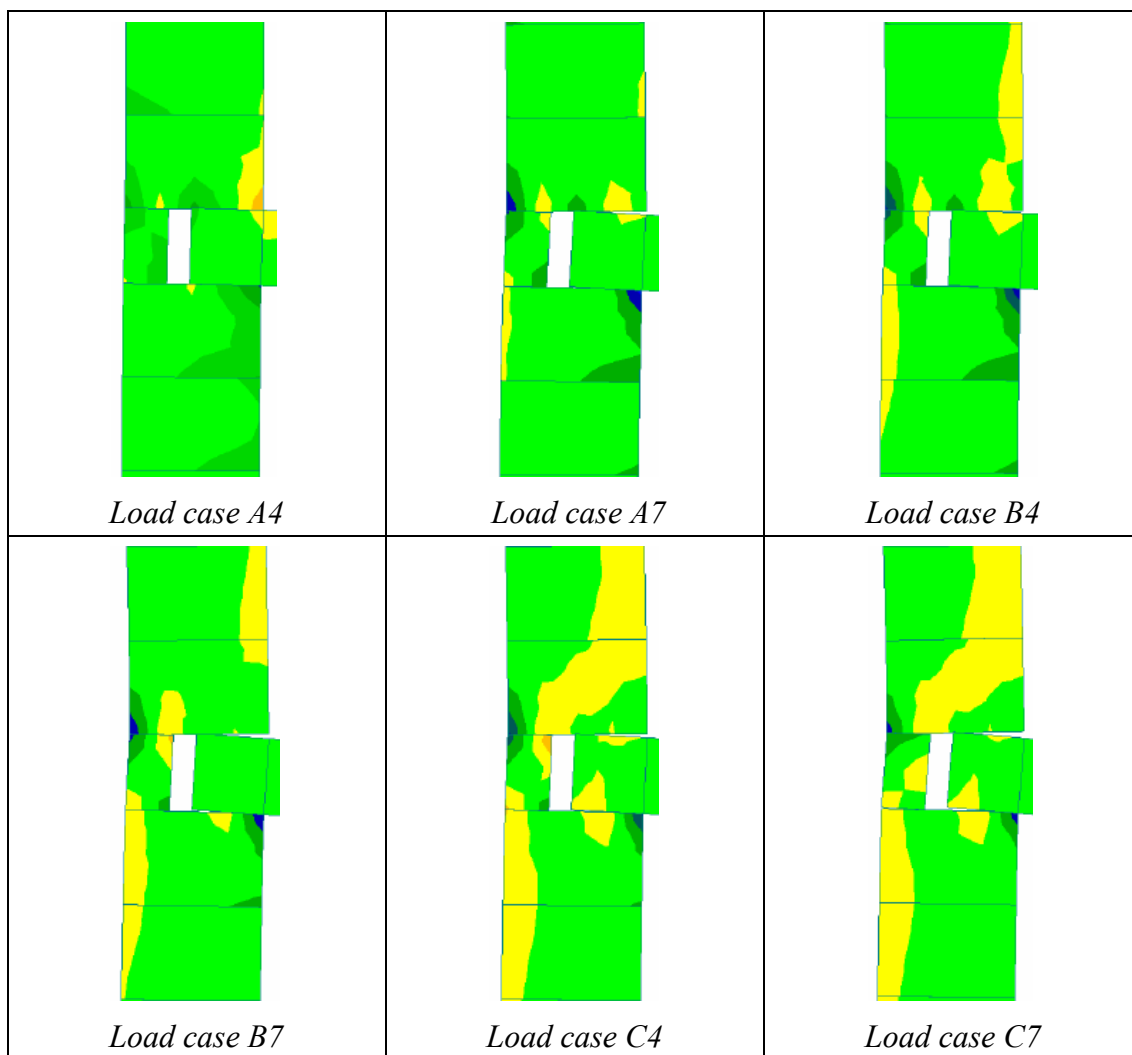


**Table 5-11 Vertical stress qualitative evaluation**

For the first 3 cases, the wall/slab connection does not reach the tensile strength on the upper side of the slab, as a consequence it is capable to resist to the tensile stress transferred by the slab, which rotates due to the action of the vertical loads  $P$ . While, for the next 2 cases (B7 and C4), the stone on the exterior side of the wall is the macro-element which contributes to transfer the vertical tensile stress from the upper wall to the lower one. In the last case (C7), only the lower connections are capable to transfer the tensile stress, while on the upper side there is no connections between the macro-elements, i.e. the tensile stress exceeded the tensile strength of the mortar interface.

## 6 Load Bearing Capacity evaluation

The load bearing capacity is evaluated with the theoretical model developed by Awni/A.W. Hendry and then the results are compared to the DIN formulation. The normative considers a frame system where the loss of rigidity is associated to a reduction factor which depends by the rigidity of the beams, but does not takes in account the non-linear behavior of the structure. Furthermore, the simplified method suggested by DIN for the bending moment calculation, does not consider the influence of the vertical force applied on the top of the wall, or the relative position of the slab compared to the edge of the wall, which are actually important for the calculation of the eccentricity.

Following, the bending moments, the eccentricities and finally the load bearing capacity are estimated with a FEM numerical model by using a non-linear analysis, in order to compare the results to the analytics solutions.

For this purpose the geometry considered is a wall/slab joint, where the slab is completely inserted into the joint.



**Figure 6.1 Model used for the load bearing capacity evaluation**

The geometrical parameters are shown below:

- Wall thickness  $t = 365 \text{ mm}$
- Wall height  $h_1 = h_2 = 1.25 \text{ m}$
- Wall width  $b = 1 \text{ m}$
- Slab length  $l = 4.90 \text{ m}$
- Slab thickness  $s = 200 \text{ mm}$

The results are divided by considering the upper side and the lower side of the slab separately. Following, a comparison between the bending moments and the eccentricities was made in order to understand the differences between the numerical analysis and the simplified method proposed by DIN. The characteristics values were considered.

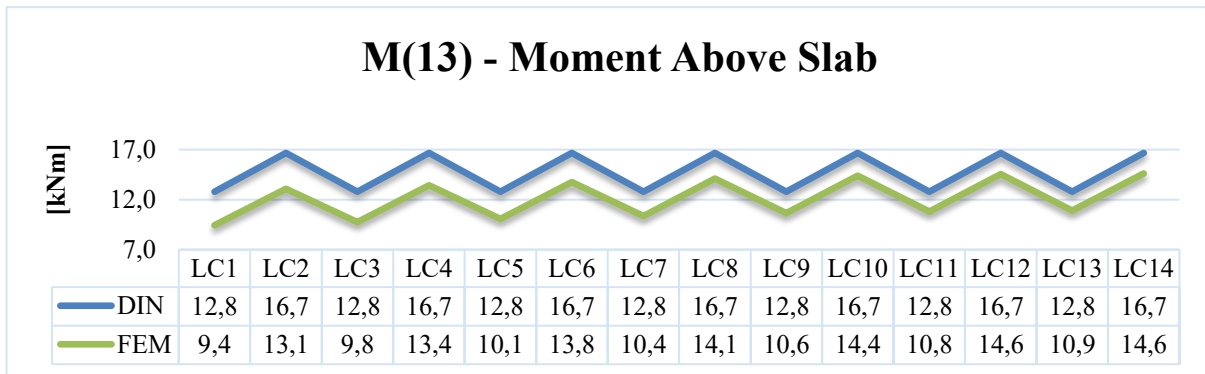


Figure 6.2 Bending moment comparison above the slab

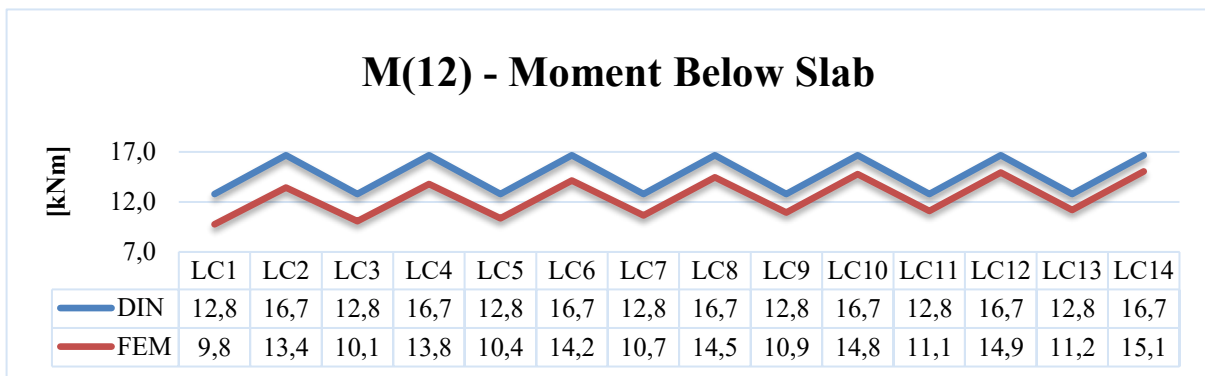


Figure 6.3 Bending moment comparison below the slab

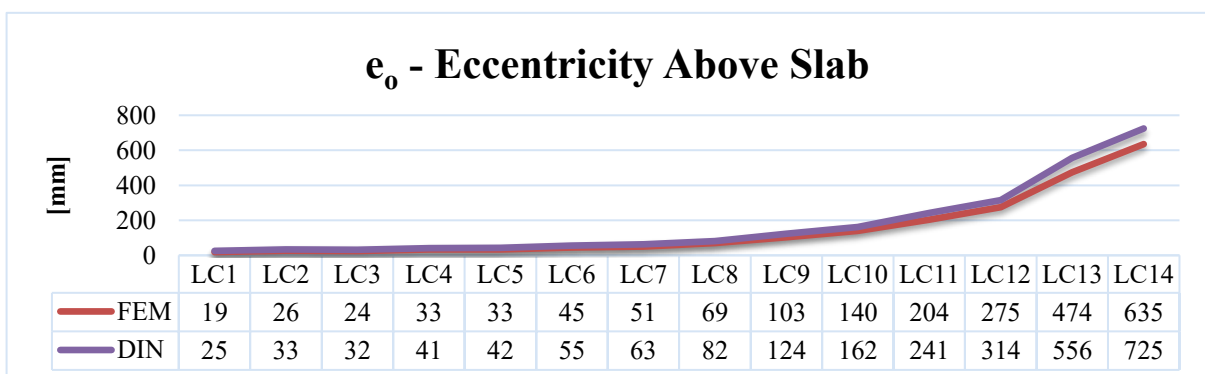


Figure 6.4 Eccentricity comparison above the slab

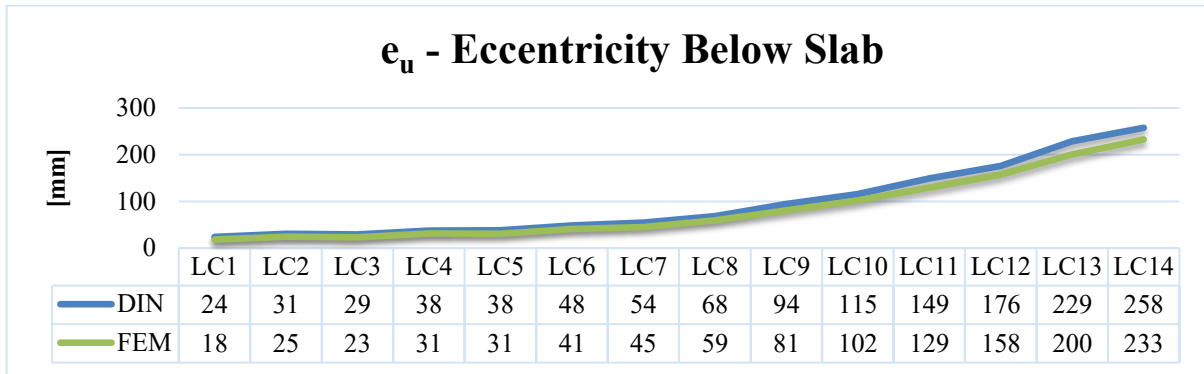


Figure 6.5 Eccentricity comparison below the slab

### Error [%]

Load case	M(13)	M(12)	$e_o$	$e_u$
LC1	35,5	31,0	35,5	31,0
LC2	27,5	24,1	27,5	24,1
LC3	31,1	27,1	31,1	27,1
LC4	24,1	20,9	24,1	20,9
LC5	27,1	23,4	27,1	23,4
LC6	21,1	17,8	21,1	17,8
LC7	23,4	20,0	23,4	20,0
LC8	18,3	15,1	18,3	15,1
LC9	20,1	17,0	20,1	17,0
LC10	15,8	12,8	15,8	12,8
LC11	18,4	15,4	18,4	15,4
LC12	14,5	11,7	14,5	11,7
LC13	17,3	14,3	17,3	14,3
LC14	14,0	10,7	14,0	10,7

Table 6-1 Error evaluation

Either the FEM results and the DIN results, show a similar trend. The difference between the two cases is that the DIN formulations overestimate the bending moment acting to the node.

It can be observed that in this geometrical case, the vertical force applied on the top of the wall is not the principal parameter that influences the transferred moment from the wall/slab connection. As a matter of fact, there are small differences of the bending moment results for the different load cases. On the contrary, the lower the vertical force applied on the top of the wall is, the higher the eccentricity resulting is.

## 6 Load Bearing Capacity evaluation

Following the load bearing capacity is estimated. It is supposed that, for the geometrical situation taken into account, the compressive failure anticipates the buckling failure (see chapter 2).

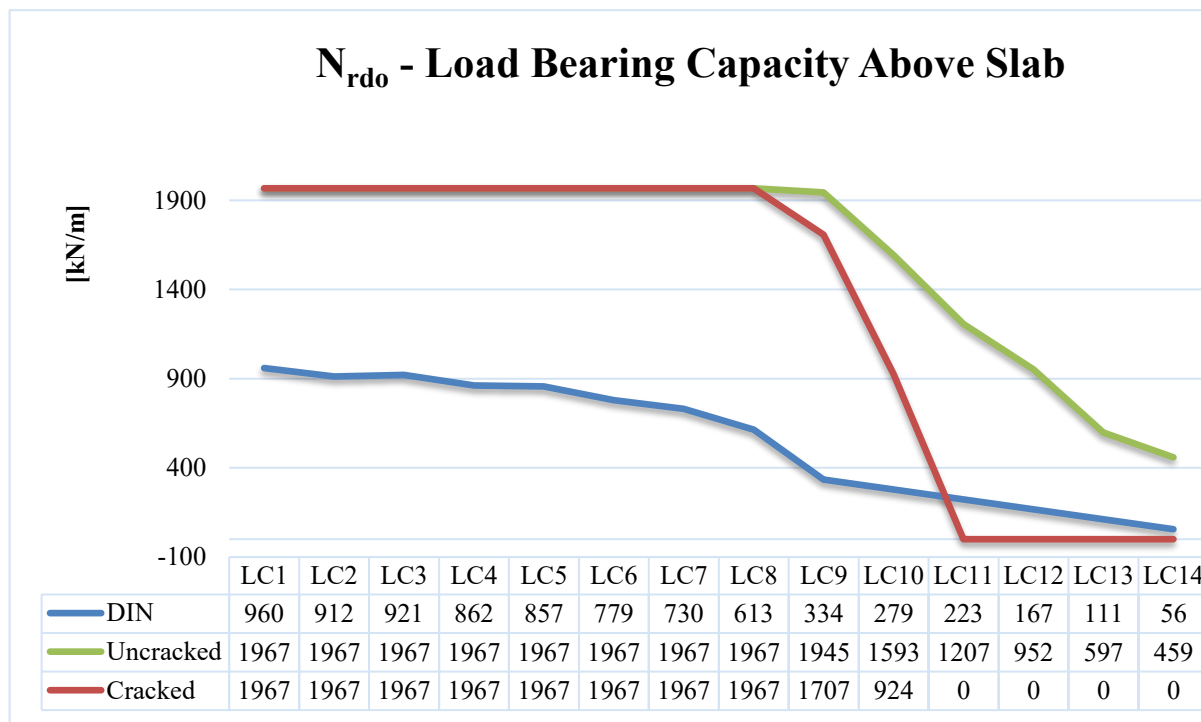


Figure 6.6 Load bearing capacity above the slab comparison

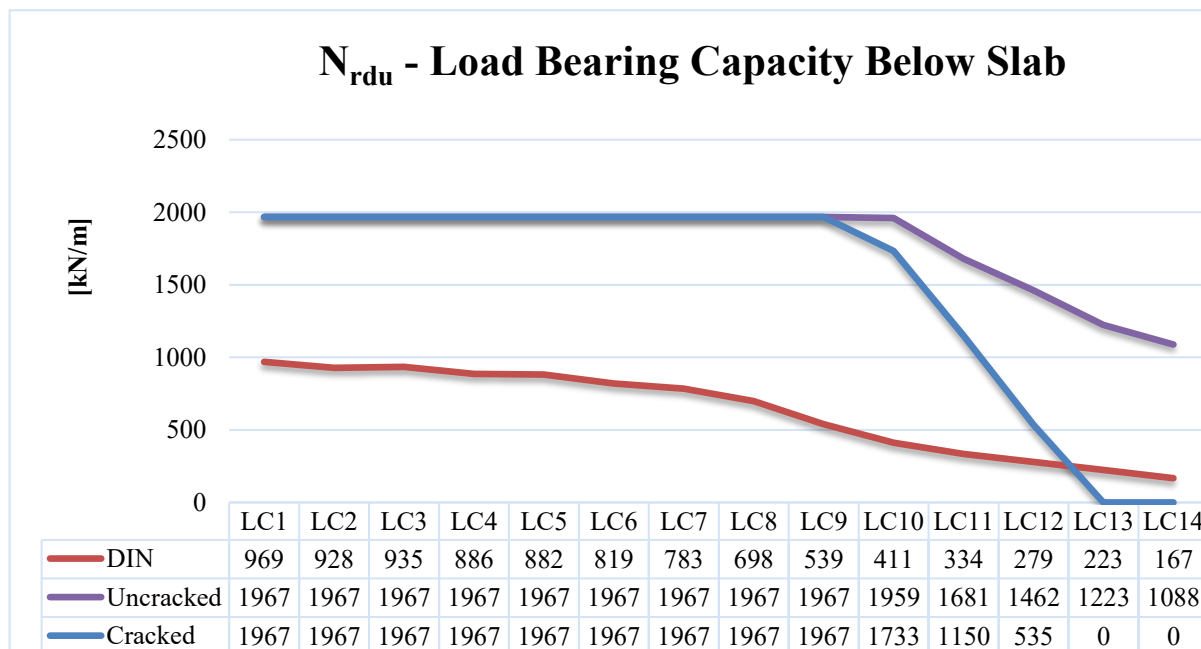
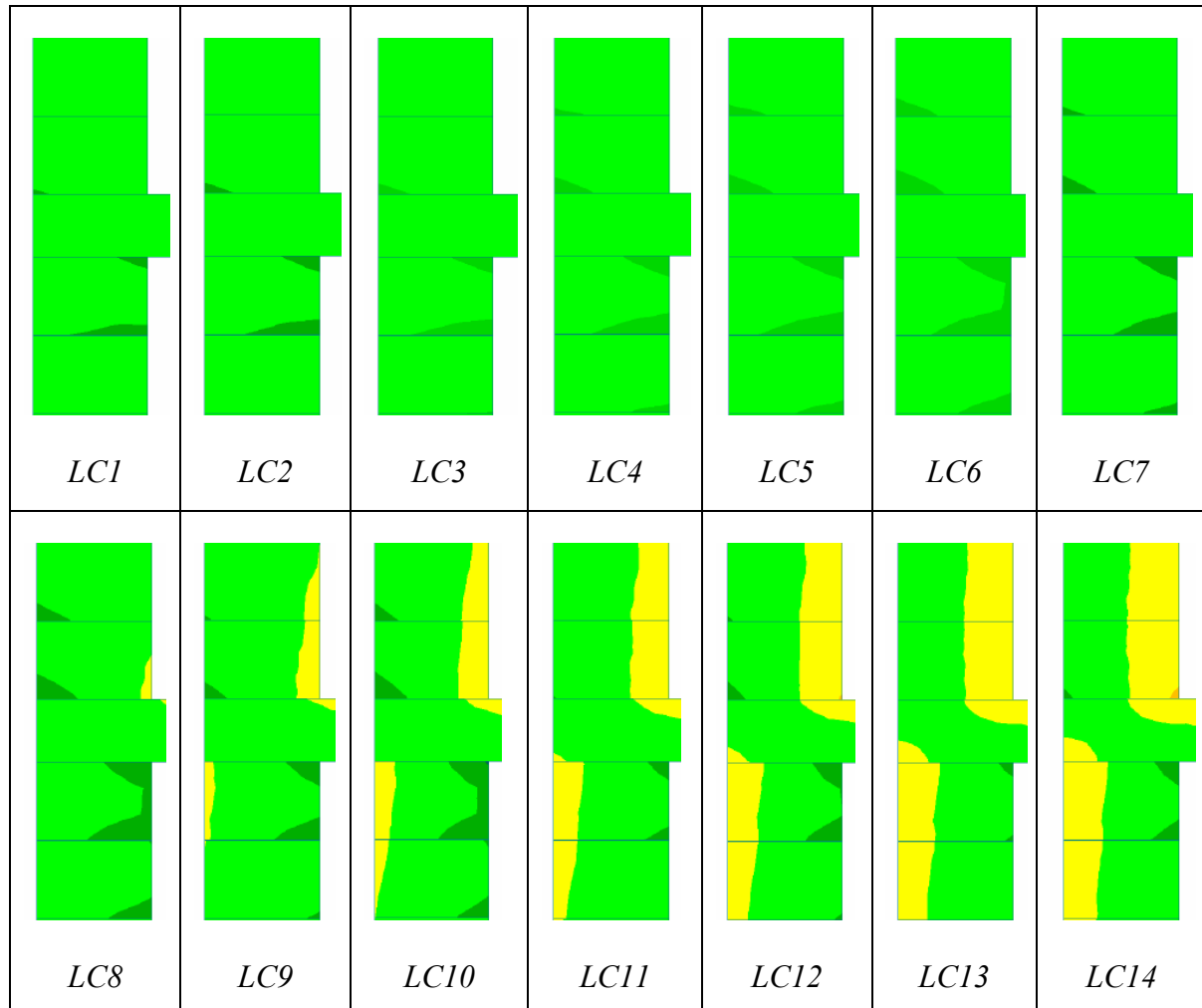


Figure 6.7 Load bearing capacity below the slab comparison

The calculation of the load bearing capacity is carried out using the FEM eccentricity results, regarding the *uncracked* and *cracked* state, and using the simplified method for the DIN results.

The DIN formulation consider the masonry with no tensile strength, which is actually a wrong approximation of the real behaviour of the structure. In order to understand the real behaviour of the structure, it is possible to analyze the vertical stress  $\sigma_{zz}$  resulting from FEM calculations acting to the node.



**Table 6-2 Vertical stress qualitative evaluation**

The green area indicates the compressive stress. Instead, the yellow area indicates the tensile stress acting to the node. The stress values of the iso-areas are shown in the Annex D.

The structure, for this geometrical case, does not reach the tensile strength on the wall/slab connection, even for low value of the vertical load on the top of the wall, and results to be in *uncracked state*.

Also the *cracked state* with no tensile strength is considered. In this case the load bearing capacity decrease to zero for lower values of the vertical force on the top of the wall.

The DIN formulations considers, for high values of eccentricity, the minimal compressive area lower to 0.33 times the effective area capable to resist to compressive stress. This consideration is in a safety side, but it is not realistic because the structure is actually capable to resist to low values of tensile stress, which increases the real value of load bearing capacity.

## 7 Influence of Slab position

In order to calculate the load bearing capacity, the DIN does not take in consideration the relative position of the slab compared to the edge of the wall, or the different behavior of the upper side of the slab respect the lower side.

For this reason a series of simulations were achieved, setting different load cases with different values of the vertical load on the upper side of the wall. For each simulation the relative position of the structural elements were changed, so as to understand the influence of the two parameters on the structural behavior.

The determination of the bending moment using the DIN formulation takes in consideration only the geometrical characteristics of the masonry, but does not consider the influence of the slab position or the vertical load acting to the wall.

When the value of the slab distance from the edge of the wall increases, there is a different behavior compared to the simplified model, due to the non-linear relations between the slab and the masonry wall.

As a matter of fact, the loss of stiffness in the node region leads to a redistribution of the forces which is not considered from the DIN formulations. Until the interface is connected within the two elements, the bending moments in both sides are similar, and the FEM values have a similar trend compared to those calculated with the simplified method. When the upper interface fails (*cracked state*), i.e. the tensile stress overcome the tensile resistance of the mortar in the wall/slab connection, the bending moment drastically decreases and, as a consequence, also the actual eccentricity decreases.

All these phenomena are analyzed in the following chapters by the confrontation of the theoretical calculations and the FEM results.

The parameters taken in consideration are the distance of the slab from the edge of the wall  $a$  and the vertical force applied on the top of the wall  $N$ .

- $a$  = variable
- $t$  = 365 mm
- $d$  = 200 mm

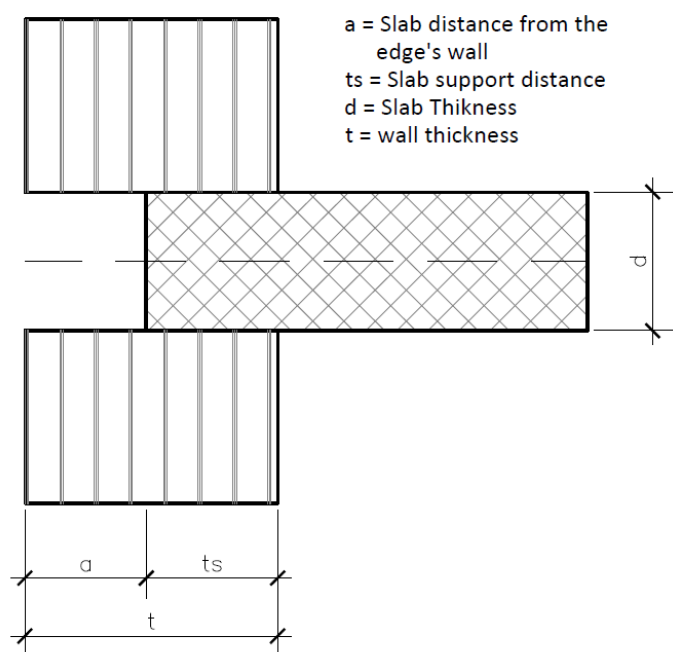


Figure 7.1 Wall/Slab connection detail

### 7.1 a= 50 mm

The following case takes in consideration the wall slab connection in which the slab is situated 50 mm far from the edge of the wall.



Figure 7.2 Structure geometry a= 50 mm

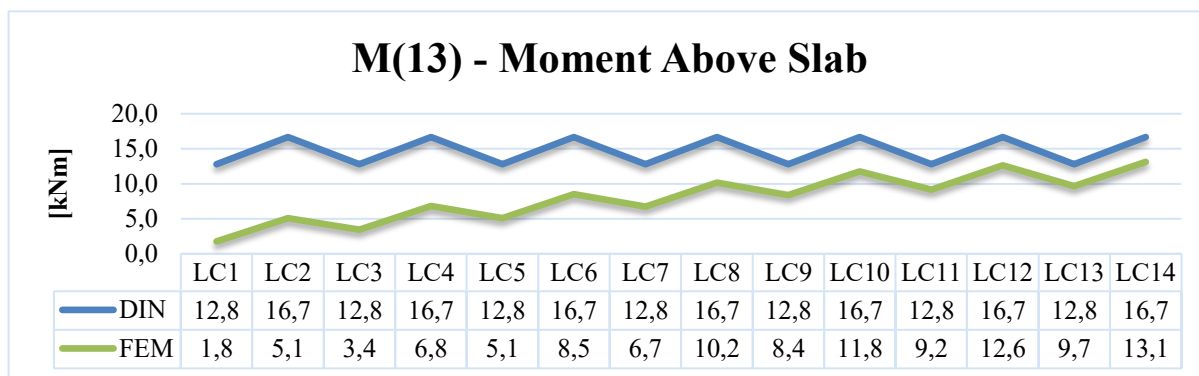


Figure 7.3 Bending moment comparison above the slab

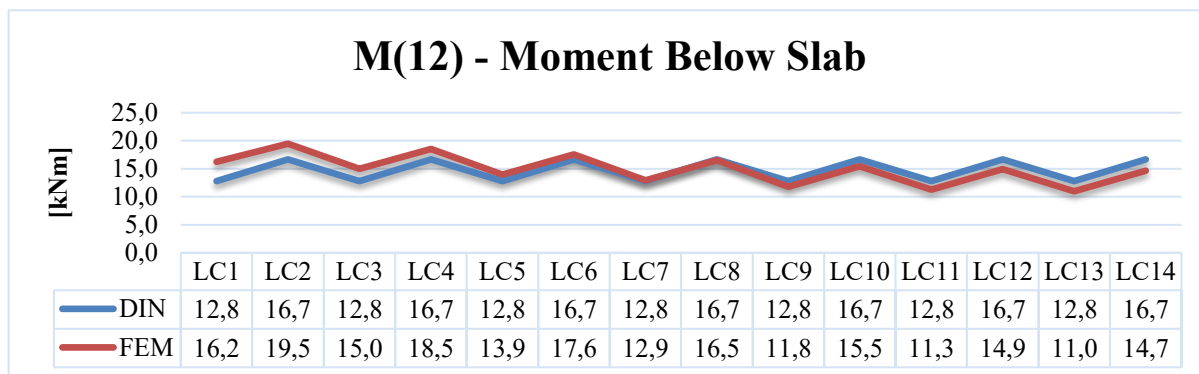


Figure 7.4 Bending moment comparison below the slab

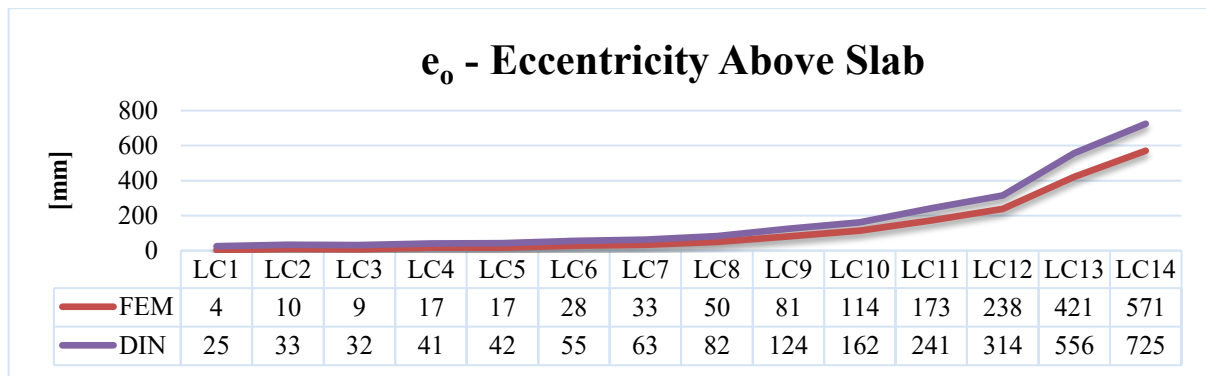


Figure 7.5 Eccentricity comparison above the slab

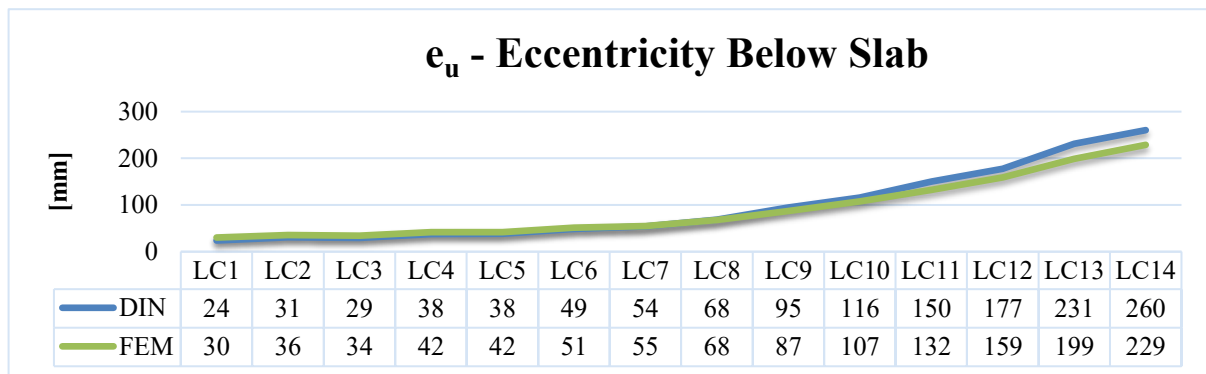


Figure 7.6 Eccentricity comparison below the slab

**Error [%]**

Load case	M(13)	M(12)	$e_o$	$e_u$
L1	623,1	21,2	623,1	21,2
L2	226,7	14,4	226,7	14,4
L3	271,5	14,5	271,5	14,5
L4	144,5	10,0	144,5	10,0
L5	150,6	8,2	150,6	8,2
L6	95,7	5,1	95,7	5,1
L7	89,7	0,9	89,7	0,9
L8	63,9	0,8	63,9	0,8
L9	53,0	8,3	53,0	8,3
L10	41,5	7,9	41,5	7,9
L11	39,4	13,4	39,4	13,4
L12	32,1	11,7	32,1	11,7
L13	32,2	16,5	32,2	16,5
L14	27,0	13,8	27,0	13,8

Table 7-1 Error evaluation

It is possible to recognize two different behaviors considering the upper or the lower side of the wall/slab connection. Firstly, the bending moment acting above the slab, when the latter is situated at about 0.15 time the wall thickness, shows a sensible increment of the values when

the vertical force applied on the top of the wall decreases. Furthermore, the lower the vertical force applied on the top of the wall is, the higher the DIN formulation's precision is.

On the contrary, below the slab, the bending moments show a similar trend compared to the DIN formulation, and the vertical force does not influence so much the results, like in the previous situation. The FEM values shows a slight decrement when N decreases and the precision of the DIN formulation is higher compared with the upper side.

## 7.2 a= 100 mm

In this case the slab is situated 100 mm far from the edge of the wall.



Figure 7.7 Structure geometry a=100 mm

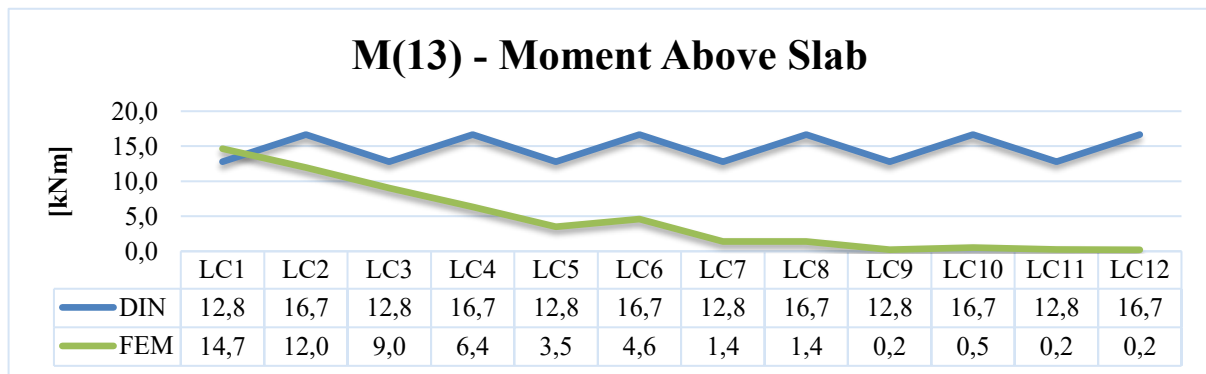


Figure 7.8 Bending moment comparison above the slab

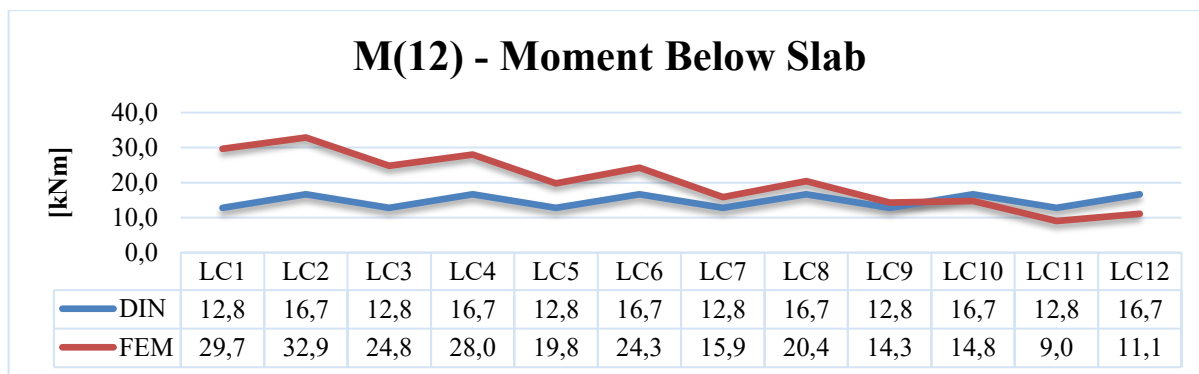


Figure 7.9 Bending moment comparison below the slab

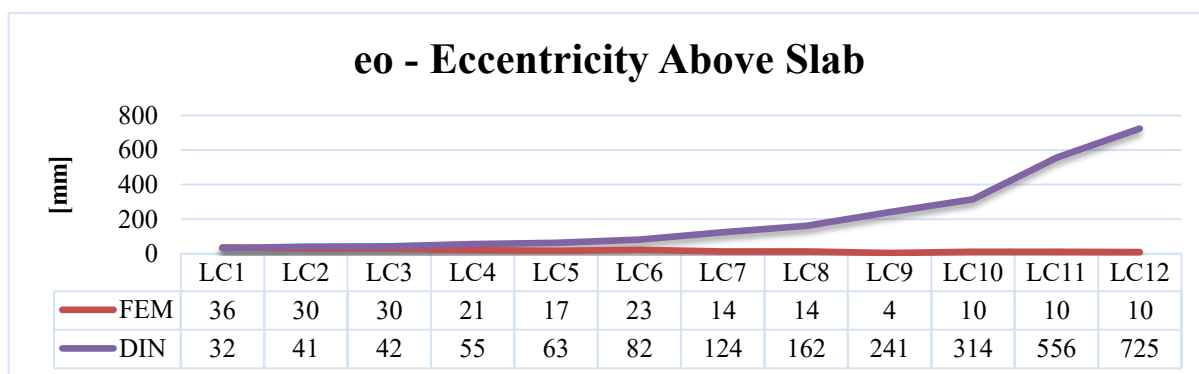


Figure 7.10 Eccentricity comparison above the slab

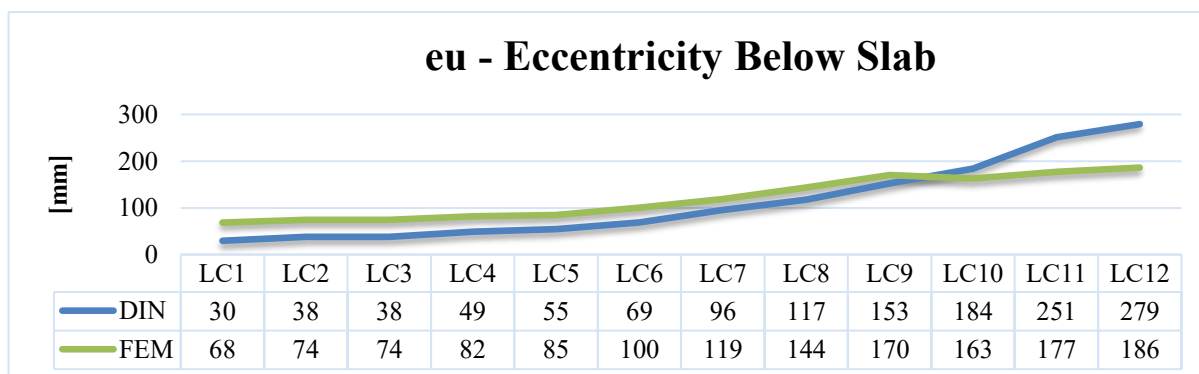


Figure 7.11 Eccentricity comparison below the slab

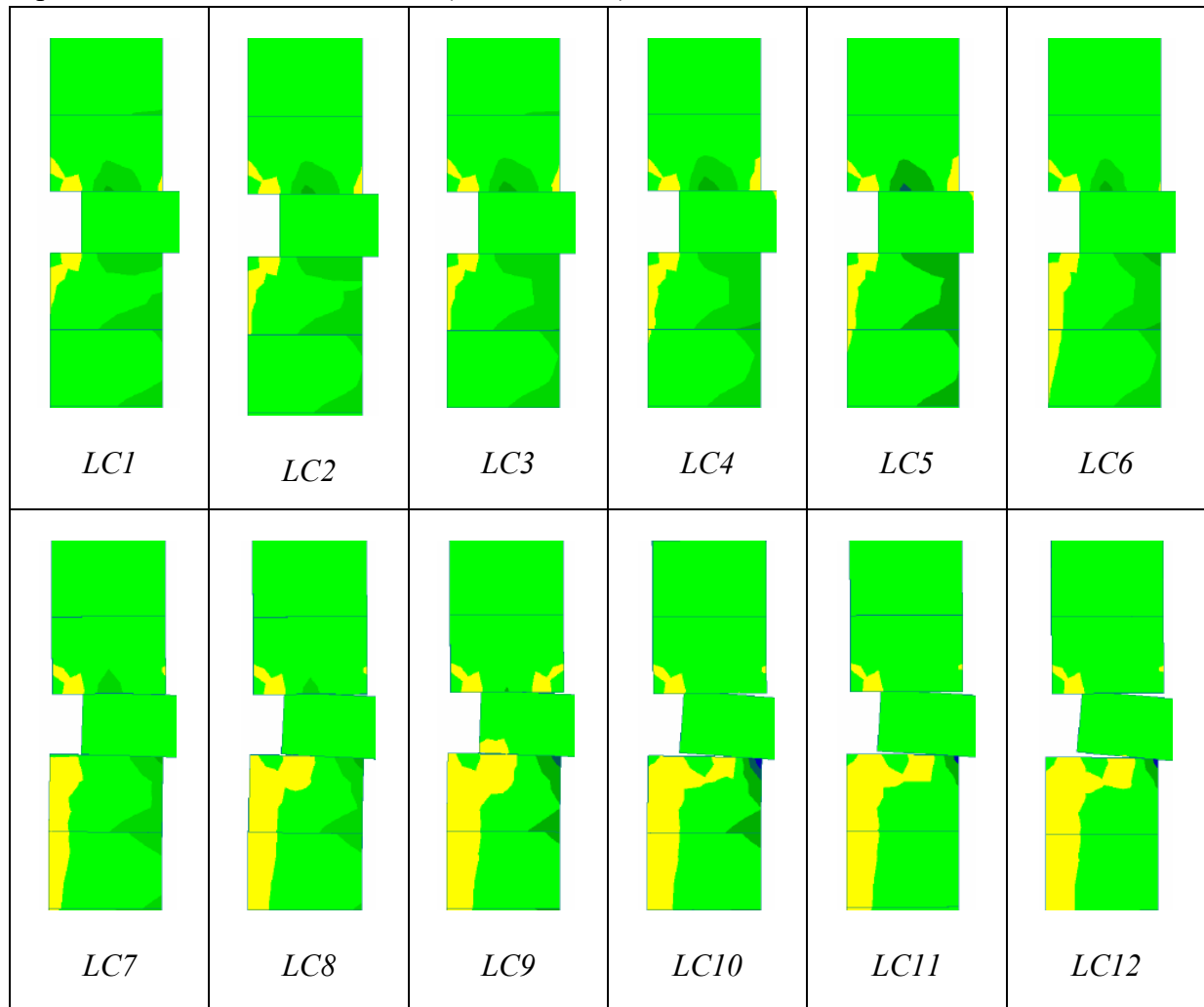
Load case	Error [%]			
	M(13)	M(12)	$e_o$	$e_u$
LC1	12,7	56,9	12,7	56,9
LC2	39,3	49,3	39,3	49,3
LC3	41,5	48,4	41,5	48,4
LC4	162,4	40,5	162,4	40,5
LC5	265,7	35,4	265,7	35,4
LC6	262,7	31,4	262,7	31,4
LC7	811,1	19,5	811,1	19,5
LC8	1094,6	18,3	1094,6	18,3
LC9	5527,9	10,3	5527,9	10,3
LC10	2945,9	13,0	2945,9	13,0
LC11	5245,6	41,6	5245,6	41,6
LC12	7048,5	50,0	7048,5	50,0

Table 7-2 Error evaluation

When the slab is far about 0.3 times the wall thickness from the edge of the wall, the structural behavior is different compared to the previous case analyzed before. In this case, the actual moment transferred by the upper side of the slab starts from a similar value compared to the analytic calculation but next, a drastic decrement is registered. This behavior is due to the loss of contact between the slab and the wall (*cracked state*), because the interface's tensile strength has been exceeded by the tensile stress acting to the node. As a consequence, the eccentricity on the upper side tend to assume really small values compared to those calculated with the formulations provided by the DIN.

Regarding the lower side of the slab, the decrement of the upper vertical force  $N$  cause a decrement of the bending moment into the joint connection.

By looking the following pictures, which show the vertical stress acting to the node, it is possible to qualitatively understand in which way the loss of contact between the slab and the wall occurs. In particular, the first 5 load cases show that the interface is able to resist to the tensile stress (yellow area) transferred by the slab to the wall. Starting from the load case LC6, the loss of contact within the two surfaces leads to a redistribution of the forces. For this reason on the upper side of the wall the bending moment decreases drastically and the node is no longer capable to resist to tensile stresses (*cracked state*).



**Table 7-3 Vertical stress qualitative evaluation**

In these cases the errors between the analytic solution and the FEM results are large.

### 7.3 a= 150 mm

This case is similar to the previous cases. The results are shown in the Annex B.



Figure 7.12 Structure geometry a= 150 mm

### 7.4 a= 200 mm

In this case the slab is situated 200 mm far from the edge of the wall.



Figure 7.13 Structure geometry a=200 mm

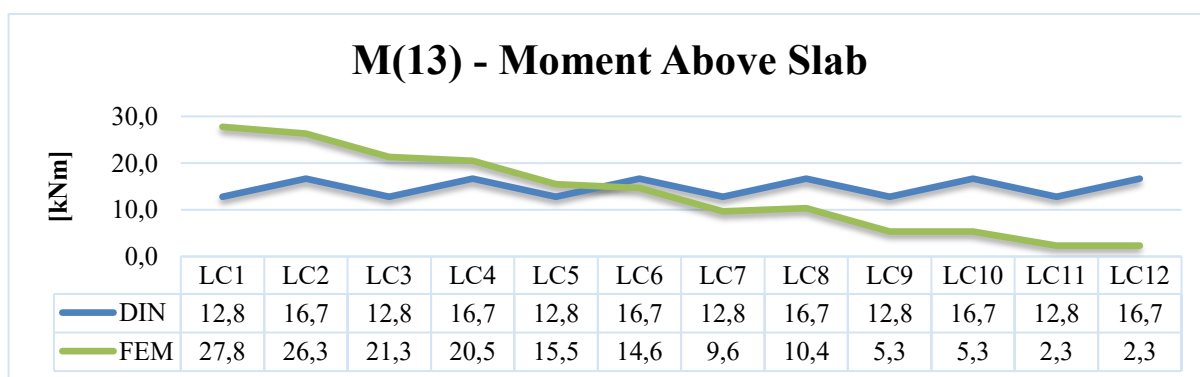


Figure 7.14 Bending moment comparison above the slab

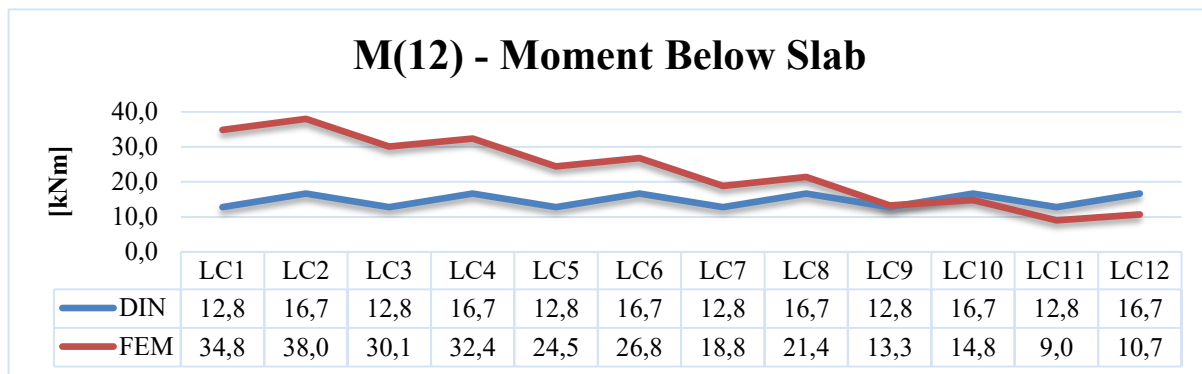


Figure 7.15 Bending moment comparison below the slab

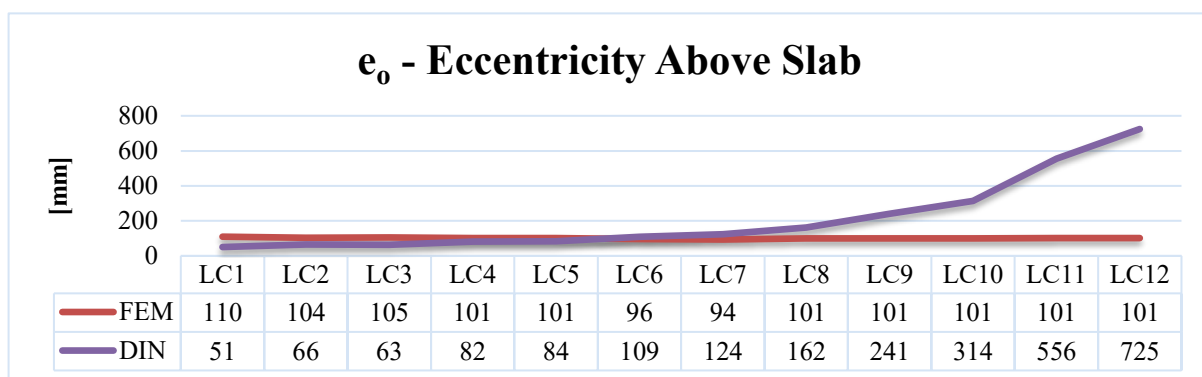


Figure 7.16 Eccentricity comparison above the slab

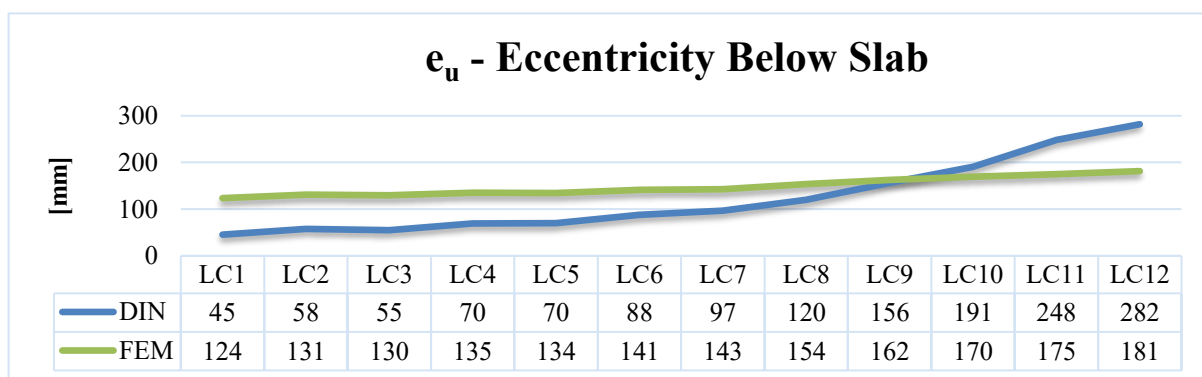


Figure 7.17 Eccentricity comparison below the slab

**Error [%]**

Load case	M(13)	M(12)	$e_o$	$e_u$
LC1	53,9	63,3	53,9	63,3
LC2	36,7	56,1	36,7	56,1
LC3	40,0	57,4	40,0	57,4
LC4	18,7	48,6	18,7	48,6
LC5	17,3	47,7	17,3	47,7
LC6	13,9	37,9	13,9	37,9
LC7	32,8	32,1	32,8	32,1
LC8	60,7	22,1	60,7	22,1
LC9	139,7	3,7	139,7	3,7
LC10	212,1	12,5	212,1	12,5
LC11	451,3	41,8	451,3	41,8
LC12	617,9	55,3	617,9	55,3

**Table 7-4 Error evaluation**

When the slab is far about 0.5 times the thickness of the wall from the edge of the latter, both of the upper side and the lower side of the slab show a similar trend. The bending moment decrease as the vertical force  $N$  decreases. While the eccentricities remains quite constant for the different load cases, and does not prove the trend shown in the previous geometric situations. The eccentricities calculated above the slab remain quite constant for all the load cases. On the contrary, below the slab the eccentricities tend to increase slowly when the vertical load  $N$  decreases.

Following the vertical stress  $\sigma_{zz}$  acting to the node is qualitatively analyzed.

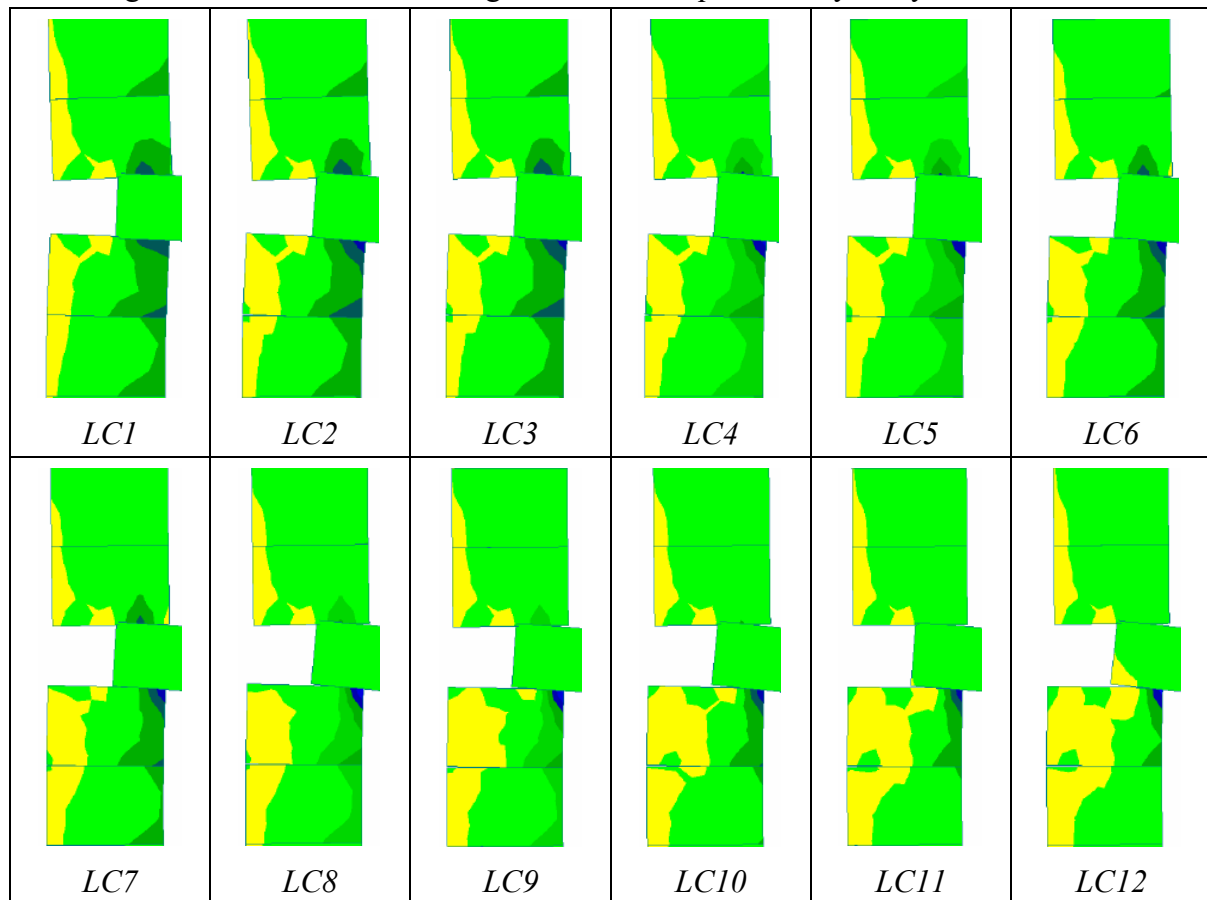


**Table 7-5 Vertical stress qualitative evaluation**

In this geometrical situation, when the slab is situated far over 0.5 times the wall thickness from the edge of the wall, there is not the development of tensile stress on the connection above the slab, which is stressed mainly by compressive load. The acting bending moment decreases when the vertical force applied on the top of the wall decreases. After the load case LC7 the interface starts to fail.

On the contrary, above the slab there is tensile stress development only in the last load cases, starting from LC9. It is possible to notice a concentration of compressive stress on the edge of the wall connected with the slab (blue area).

### 7.5 $a = 250 \text{ mm}$

This geometrical cases shows a similar behavior compared to the previous case. The results are shown in Annex B.



Figure 7.18 Structure geometry  $a=250 \text{ mm}$

## 8 Influence of Wall Thickness

The next simulations have the aim to understand the effect of the wall thickness to the structural behavior. The wall thickness is one of the parameters which influence the slenderness of the wall, which represent the ratio between the wall height  $h$  and the wall thickness  $t$ . The slenderness is important because the buckling failure is really influenced by this parameter. For slender wall, the buckling failure is more likely to occur compared to the compressive material failure, when the vertical force applied on the wall is eccentric. For this reason the slenderness ratio should be limited, in order to exercise a control on the flexural tension stress within the wall.

When slenderness increases, the tensile strength has a larger influence on the load bearing capacity, due to role on the flexural mechanism in the activation of the failure. For cases with large eccentricity, the tensile strength significantly increases the load capacity. In these cases, neglecting the tensile strength can cause a severe underestimation of the load bearing capacity of walls. Therefore, the contribution of the tensile strength of the unit–mortar interface on the load bearing capacity of masonry walls increases significantly with the slenderness ratio and the load eccentricity. Conversely, for small or null eccentricities the failure is mostly due to compression crushing, in these cases the tensile strength have not noticeable effect to the final load bearing capacity.

The FEM results were compared with the DIN formulation. The load cases are similar to the previous simulations. The vertical force on the top of the wall decreases while the vertical forces on the slab change between the same two values.

### 8.1 $t = 365$ mm

This is the same case analyzed in chapter 6.

Load case	Error [%]			
	M(13)	M(12)	$e_o$	$e_u$
LC1	35,5	31,0	35,5	31,0
LC2	27,5	24,1	27,5	24,1
LC3	31,1	27,1	31,1	27,1
LC4	24,1	20,9	24,1	20,9
LC5	27,1	23,4	27,1	23,4
LC6	21,1	17,8	21,1	17,8
LC7	23,4	20,0	23,4	20,0
LC8	18,3	15,1	18,3	15,1
LC9	20,1	17,0	20,1	17,0
LC10	15,8	12,8	15,8	12,8
LC11	18,4	15,4	18,4	15,4
LC12	14,5	11,7	14,5	11,7
LC13	17,3	14,3	17,3	14,3
LC14	14,0	10,7	14,0	10,7

Table 8-1 Error evaluation

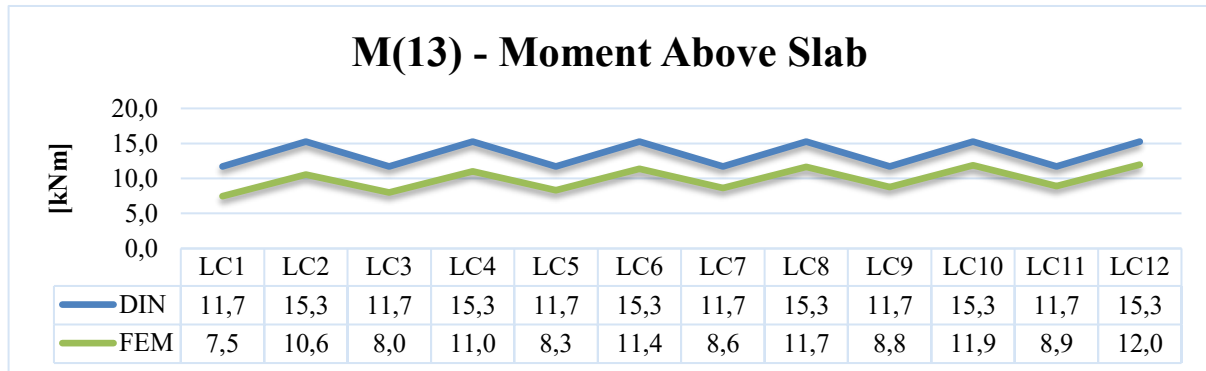
8.2  $t = 315 \text{ mm}$ 

Figure 8.1 Bending moment comparison above the slab

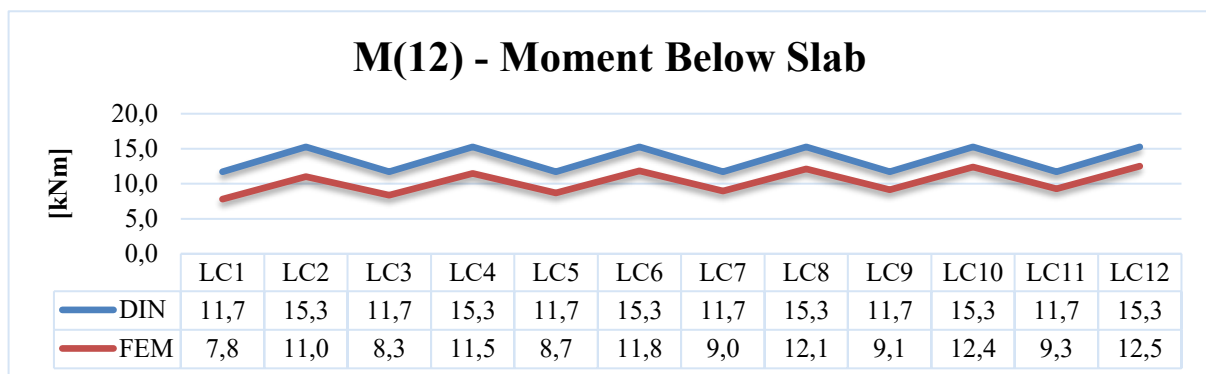


Figure 8.2 Bending moment comparison below the slab

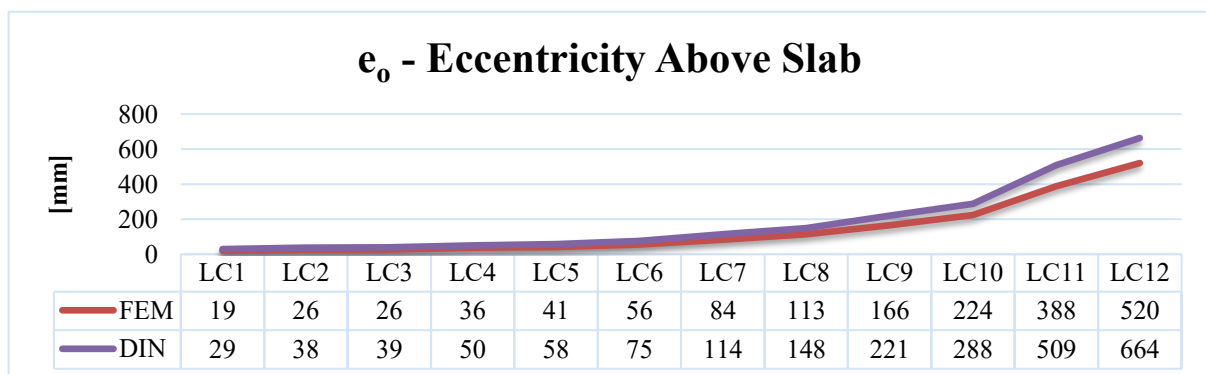


Figure 8.3 Eccentricity comparison above the slab

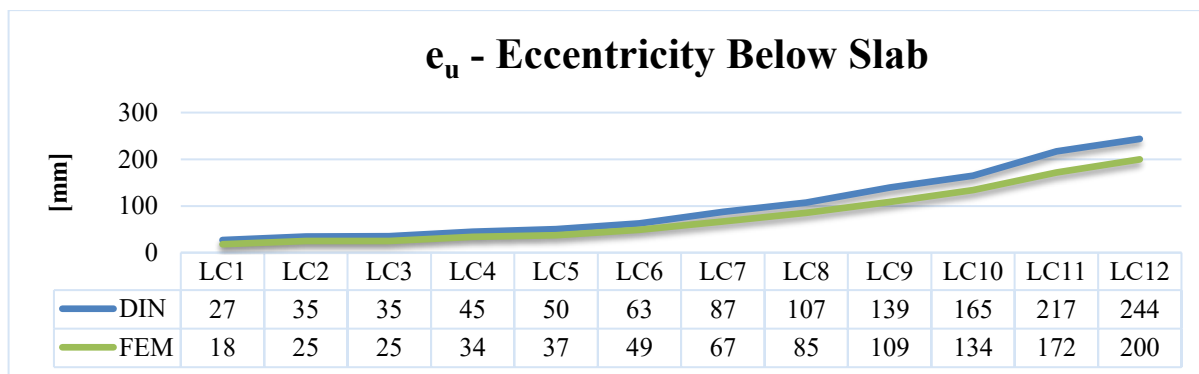


Figure 8.4 Eccentricity comparison below the slab

### Error [%]

Load case	M(13)	M(12)	e <sub>o</sub>	e <sub>u</sub>
L1	56,8	50,1	56,8	50,1
L2	44,3	38,4	44,3	38,4
L3	46,9	40,3	46,9	40,3
L4	38,5	32,8	38,5	32,8
L5	40,8	34,9	40,8	34,9
L6	34,4	29,0	34,4	29,0
L7	35,9	30,6	35,9	30,6
L8	30,9	25,9	30,9	25,9
L9	33,4	28,3	33,4	28,3
L10	28,3	23,3	28,3	23,3
L11	31,2	26,0	31,2	26,0
L12	27,5	22,0	27,5	22,0

Table 8-2 Error evaluation

### 8.3 t= 265 mm

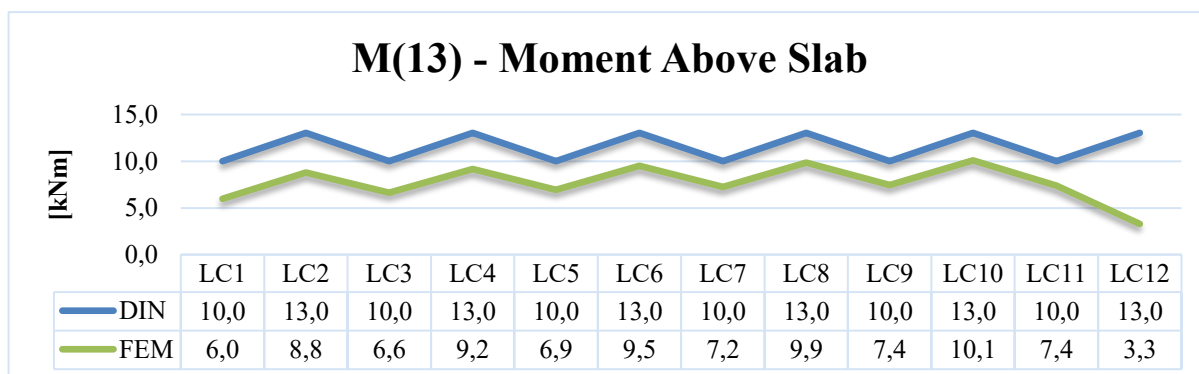


Figure 8.5 Bending moment comparison above the slab

The last load case shows a decrement of the bending moment, caused by the loss of contact between the elements on the wall/slab connection.

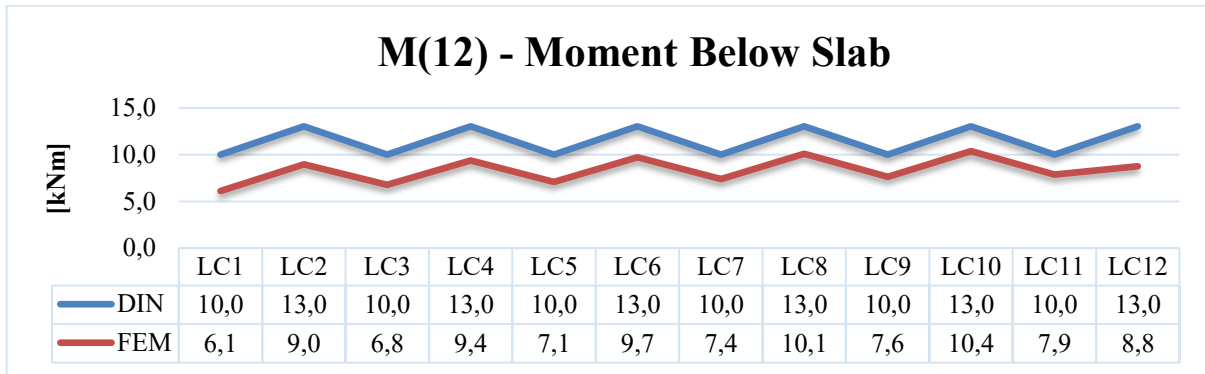


Figure 8.6 Bending moment comparison below the slab

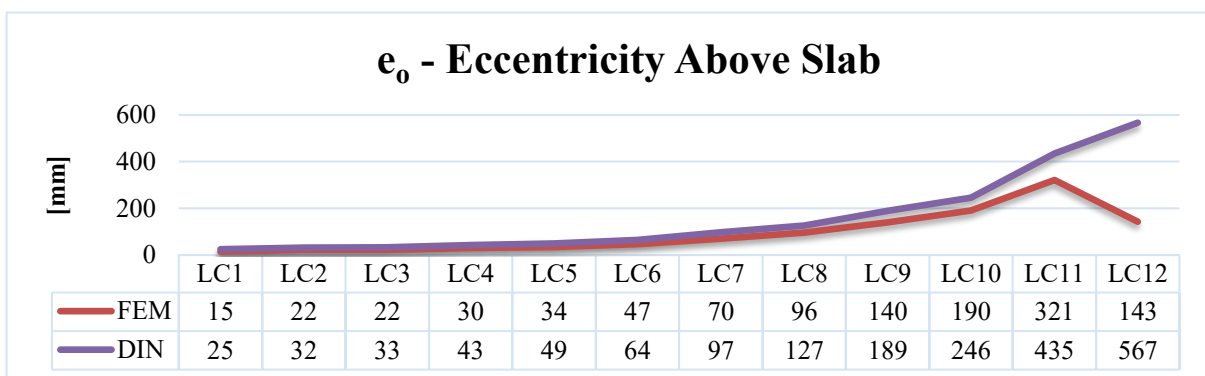


Figure 8.7 Eccentricity comparison above the slab

The last load case LC12 shows a significant decrement of the eccentricity, because of the loss of contact between the wall/slab interface.

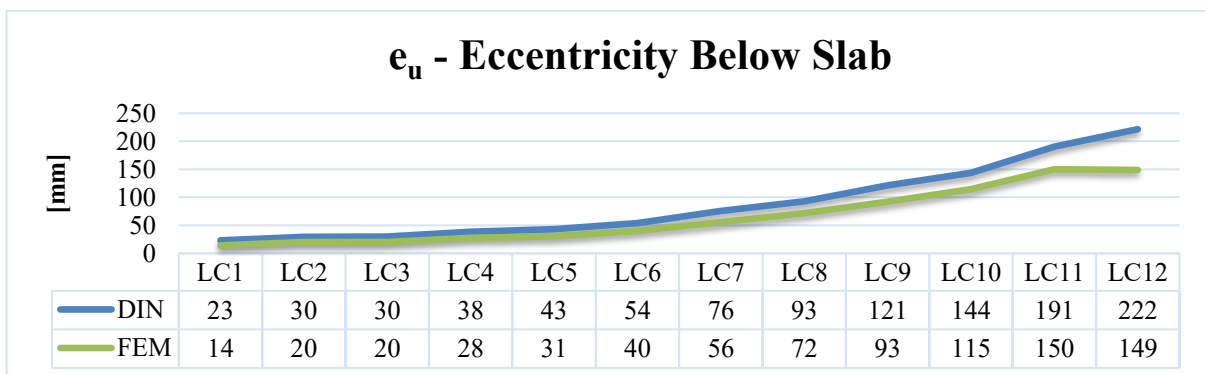


Figure 8.8 Eccentricity comparison below the slab

**Error [%]**

Load case	M(13)	M(12)	e <sub>o</sub>	e <sub>u</sub>
L1	67,2	63,7	67,2	63,7
L2	48,4	45,2	48,4	45,2
L3	51,2	47,5	51,2	47,5
L4	42,2	39,0	42,2	39,0
L5	44,4	41,0	44,4	41,0
L6	37,2	34,1	37,2	34,1
L7	38,3	35,2	38,3	35,2
L8	32,2	29,1	32,2	29,1
L9	34,4	31,2	34,4	31,2
L10	29,2	25,6	29,2	25,6
L11	35,4	27,1	35,4	27,1
L12	296,9	48,8	296,9	48,8

**Table 8-3 Error evaluation**

**8.4 t= 215 mm**

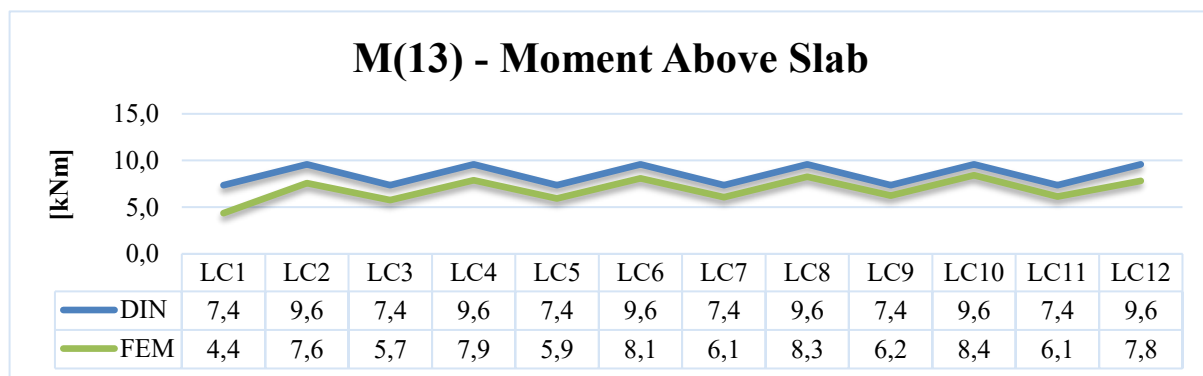


**Figure 8.9 Bending moment comparison above the slab**

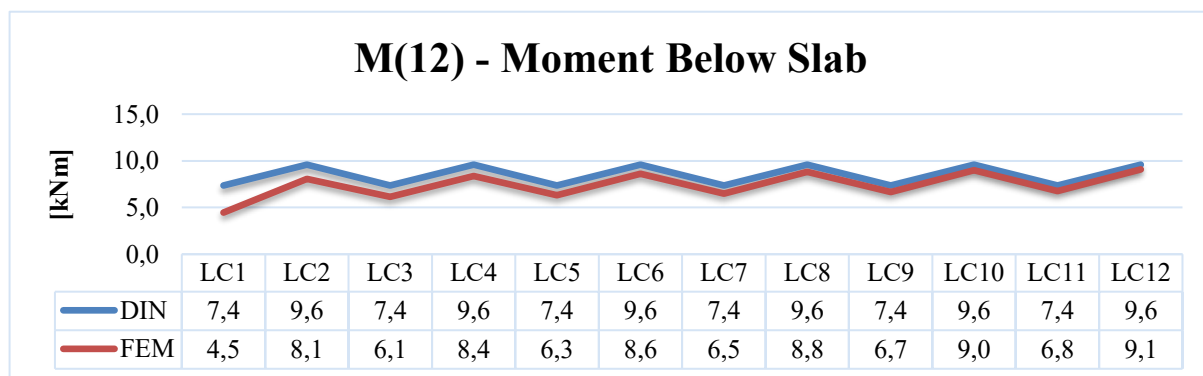


**Figure 8.10 Bending moment comparison below the slab**

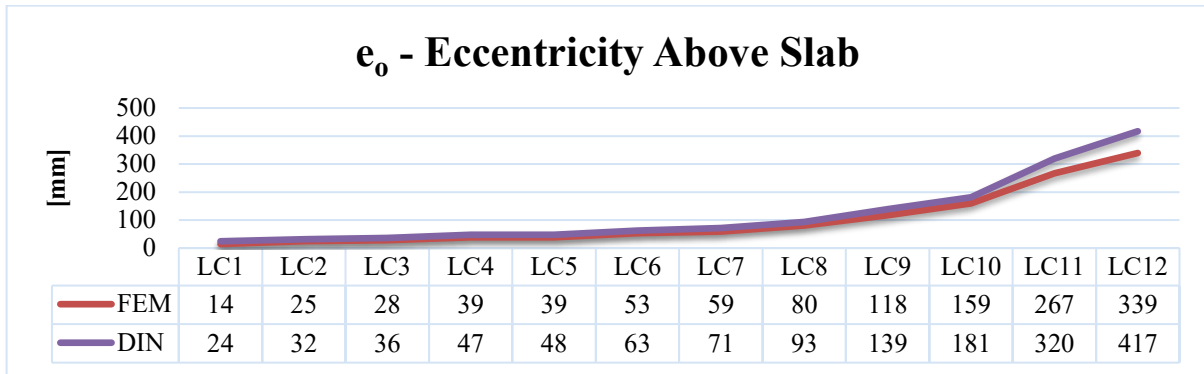


Figure 8.11 Eccentricity comparison above the slab

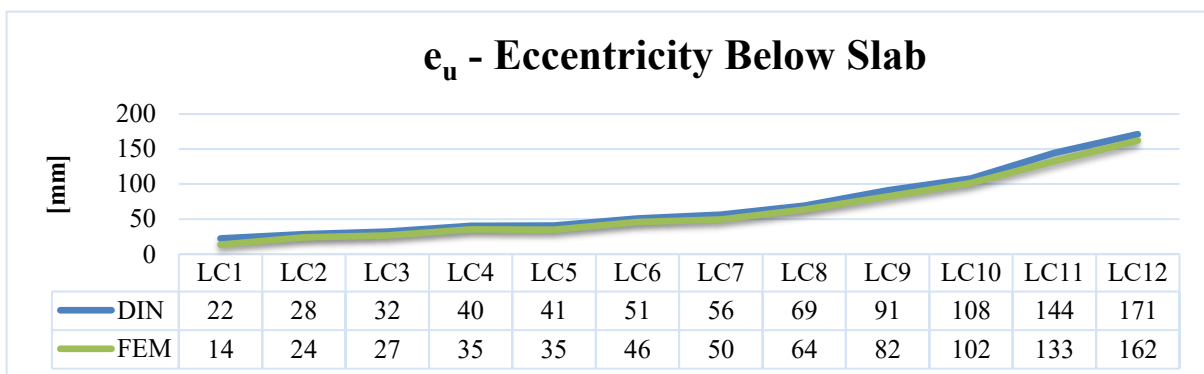


Figure 8.12 Eccentricity comparison below the slab

### Error [%]

Load case	M(13)	M(12)	$e_o$	$e_u$
L1	68,7	65,0	68,7	65,0
L2	26,6	19,0	26,6	19,0
L3	28,1	19,9	28,1	19,9
L4	21,7	14,4	21,7	14,4
L5	24,3	16,3	24,3	16,3
L6	18,6	11,3	18,6	11,3
L7	21,0	13,2	21,0	13,2
L8	15,9	8,7	15,9	8,7
L9	18,1	10,4	18,1	10,4
L10	13,8	6,5	13,8	6,5
L11	19,9	8,9	19,9	8,9
L12	22,9	5,6	22,9	5,6

Table 8-4 Error evaluation

8.5  $t = 175 \text{ mm}$

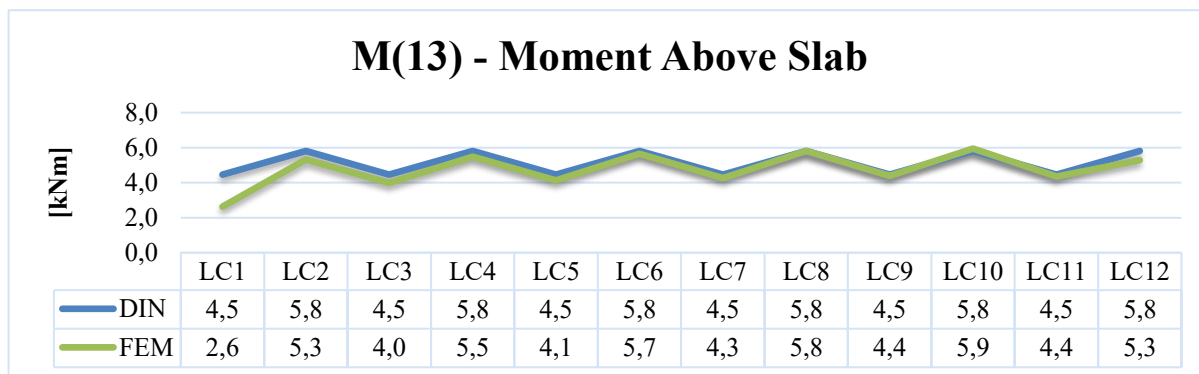


Figure 8.13 Bending moment comparison above the slab

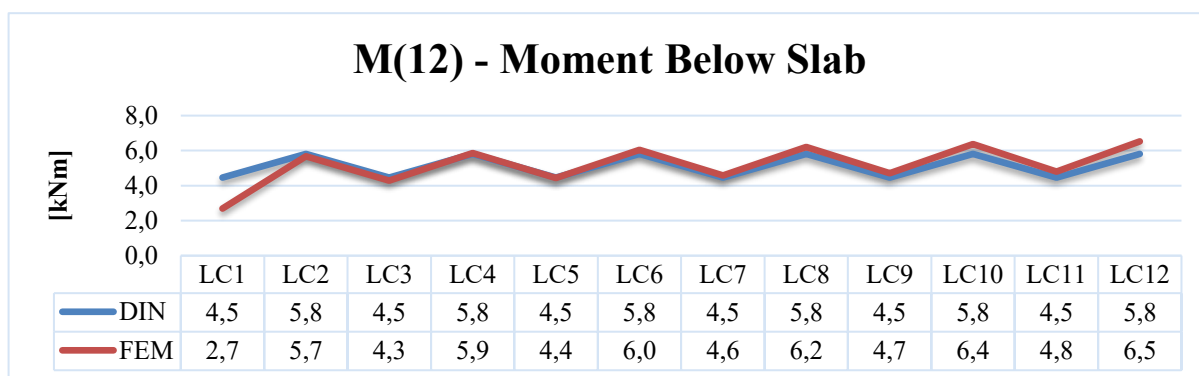


Figure 8.14 Bending moment comparison below the slab

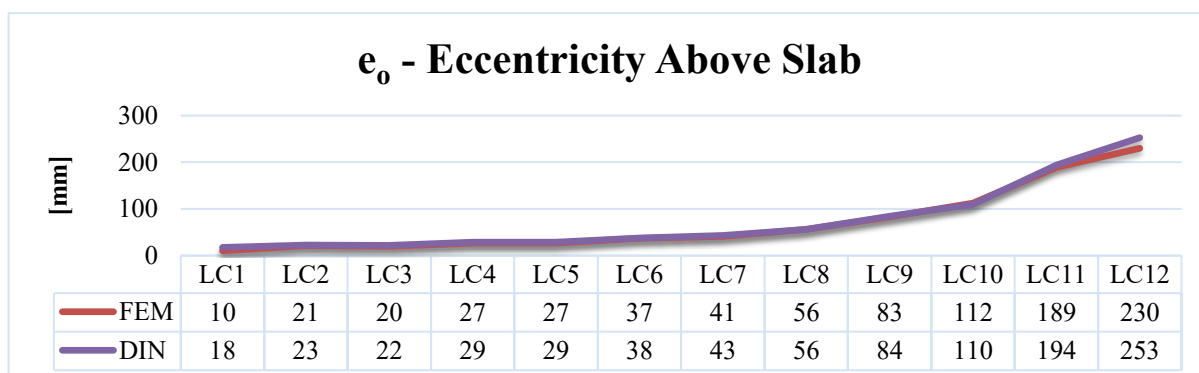


Figure 8.15 Eccentricity comparison above the slab

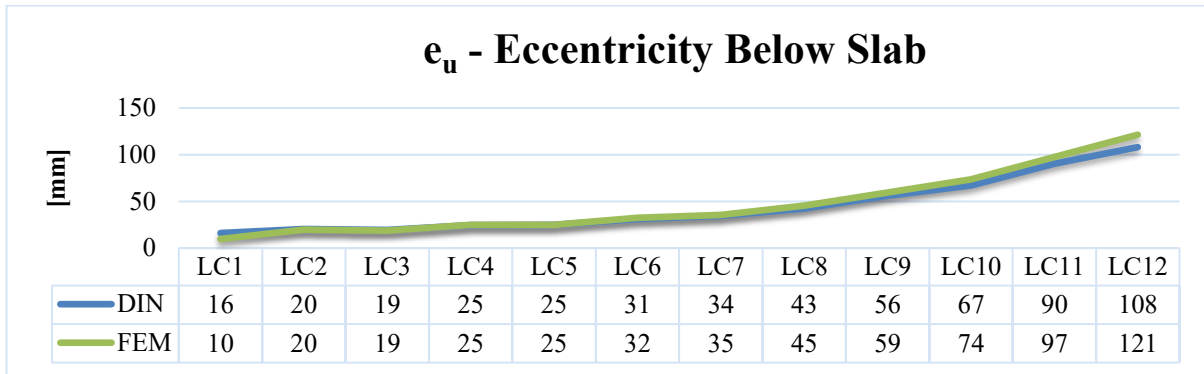


Figure 8.16 Eccentricity comparison below the slab

**Error [%]**

Load case	M(13)	M(12)	$e_o$	$e_u$
L1	69,7	65,6	69,7	65,6
L2	9,4	2,5	9,4	2,5
L3	12,0	4,2	12,0	4,2
L4	5,9	0,8	5,9	0,8
L5	8,0	0,6	8,0	0,6
L6	2,8	3,7	2,8	3,7
L7	4,6	2,5	4,6	2,5
L8	0,1	6,5	0,1	6,5
L9	1,5	5,4	1,5	5,4
L10	2,2	8,8	2,2	8,8
L11	2,4	7,3	2,4	7,3
L12	9,9	11,0	9,9	11,0

Table 8-5 Error evaluation

Through the analysis of the results obtained by the different simulations it is possible to notice that the higher the slenderness is, the lower the bending moment acting into the node is.

The error committed by the DIN formulation is higher for low value of slenderness. In addition, when the slenderness increases, the bending moments are more influenced by the vertical force applied on the top of the wall. In fact, the last case with  $t$  equal to 175 mm shows that the bending moment above the slab for the load case LC1 is about 0.6 times the bending moment acting for the load case LC11.

By the comparison of the results, it can be seen that there is a relation between the slenderness and the bending moment, considering the same load case.

The next diagram shows the relation between the slenderness and the bending moment for the same load case, with  $N$  equal to 200 kN and  $P$  equal to 6.25 kN. The results are obtained from the FEM simulations.

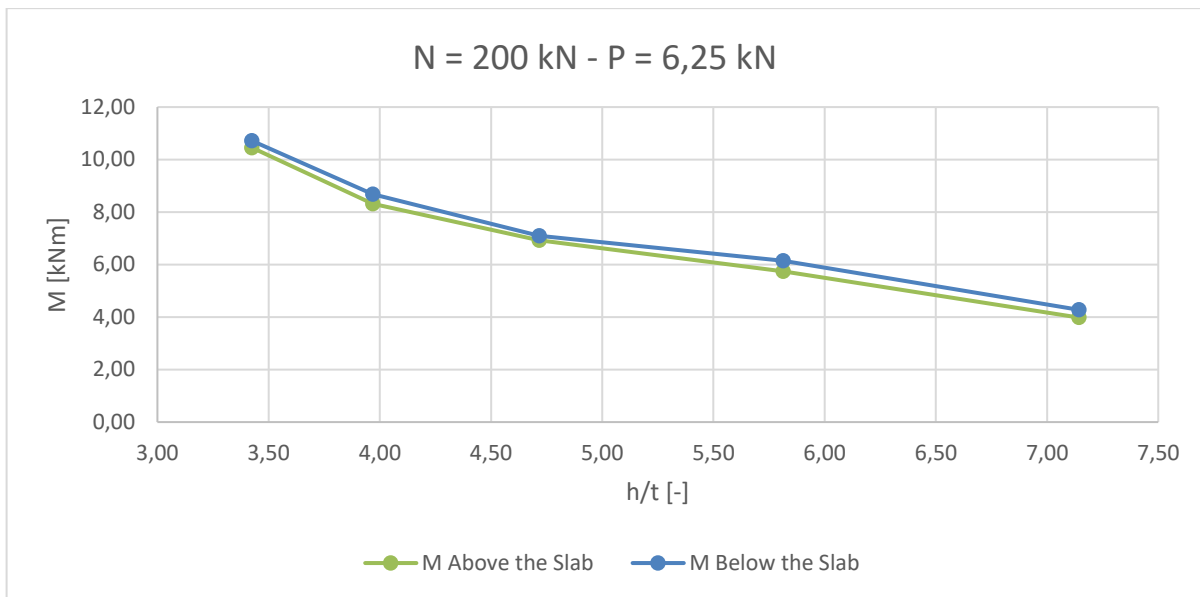


**Figure 8.17 Relation between bending moment and wall slenderness**

The eccentricities have a similar behavior compared to the bending moments.

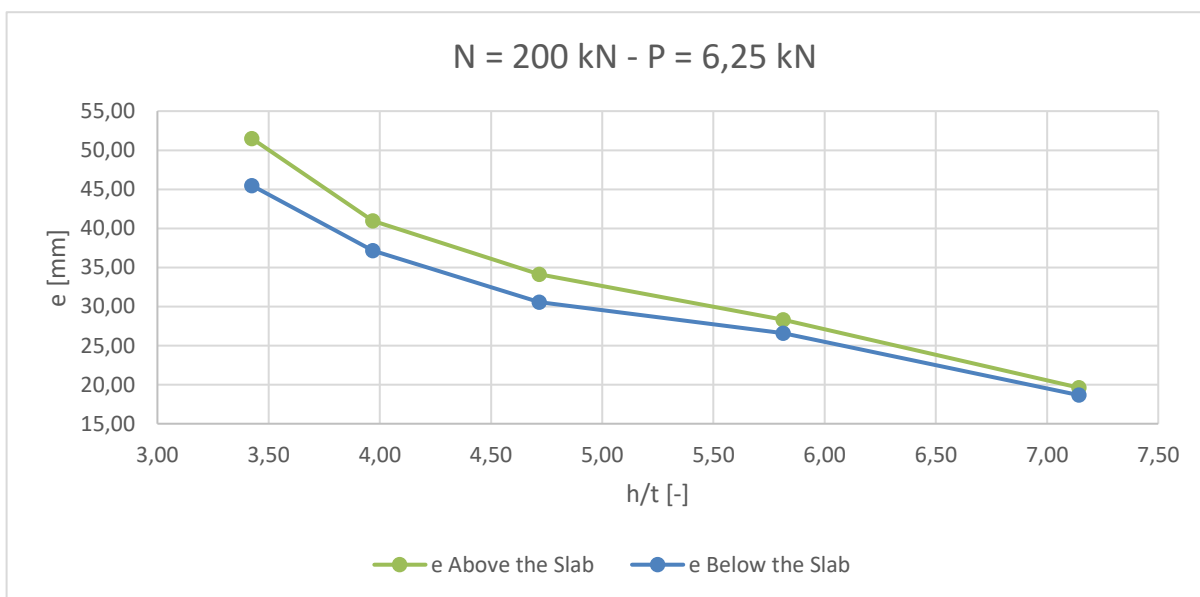


**Figure 8.18 Relation between eccentricity and wall slenderness**

For slender walls, the bending moment is lower and, as a consequence, also the eccentricity decreases.

The parameter which influences the capacity reduction factor is the rate between the eccentricity and the wall thickness  $e/t$ .

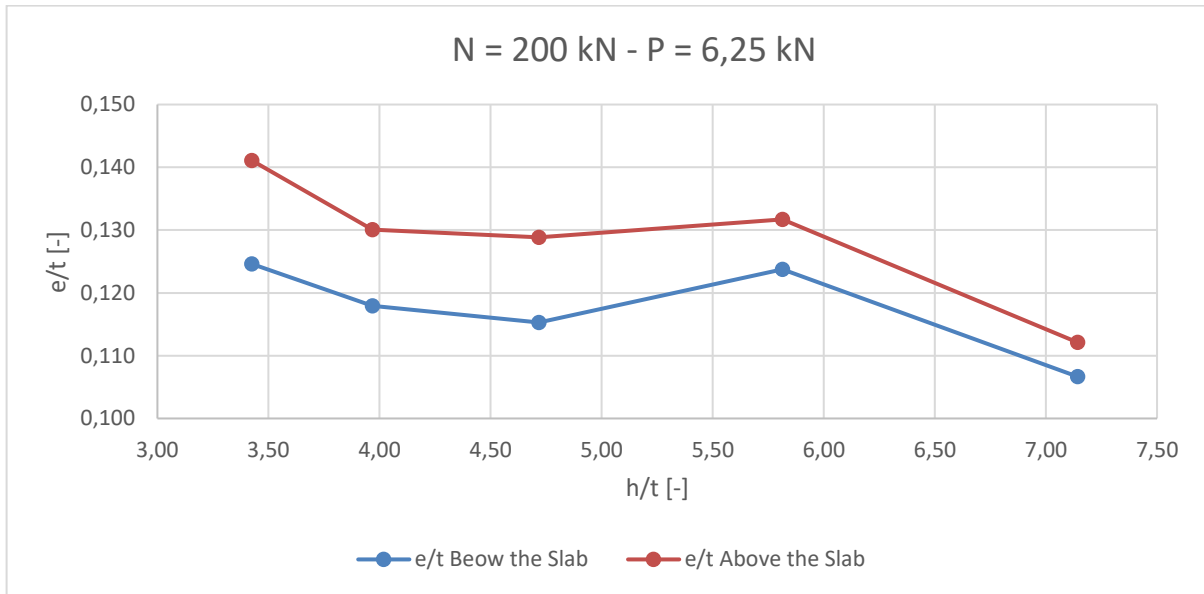


**Figure 8.19 Relation between eccentricity ratio and slenderness**

For different values of slenderness the eccentricity rate factor was calculated. For higher slenderness the capacity reduction factor will be higher because of the lower eccentricity. The load bearing capacity is calculated and the final results are shown in the following chart.

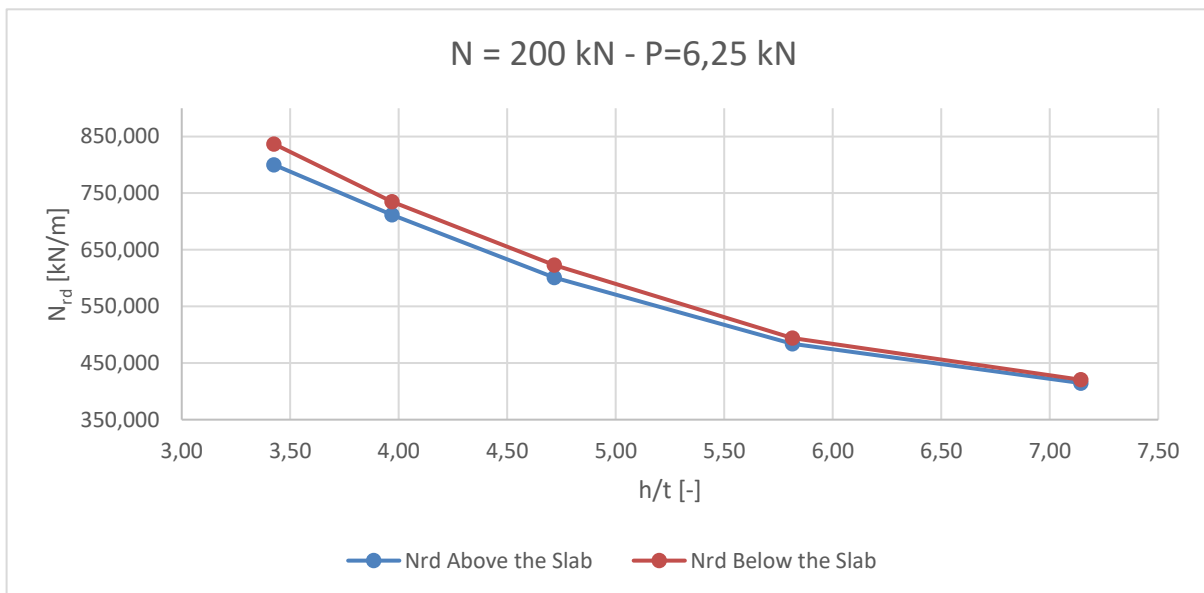


**Figure 8.20 Relation between Load Bearing Capacity and Slenderness ratio**

Even if the eccentricity decrease with increasing the slenderness, the load bearing capacity decreases, because of the lower thickness of the wall section. The load bearing capacity is calculated by using eq. (2.11) from DIN.

## 9 Influence of Wall Elastic Modulus

The following simulations are made in order to understand the influence of the wall elastic modulus on the structural behavior.

The load bearing capacity increases with the compressive strength of the wall. The compressive strength depends on the wall young modulus  $E$ . For this reason the elastic modulus of the bricks which composed the masonry is changed in relation to the compressive strength.

The elastic modulus of the wall is calculated by using the formulation suggested by the DIN. Starting from the compressive strength of the wall, which depend on the compressive strength of the bricks and the mortar, it is possible to estimate the elastic modulus with the following equation:

$$E = k_E * f_k \quad 9.1$$

Where  $k_E$  represent the wall stiffness. It is a factor which change in relation to the country. The value of  $k_E$  suggested by the EC6 is equal to 1000. While  $f_k$  is the compressive strength of the wall, calculated using the following formulation based on thin bed mortar:

$$f_k = K f_b^\alpha \quad 9.2$$

$f_b$  is the compressive strength of the brick and  $K$  is a factor which depends on the typology of the masonry units, the mortar and by the construction typology. In this case it is equal to 0.75. The value of  $\alpha$  is taken equal to 0.70.

By increasing the elastic modulus, also the wall rigidity increases. The wall rigidity influences the capacity to transfer the bending moment to the joint, because by decreasing the capacity of deformation of the materials then the transmitted forces increase.

Following different cases with different value of wall elastic modulus are analysed.

The geometry is the same used for the simulation in chapter 6.

### 9.1 $E= 2314 \text{ N/mm}^2$

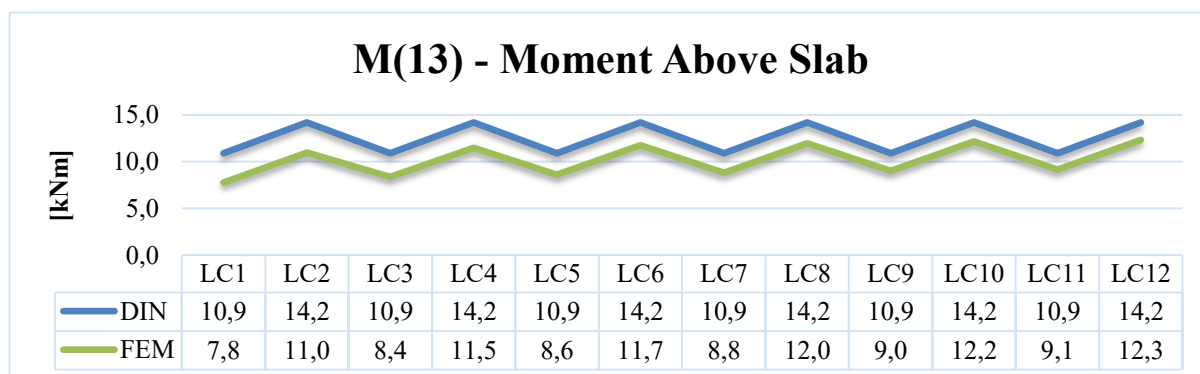


Figure 9.1 Bending moment comparison above the slab

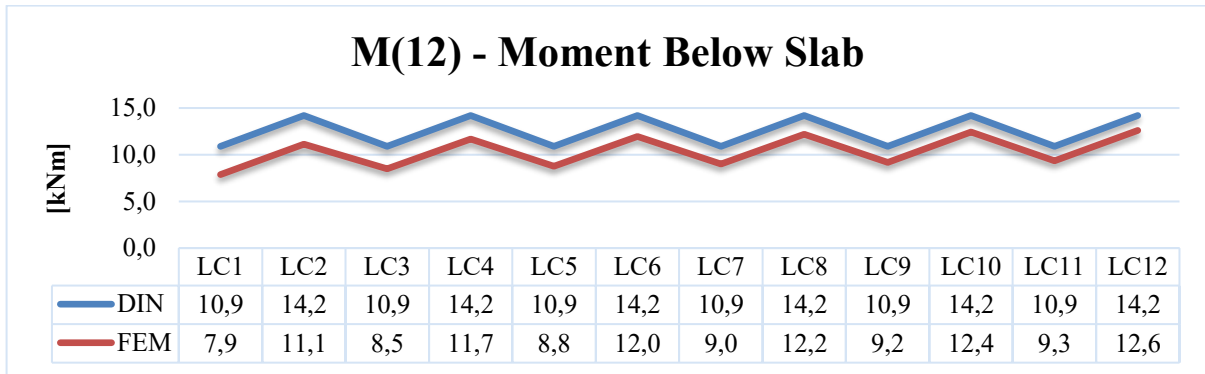


Figure 9.2 Bending moment comparison below the slab

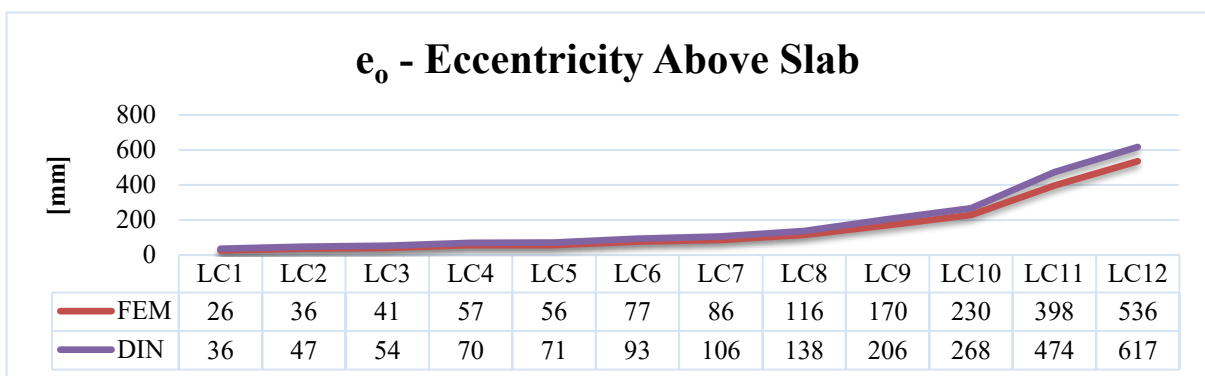


Figure 9.3 Eccentricity comparison above the slab

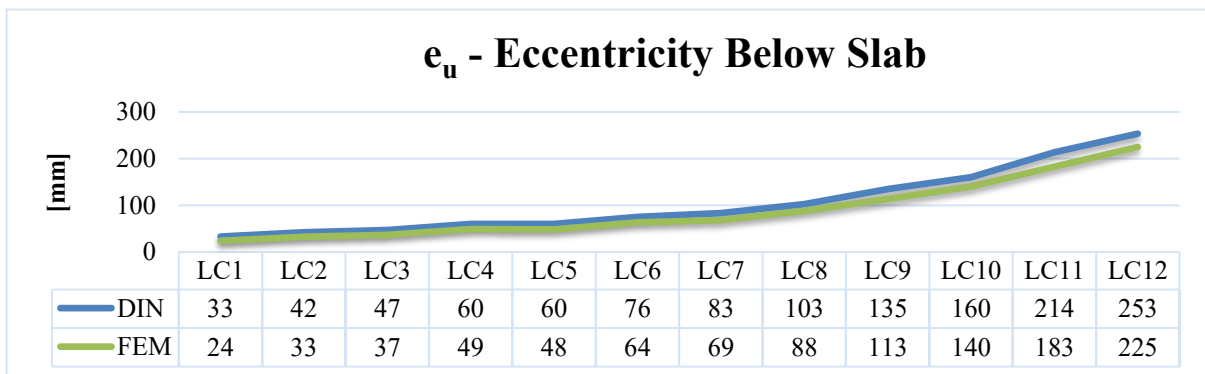


Figure 9.4 Eccentricity comparison below the slab

**Error [%]**

Load case	M(13)	M(12)	e <sub>o</sub>	e <sub>u</sub>
L1	40,4	38,4	40,4	38,4
L2	29,3	27,5	29,3	27,5
L3	30,4	28,3	30,4	28,3
L4	23,5	21,4	23,5	21,4
L5	26,6	24,3	26,6	24,3
L6	20,9	18,6	20,9	18,6
L7	23,6	21,2	23,6	21,2
L8	18,8	16,5	18,8	16,5
L9	20,9	18,6	20,9	18,6
L10	16,7	14,4	16,7	14,4
L11	19,1	16,7	19,1	16,7
L12	15,2	12,7	15,2	12,7

Table 9-1 Error evaluation

**9.2 E= 2629 N/mm<sup>2</sup>**

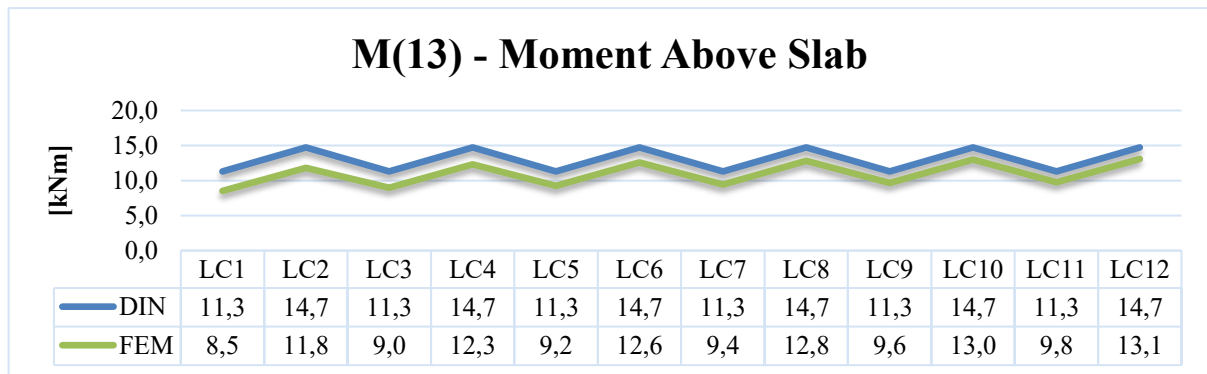


Figure 9.5 Bending moment comparison above the slab

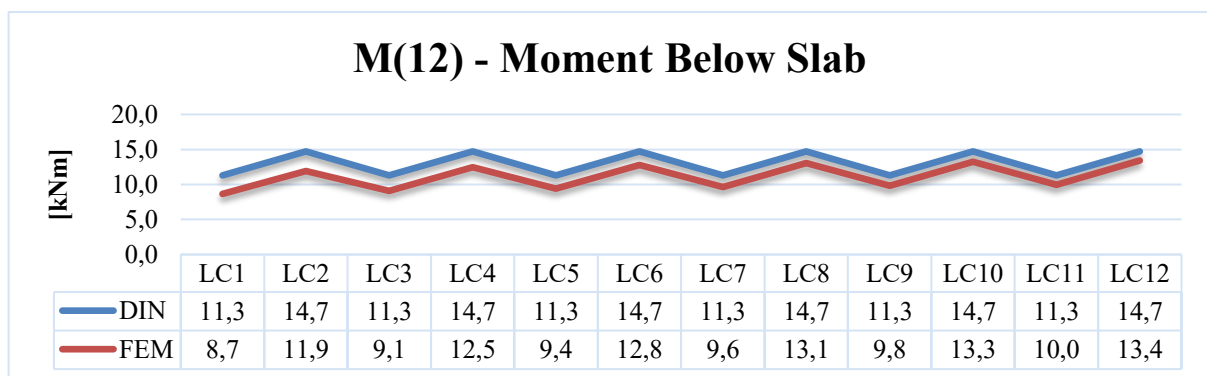


Figure 9.6 Bending moment comparison below the slab

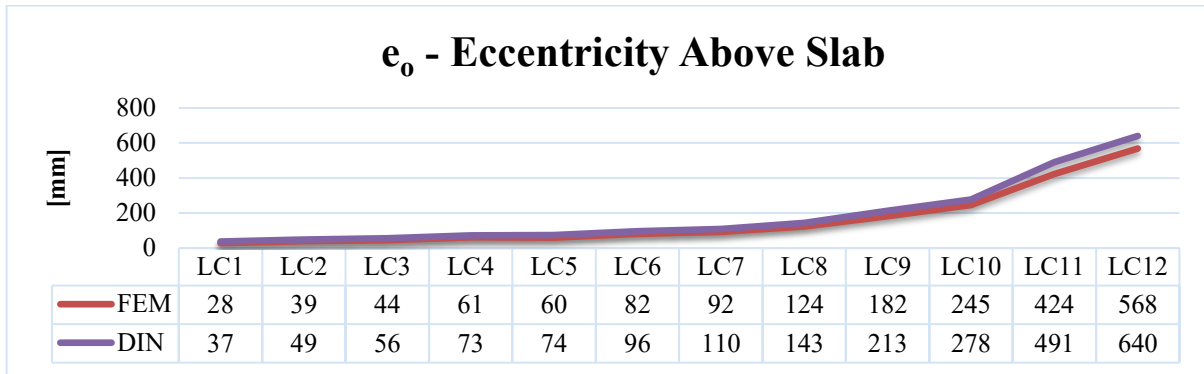


Figure 9.7 Eccentricity comparison above the slab

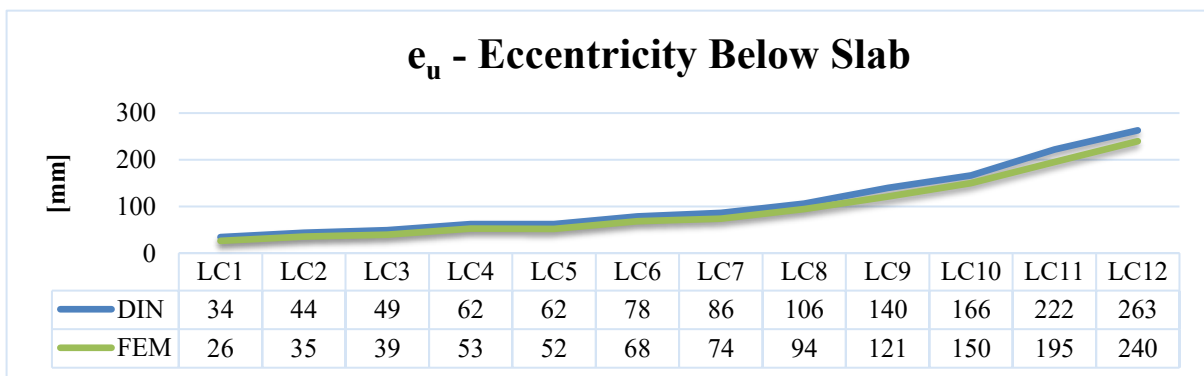


Figure 9.8 Eccentricity comparison below the slab

**Error [%]**

Load case	M(13)	M(12)	$e_o$	$e_u$
L1	32,7	30,5	32,7	30,5
L2	24,8	23,3	24,8	23,3
L3	26,1	24,3	26,1	24,3
L4	19,9	18,0	19,9	18,0
L5	22,5	20,4	22,5	20,4
L6	17,0	14,9	17,0	14,9
L7	19,6	17,4	19,6	17,4
L8	15,1	12,7	15,1	12,7
L9	17,3	15,1	17,3	15,1
L10	13,3	11,0	13,3	11,0
L11	15,8	13,6	15,8	13,6
L12	12,6	9,7	12,6	9,7

Table 9-2 Error evaluation

9.3  $E = 2928 \text{ N/mm}^2$

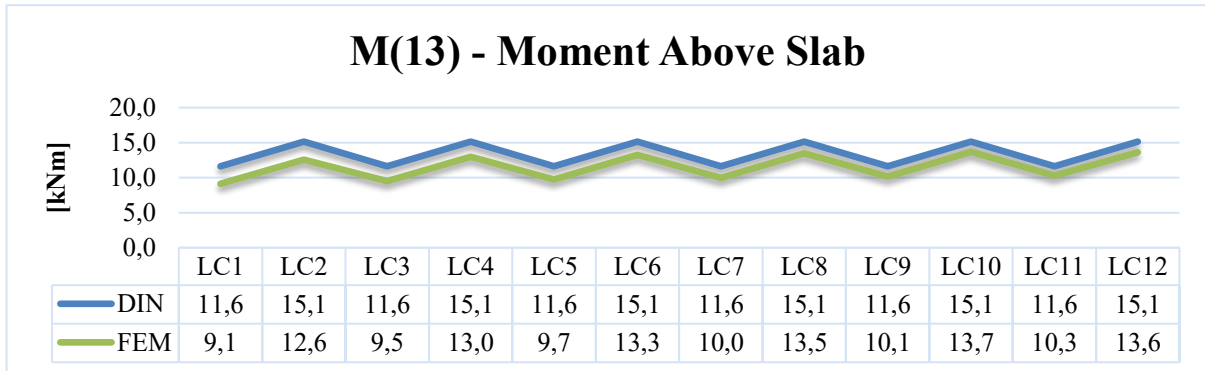


Figure 9.9 Bending moment comparison above the slab

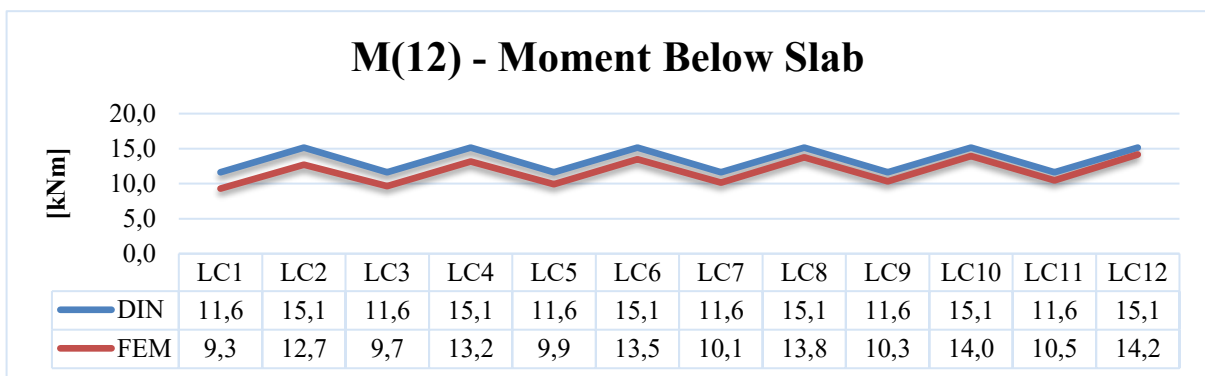


Figure 9.10 Bending moment comparison below the slab

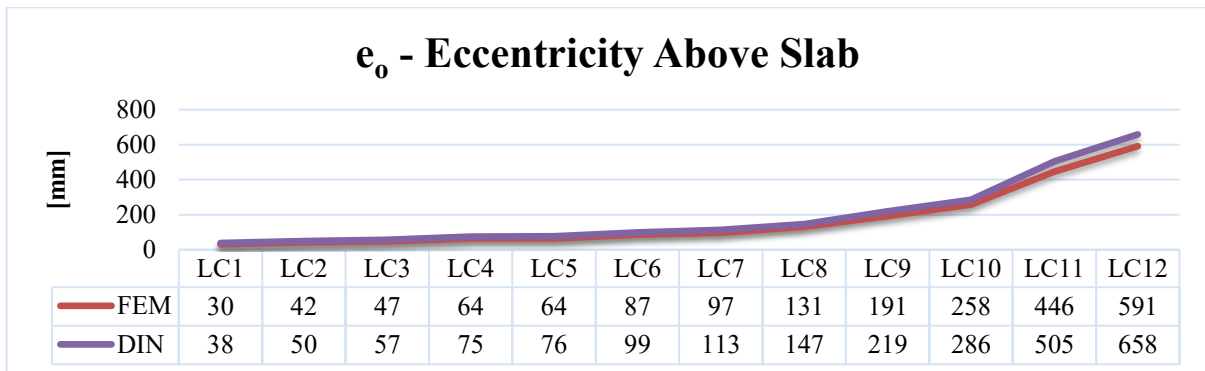


Figure 9.11 Eccentricity comparison above the slab

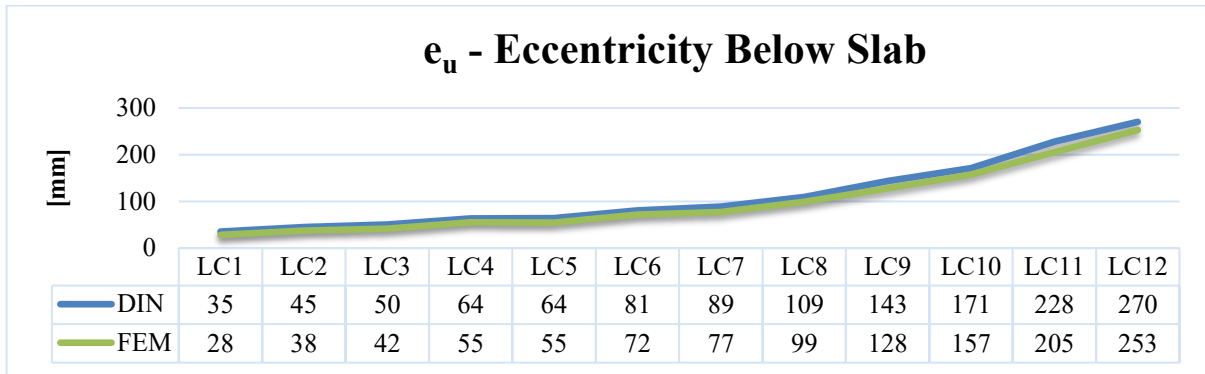


Figure 9.12 Eccentricity comparison below the slab

### Error [%]

Load case	M(13)	M(12)	e <sub>o</sub>	e <sub>u</sub>
L1	27,3	25,0	27,3	25,0
L2	20,4	19,0	20,4	19,0
L3	22,1	20,4	22,1	20,4
L4	16,6	15,0	16,6	15,0
L5	19,3	17,3	19,3	17,3
L6	14,2	12,3	14,2	12,3
L7	16,7	14,6	16,7	14,6
L8	12,2	10,1	12,2	10,1
L9	14,5	12,4	14,5	12,4
L10	10,7	8,6	10,7	8,6
L11	13,2	11,1	13,2	11,1
L12	11,4	6,9	11,4	6,9

Table 9-3 Error evaluation

## 9.4 E= 3215 N/mm<sup>2</sup>

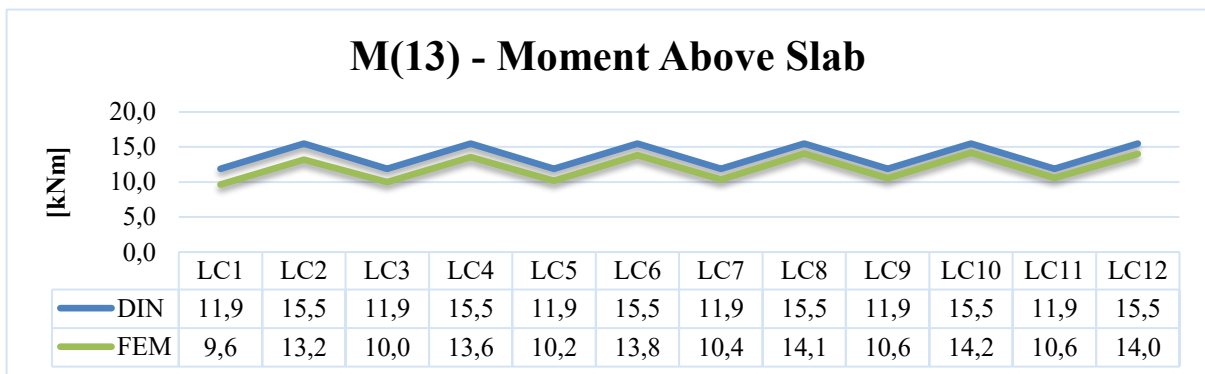


Figure 9.13 Bending moment comparison above the slab

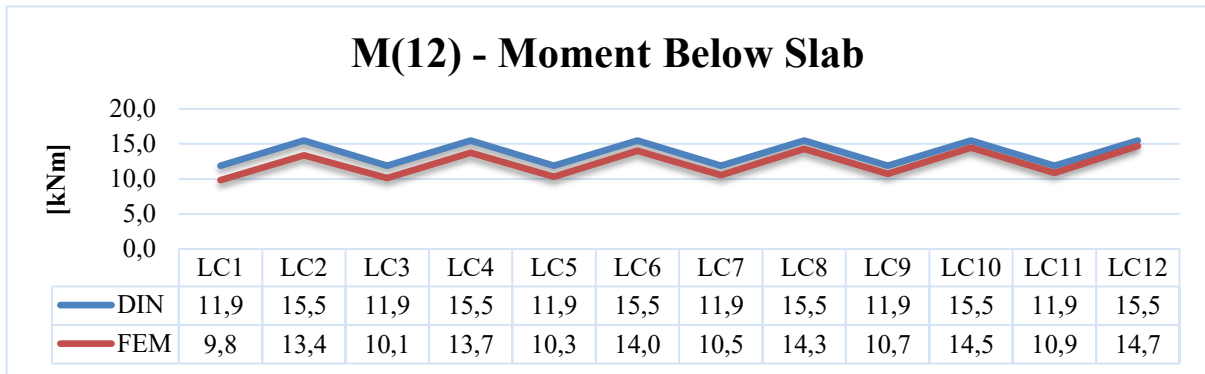


Figure 9.14 Bending moment comparison below the slab

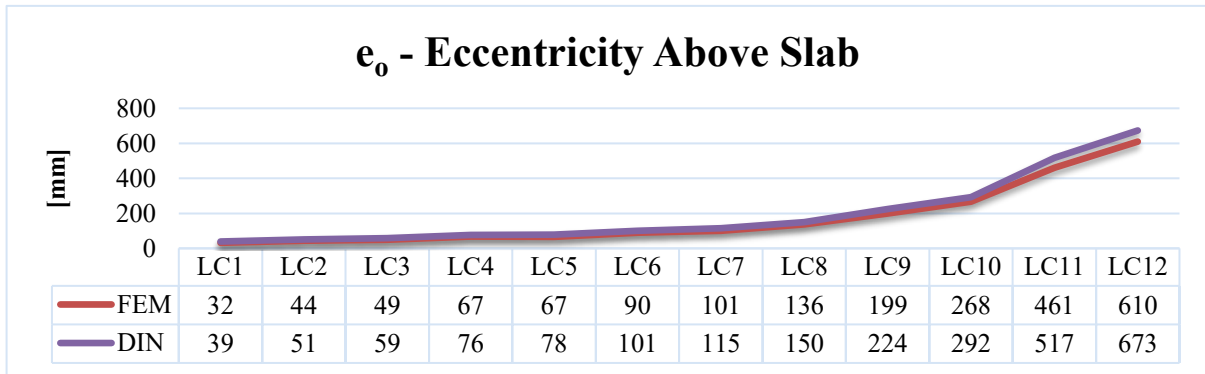


Figure 9.15 Eccentricity comparison above the slab

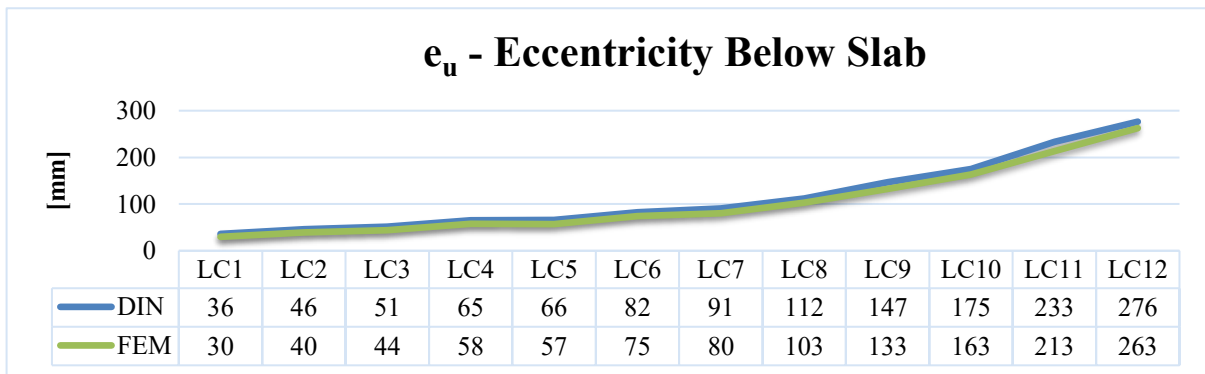


Figure 9.16 Eccentricity comparison below the slab

**Error [%]**

Load case	M(13)	M(12)	e <sub>o</sub>	e <sub>u</sub>
L1	23,3	20,9	23,3	20,9
L2	17,2	15,8	17,2	15,8
L3	19,1	17,6	19,1	17,6
L4	14,1	12,7	14,1	12,7
L5	16,8	15,1	16,8	15,1
L6	12,1	10,5	12,1	10,5
L7	14,6	12,8	14,6	12,8
L8	10,2	8,4	10,2	8,4
L9	12,6	10,7	12,6	10,7
L10	9,1	7,0	9,1	7,0
L11	12,1	9,3	12,1	9,3
L12	10,4	5,3	10,4	5,3

Table 9-4 Error evaluation

**9.5 E= 3492 N/mm<sup>2</sup>**

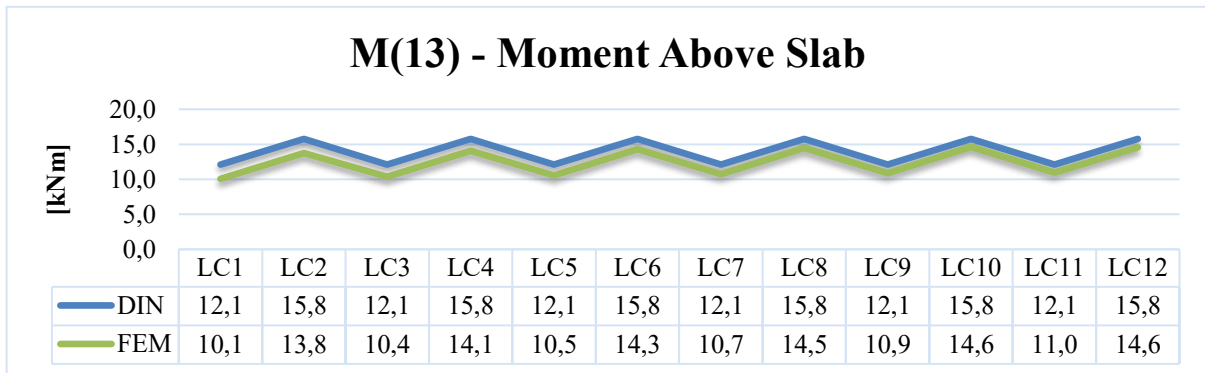


Figure 9.17 Bending moment comparison above the slab

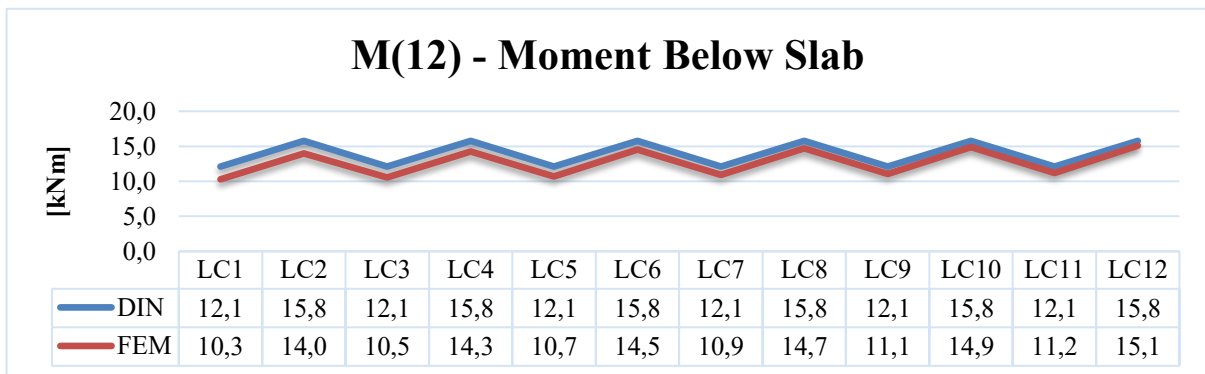


Figure 9.18 Bending moment comparison below the slab

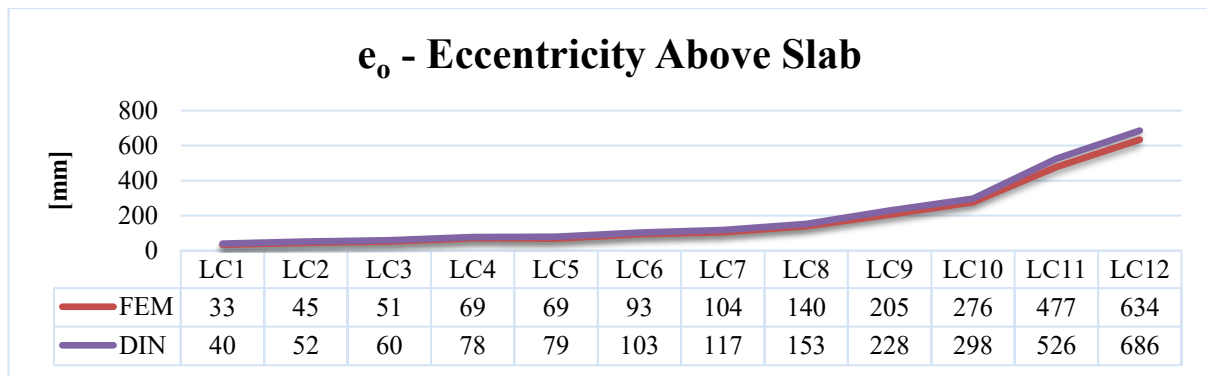


Figure 9.19 Eccentricity comparison above the slab

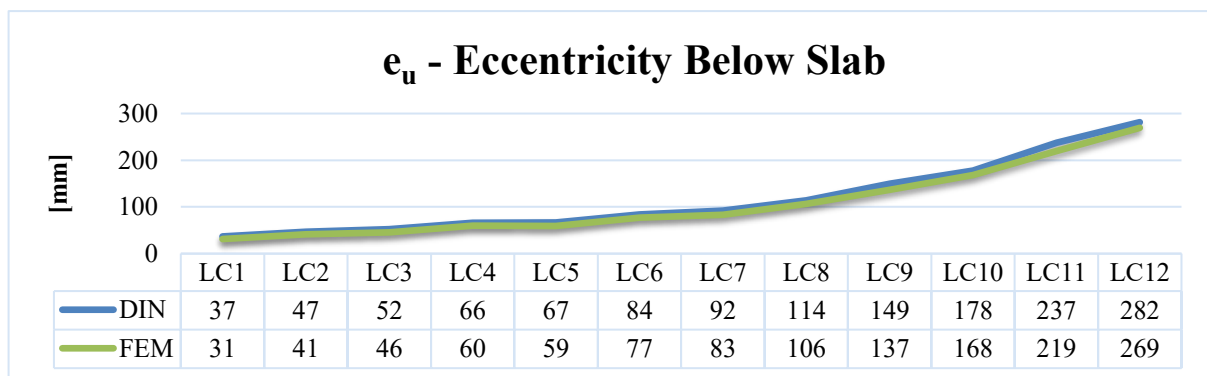


Figure 9.20 Eccentricity comparison below the slab

#### Error [%]

Load case	M(13)	M(12)	e <sub>o</sub>	e <sub>u</sub>
L1	20,2	17,7	20,2	17,7
L2	14,7	12,9	14,7	12,9
L3	16,8	14,9	16,8	14,9
L4	12,1	10,6	12,1	10,6
L5	14,9	13,0	14,9	13,0
L6	10,4	8,6	10,4	8,6
L7	13,0	10,9	13,0	10,9
L8	9,0	7,2	9,0	7,2
L9	11,3	9,3	11,3	9,3
L10	7,7	5,8	7,7	5,8
L11	10,2	8,3	10,2	8,3
L12	8,2	4,5	8,2	4,5

Table 9-5 Error evaluation

The higher the elastic modulus of the brick is, the higher the flexural rigidity of the wall is. As a consequence, the bending moment transmitted by the slab to the joint is higher when the elastic modulus of the single stone increases. Therefore, the comparison between FEM results and DIN formulations shows a higher precision when the elastic modulus increases, or for lower value of the vertical force applied on the top of the wall, by considering the *uncracked state*.

The following diagrams show the behaviour described above. By considering the same load case, with  $N$  equal to 200 kN and  $P$  equal to 6.25 kN, it is possible to notice that the higher the elastic modulus of the wall is, the higher the bending moment acting to the joint is.

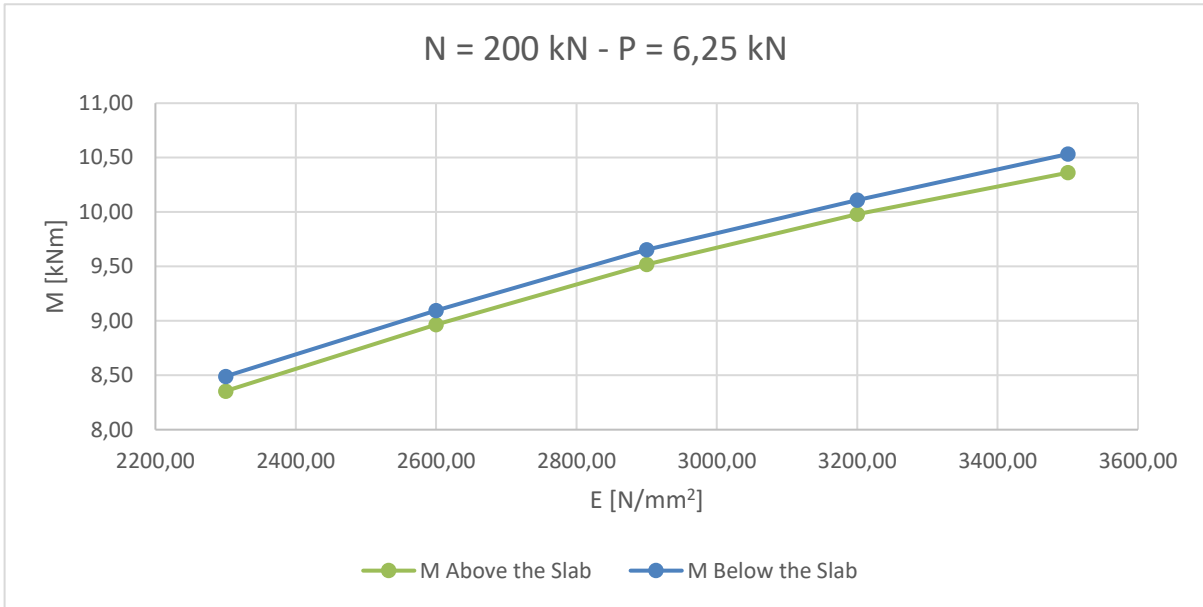


**Figure 9.21 Relation between bending moment and wall elastic modulus**

Also the eccentricity increases as the elastic modulus of the bricks increases.

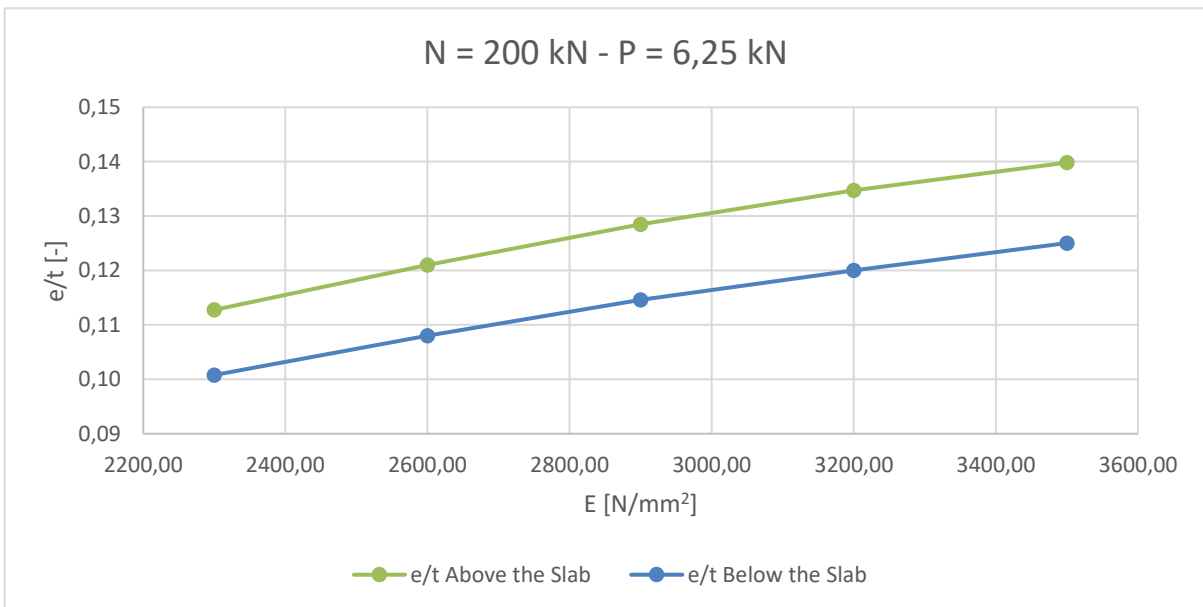


**Figure 9.22 Relation between eccentricity and wall elastic modulus**

Considering the load bearing capacity, the increasing of the elastic modulus leads to a lower value of the load bearing capacity, because of the higher eccentricity developed by the wall/slab connection. The capacity reduction factor is inversely proportional to the eccentricity.

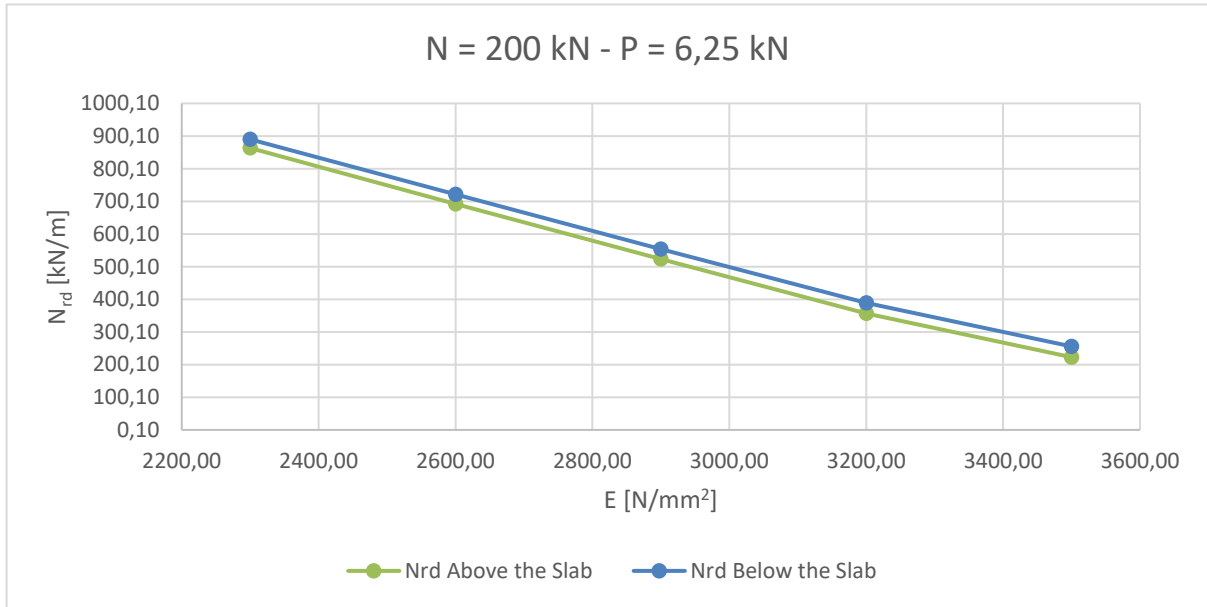


Figure 9.23 Relation between Wall Elastic Modulus and Load Bearing Capacity

The load bearing capacity is calculated using the DIN formulation.

## 10 Influence of Slab Elastic Modulus

Elastic modulus is a property of the constituent material. Stiffness is a property of a structure or component of a structure, and hence it is dependent upon various physical dimensions that describe that component. That is, the modulus is an intensive property of the material. Stiffness, on the other hand, is an extensive property of the solid body that is dependent on the material and its shape and boundary conditions.

The stiffness of a structure is of principal importance in many engineering applications, so the modulus of elasticity is often one of the primary properties considered when selecting a material. A high modulus of elasticity is sought when deflection is undesirable, while a low modulus of elasticity is required when flexibility is needed.

The elastic modulus can be defined as the ratio of the stress (force per unit area) along an axis to the strain (ratio of deformation over initial length) along that axis in the range of stress in which Hooke's law holds. It can be used to predict the elongation or compression of an object as long as the stress is less than the yield strength of the elastic material.

A solid material will deform when a load is applied to it. If it returns to its original shape after the load is removed, this is called elastic deformation. A stiff material needs more force to deform compared to a soft material, and an infinite force would be needed to deform a perfectly rigid material, implying that it would have an infinite Young's modulus. Although such a material cannot exist, a material with a very high Young's modulus can be approximated as rigid.

Concrete is a quasi-brittle material and has different behaviour in tension and compression. The experimental short term uniaxial stress–strain curve for concrete has essentially no linear range and the slope of the curve is continuous up to “failure” (see Fig. 10.1). The response of the concrete is nonlinear and, after the ultimate stress is reached, the material softens until it can no longer carry any stress. In compression, the stress-strain curve for concrete is linearly elastic up to 30 percent of the maximum compressive strength. Above this point, the stress increases gradually up to the maximum compressive strength. After it reaches the maximum compressive strength, the curve descends into a softening region, and eventually crushing failure occurs at an ultimate strain. In tension, the stress-strain curve for concrete is approximately linearly elastic up to the maximum tensile strength. After this point, the concrete cracks and strength decreases gradually to zero.

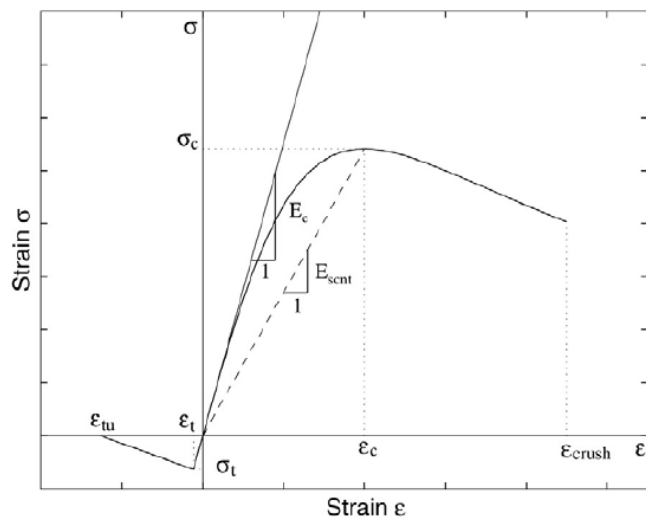


Figure 10.1 Stress strain curve for concrete

$\sigma$  is the stress,  $\varepsilon$  is the strain,  $E_c$  is the Young's modulus of the concrete,  $E_{scnt}$  is the secant modulus corresponding to the maximum stress  $\sigma_c$  and given by:

$$E_{scnt} = \frac{\sigma_c}{\varepsilon_c} \quad \text{Equation 10.1}$$

The bilinear stress–strain curve in Fig. 10.1 is used to represent the tensile behaviour of the concrete where the Young's modulus is the same as that for the compressive behaviour,  $\sigma_t$  is the tensile strength of the concrete, and  $\varepsilon_{tu}$  is the maximum tensile strain.

If the elastic modulus decreases, the concrete slab is able to reach higher deformation before to reach the cracked state.

The difference between the slab elastic modulus compared to the masonry wall's one is of about one order of magnitude.

If the slab elastic modulus increases, then it results less deformable and the flexibility is reduced. For this reason it is more easy to reach the *cracked state* in the wall slab connection. The deflection is the degree to which a structural element is displaced under a load, and it is proportional to the flexibility of the material. It may refer to an angle or a distance.

The analysis were carried out taking in consideration the structural concrete generally used in common constructions. Four typologies were considered:

- **C25/30**
- **C30/37**
- **C40/50**
- **C45/55**

The mechanical characteristics of the concrete are obtained from pre-set mechanical parameters by Atena 3D program, which are based on mechanical experimental data. The structural behaviour in Atena 3D is capable to consider the nonlinear effects due to the crack developing.

The geometry is the same used for the simulation in Chapter 6.

10.1 C25/30 (E= 31000 N/mm<sup>2</sup>)

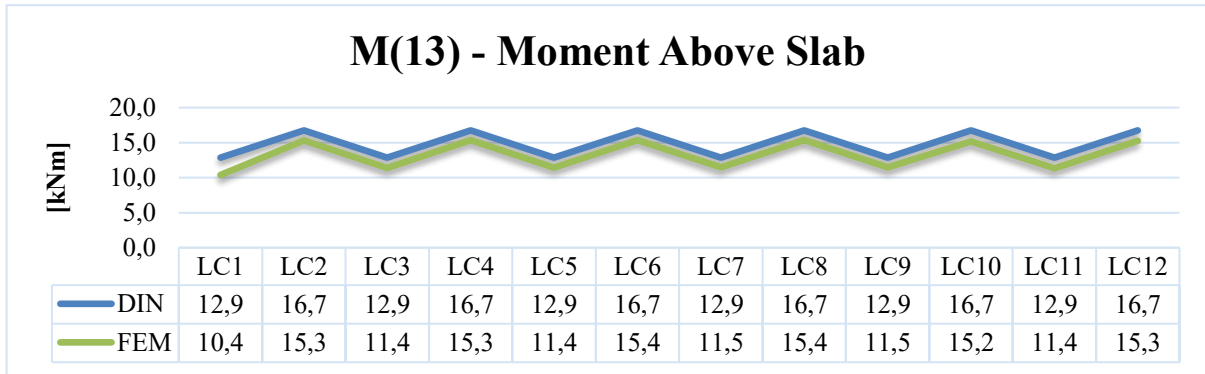


Figure 10.2 Bending moment comparison above the slab

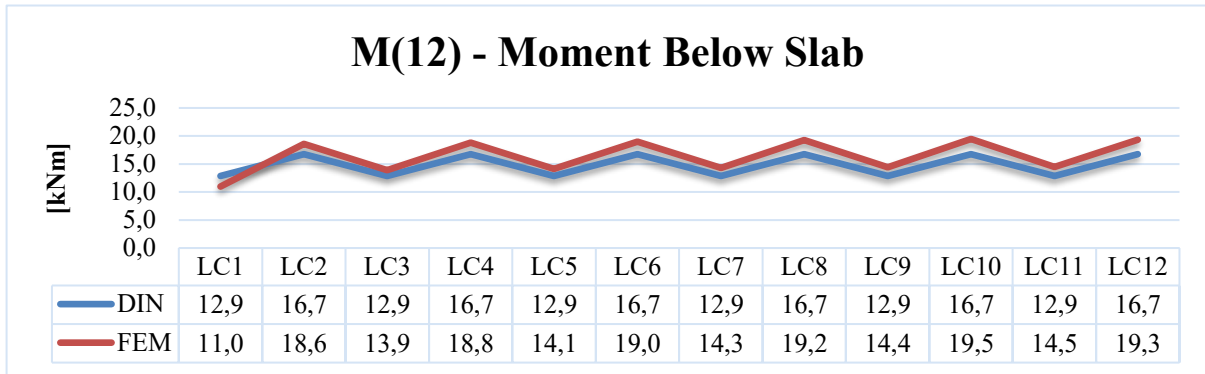


Figure 10.3 Bending moment comparison below the slab

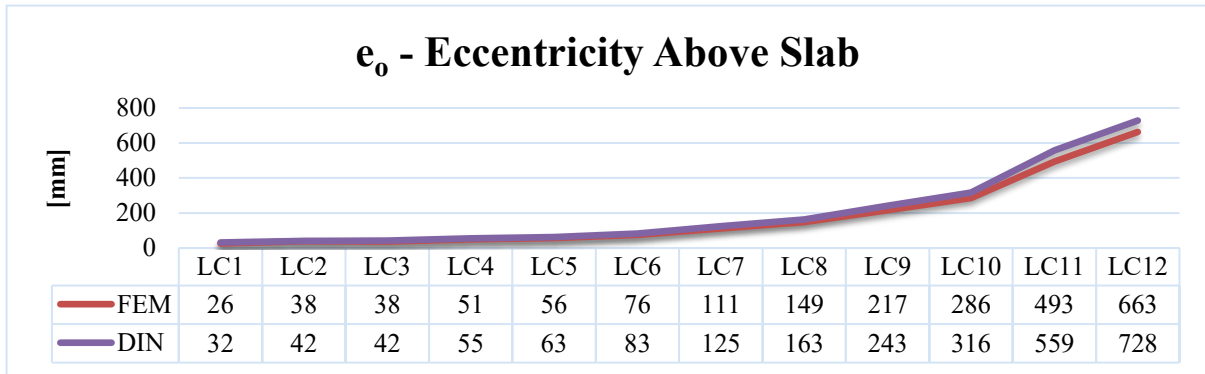


Figure 10.4 Eccentricity comparison above the slab

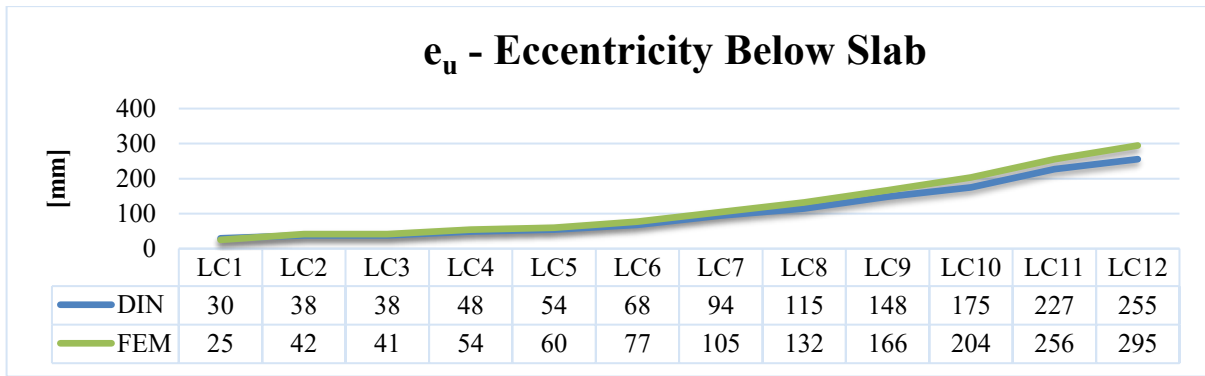


Figure 10.5 Eccentricity comparison below the slab

### Error [%]

Load case	M(13)	M(12)	e <sub>o</sub>	e <sub>u</sub>
L1	23,8	17,2	23,8	17,2
L2	9,5	9,8	9,5	9,8
L3	13,0	7,6	13,0	7,6
L4	9,2	10,8	9,2	10,8
L5	12,5	8,9	12,5	8,9
L6	9,1	11,8	9,1	11,8
L7	11,9	10,1	11,9	10,1
L8	8,9	12,9	8,9	12,9
L9	12,0	10,8	12,0	10,8
L10	10,4	13,9	10,4	13,9
L11	13,3	11,2	13,3	11,2
L12	9,8	13,3	9,8	13,3

Table 10-1 Error evaluation

## 10.2 C30/37 (E= 33000 N/mm<sup>2</sup>)

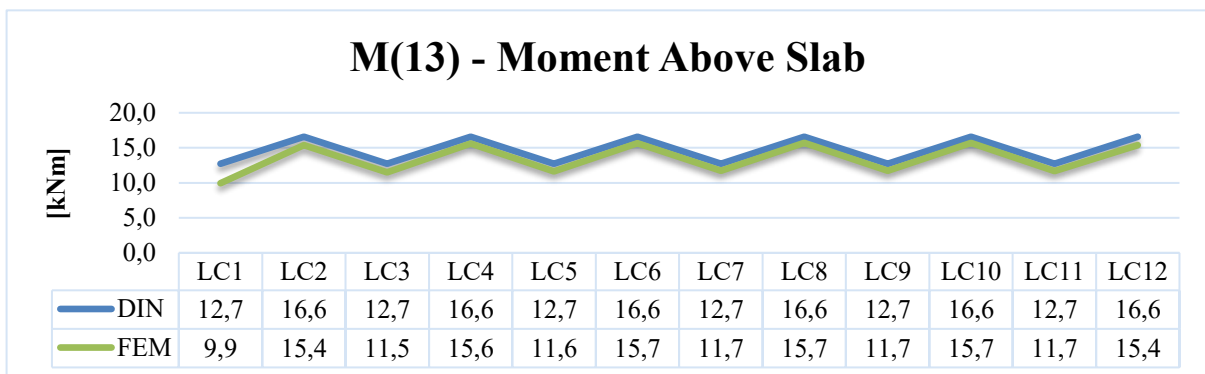


Figure 10.6 Bending moment comparison above the slab

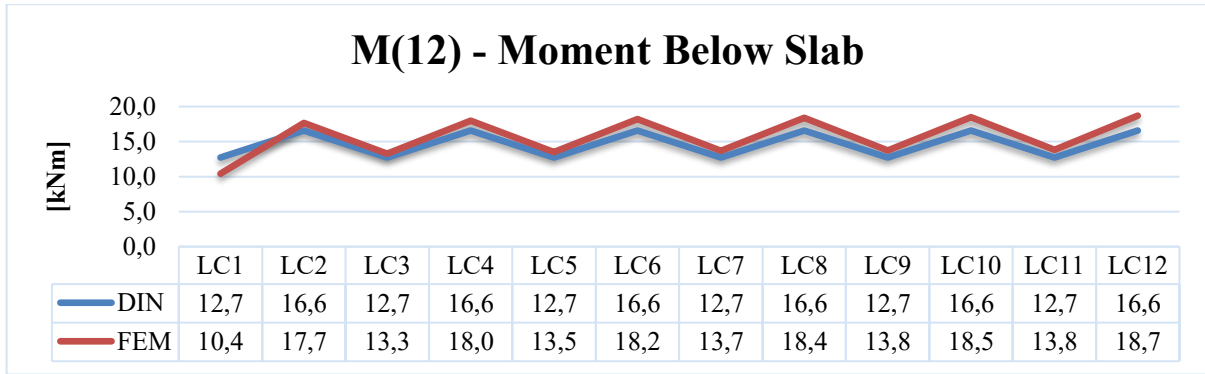


Figure 10.7 Bending moment comparison below the slab

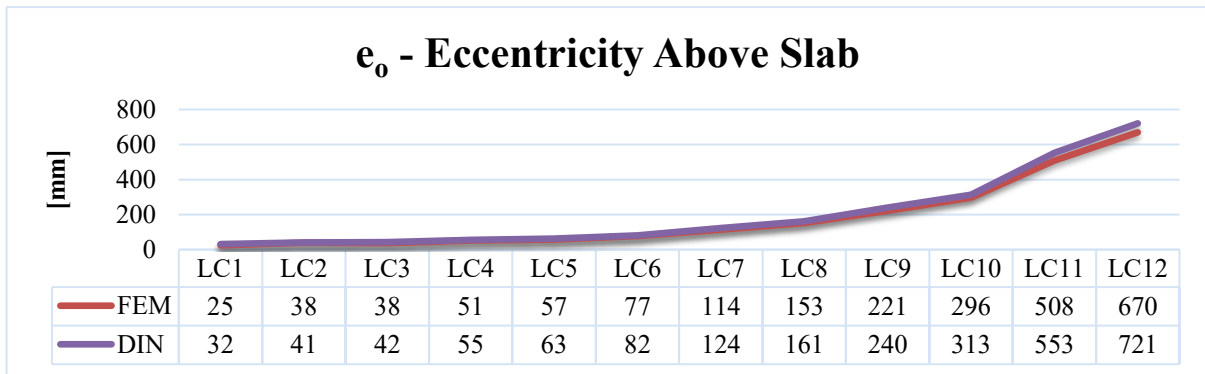


Figure 10.8 Eccentricity comparison above the slab

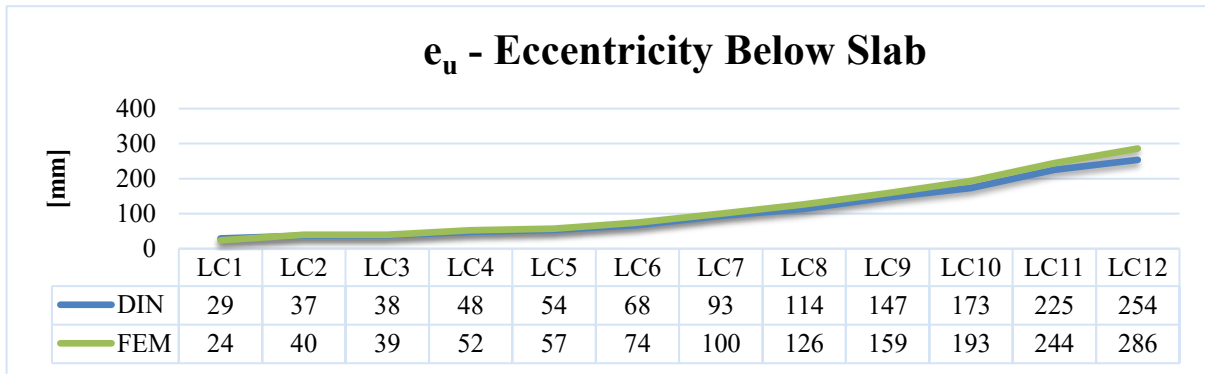


Figure 10.9 Eccentricity comparison below the slab

**Error [%]**

Load case	M(13)	M(12)	e <sub>o</sub>	e <sub>u</sub>
L1	28,0	22,2	28,0	22,2
L2	7,8	6,2	7,8	6,2
L3	10,8	4,1	10,8	4,1
L4	6,4	7,8	6,4	7,8
L5	9,3	5,8	9,3	5,8
L6	5,8	9,0	5,8	9,0
L7	8,4	6,9	8,4	6,9
L8	5,5	9,8	5,5	9,8
L9	8,6	7,5	8,6	7,5
L10	5,7	10,3	5,7	10,3
L11	8,9	8,0	8,9	8,0
L12	7,7	11,3	7,7	11,3

Table 10-2 Error evaluation

**10.3 C40/50 (E=35000 N/mm<sup>2</sup>)**

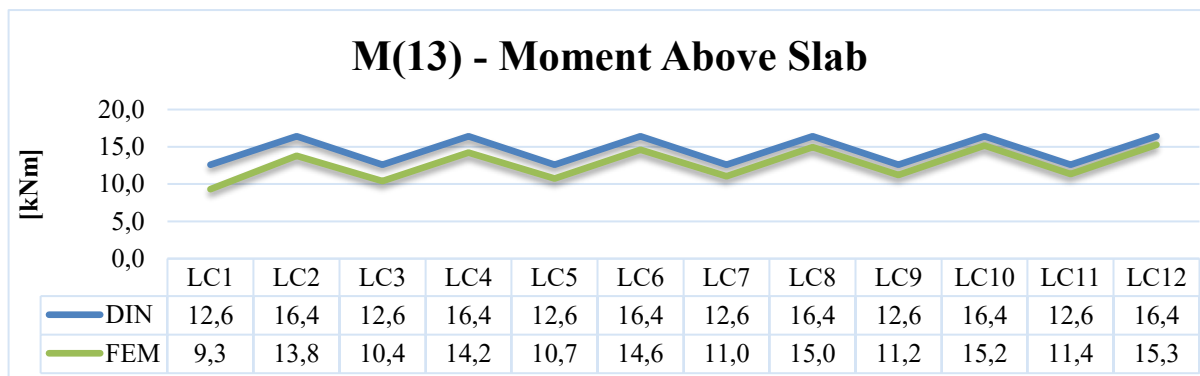


Figure 10.10 Bending moment comparison above the slab

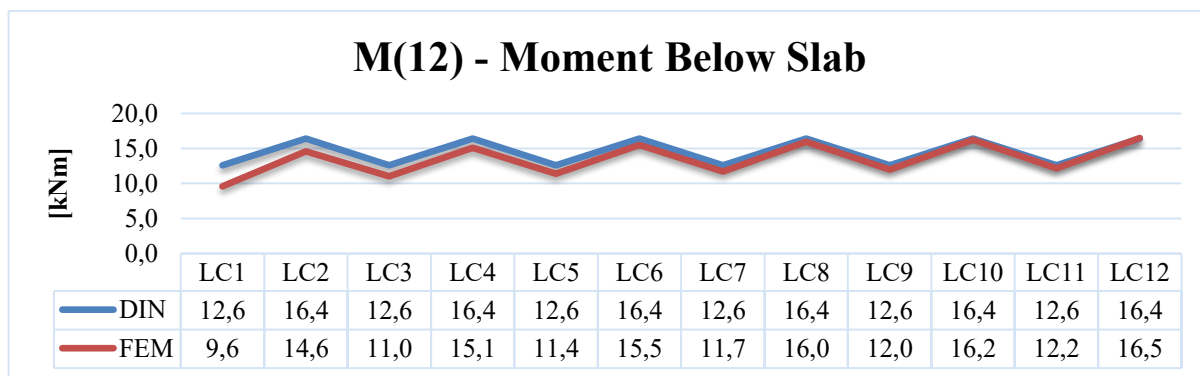


Figure 10.11 Bending moment comparison below the slab

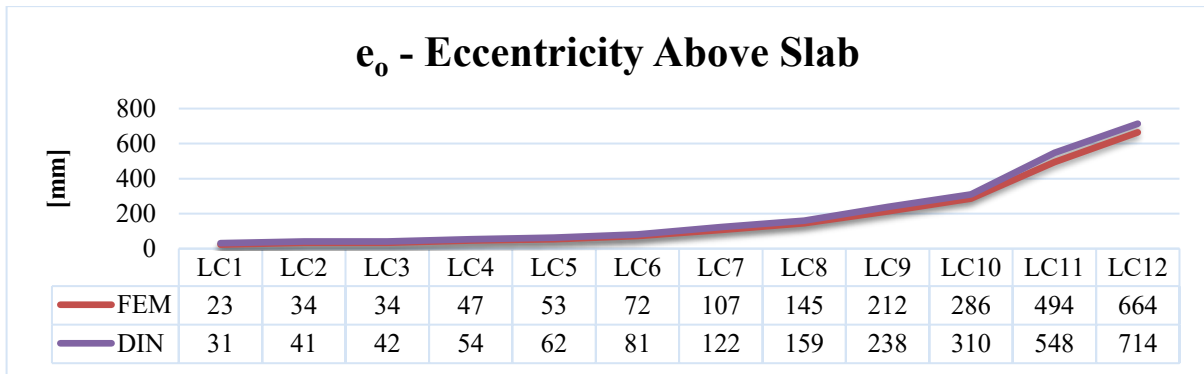


Figure 10.12 Eccentricity comparison above the slab

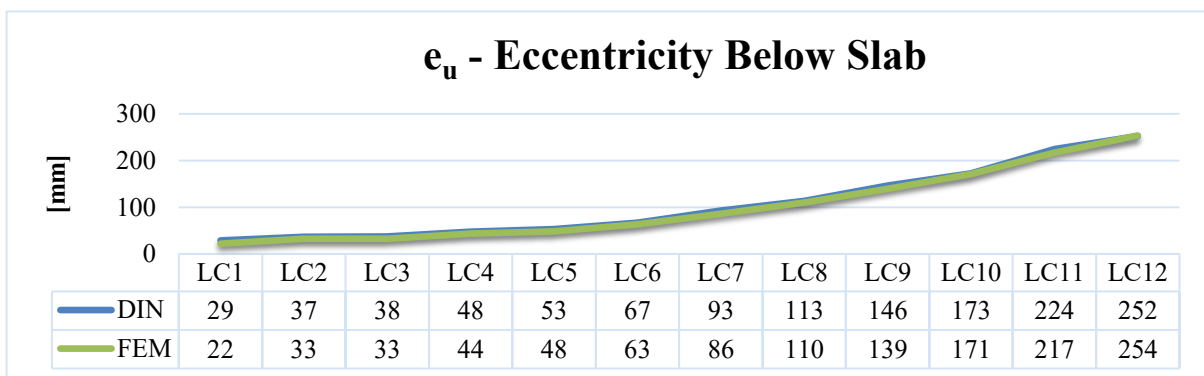


Figure 10.13 Eccentricity comparison below the slab

**Error [%]**

Load case	M(13)	M(12)	$e_o$	$e_u$
L1	35,2	31,3	35,2	31,3
L2	18,8	12,6	18,8	12,6
L3	21,2	14,4	21,2	14,4
L4	15,3	8,9	15,3	8,9
L5	17,4	10,6	17,4	10,6
L6	12,4	5,9	12,4	5,9
L7	14,2	7,4	14,2	7,4
L8	9,7	2,8	9,7	2,8
L9	12,1	5,0	12,1	5,0
L10	8,3	1,2	8,3	1,2
L11	10,9	3,4	10,9	3,4
L12	7,5	0,4	7,5	0,4

Table 10-3 Error evaluation

10.4 C45/55 ( $E = 36000 \text{ N/mm}^2$ )

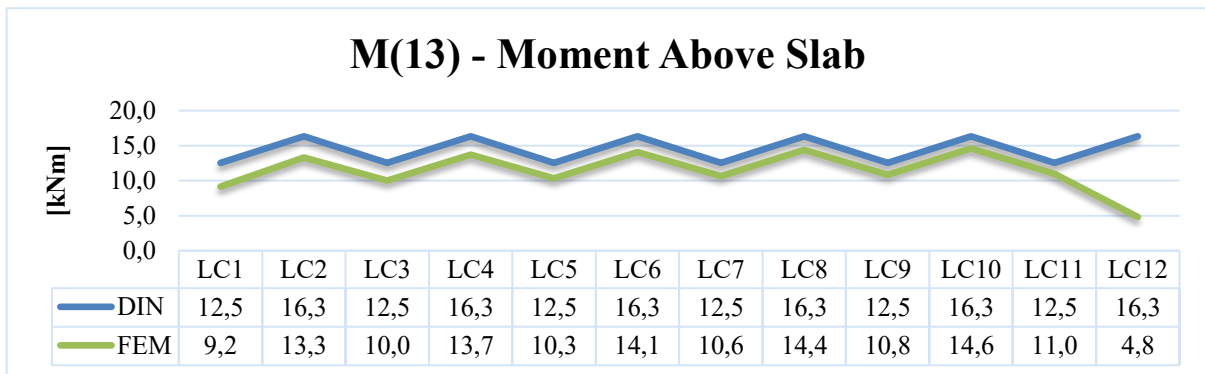


Figure 10.14 Bending moment comparison above the slab

The last load case LC12 shows the loss of contact on the interface above the slab.

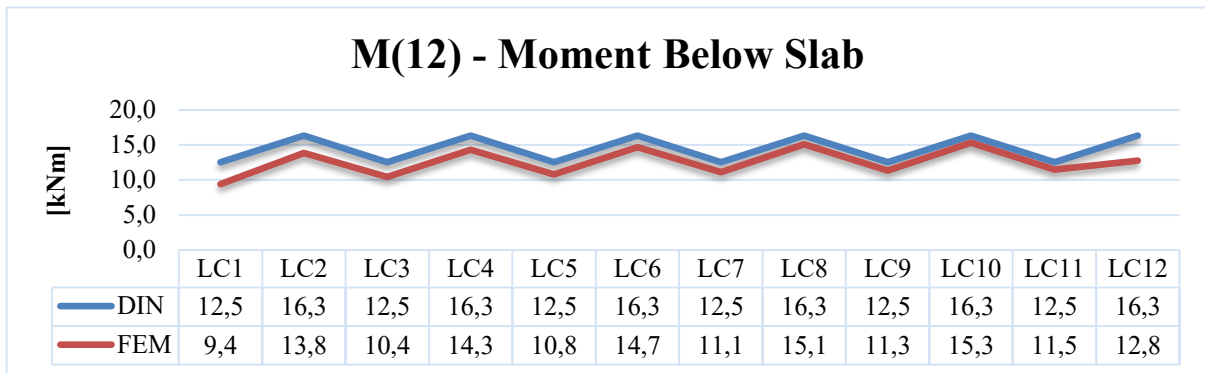


Figure 10.15 Bending moment comparison below the slab

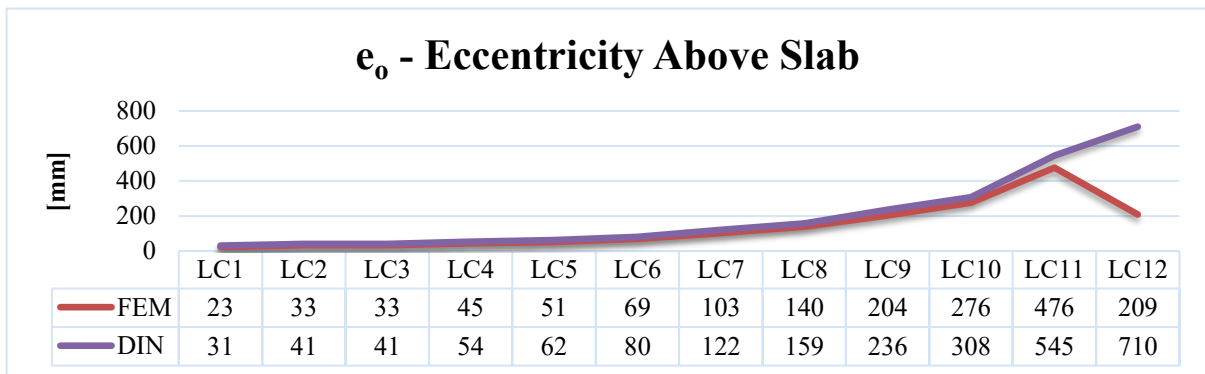


Figure 10.16 Eccentricity comparison above the slab

In load case LC12 there is a loss of contact between the slab and the wall.

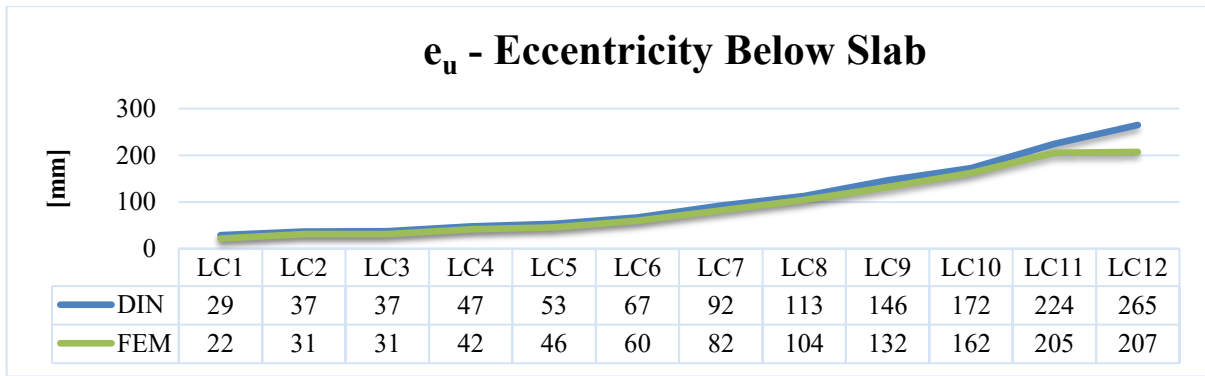


Figure 10.17 Eccentricity comparison below the slab

### Error [%]

Load case	M(13)	M(12)	e <sub>o</sub>	e <sub>u</sub>
L1	36,9	33,2	36,9	33,2
L2	22,9	18,0	22,9	18,0
L3	25,5	20,0	25,5	20,0
L4	19,2	14,2	19,2	14,2
L5	21,4	16,1	21,4	16,1
L6	16,1	11,1	16,1	11,1
L7	17,8	12,7	17,8	12,7
L8	13,4	8,3	13,4	8,3
L9	15,8	10,7	15,8	10,7
L10	11,8	6,6	11,8	6,6
L11	14,4	9,1	14,4	9,1
L12	239,1	27,8	239,1	27,8

Table 10-4 Error evaluation

The higher the elastic modulus of the slab is, the lower the bending moment transferred is.

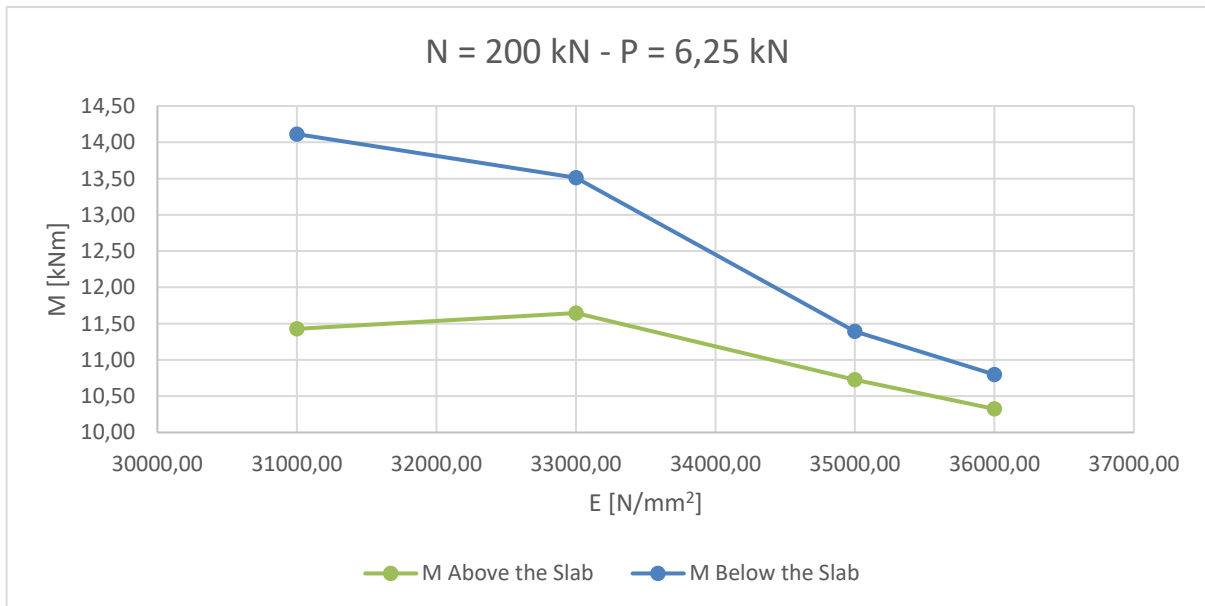
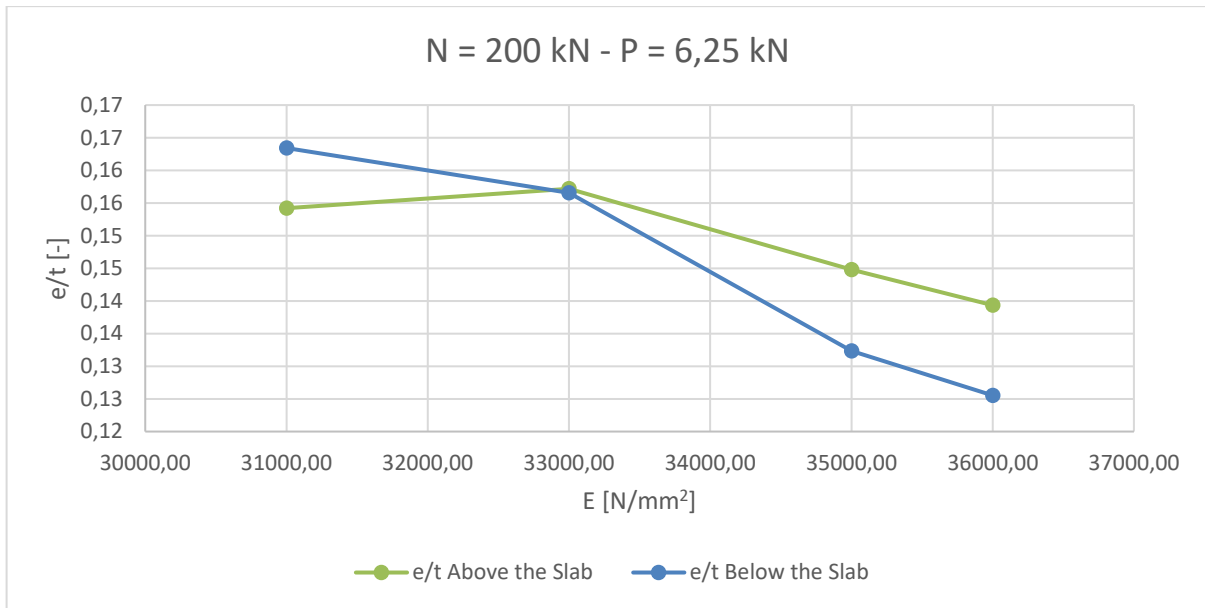


Figure 10.18 Relation between bending moment and slab elastic modulus

Also the eccentricity shows a similar behaviour compared to the bending moments.



**Figure 10.19 Relation between eccentricity and slab elastic modulus**

More rigid slab leads to a reduction of the bending moment acting to the wall/slab connection but, it is more likely that the interface failure occurs, because the deformability is reduced, while the wall deformability is higher. Instead, in the last load cases of the chapter 10.4, when the elastic modulus is equal to 36000 N/mm<sup>2</sup>, the interface fails and the acting bending moment drastically decreases.

The effect of the slab thickness variation is more marked below the slab.

The EC 6 precision is higher for low values of the elastic modulus of the slab.

For high values of wall elastic modulus, the eccentricity is lower and the load bearing capacity will have higher value because the capacity reduction factor will be higher for low values of eccentricity.

The next chart shows the relation between the load bearing capacity calculated with the DIN formulation and the elastic modulus of the slab.

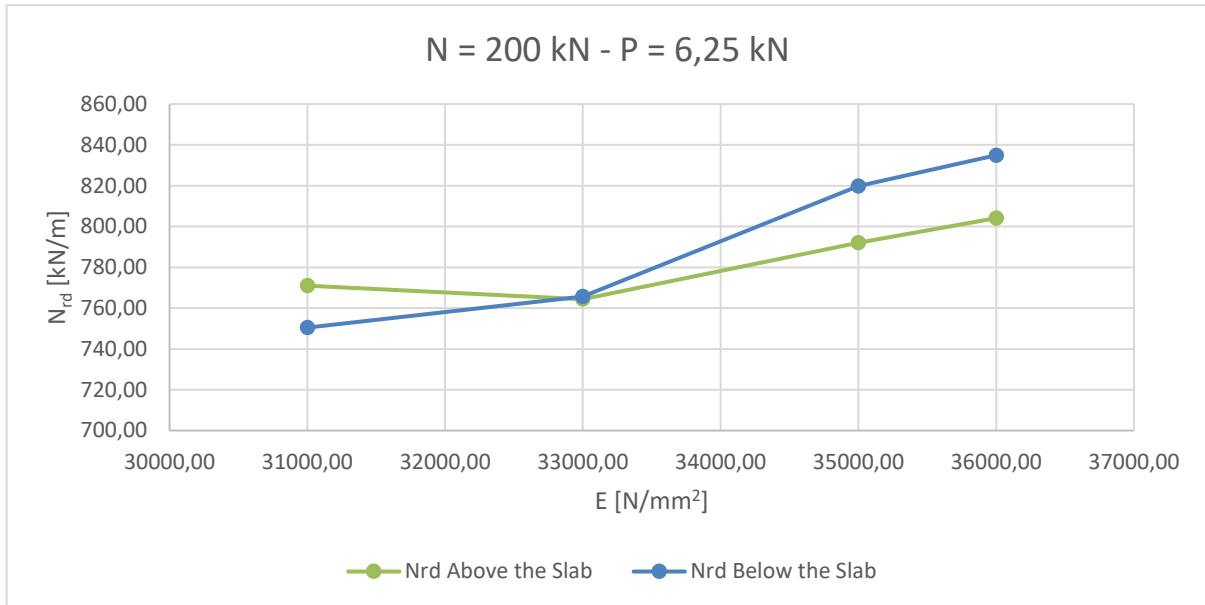


Figure 10.20 Relation between Slab Elastic Modulus and Load Bearing Capacity

## 11 Conclusions

The main parameters involved on the ultimate response of masonry walls under vertical loading are the slenderness ratio, the load eccentricity, the masonry stiffness and the tensile strength of the unit-mortar interface. The consideration of realistic value of the tensile strength of the unit-mortar interface can improve significantly the prediction of the structural behaviour and of the resistance capacity of walls with large slenderness, large eccentricity or low masonry stiffness, leading to a less conservative evaluation.

The DIN simplified formulation does not consider different factors on the calculation of the acting bending moment to the wall/slab connection. For instance, the vertical load applied on the top of the wall or the actual evolution of the interfaces stiffness.

- The loss of stiffness due to the development of the *cracked state*, i.e. when the tensile strength of the interface is exceeded by the tensile stress acting to the wall/slab connection, leads the bending moments to drastically decrease and, as a consequence, the eccentricity decreases to a small value. When the interface fails, the DIN formulation does not consider the actual behaviour of the cracked structure. In *cracked state*, the calculation of the eccentricity used to calculate the load bearing capacity shall be made using non-linear analysis, which consider the loss of contact and the redistribution of the forces. This behavior is discussed in Chapter 7.
- The precision of the DIN formulation is analyzed with respect to the FEM simulations. It is possible to notice that the bending moment calculated in the *uncracked state* with the analytic formulation are generally higher than those obtained with non-linear FEM analysis. This leads to an underestimation of the real load bearing capacity for short walls in *uncracked state*. Furthermore, the precision is higher for low value of the vertical force applied on the upper wall. This is discussed in Chapter 6.
- The DIN formulation does not consider the vertical force applied on the top of the wall, which is actually important for the bending moment calculation, especially for the *cracked state* of the wall/slab connection. For low value of the vertical load applied on the upper wall, it is more likely that the interface going to fail. As a consequence of the interface failure, the bending moment decreases drastically for lower value of the vertical force on the top of the wall when the *cracked state* involves.
- The DIN simplified method described in Annex C, does not takes in account the different behaviour between the upper and the lower side of the slab. The upper side is that one more stressed by tensile stress and, as a consequence, the first one to fail when the slab is vertically loaded.

The structural geometry influences the final structure's behaviour. In particular, the slab position respect to the edge of the wall and the variation of the wall thickness were investigated under different load cases.

- Thanks to the FEM simulations three different behaviour are identified in relation to the relative position of the slab to the wall. Those are described in Chapter 7.
- The wall thickness is a parameter which changes the wall slenderness. Different wall thickness cases were analysed. As a result, a reduction of the actual bending moment acting to the wall slab connection was detected on the basis of the reduction of the wall slenderness. The load bearing capacity shows a decrement whit increment of wall slenderness. The results are discussed in Chapter 8.

The mechanical parameters were investigated, varying the elastic modulus of the different elements of the structure, in particular the masonry wall and the slab.

- The wall rigidity is influenced by the rigidity of the single elements which composed the masonry and by the mortar interface mechanical characteristics, like the interface tensile strength. The higher the single stone elastic modulus is, the higher the bending moment transferred to the wall slab connection is, because the flexural stiffness is proportional to the elastic modulus of the wall. The higher moments leads to higher eccentricity, which influenced the load bearing capacity, by decreasing it. The results are discussed in Chapter 9.
- The slab rigidity depends on the mechanical characteristics of the concrete. The higher the slab elastic modulus is, the lower the bending moment transferred to the joint is. For this reason the eccentricity developed will be lower and, on the contrary, the load bearing capacity will be higher, until there is the *uncracked state*.

## 12 References

- A.W.Hendry, B.P.Sinha, & S.R.Davies. (2004). Design of Masonry Structures. *Third edition of Load Bearing Brickwork Design*. Edinburgh.
- ATENA Program Documentation. (2016).
- Awni, & Hendry, A. W. (1981). The Compressive Strength of Brick Masonry Walls with reference to Wall/Floor Slab interaction. Edinburgh.
- Awni, A., & Hendry, A. W. (n.d.). A Simplified Method for Eccentricity Calculation.
- Colville, J. (1978). Simplified Design of Load Bearing Brick. *Proceedings of the British Ceramic society*.
- Curtin, W., Shaw, G., Beck, J., & Bray, W. (1983). *Loadbearing brickwork crosswall construction*.
- DIN EN 1052-1. (1998). *Prüfverfahren für Mauerwerk. Teil 1: Bestimmung der Druckfestigkeit*.
- DIN EN 1996-1-1/NA:2012-05 National Annex - Nationally determined parameters - Eurocode 6: Design of masonry structures - Part 1-1: General rules for reinforced and unreinforced masonry structures. (2012).
- DIN EN 772-1. (2000). *Prüfverfahren für Mauersteine. Teil 1: Bestimmung der Druckfestigkeit*. Berlin.
- EN 1996 1-1. (2005). *Design of masonry structures. Part 1-1: General rules for reinforced and unreinforced masonry structures*.
- Graubner, C.-A. (2014). *Statikhandbuch Berechnung, Bemessung, Beispiele*. Darmstadt: Kaksandstein.
- Hailer, P. (1969). *Load capacity of Brick Masonry*. Gulf Pub Co.
- Hilsdorf, H. K. (1969). *Investigation into the failure mechanism of Brick Masonry loaded in axial compression*. Gulf Pub Co.
- Islam, M. M., Siddique, A., & Chowdhury, M. A. (2014). Critical investigation of the finite element models of steel fiber reinforced concrete (SFRC): evaluation of the governing parameters to predict the flexural capacities.
- Jäger, W., & Baier, G. (2007). *Außenwand-Decken-Knoten im einschaligen Mauerwerk mit nur teilweise eingebundener Decke nach EC 6*. Dresden.
- Jäger, W., Baier, G., & Thieme, M. (2004). Kosteneinsparung durch wirklichkeitsnahe Erfassung des Tragverhaltens von Mauerwerksbauten.
- Jäger, W., Pflücke, T., Waurig, R., Figge, D., & Meyer, U. (2002). *Bemessung von Ziegelmauerwerk*.
- Kukulski, W. a. (1966). Resistance des Murs en Béton non Armé Soumis à des Charges Verticales. *Cahiers CSTB NO. 681*.
- Lourenco, & B., P. (1996). Computational Strategy for Masonry Structures.

- Mier, J. V. (1984). *Strain-softening of concrete under multiaxial loading conditions*. Eindhoven.
- Pi, Y.-L., & Gilbert, R. I. (2007). Geometric and material nonlinear analyses of elastically restrained arches. *Engineering Structures* · March 2007.
- Pluijm, R. V. (1992). Material properties of masonry and its components under tension and shear. *Proc. 6th Canadian Masonry Symposium*.
- Pluijm, R. V. (1993). Shear behavior of bed joints. *Proc. 6th North American Masonry Conference*.
- Recommended Practice for Engineered Brick Masonry. (1969). *Brick institute of America*.
- Sahlin, S. (1959). *Structural Interaction of Walls and Floor*.
- Sahlin, S. (1971). *Structural Masonry*. Prentice-Hall.
- Sahlin, S. (2004). Plea for an EN Standard Test of Floor/Sill Joint.
- Sandoval, C. (2011). Testing and numerical modelling of buckling failure of masonry walls. *Construction and Building Materials*.
- Schubert, P. a. (1994). Compressive strength of mortar in masonry: Significance, influences, test methods, requirements. *Proc. 10th Int. Brick and Block Masonry Conference*.
- Vonk, R. (1992). *Softening of concrete loaded in compression*. Eindhoven.

## Annex A – Load Cases

### - Variation of slab position

**a=0 mm**

Load case	N [kN]	P [kN]
LC1	500	6,25
LC2	500	10,00
LC3	400	6,25
LC4	400	10,00
LC5	300	6,25
LC6	300	10,00
LC7	200	6,25
LC8	200	10,00
LC9	100	6,25
LC10	100	10,00
LC11	50	6,25
LC12	50	10,00
LC13	20	6,25
LC14	20	10,00

Table 12-1 Load cases

**a=50 mm**

Load case	N [kN]	P [kN]
LC1	500	6,25
LC2	500	10,00
LC3	400	6,25
LC4	400	10,00
LC5	300	6,25
LC6	300	10,00
LC7	200	6,25
LC8	200	10,00
LC9	100	6,25
LC10	100	10,00
LC11	50	6,25
LC12	50	10,00
LC13	20	6,25
LC14	20	10,00

Table 12-2 Load cases

**a=100 mm**

Load case	N [kN]	P [kN]
LC1	400	6,25
LC2	400	10,00
LC3	300	6,25
LC4	300	10,00
LC5	200	6,25
LC6	200	10,00
LC7	100	6,25
LC8	100	10,00
LC9	50	6,25
LC10	50	10,00
LC11	20	6,25
LC12	20	10,00

Table 12-3 Load cases

**a=150 mm**

Load case	N [kN]	P [kN]
LC1	400	6,25
LC2	400	10,00
LC3	300	6,25
LC4	300	10,00
LC5	200	6,25
LC6	200	10,00
LC7	100	6,25
LC8	100	10,00
LC9	50	6,25
LC10	50	10,00
LC11	20	6,25
LC12	20	10,00

Table 12-4 Load cases

**a=200 mm**

Load case	N [kN]	P [kN]
LC1	250	6,25
LC2	250	10,00
LC3	200	6,25
LC4	200	10,00
LC5	150	6,25
LC6	150	10,00
LC7	100	6,25
LC8	100	10,00
LC9	50	6,25
LC10	50	10,00
LC11	20	6,25
LC12	20	10,00

Table 12-5 Load cases

**a=250 mm**

Load case	N [kN]	P [kN]
LC1	250	6,25
LC2	250	10,00
LC3	200	6,25
LC4	200	10,00
LC5	150	6,25
LC6	150	10,00
LC7	100	6,25
LC8	100	10,00
LC9	50	6,25
LC10	50	10,00
LC11	20	6,25
LC12	20	10,00

Table 12-6 Load cases

- Variation of wall thickness

**t=365 mm**

Load case	N [kN]	P [kN]
LC1	500	6,25
LC2	500	10,00
LC3	400	6,25
LC4	400	10,00
LC5	300	6,25
LC6	300	10,00
LC7	200	6,25
LC8	200	10,00
LC9	100	6,25
LC10	100	10,00
LC11	50	6,25
LC12	50	10,00
LC13	20	6,25
LC14	20	10,00

Table 12-7 Load cases

**t=315 mm**

Load case	N [kN]	P [kN]
LC1	400	6,25
LC2	400	10,00
LC3	300	6,25
LC4	300	10,00
LC5	200	6,25
LC6	200	10,00
LC7	100	6,25
LC8	100	10,00
LC9	50	6,25
LC10	50	10,00
LC11	20	6,25
LC12	20	10,00

Table 12-8 Load cases

**t=215 mm**

Load case	N [kN]	P [kN]
LC1	300	6,25
LC2	300	10,00
LC3	200	6,25
LC4	200	10,00
LC5	150	6,25
LC6	150	10,00
LC7	100	6,25
LC8	100	10,00
LC9	50	6,25
LC10	50	10,00
LC11	20	6,25
LC12	20	10,00

Table 12-9 Load cases

**t=175 mm**

Load case	N [kN]	P [kN]
LC1	250	6,25
LC2	250	10,00
LC3	200	6,25
LC4	200	10,00
LC5	150	6,25
LC6	150	10,00
LC7	100	6,25
LC8	100	10,00
LC9	50	6,25
LC10	50	10,00
LC11	20	6,25
LC12	20	10,00

Table 12-10 Load cases

- Variation of wall elastic modulus

**E=2314 N/mm<sup>2</sup>**

Load case	N [kN]	P [kN]
LC1	300	6,25
LC2	300	10,00
LC3	200	6,25
LC4	200	10,00
LC5	150	6,25
LC6	150	10,00
LC7	100	6,25
LC8	100	10,00
LC9	50	6,25
LC10	50	10,00
LC11	20	6,25
LC12	20	10,00

Table 12-11 Load cases

**E=2629 N/mm<sup>2</sup>**

Load case	N [kN]	P [kN]
LC1	300	6,25
LC2	300	10,00
LC3	200	6,25
LC4	200	10,00
LC5	150	6,25
LC6	150	10,00
LC7	100	6,25
LC8	100	10,00
LC9	50	6,25
LC10	50	10,00
LC11	20	6,25
LC12	20	10,00

Table 12-12 Load cases

**E=2928 N/mm<sup>2</sup>**

Load case	N [kN]	P [kN]
LC1	300	6,25
LC2	300	10,00
LC3	200	6,25
LC4	200	10,00
LC5	150	6,25
LC6	150	10,00
LC7	100	6,25
LC8	100	10,00
LC9	50	6,25
LC10	50	10,00
LC11	20	6,25
LC12	20	10,00

Table 12-13 Load cases

**E=3215 N/mm<sup>2</sup>**

Load case	N [kN]	P [kN]
LC1	300	6,25
LC2	300	10,00
LC3	200	6,25
LC4	200	10,00
LC5	150	6,25
LC6	150	10,00
LC7	100	6,25
LC8	100	10,00
LC9	50	6,25
LC10	50	10,00
LC11	20	6,25
LC12	20	10,00

Table 12-14 Load cases

$$E=3492 \text{ N/mm}^2$$

Load case	N [kN]	P [kN]
LC1	300	6,25
LC2	300	10,00
LC3	200	6,25
LC4	200	10,00
LC5	150	6,25
LC6	150	10,00
LC7	100	6,25
LC8	100	10,00
LC9	50	6,25
LC10	50	10,00
LC11	20	6,25
LC12	20	10,00

Table 12-15 Load cases

- Variation of slab elastic modulus

$$E= 31000 \text{ N/mm}^2$$

Load case	N [kN]	P [kN]
LC1	400	6,25
LC2	400	10,00
LC3	300	6,25
LC4	300	10,00
LC5	200	6,25
LC6	200	10,00
LC7	100	6,25
LC8	100	10,00
LC9	50	6,25
LC10	50	10,00
LC11	20	6,25
LC12	20	10,00

Table 12-16 Load cases

**E= 33000 N/mm<sup>2</sup>**

Load case	N [kN]	P [kN]
LC1	400	6,25
LC2	400	10,00
LC3	300	6,25
LC4	300	10,00
LC5	200	6,25
LC6	200	10,00
LC7	100	6,25
LC8	100	10,00
LC9	50	6,25
LC10	50	10,00
LC11	20	6,25
LC12	20	10,00

Table 12-17 Load cases

**E= 35000 N/mm<sup>2</sup>**

Load case	N [kN]	P [kN]
LC1	400	6,25
LC2	400	10,00
LC3	300	6,25
LC4	300	10,00
LC5	200	6,25
LC6	200	10,00
LC7	100	6,25
LC8	100	10,00
LC9	50	6,25
LC10	50	10,00
LC11	20	6,25
LC12	20	10,00

Table 12-18 Load cases

$$E = 36000 \text{ N/mm}^2$$

Load case	N [kN]	P [kN]
LC1	400	6,25
LC2	400	10,00
LC3	300	6,25
LC4	300	10,00
LC5	200	6,25
LC6	200	10,00
LC7	100	6,25
LC8	100	10,00
LC9	50	6,25
LC10	50	10,00
LC11	20	6,25
LC12	20	10,00

Table 12-19 Load cases

## Annex B – FEM result for different Slab Positions

- a=150 mm

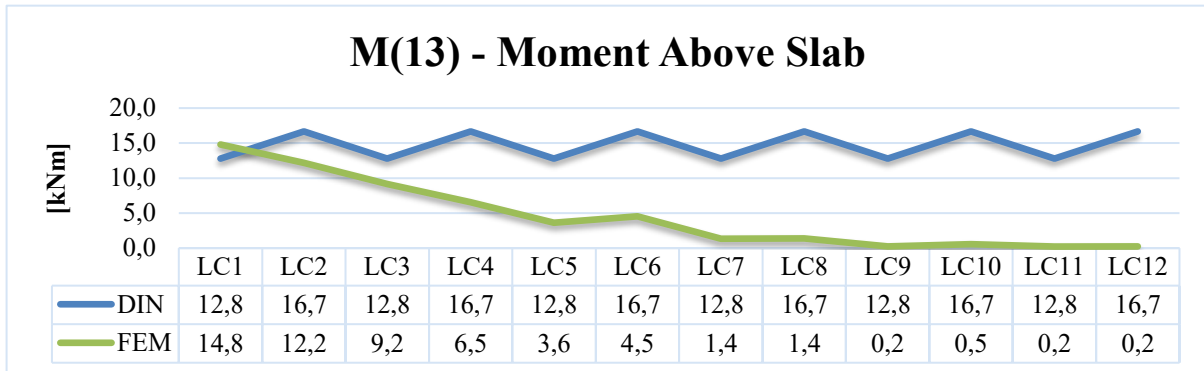


Figure B12.1 Bending moment comparison above the slab

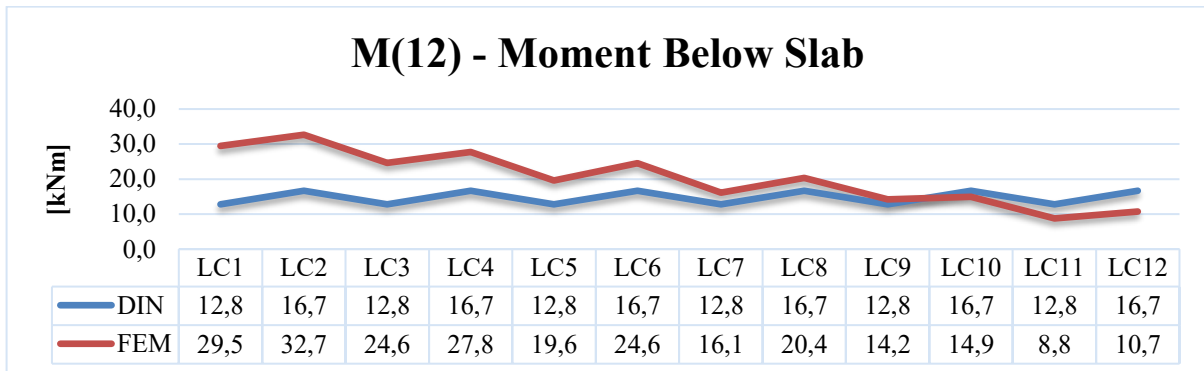


Figure B.2 Bending moment comparison below the slab

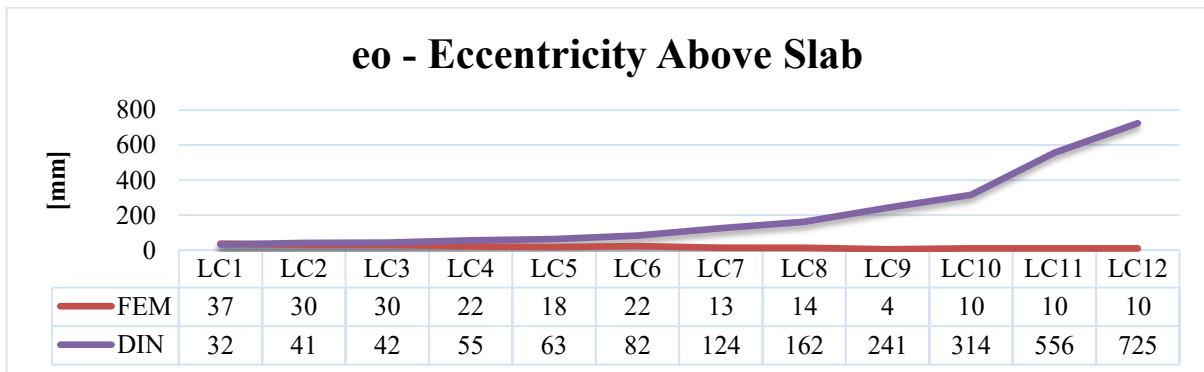


Figure B.3 Eccentricity comparison above the slab

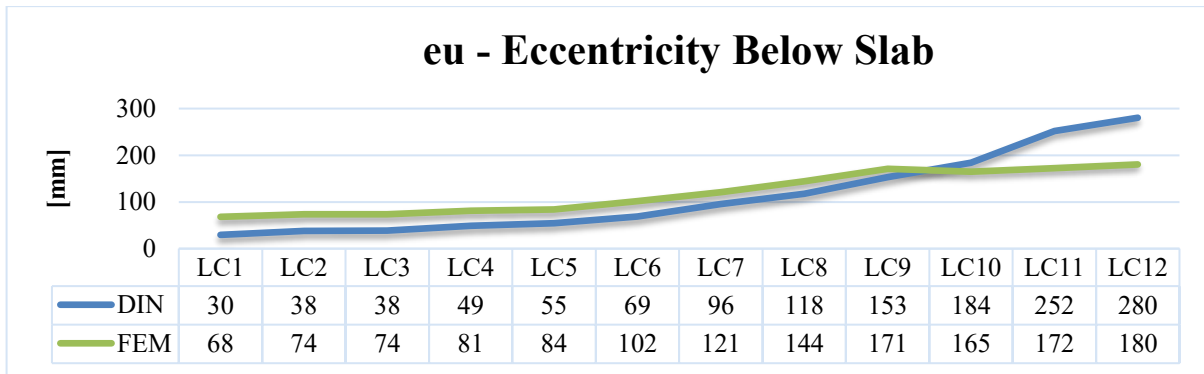


Figure B.4 Eccentricity comparison below the slab

### Error [%]

Load case	M(13)	M(12)	e <sub>o</sub>	e <sub>u</sub>
L1	13,6	56,6	13,6	56,6
L2	37,0	49,0	37,0	49,0
L3	39,3	48,1	39,3	48,1
L4	154,7	40,0	154,7	40,0
L5	252,0	34,9	252,0	34,9
L6	266,4	32,1	266,4	32,1
L7	841,3	20,6	841,3	20,6
L8	1087,2	18,2	1087,2	18,2
L9	5319,2	10,1	5319,2	10,1
L10	2940,3	11,6	2940,3	11,6
L11	5430,5	45,9	5430,5	45,9
L12	7056,2	55,4	7056,2	55,4

Table B-20 Error evaluation

- a=250 mm

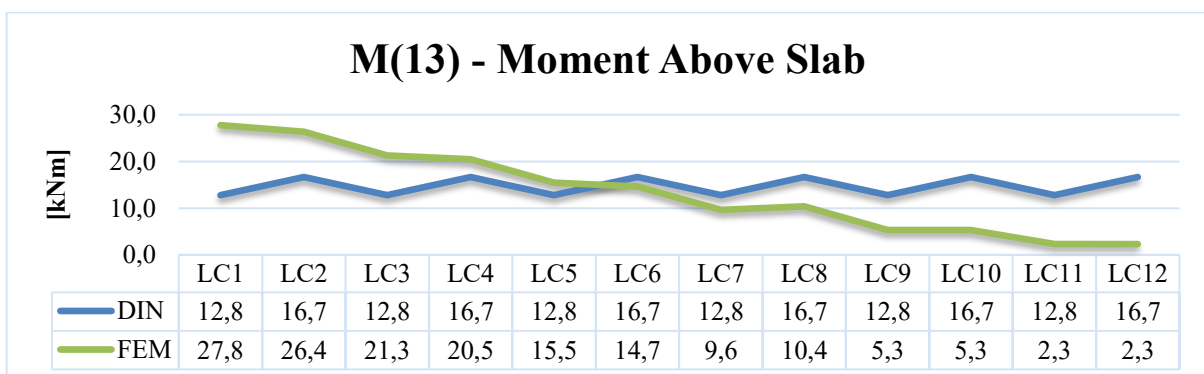
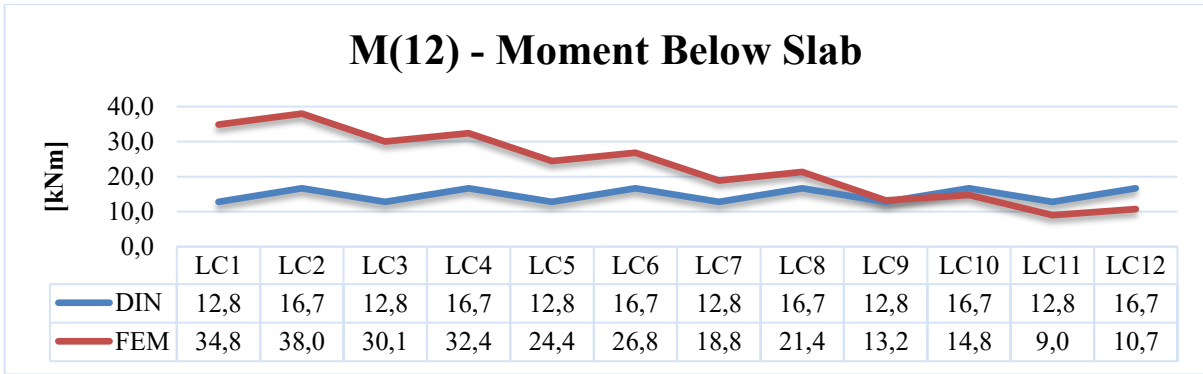
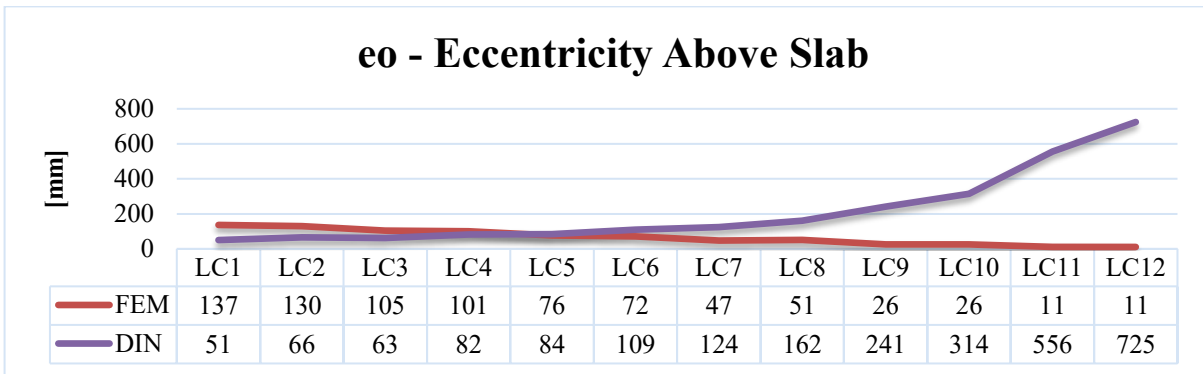


Figure B.5 Bending moment comparison above the slab



**Figure B.6 Bending moment comparison below the slab**



**Figure B.7 Eccentricity comparison above the slab**

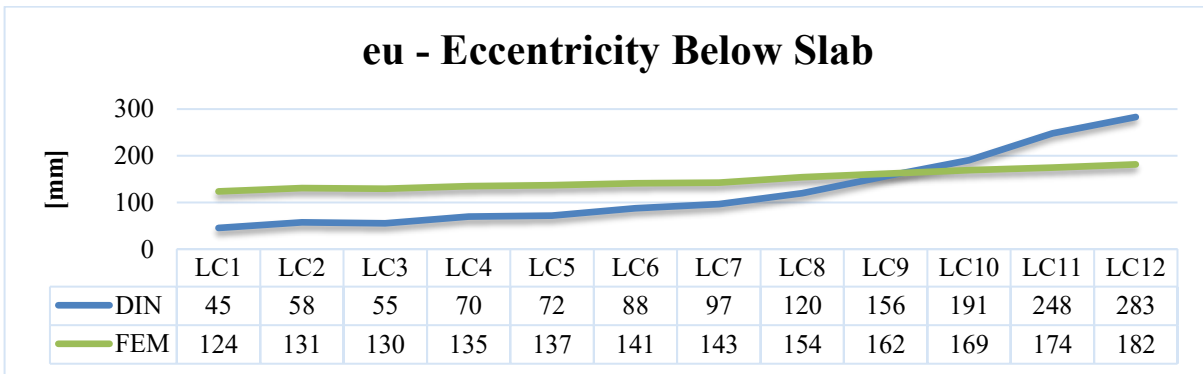


**Figure B.8 Eccentricity comparison below the slab**

### Error [%]

Load case	M(13)	M(12)	e <sub>o</sub>	e <sub>u</sub>
LC1	54,0	63,3	63,1	63,3
LC2	36,8	56,1	49,3	56,1
LC3	40,0	57,4	40,0	57,4
LC4	18,7	48,6	18,7	48,6
LC5	17,4	47,7	9,7	47,7
LC6	13,8	37,9	50,9	37,9
LC7	32,7	32,1	161,5	32,1
LC8	60,7	22,0	216,7	22,0
LC9	139,7	3,4	818,0	3,4
LC10	212,1	12,7	1095,3	12,7
LC11	451,3	42,4	4765,5	42,4
LC12	617,9	55,9	6236,5	55,9

Table B-21 Error evaluation

## Annex C – Experimental and FEM Results comparison

### EXP

Load case	Av [kN]	Cv [kN]
A4	117,84	10,53
A7	125,16	17,7
B4	66,67	11,27
B7	73,88	18,59
C4	26,95	11,92
C7	34,27	19,27

**Table C - 1 Experimental vertical binding reactions**

### FEM

Load case	Av [kN]	Cv [kN]
A4	117,41	10,96
A7	124,83	18,03
B4	66,37	11,48
B7	74,14	18,72
C4	27,69	12,14
C7	34,26	19,57

**Table C - 2 FEM vertical binding reaction**

### Error [%]

Av	Cv
0,36	4,08
0,26	1,86
0,45	1,91
0,35	0,69
2,75	1,82
0,03	1,53

**Table C - 3 Error evaluation**

## Annex D – FEM Simulation Results

- Geometrical case used for the calibration of the model

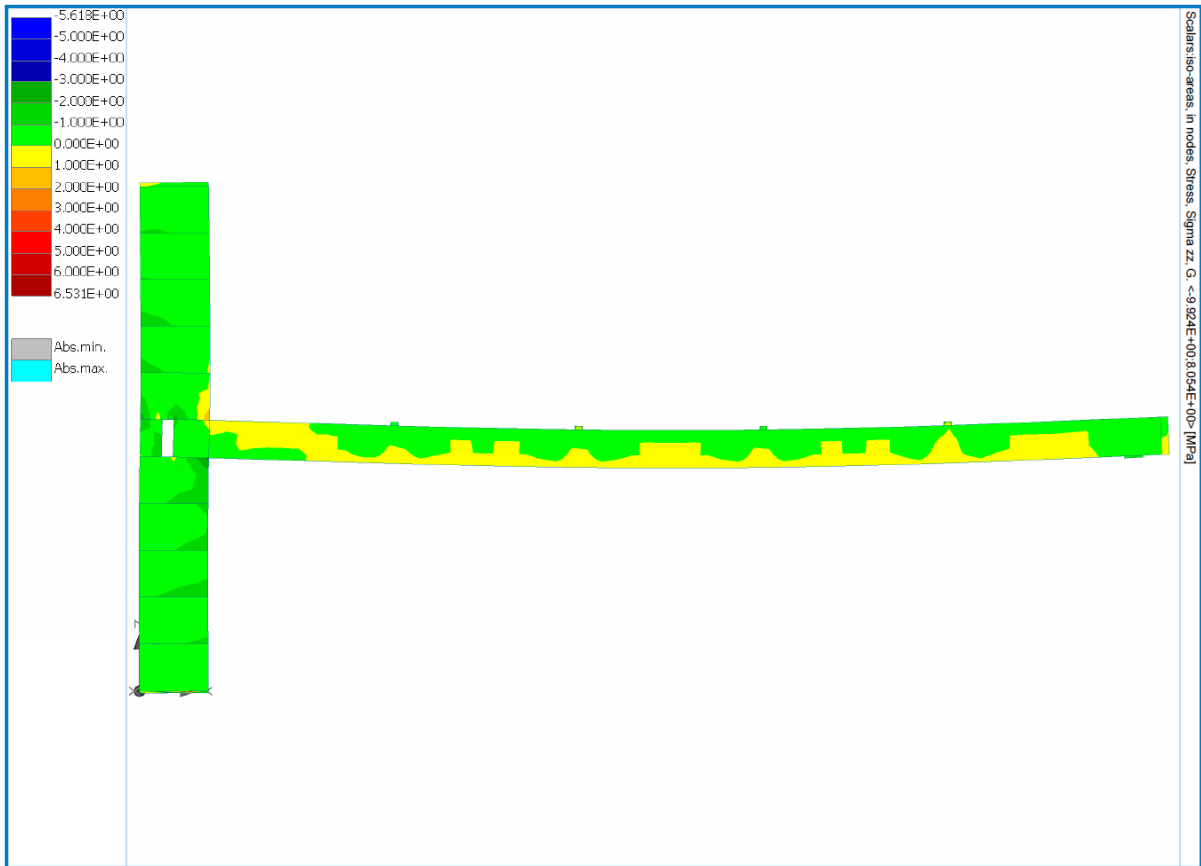


Figure D - 1 Vertical stress  $\sigma_{zz}$  iso-areas Load Case A4

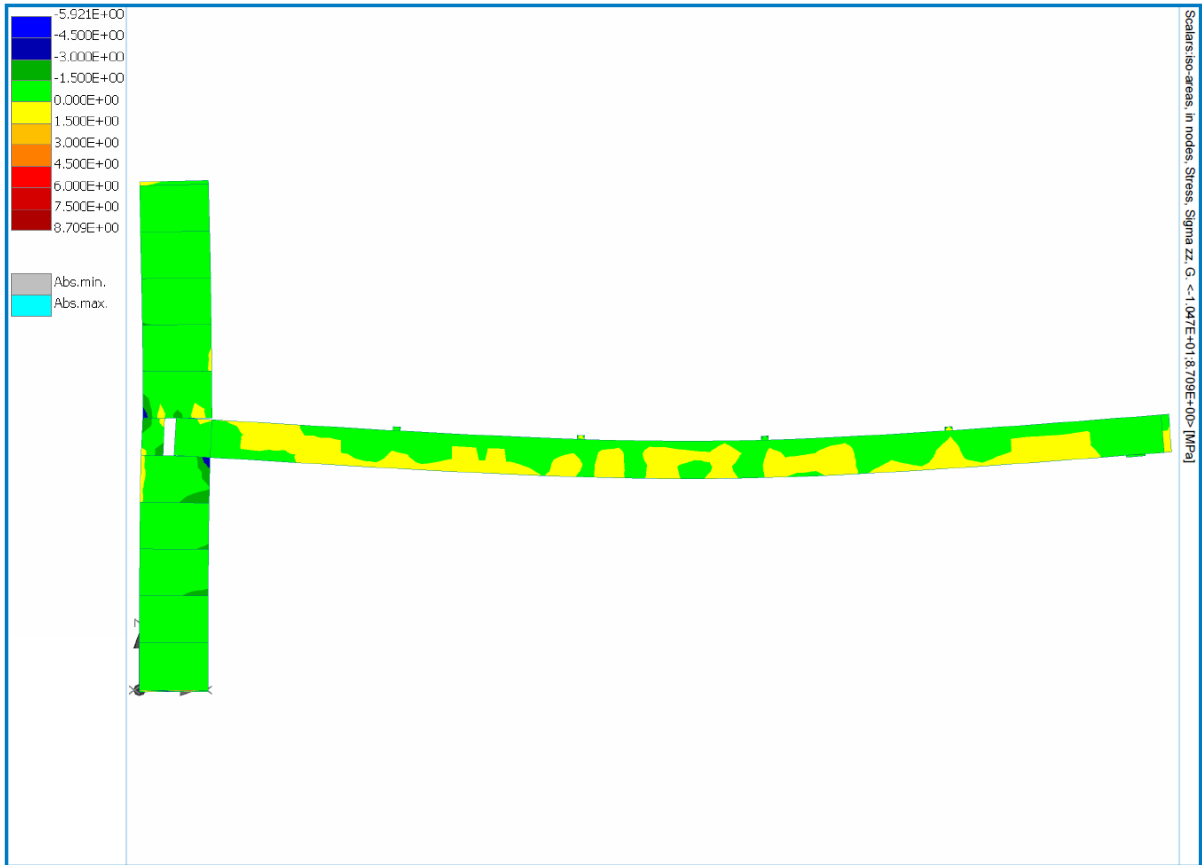


Figure D - 2 Vertical stress  $\sigma_{zz}$  iso-areas Load Case A7

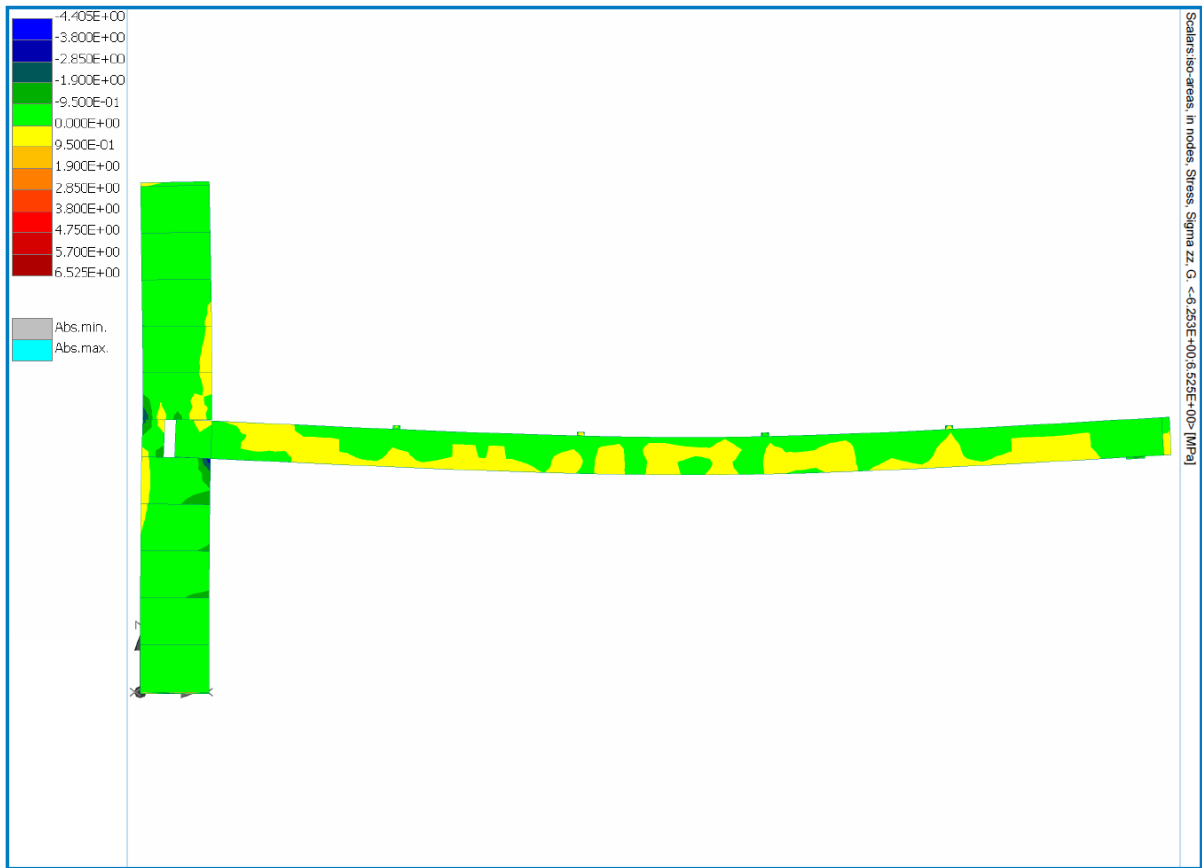


Figure D - 3 Vertical stress  $\sigma_{zz}$  iso-areas Load Case B4

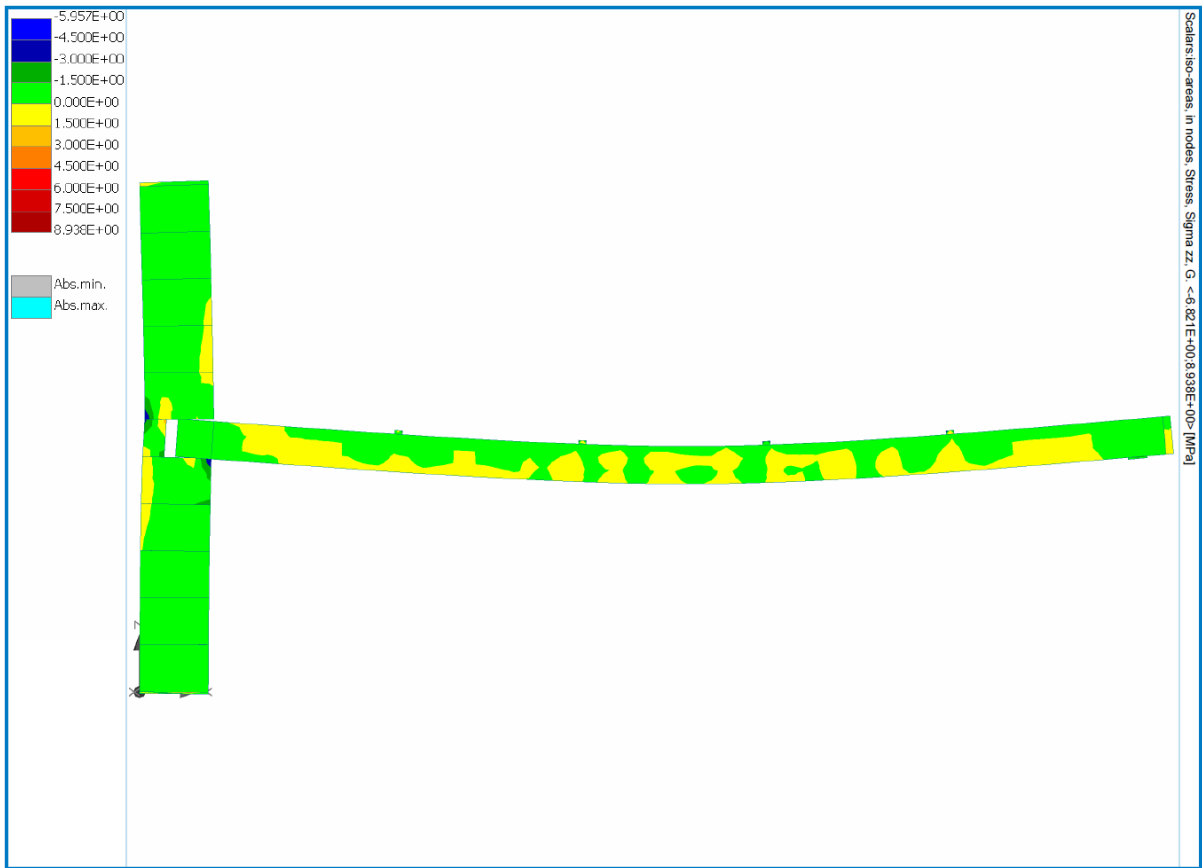


Figure D - 4 Vertical stress  $\sigma_{zz}$  iso-areas Load Case B7



Figure D - 5 Vertical stress  $\sigma_{zz}$  iso-areas Load Case C4

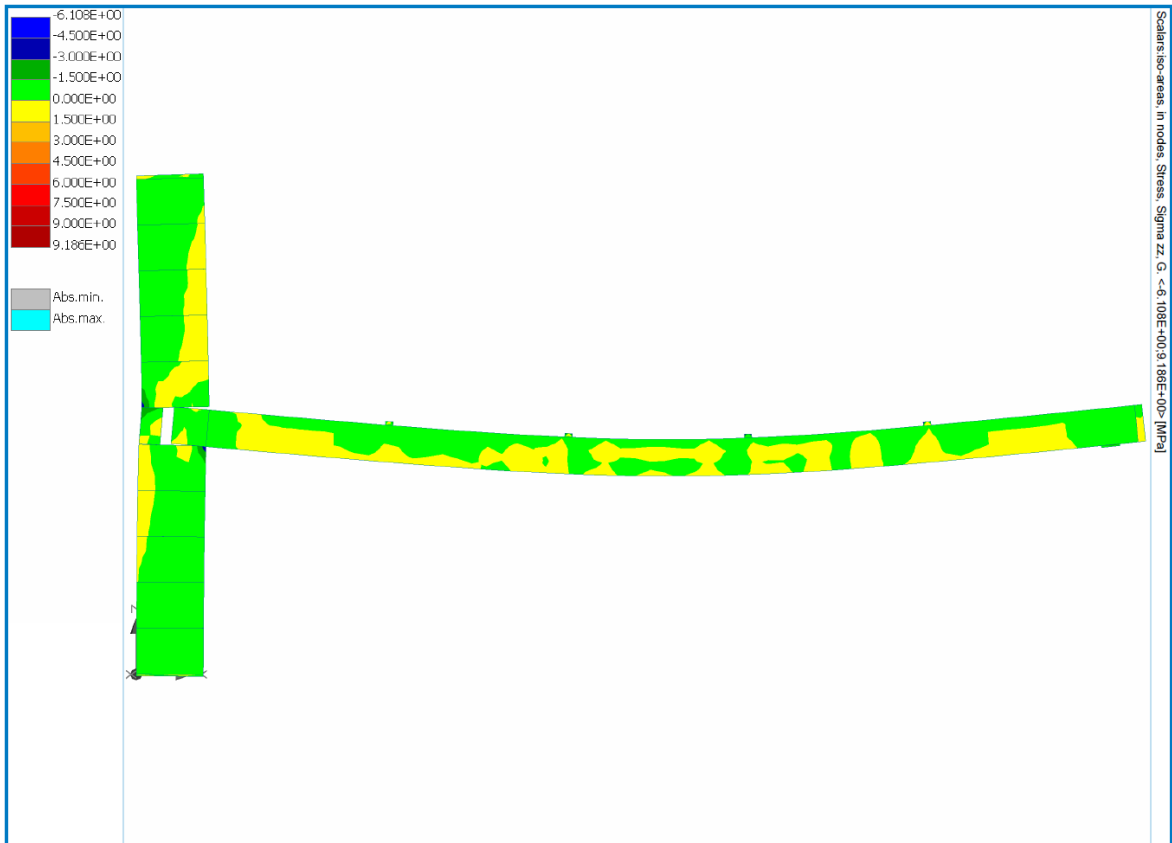


Figure D - 6 Vertical stress  $\sigma_{zz}$  iso-areas Load Case C7

- Geometrical case used for the evaluation of the load bearing capacity (a=0)

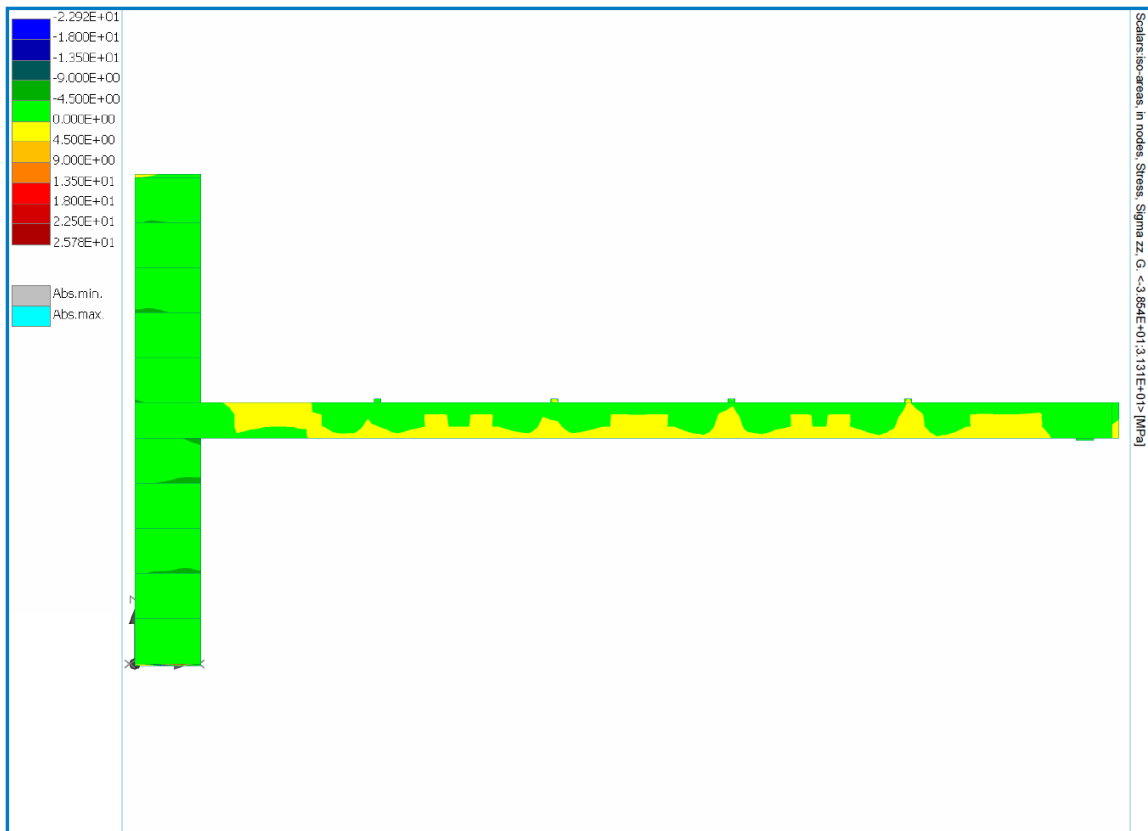


Figure D - 7 Vertical stress  $\sigma_{zz}$  iso-areas Load Case 1

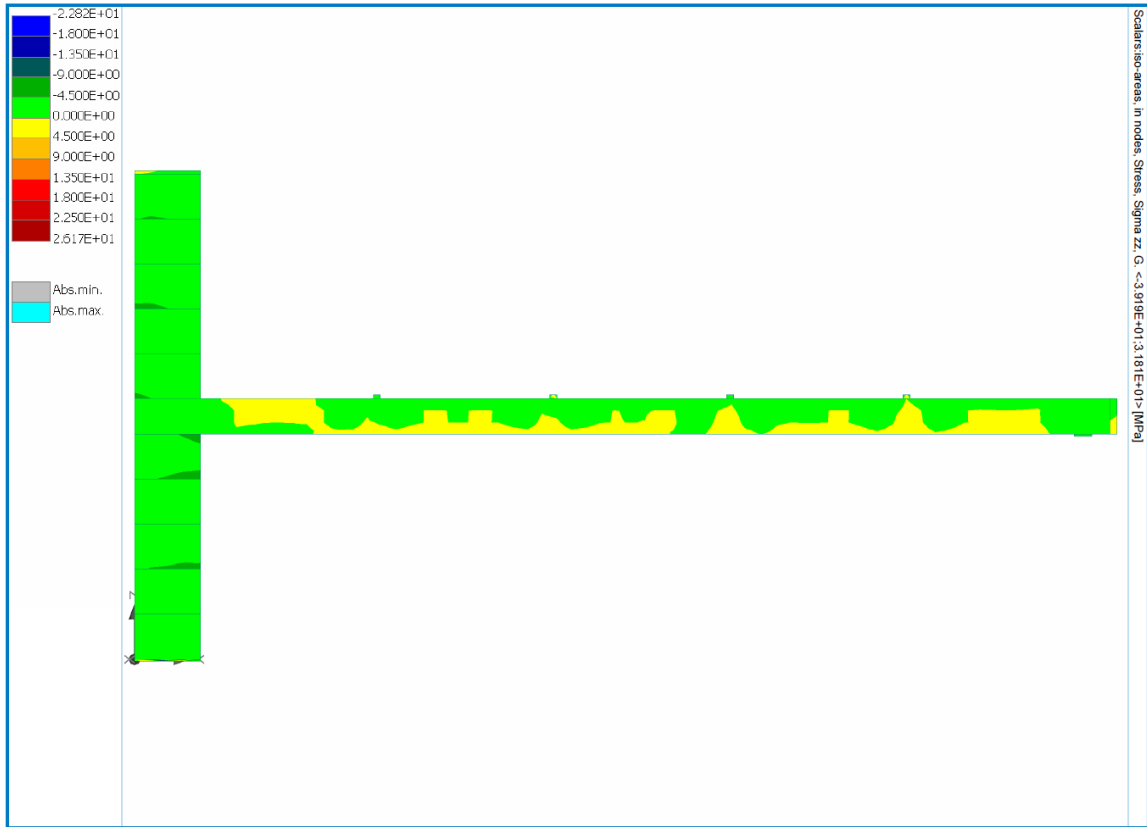


Figure D - 8 Vertical stress  $\sigma_{zz}$  iso-areas Load Case 2

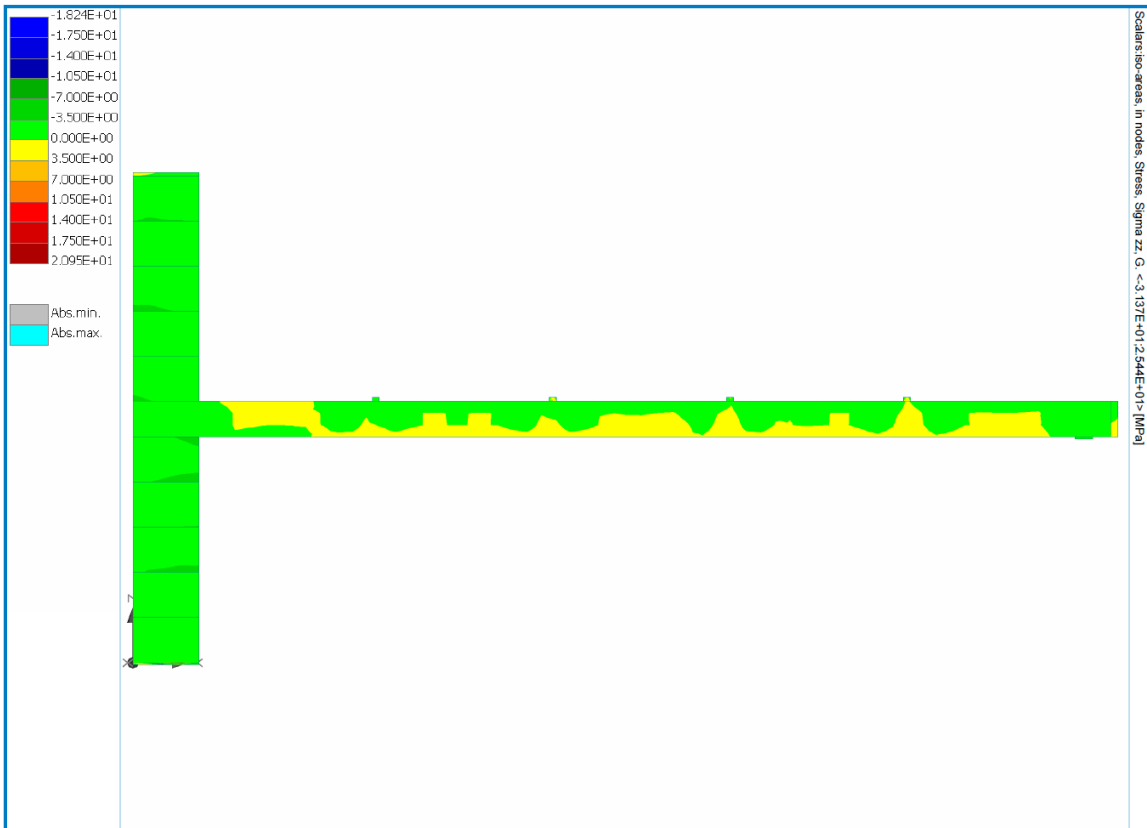


Figure D - 9 Vertical stress  $\sigma_{zz}$  iso-areas Load Case 3

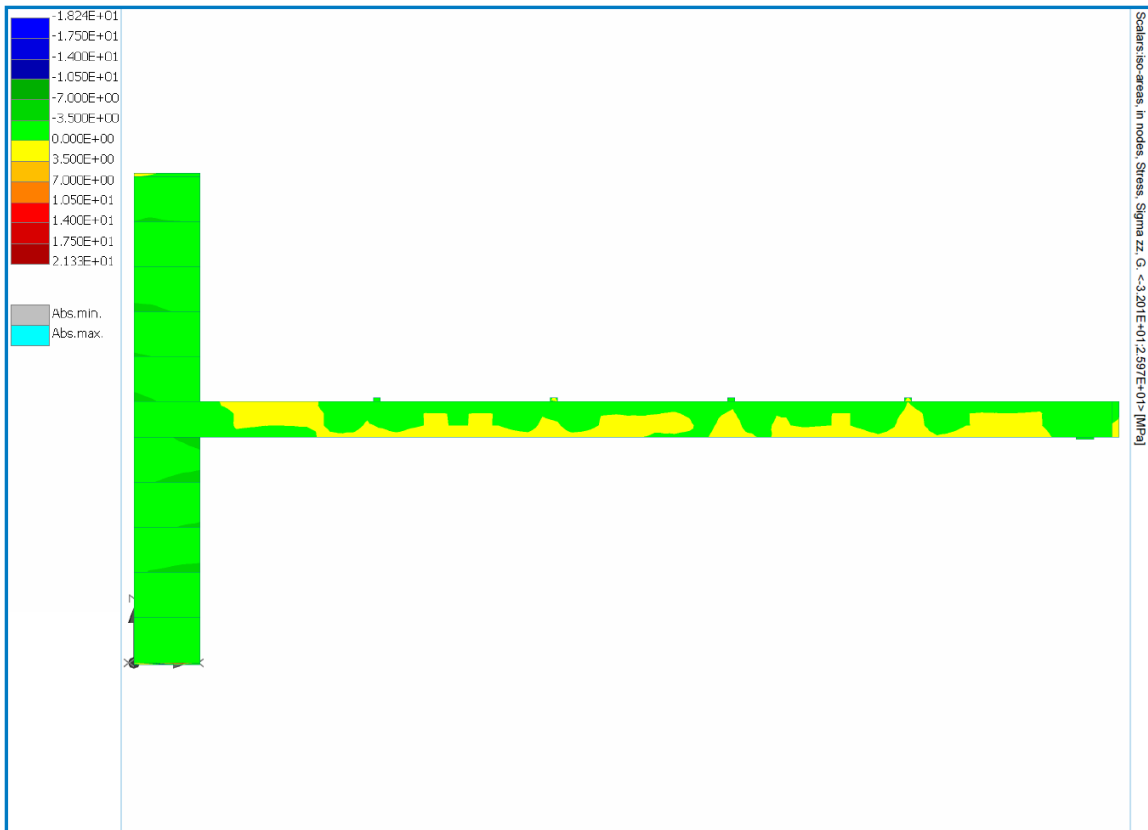


Figure D - 10 Vertical stress  $\sigma_{zz}$  iso-areas Load Case 4

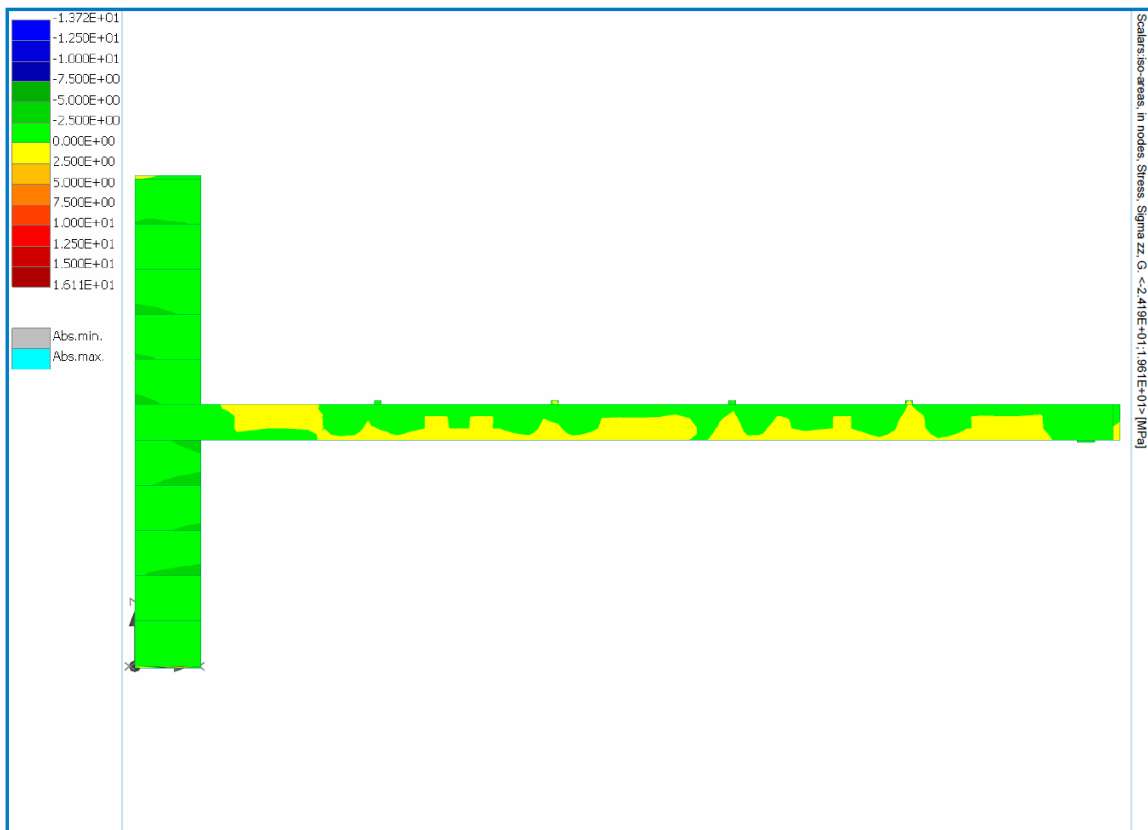


Figure D - 11 Vertical stress  $\sigma_{zz}$  iso-areas Load Case 5

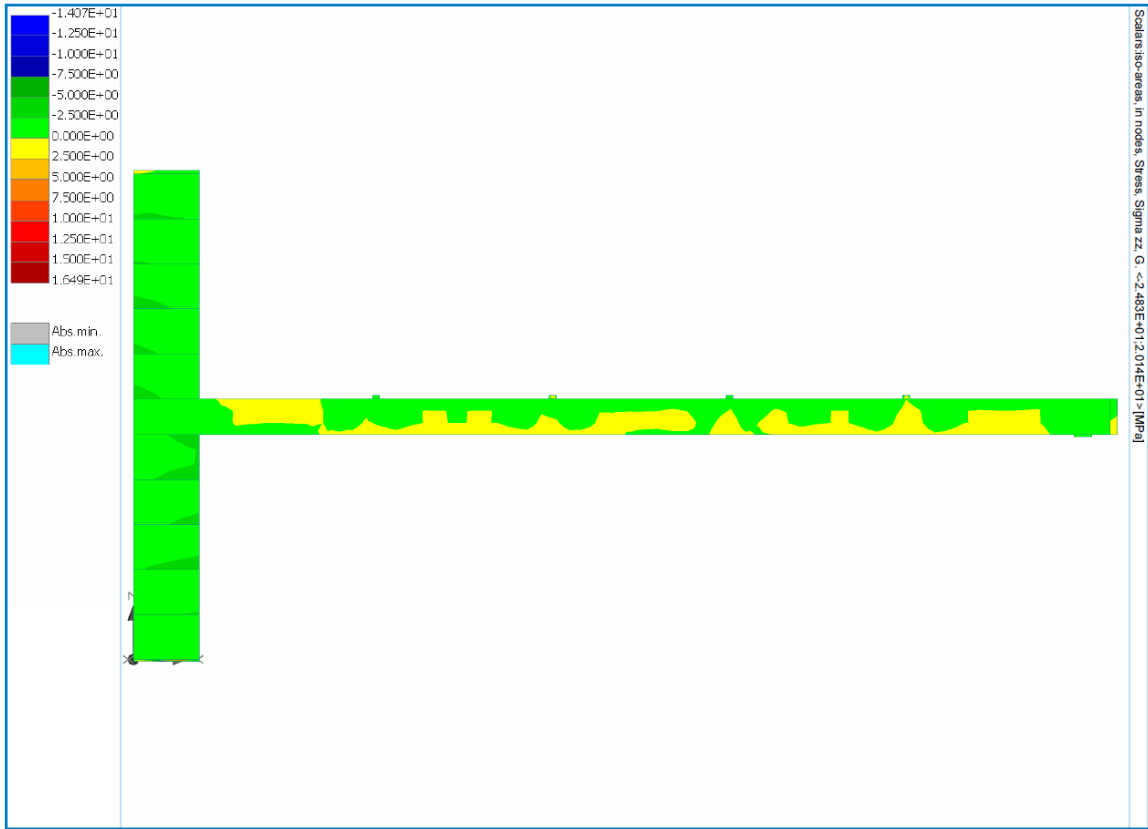


Figure D - 12 Vertical stress  $\sigma_{zz}$  iso-areas Load Case 6

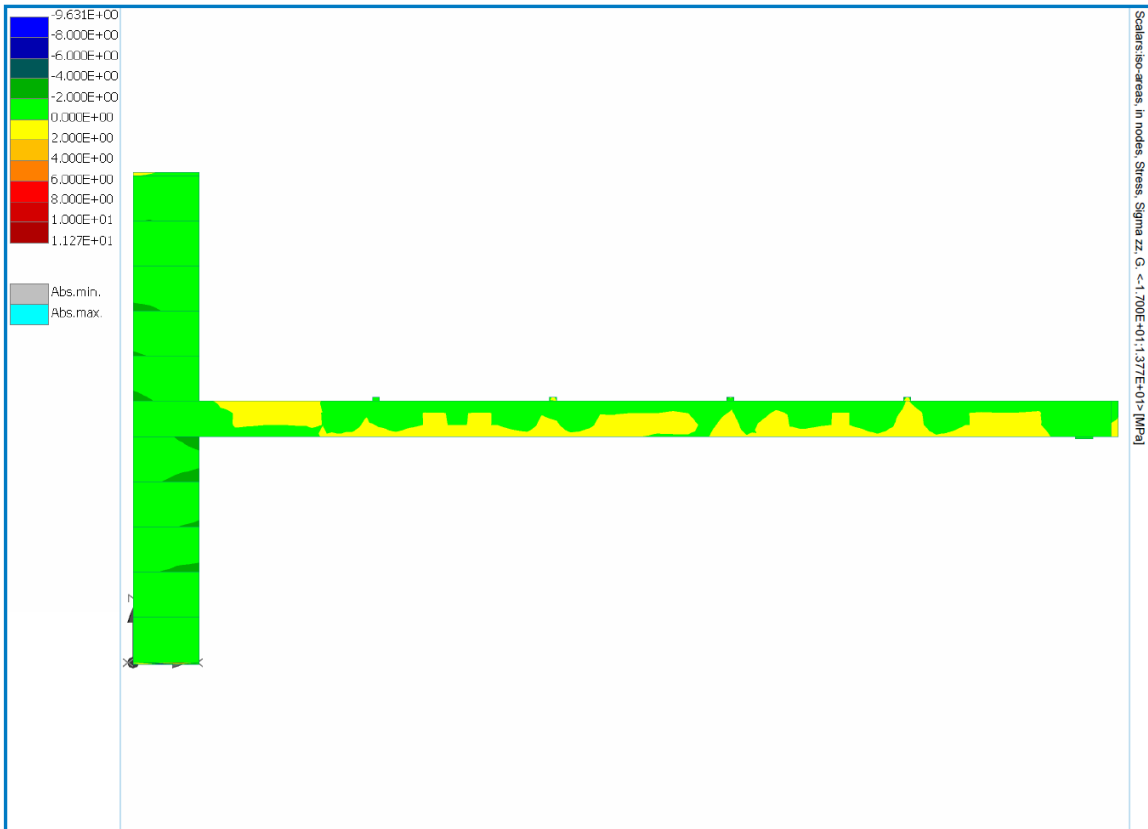


Figure D - 13 Vertical stress  $\sigma_{zz}$  iso-areas Load Case 7

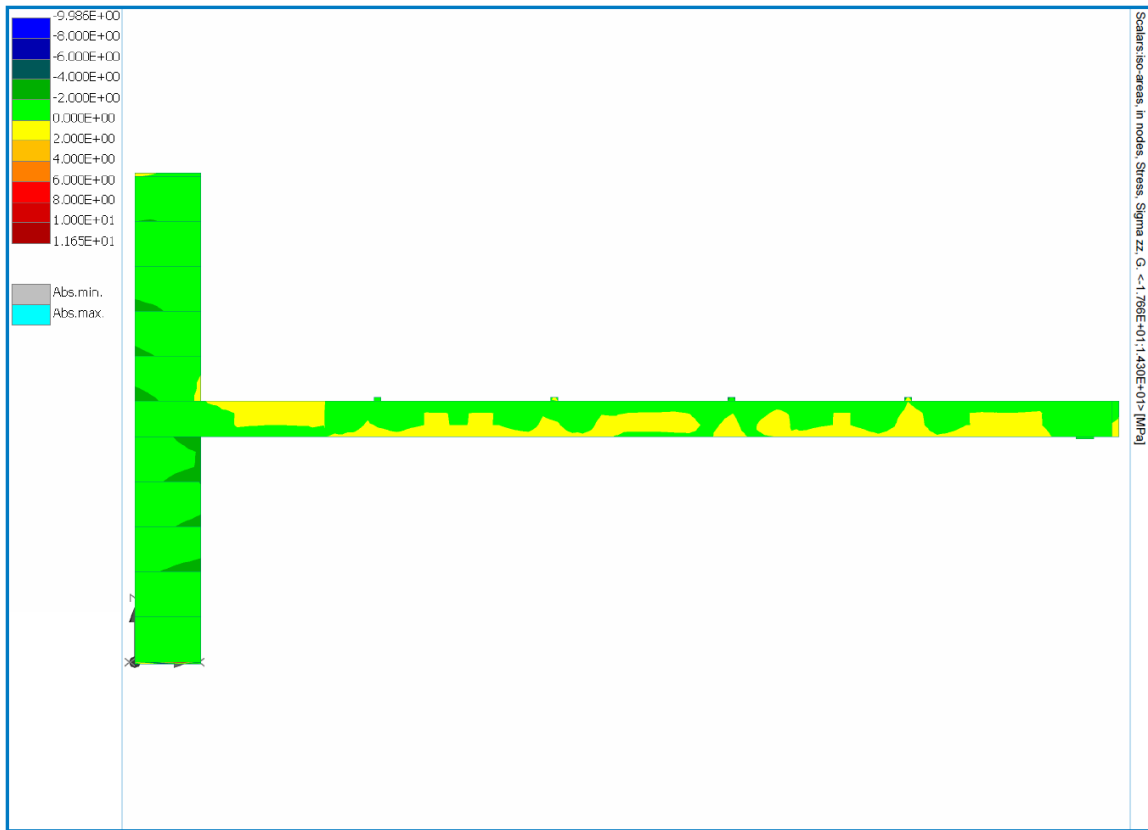


Figure D - 14 Vertical stress  $\sigma_{zz}$  iso-areas Load Case 8

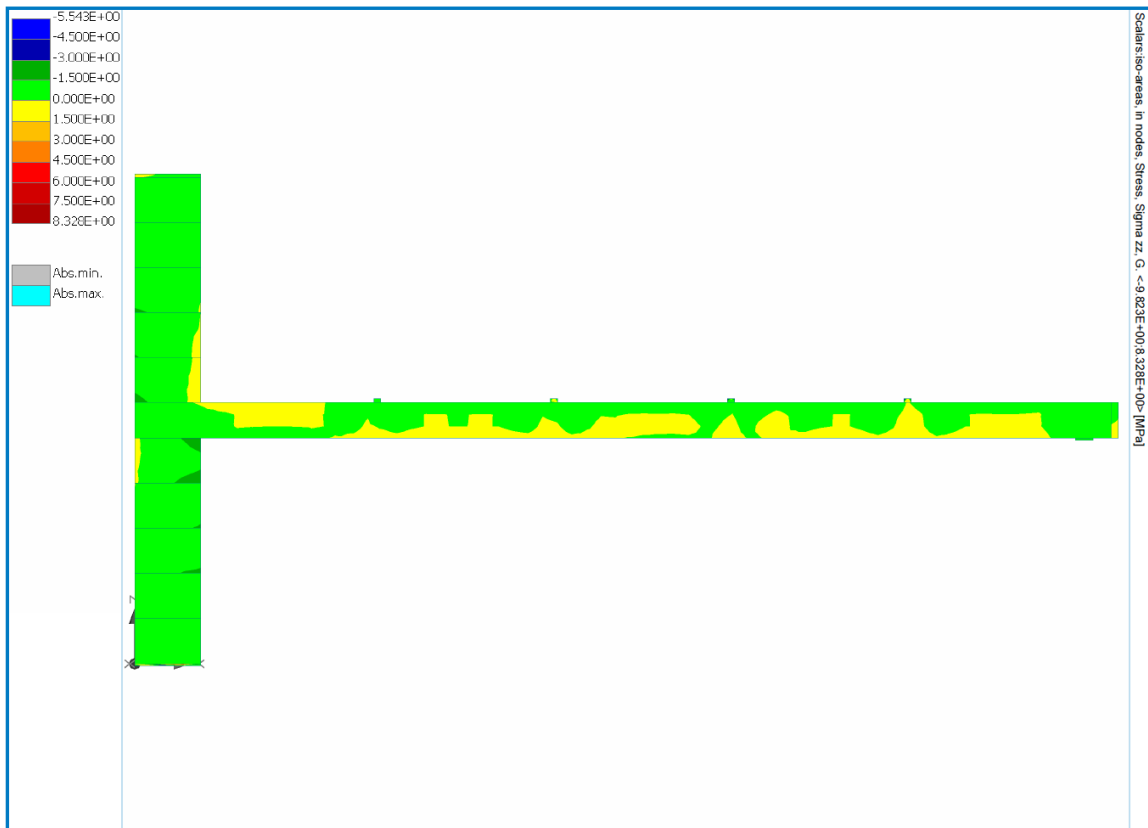


Figure D - 15 Vertical stress  $\sigma_{zz}$  iso-areas Load Case 9

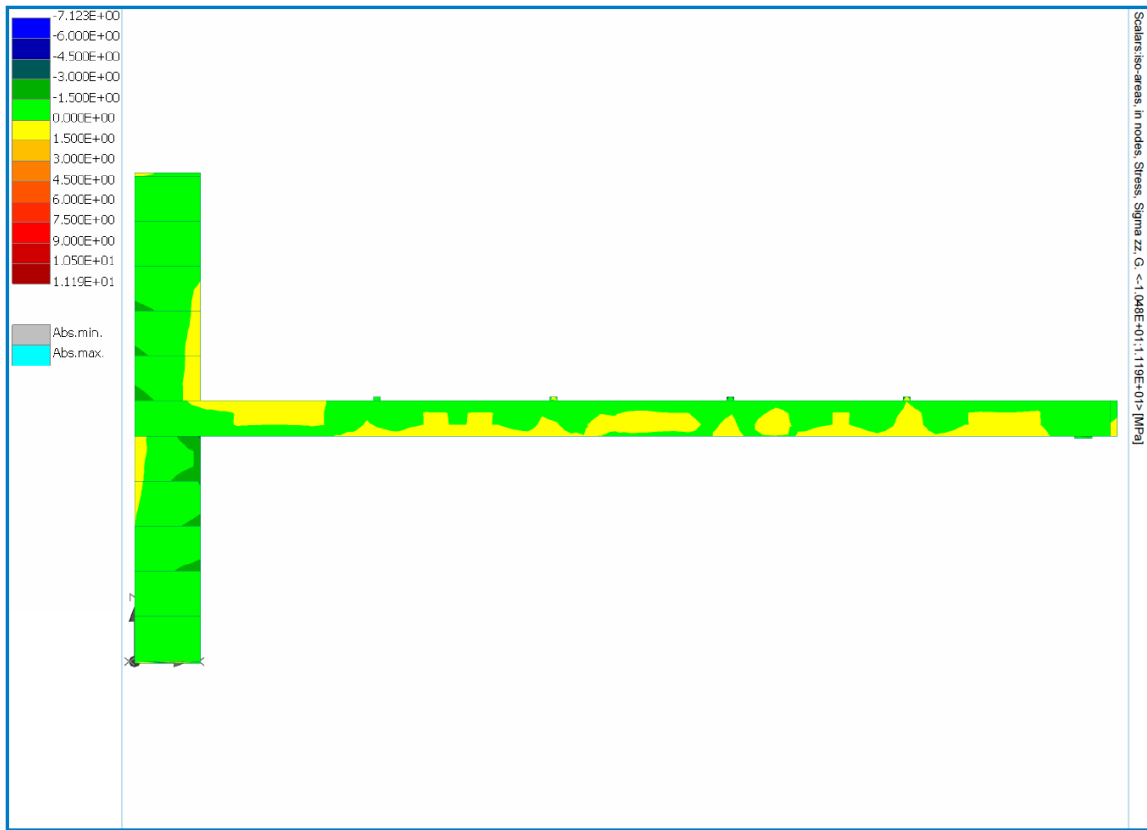


Figure D - 16 Vertical stress  $\sigma_{zz}$  iso-areas Load Case 10

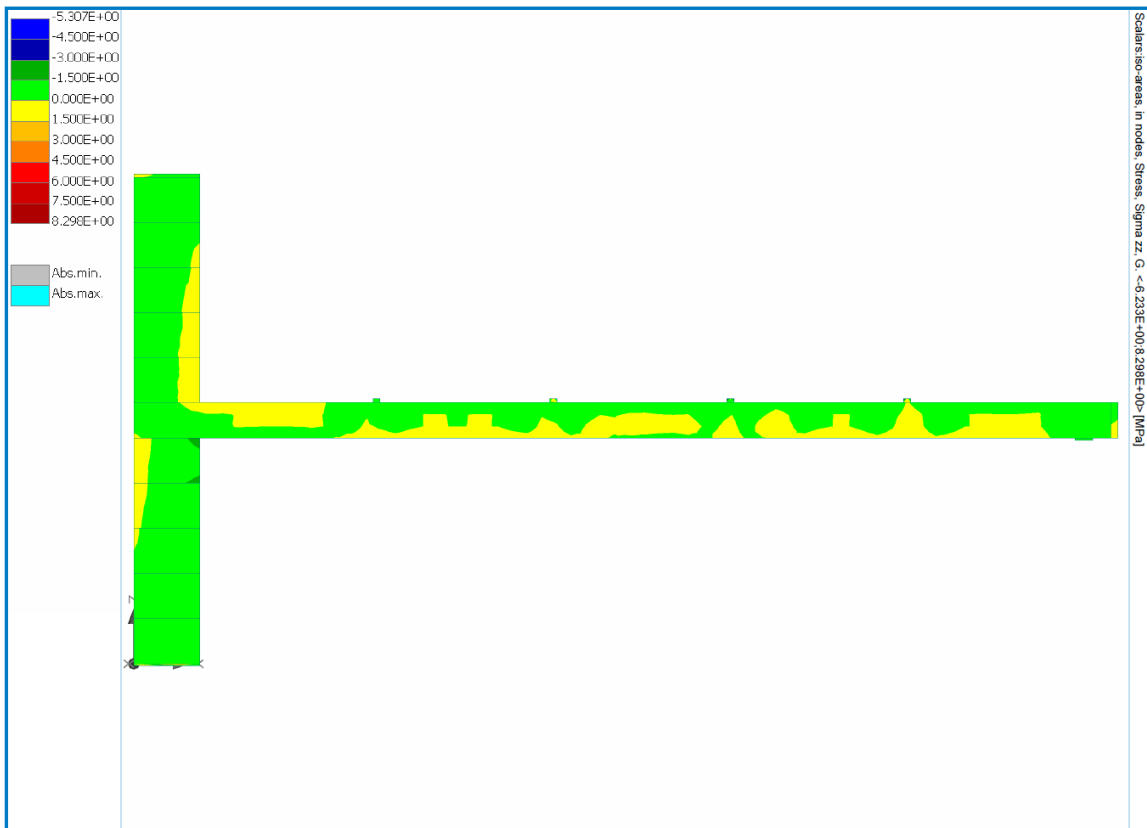


Figure D - 17 Vertical stress  $\sigma_{zz}$  iso-areas Load Case 11

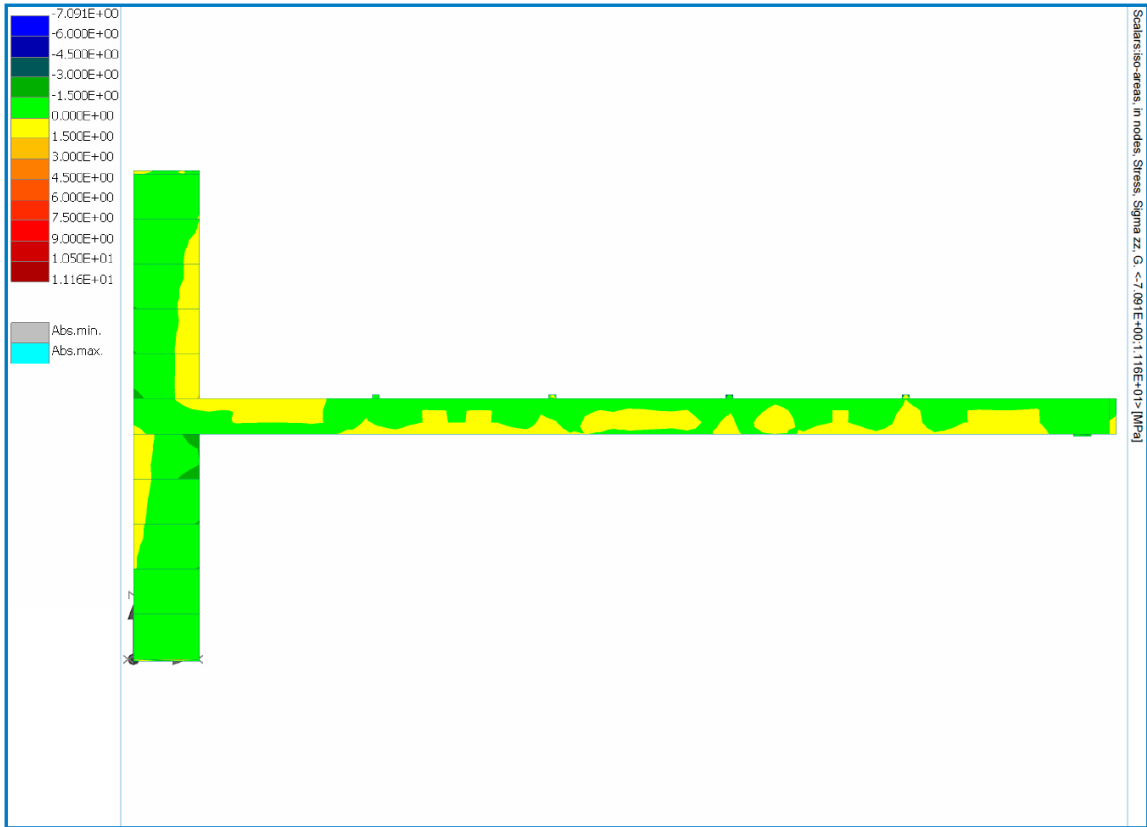


Figure D - 18 Vertical stress  $\sigma_{zz}$  iso-areas Load Case 12

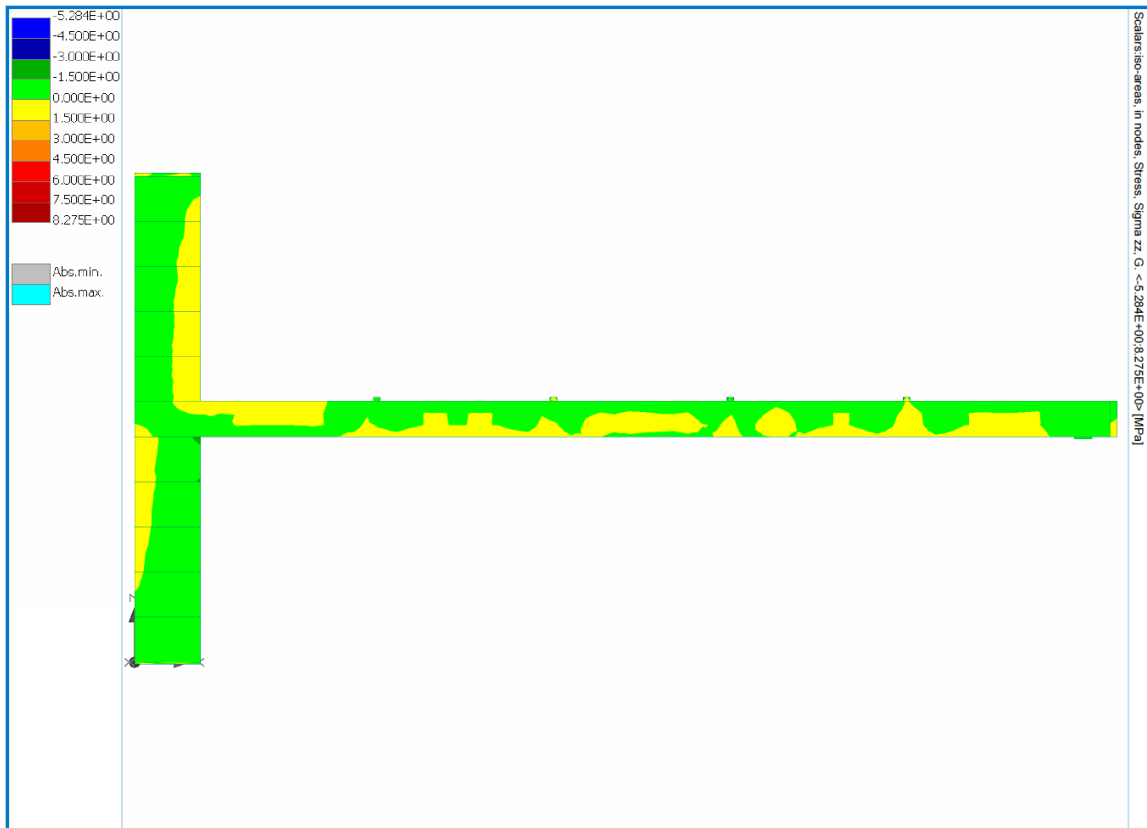
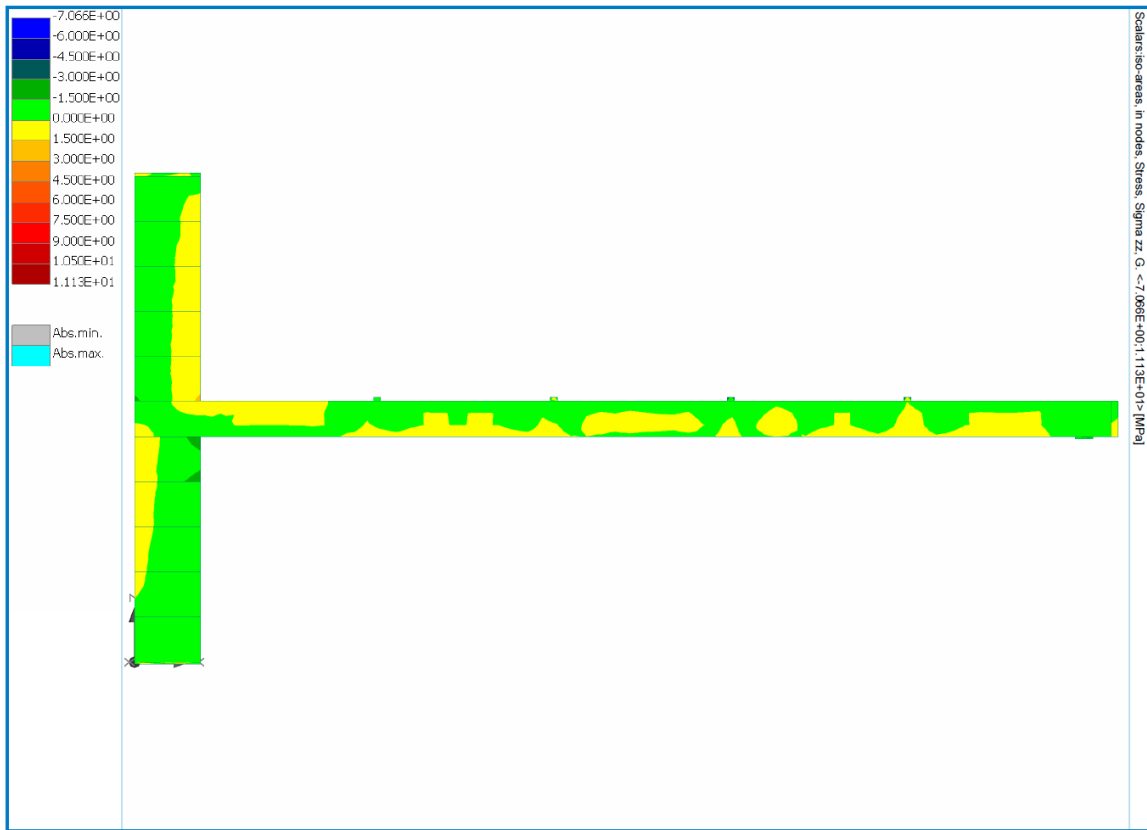


Figure D - 19 Vertical stress  $\sigma_{zz}$  iso-areas Load Case 13



**Figure D - 20 Vertical stress  $\sigma_{zz}$  iso-areas Load Case 14**

- Geometrical case: a=100 mm

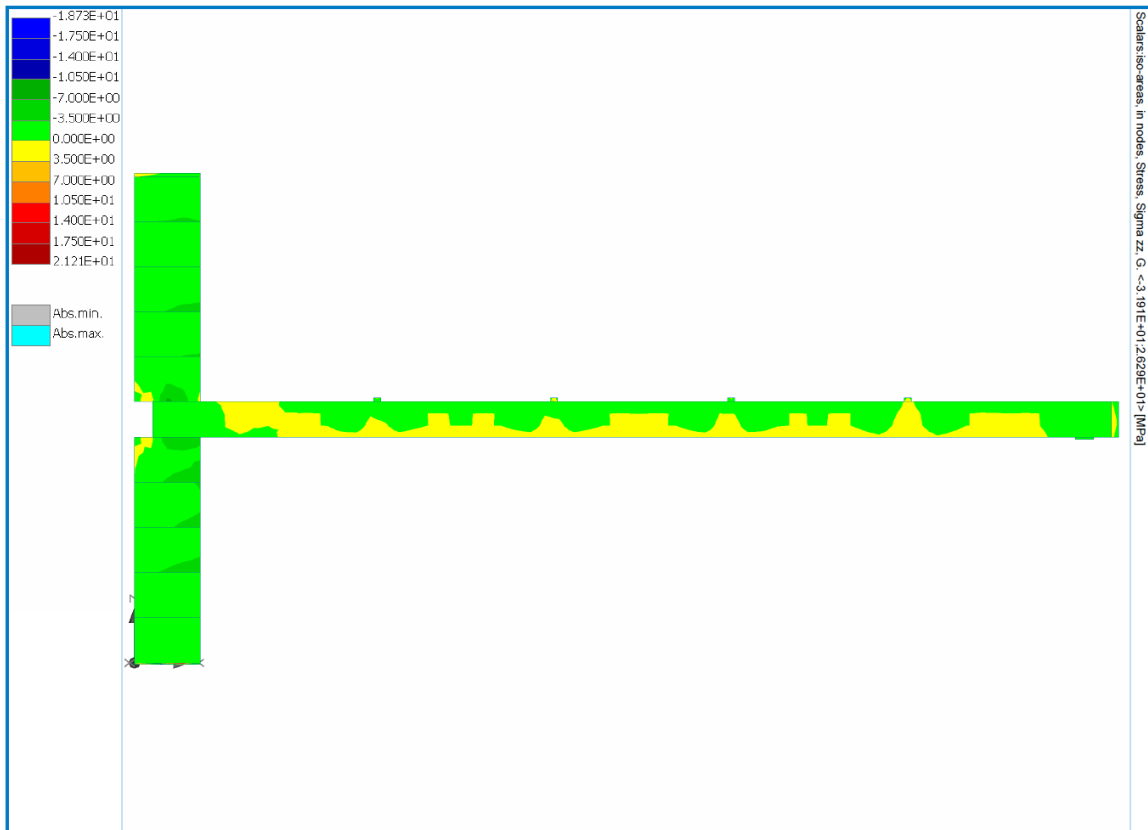


Figure D - 21 Vertical stress  $\sigma_{zz}$  iso-areas Load Case 1

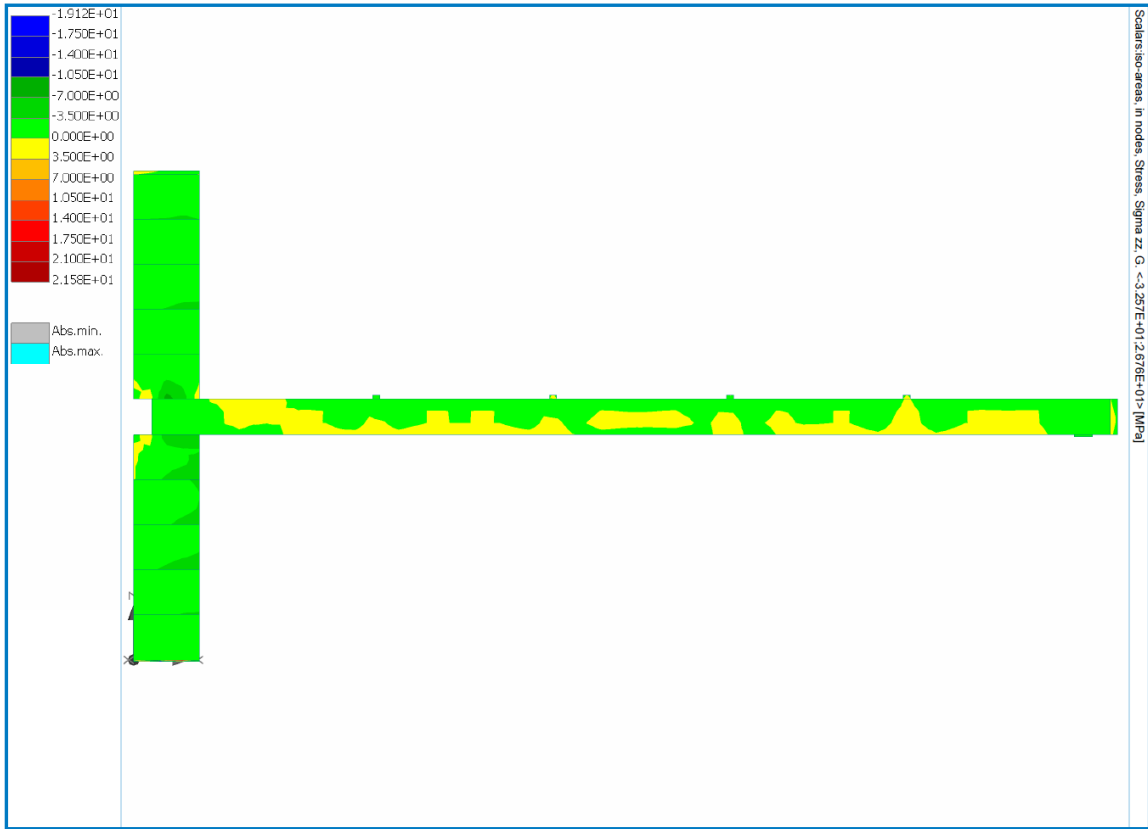


Figure D - 22 Vertical stress  $\sigma_{zz}$  iso-areas Load Case 2

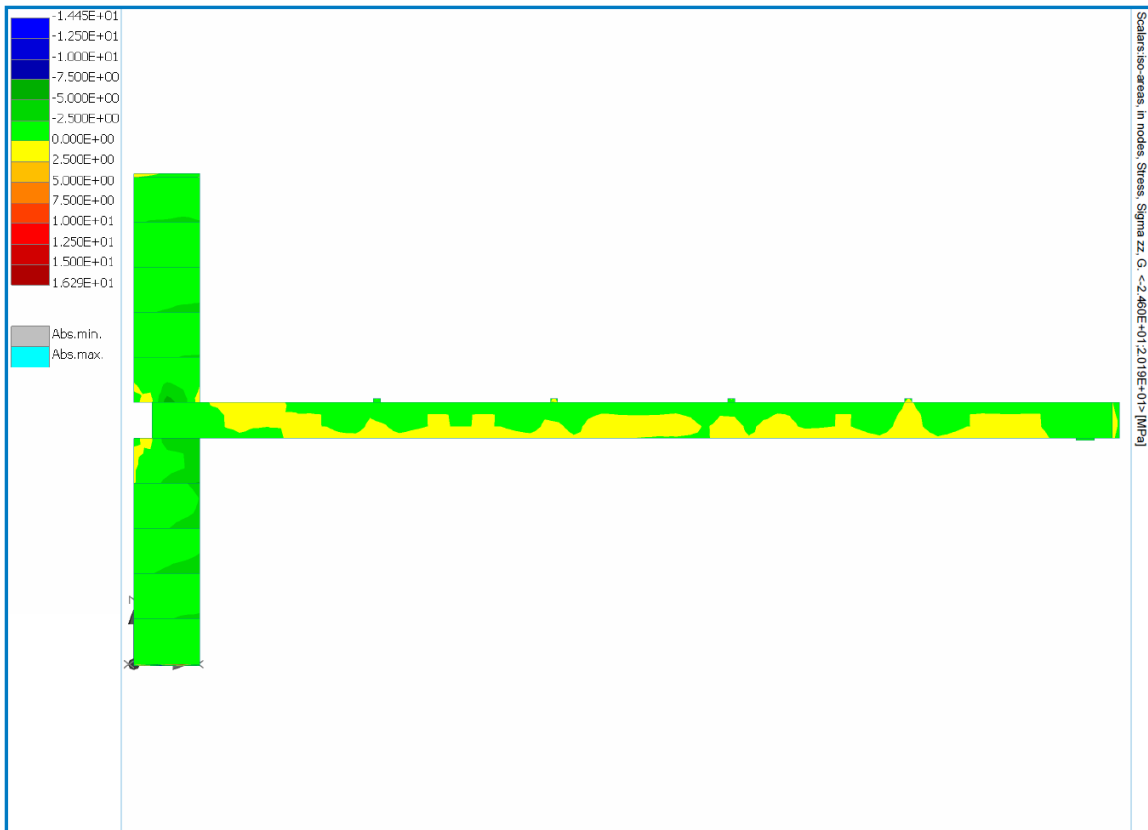


Figure D - 23 Vertical stress  $\sigma_{zz}$  iso-areas Load Case 3

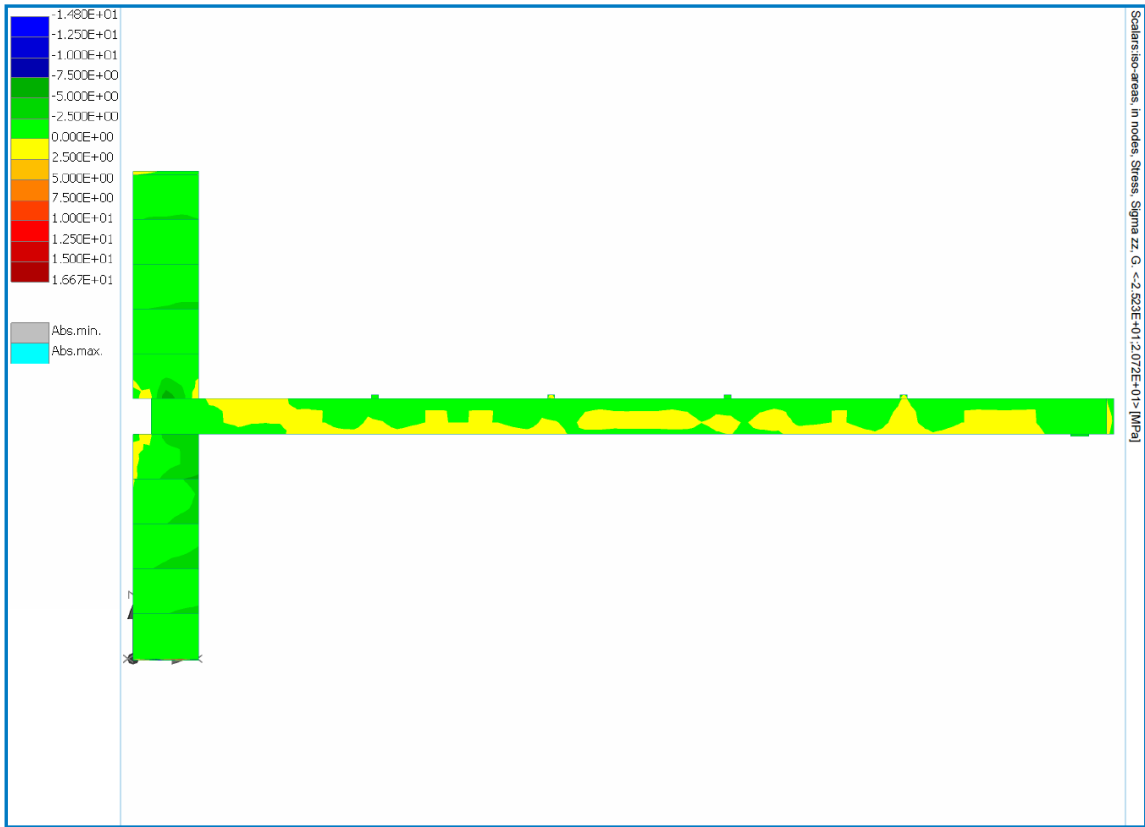


Figure D - 24 Vertical stress  $\sigma_{zz}$  iso-areas Load Case 4

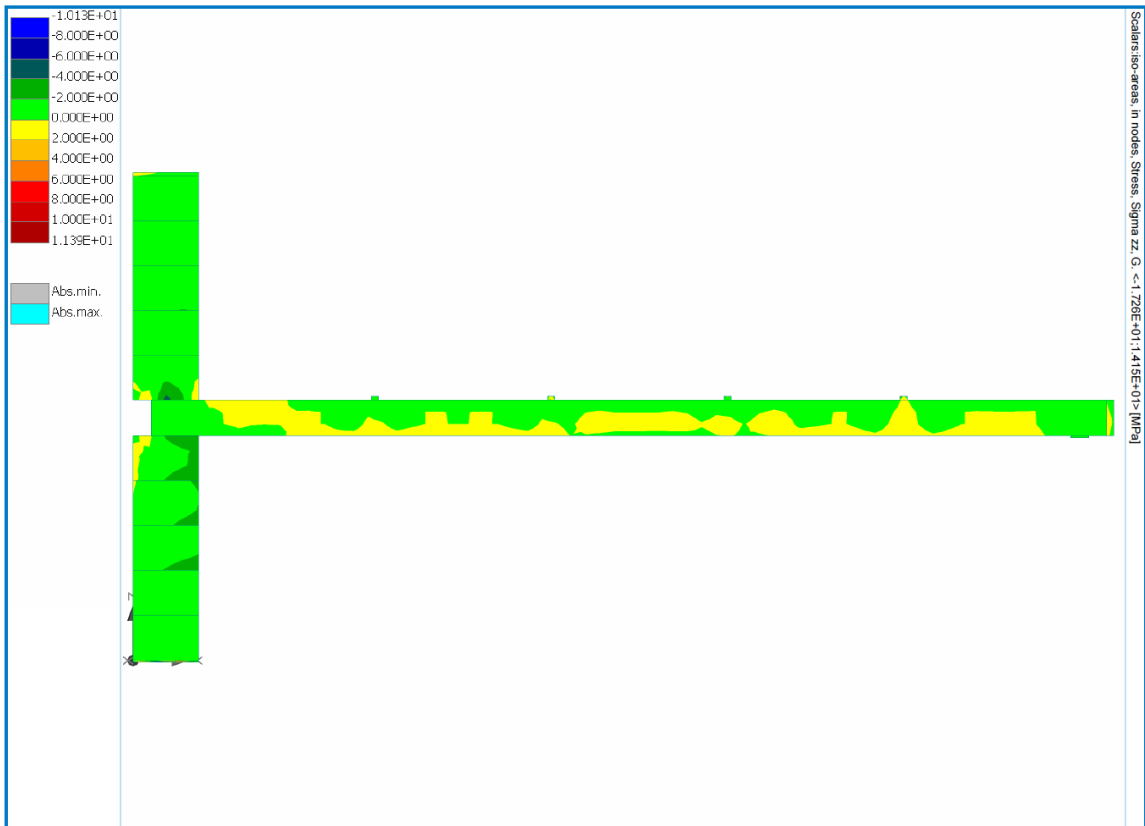


Figure D - 25 Vertical stress  $\sigma_{zz}$  iso-areas Load Case 5

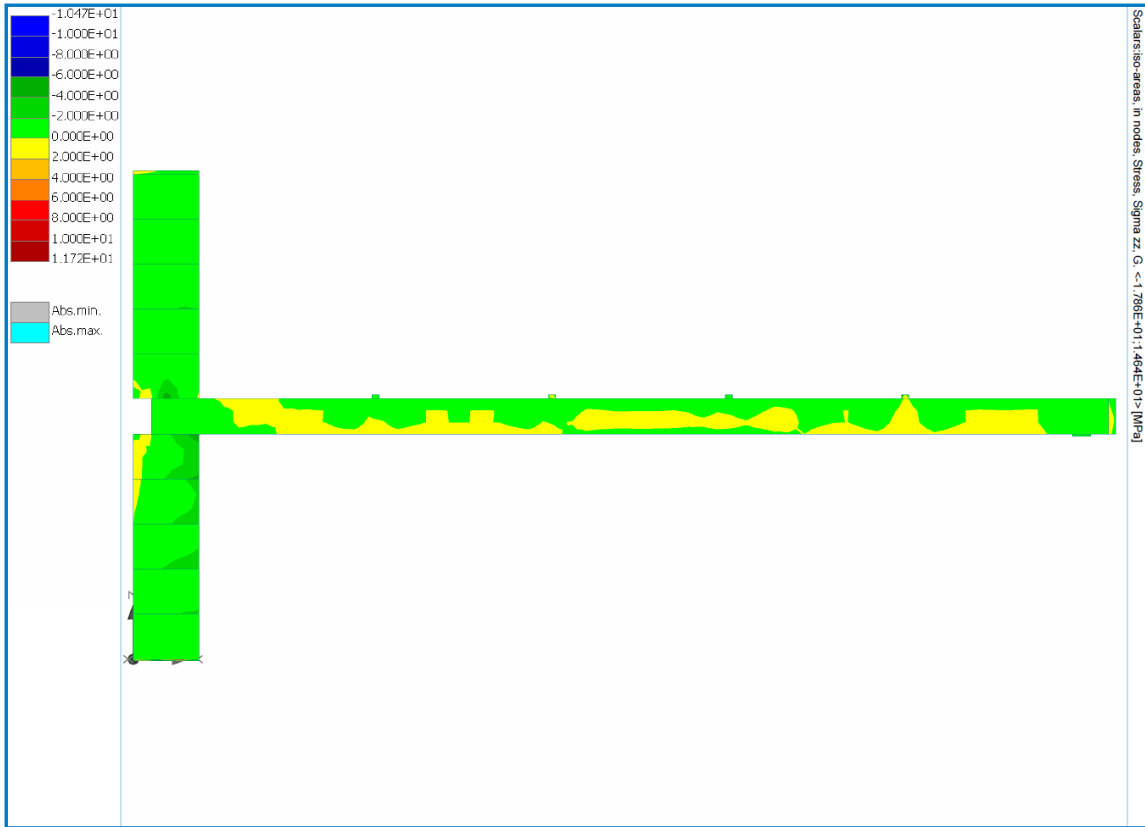


Figure D - 26 Vertical stress  $\sigma_{zz}$  iso-areas Load Case 6

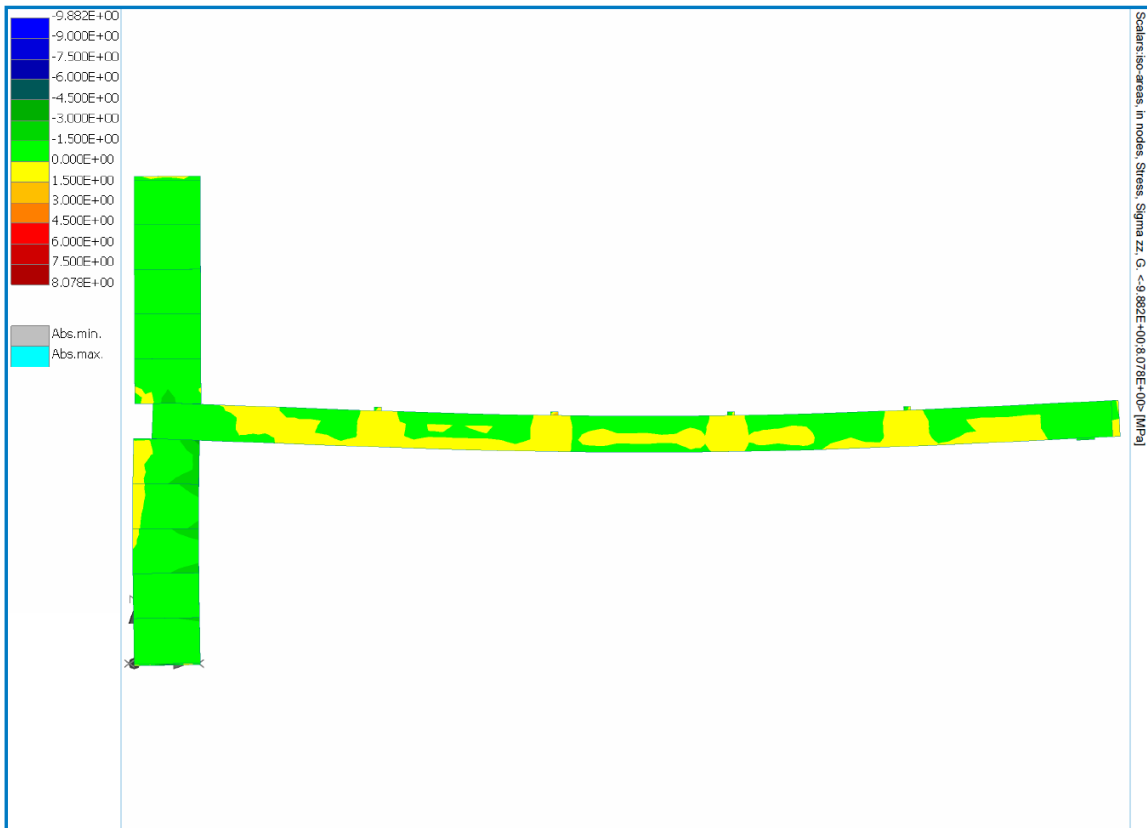


Figure D - 27 Vertical stress  $\sigma_{zz}$  iso-areas Load Case 7

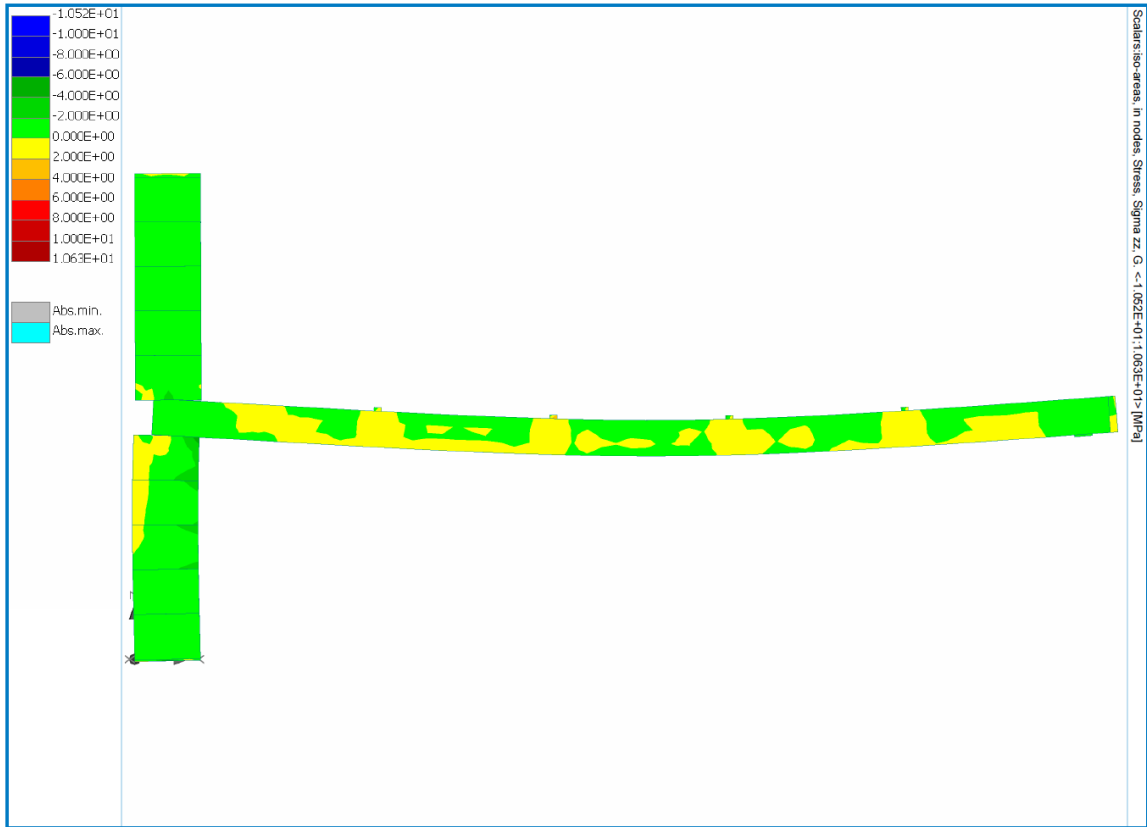


Figure D - 28 Vertical stress  $\sigma_{zz}$  iso-areas Load Case 8

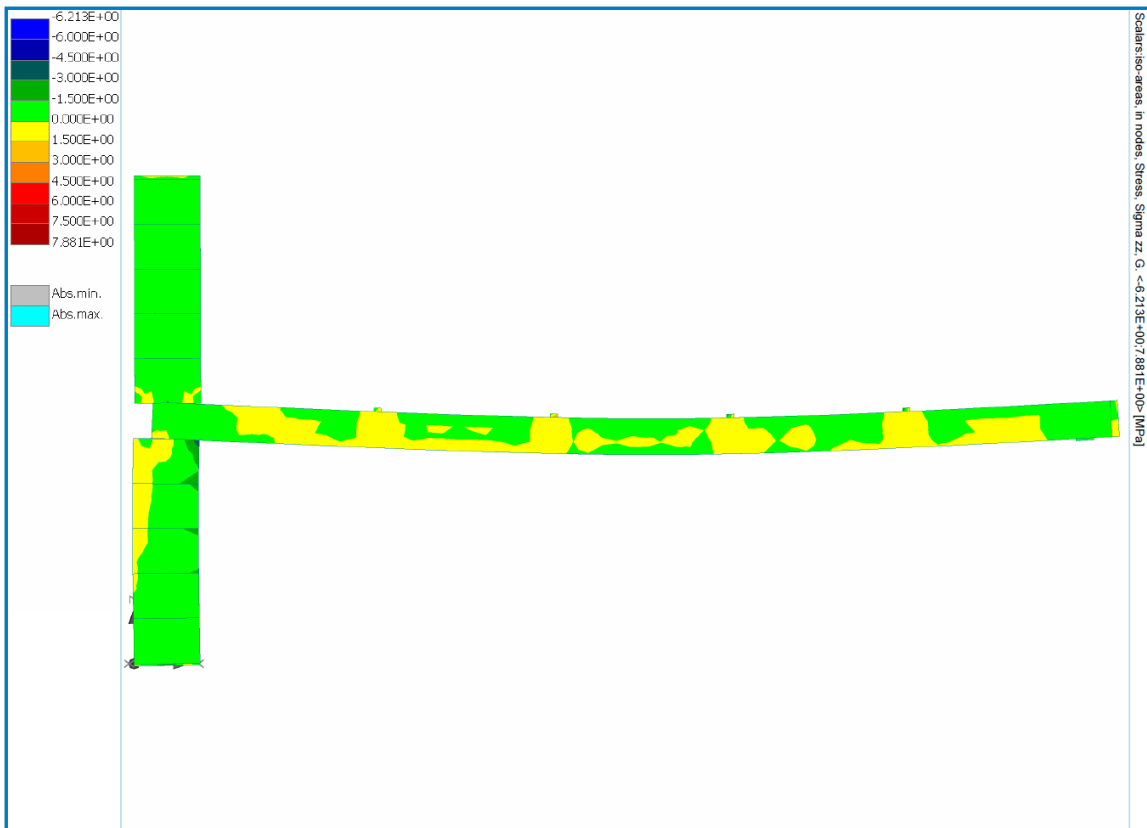


Figure D - 29 Vertical stress  $\sigma_{zz}$  iso-areas Load Case 9

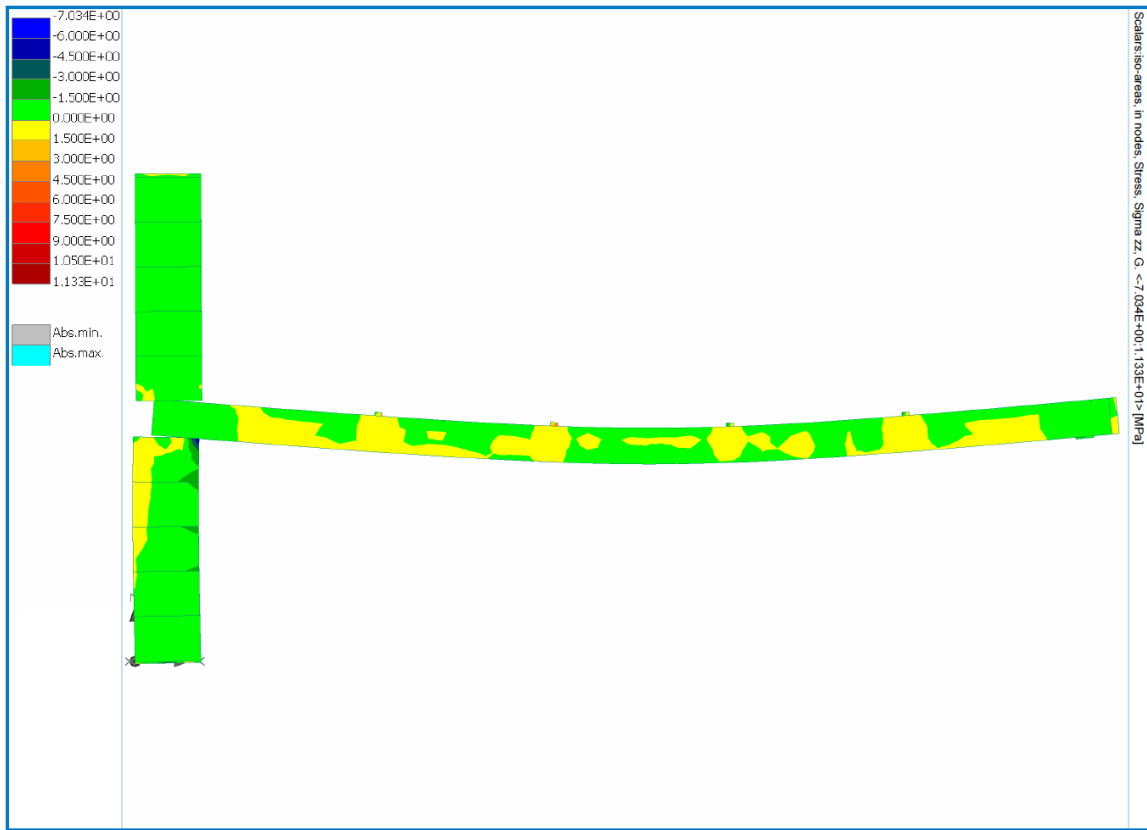


Figure D - 30 Vertical stress  $\sigma_{zz}$  iso-areas Load Case 10

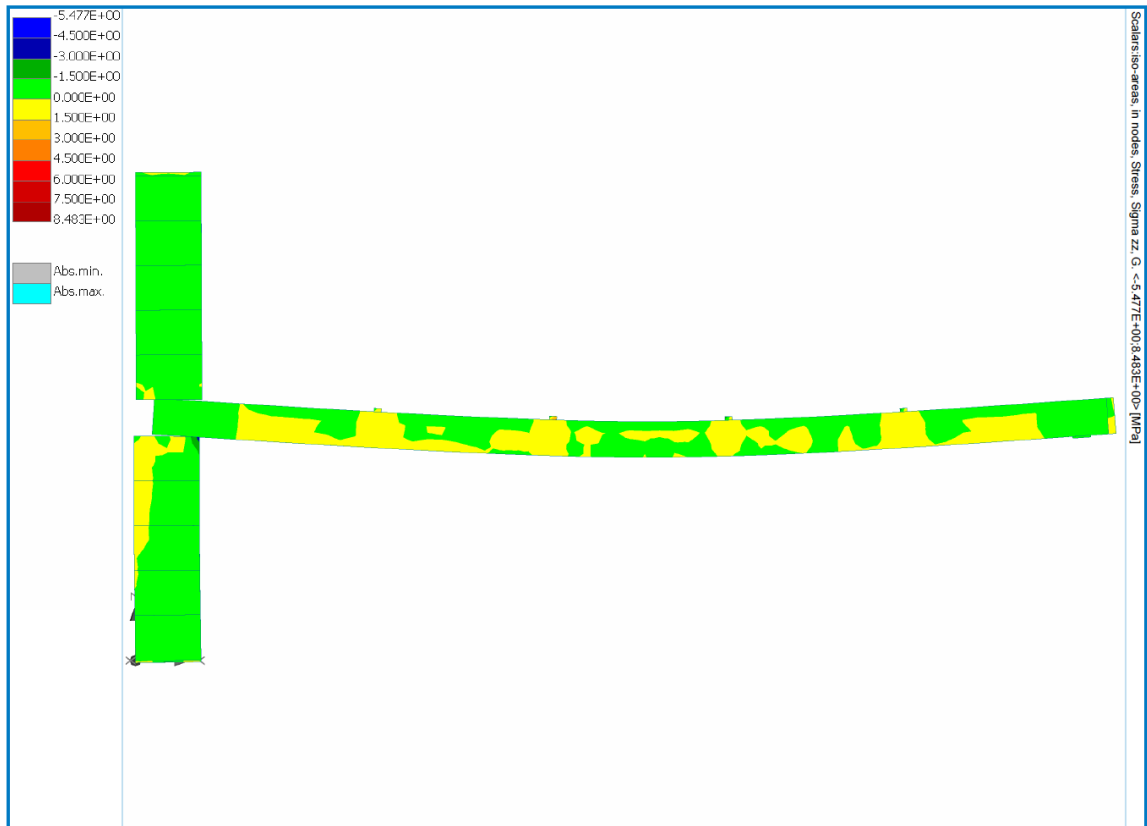
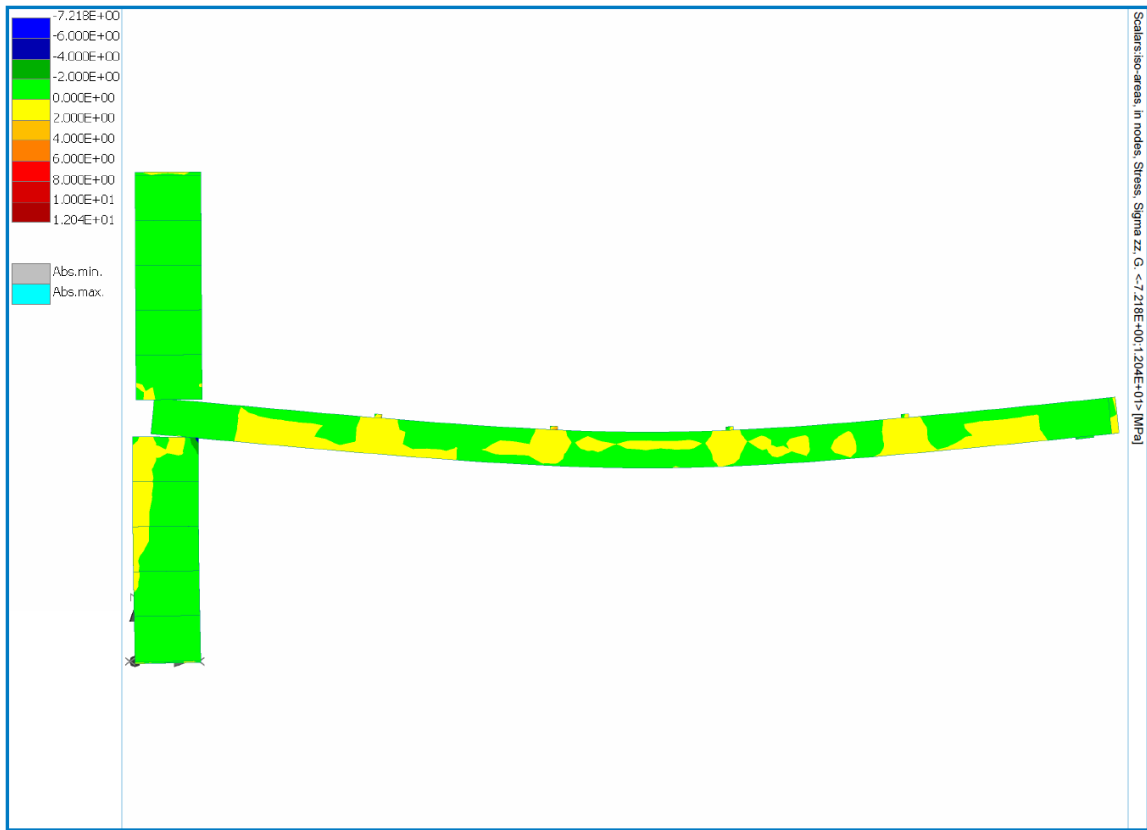


Figure D - 31 Vertical stress  $\sigma_{zz}$  iso-areas Load Case 11



**Figure D - 32 Vertical stress  $\sigma_{zz}$  iso-areas Load Case 12**

- Geometrical case: a= 200 mm

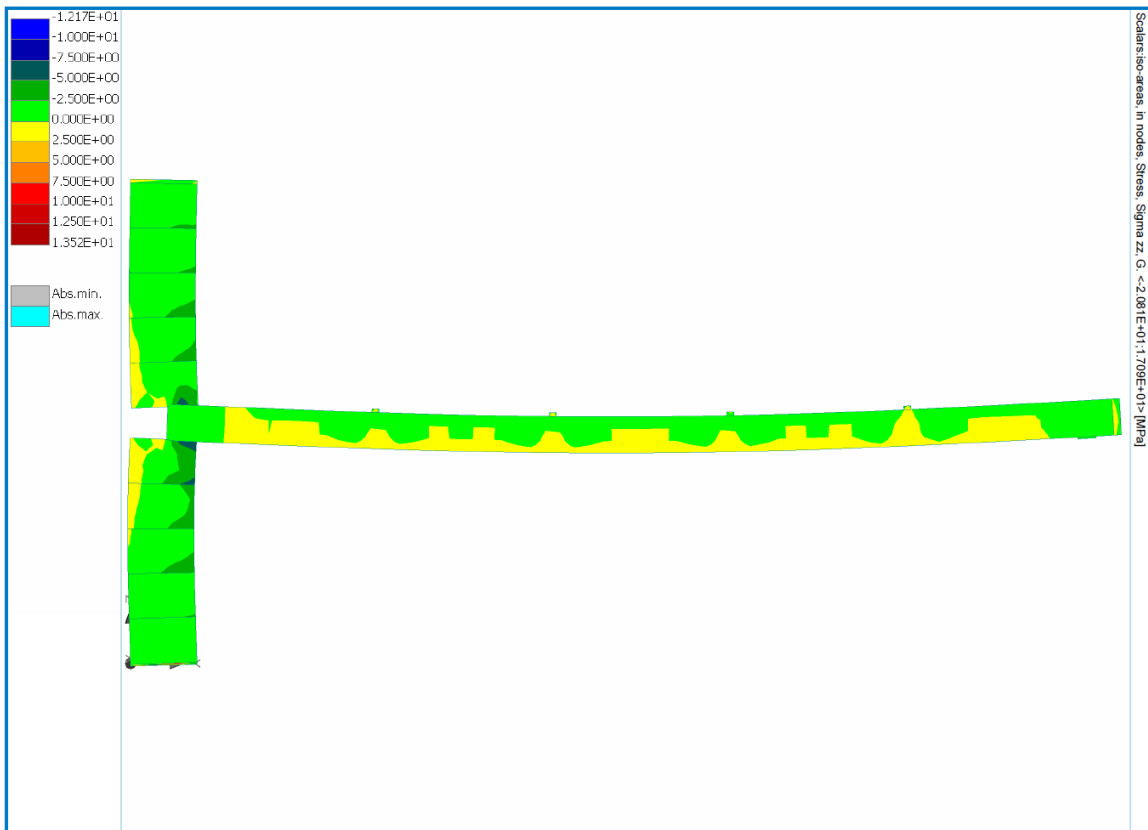


Figure D - 33 Vertical stress  $\sigma_{zz}$  iso-areas Load Case 1

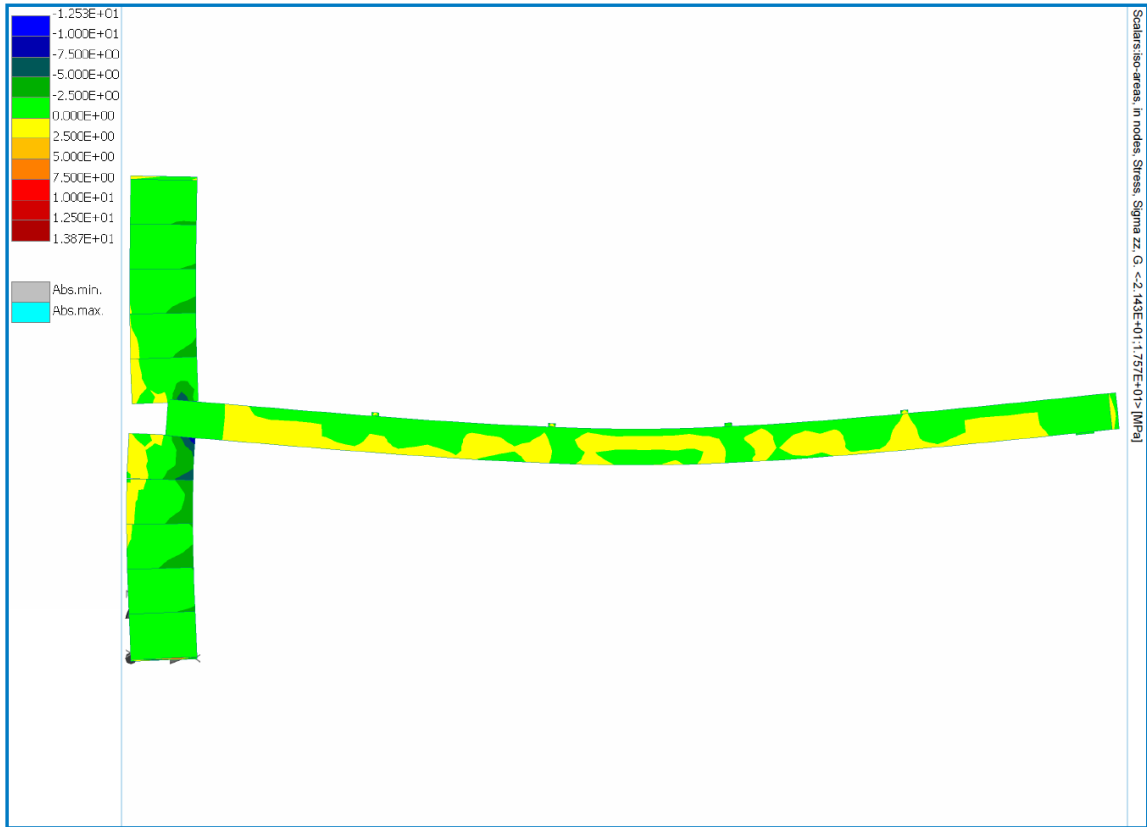


Figure D - 34 Vertical stress  $\sigma_{zz}$  iso-areas Load Case 2

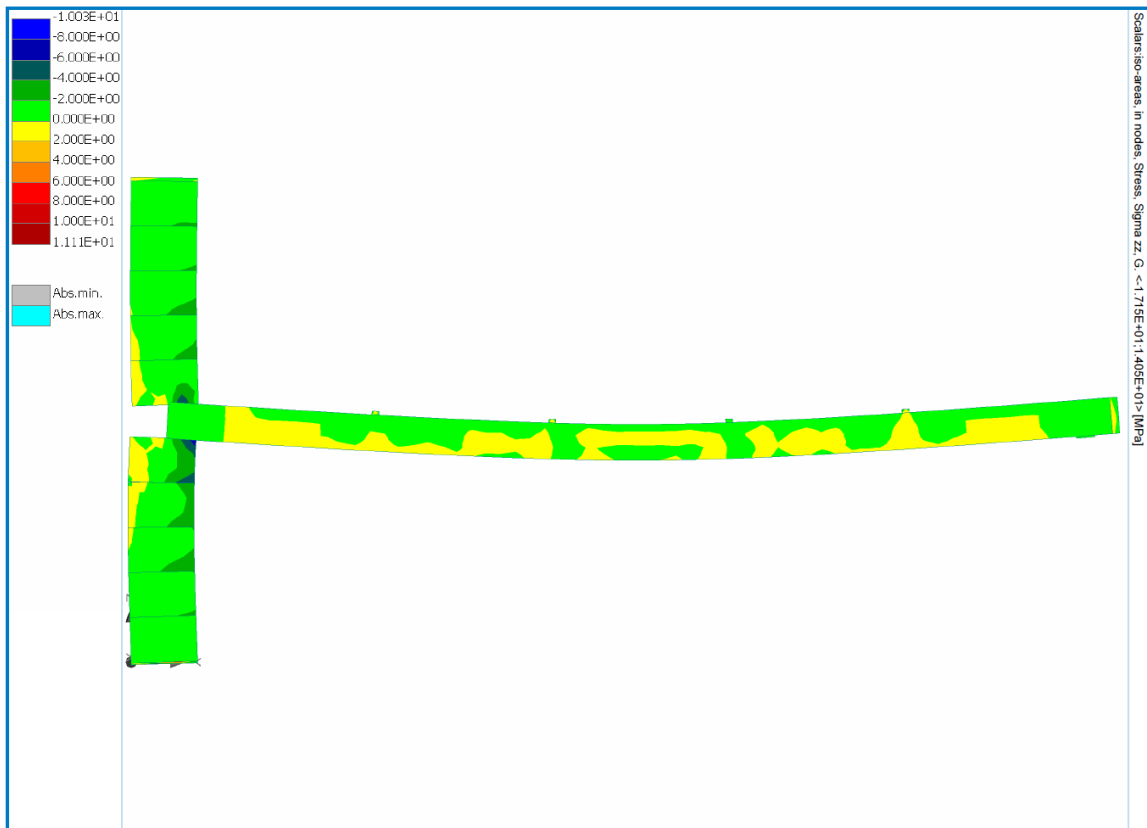


Figure D - 35 Vertical stress  $\sigma_{zz}$  iso-areas Load Case 3

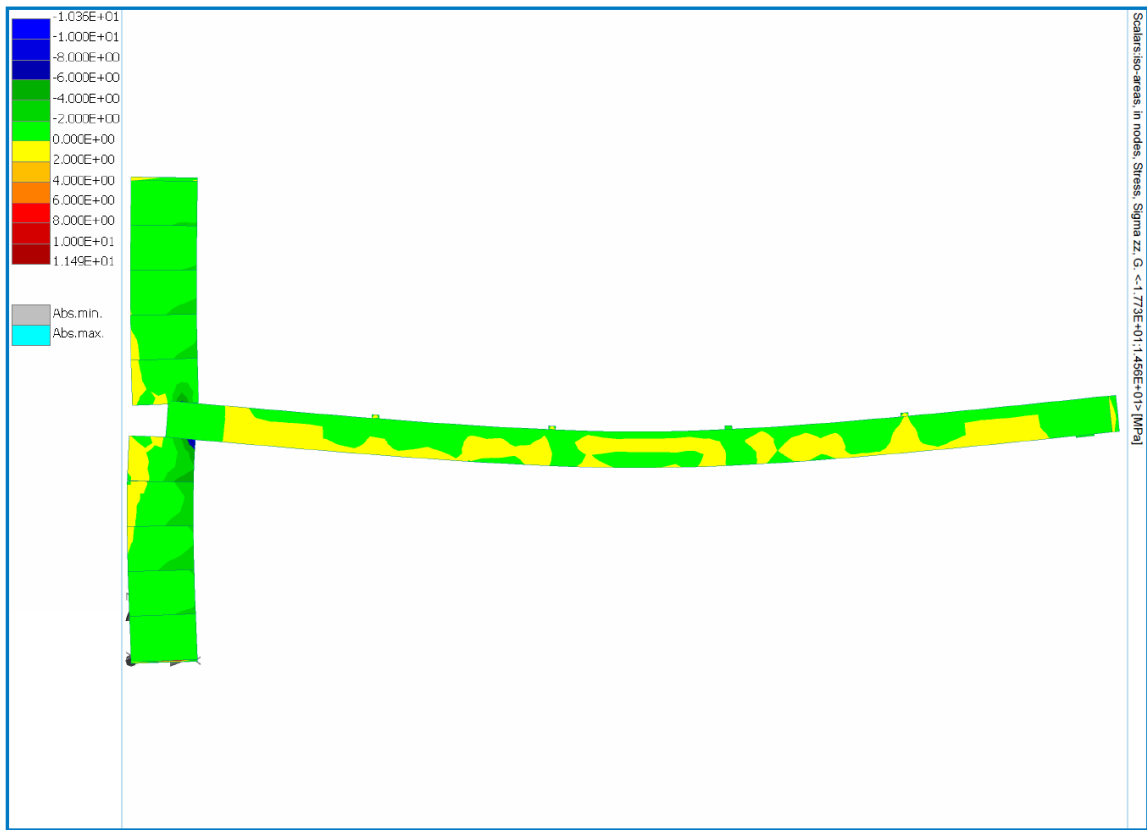


Figure D - 36 Vertical stress  $\sigma_{zz}$  iso-areas Load Case 4

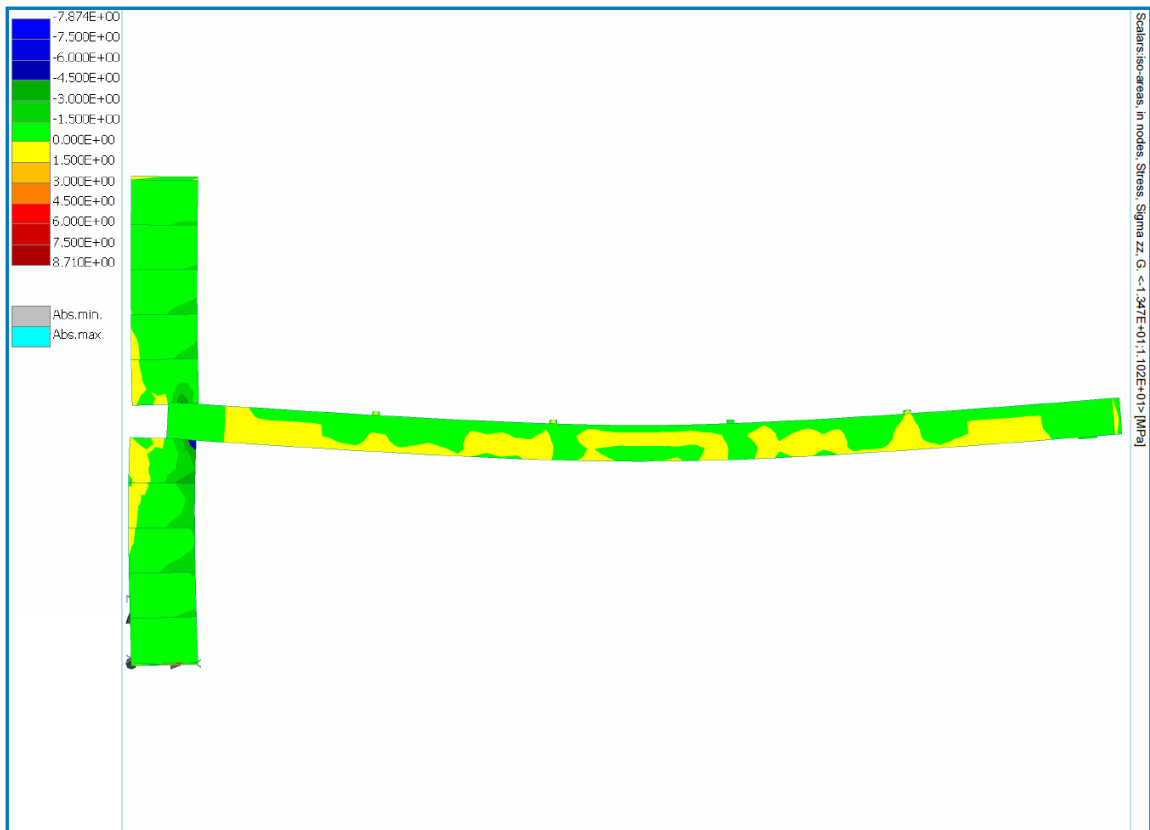


Figure D - 37 Vertical stress  $\sigma_{zz}$  iso-areas Load Case 5

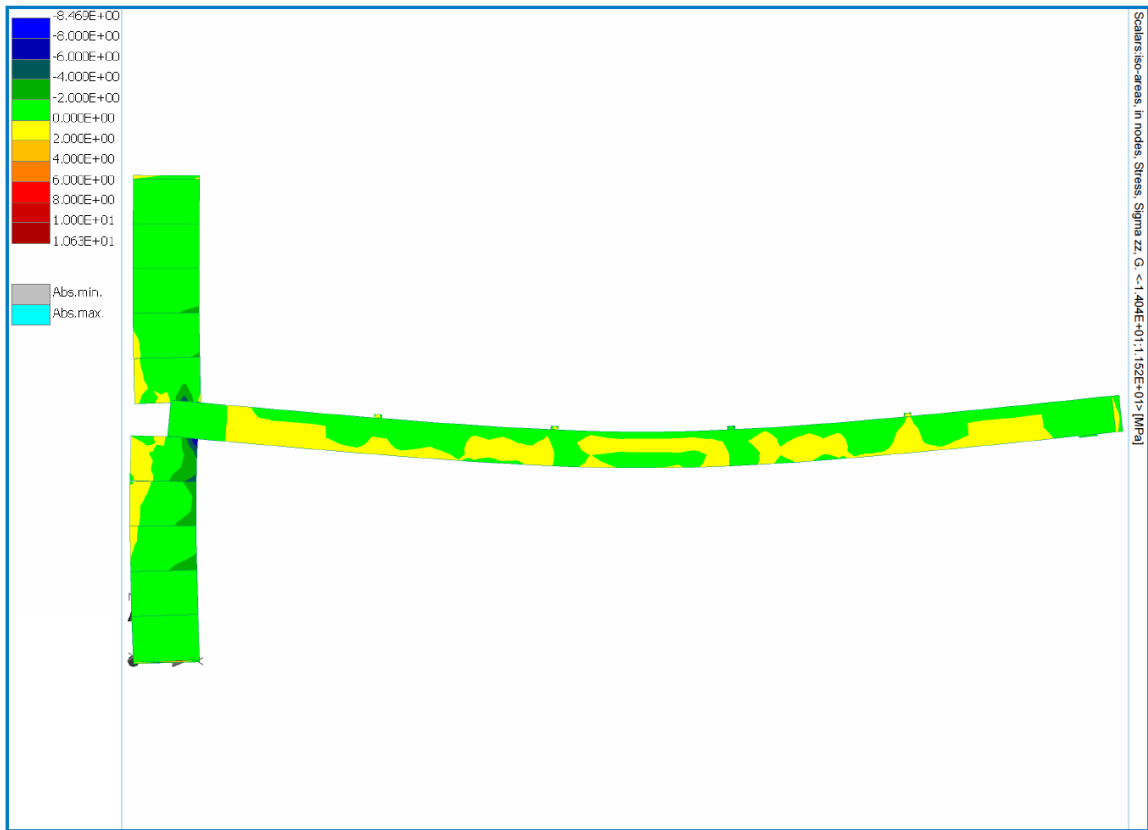


Figure D - 38 Vertical stress  $\sigma_{zz}$  iso-areas Load Case 6

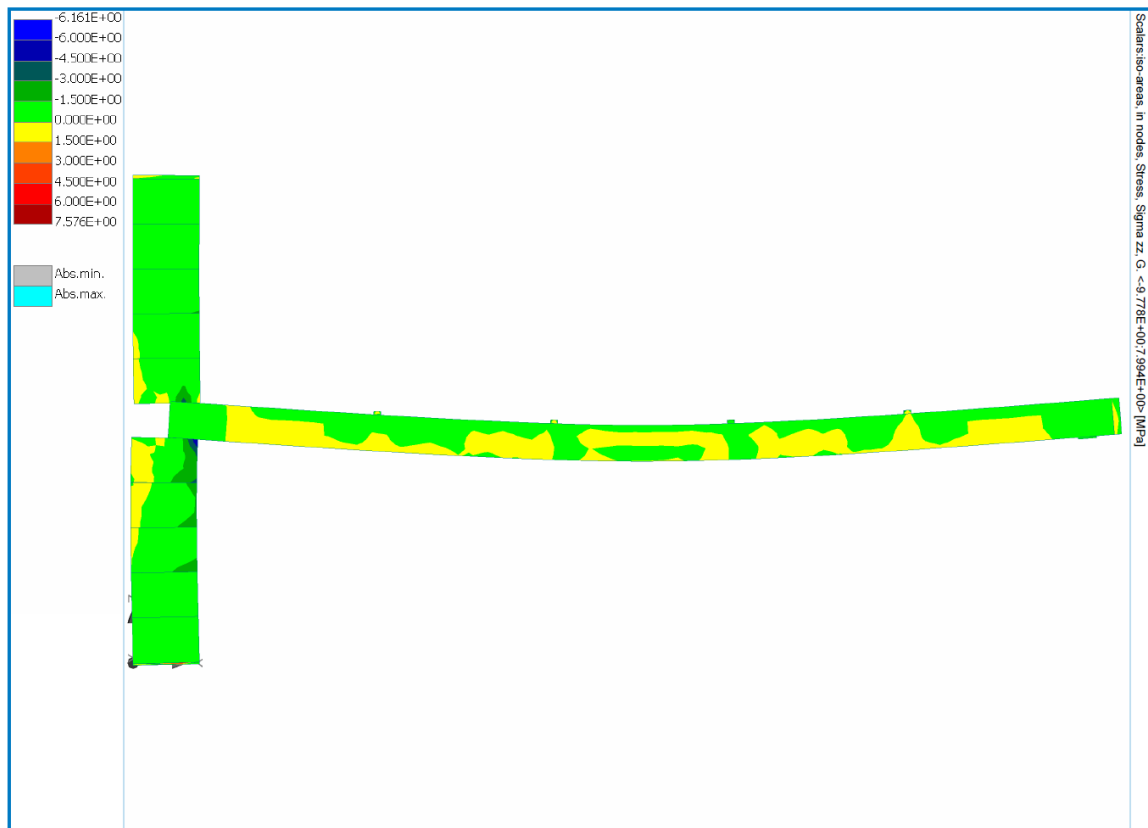


Figure D - 39 Vertical stress  $\sigma_{zz}$  iso-areas Load Case 7

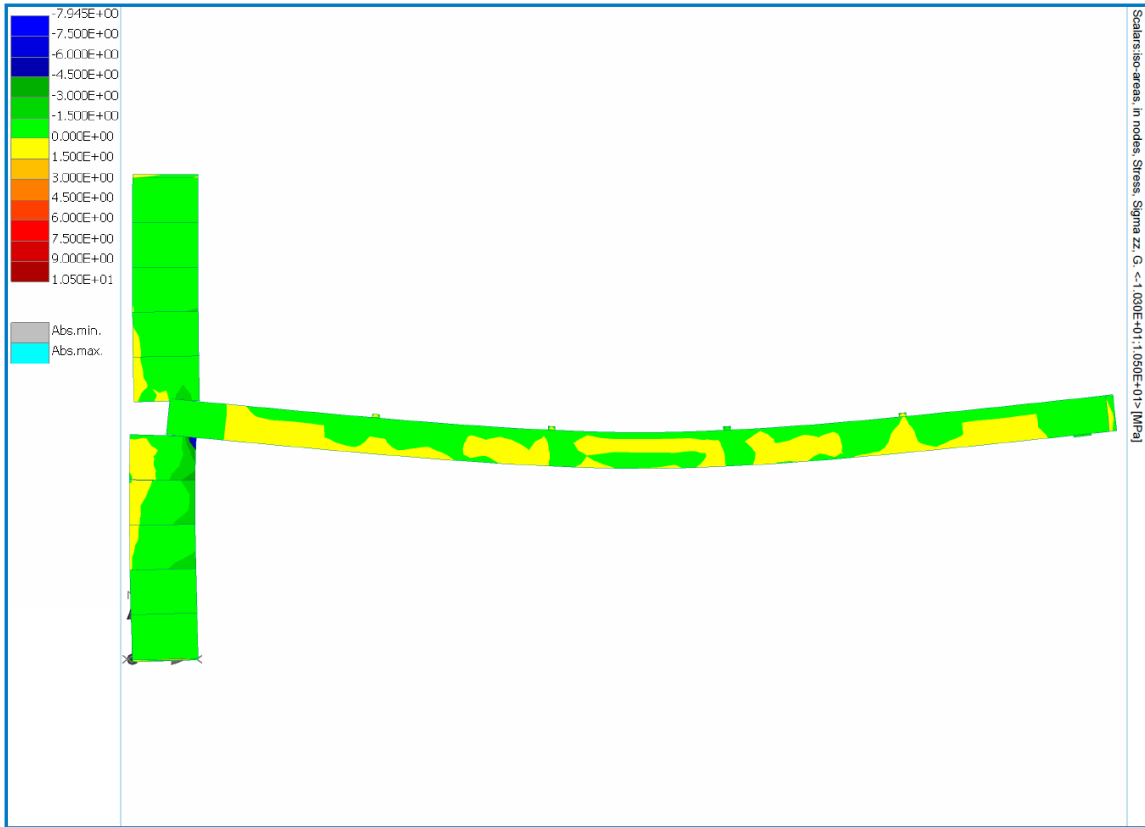


Figure D - 40 Vertical stress  $\sigma_{zz}$  iso-areas Load Case 8

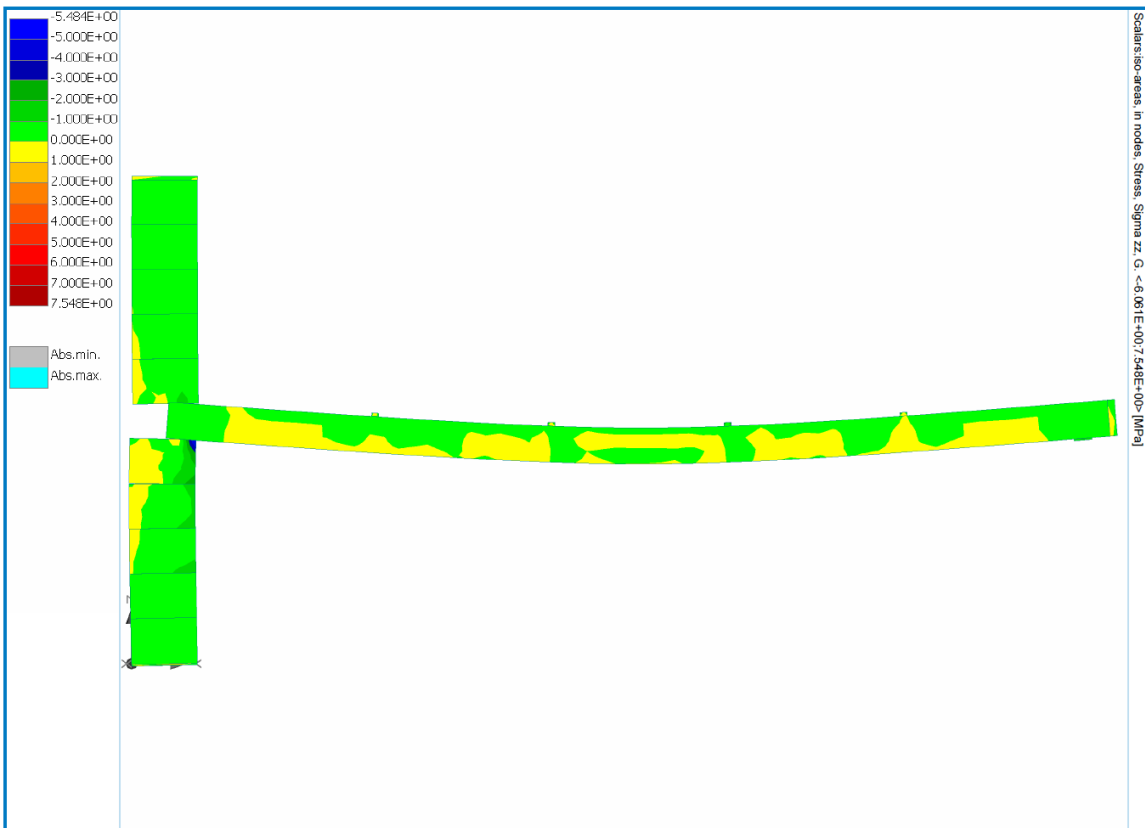


Figure D - 41 Vertical stress  $\sigma_{zz}$  iso-areas Load Case 9

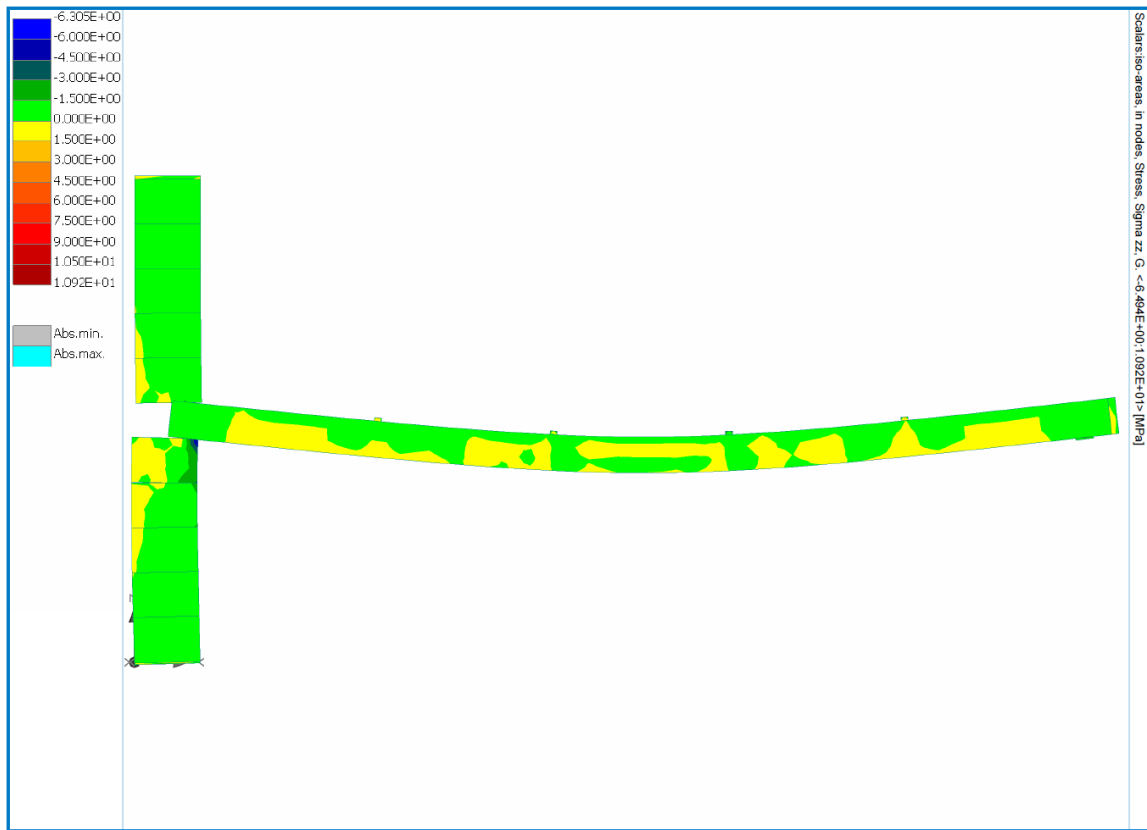


Figure D - 42 Vertical stress  $\sigma_{zz}$  iso-areas Load Case 10

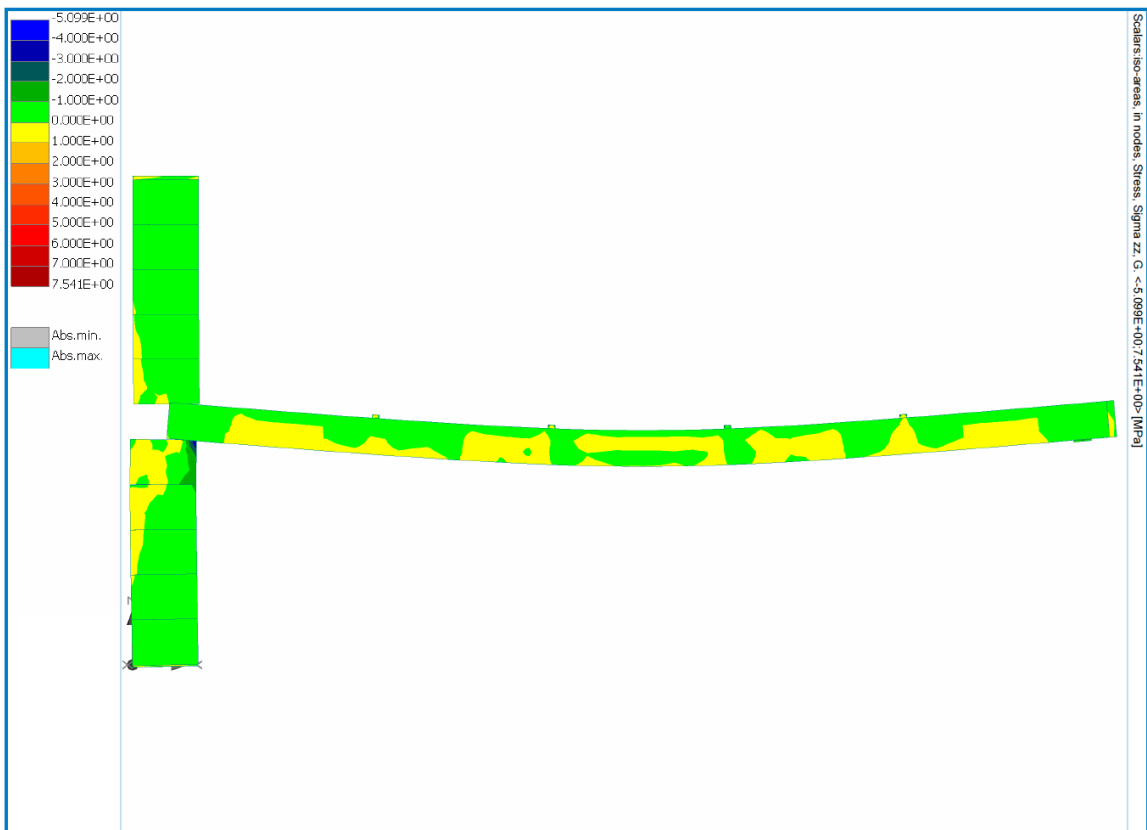
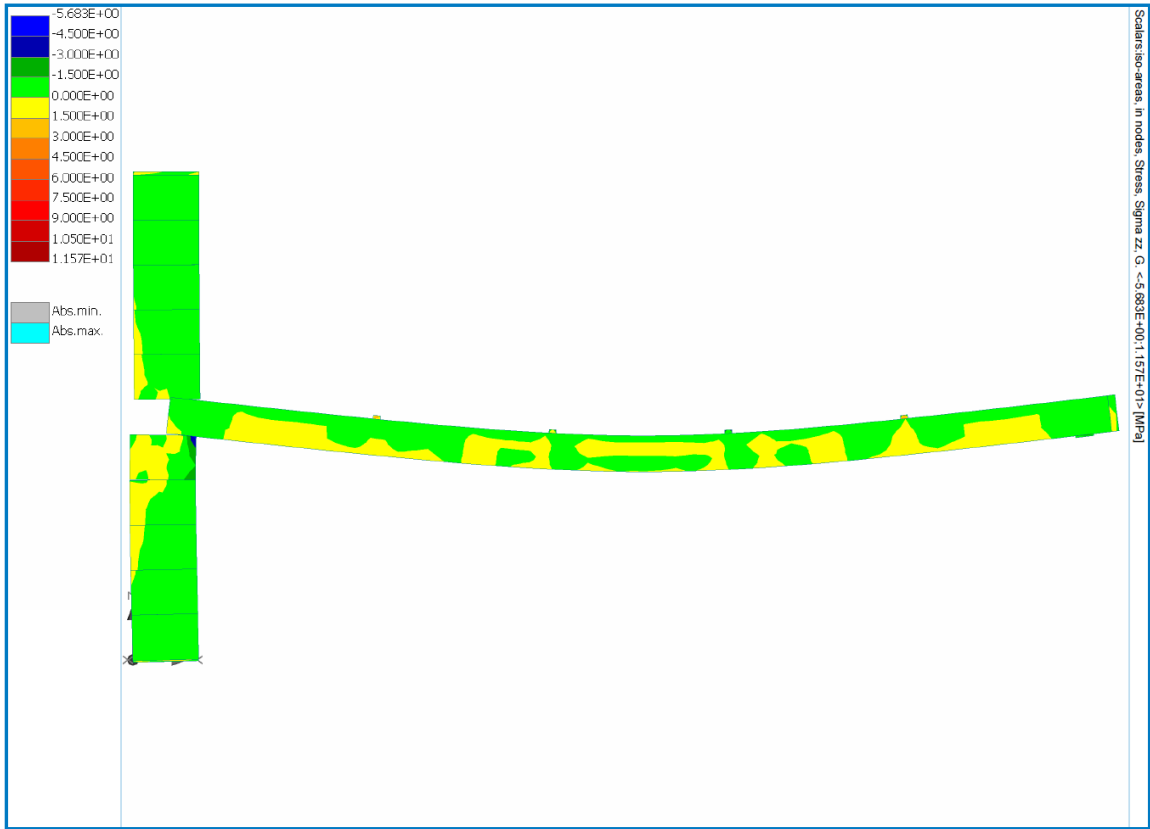


Figure D - 43 Vertical stress  $\sigma_{zz}$  iso-areas Load Case 11



**Figure D - 44 Vertical stress  $\sigma_{zz}$  iso-areas Load Case 12**

## Annex E – Geometrical parameters of Experimental and FEM structure

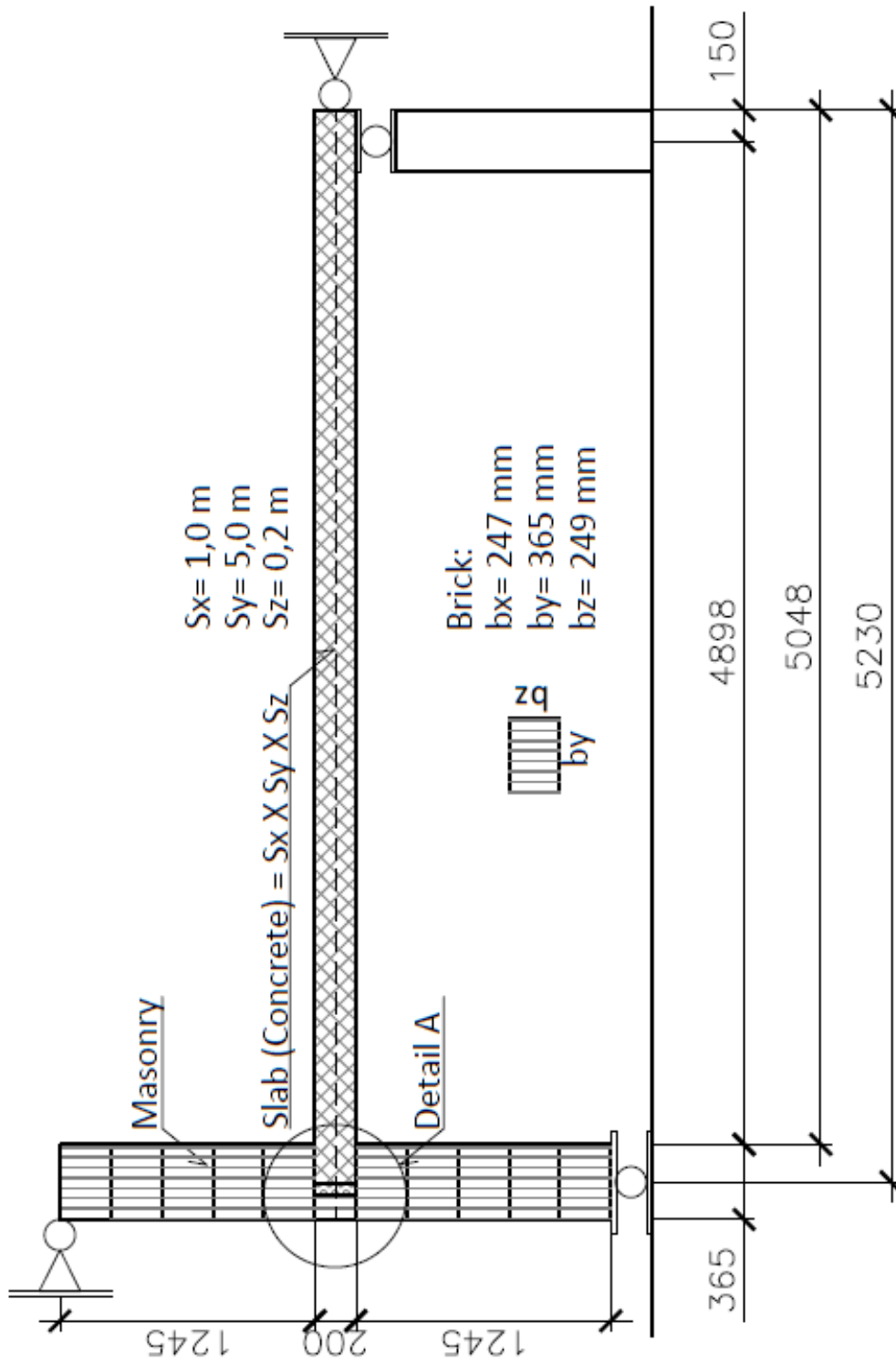


Figure E - 1 Vertical Section

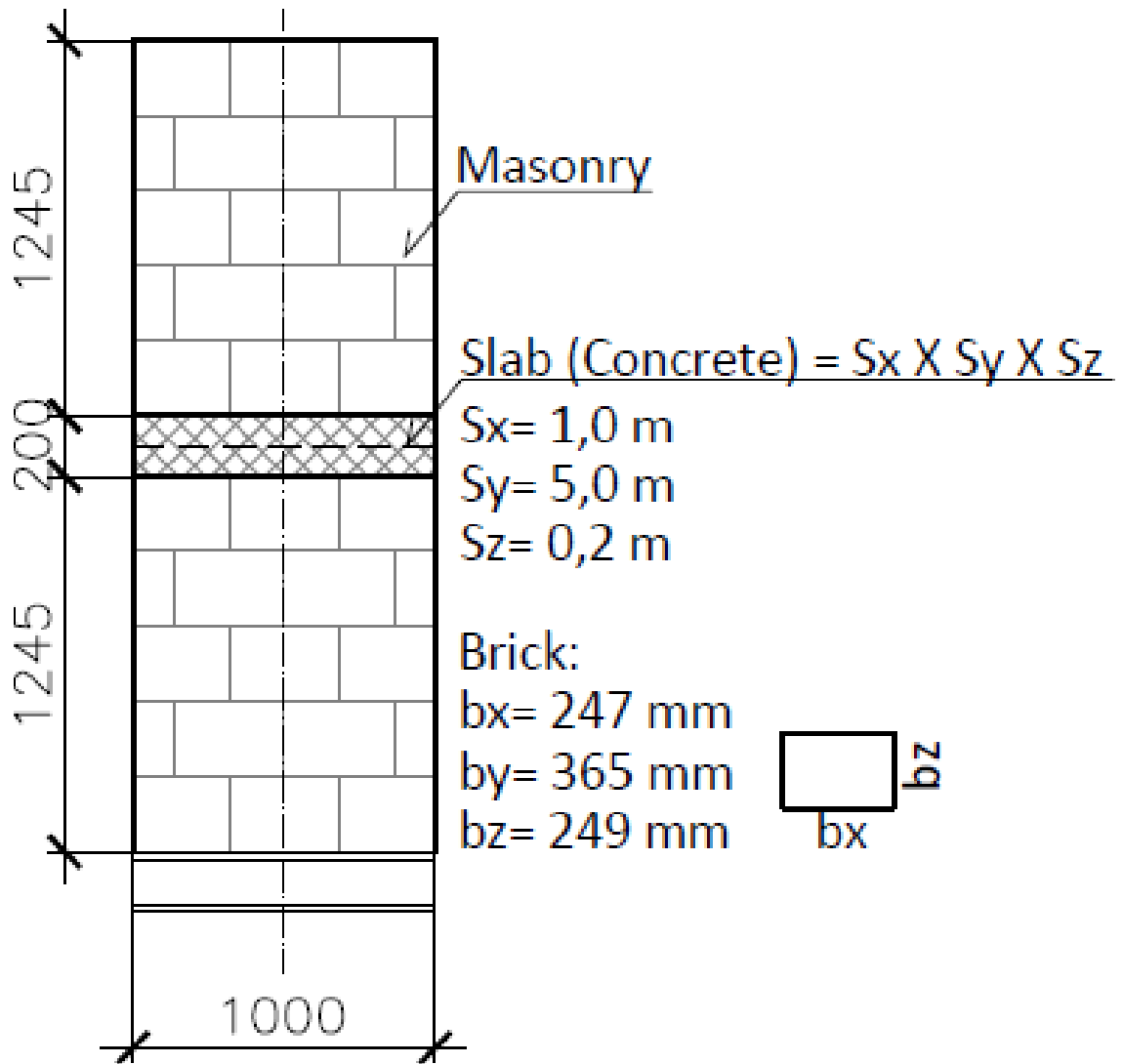


Figure E - 2 Back view

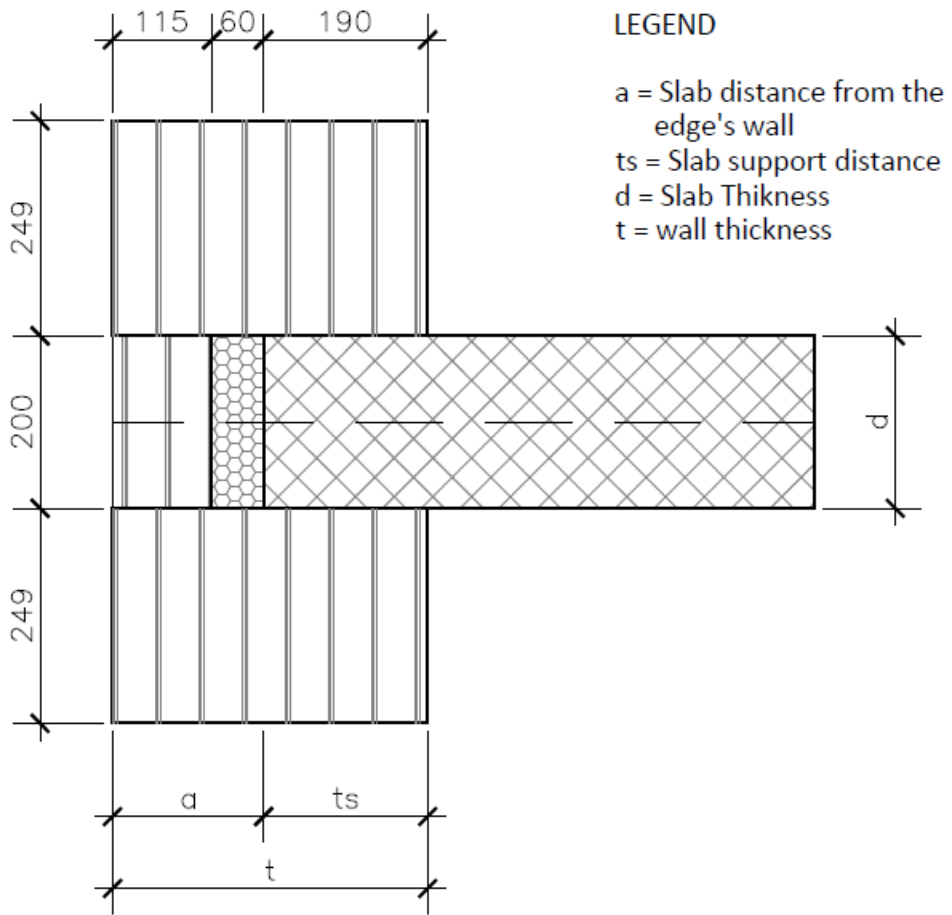
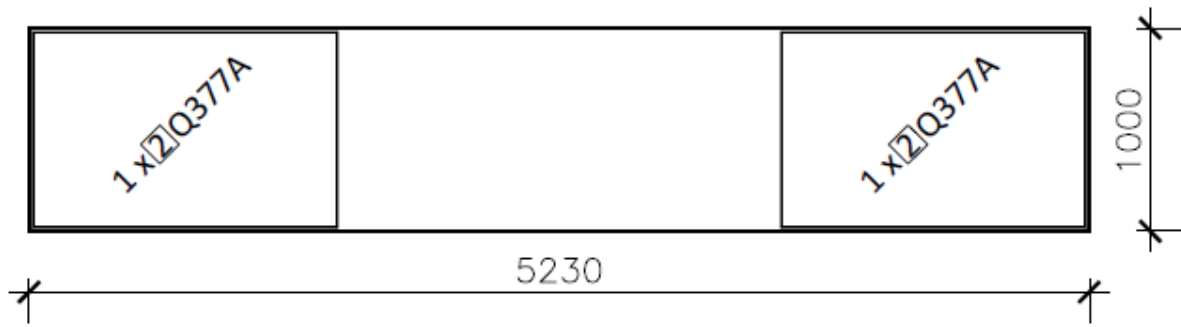
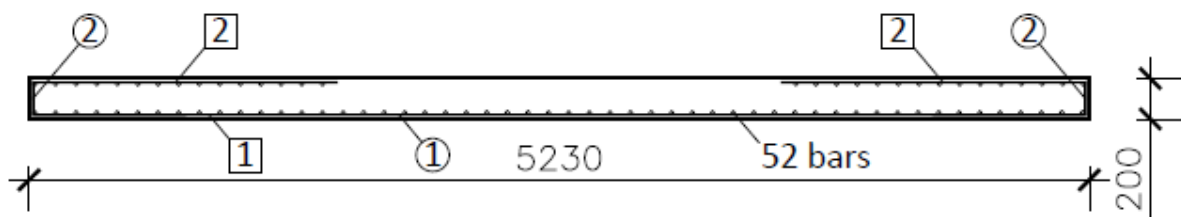


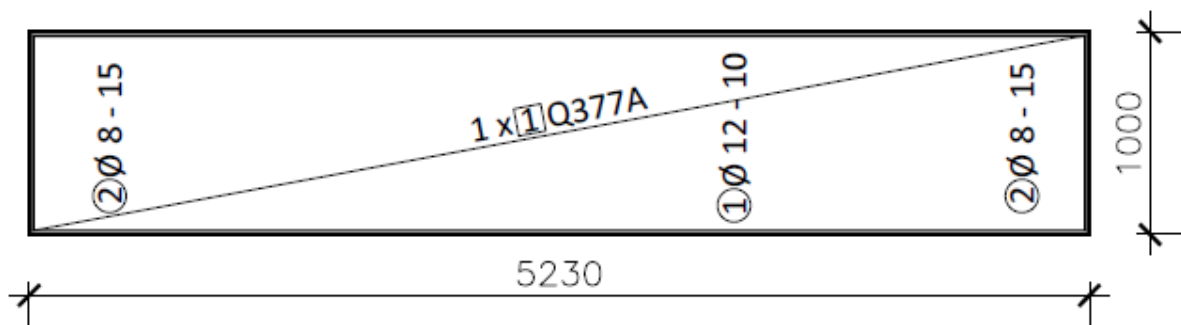
Figure E - 3 Detail A of the Wall/Slab



Longitudinal Vertical section - 1:50



Lower view - 1:50



[1]	1 Stk. Q377A		5,18 x 0,95 m <sup>2</sup>	B25
[2]	2 Stk. Q377A		1,50 x 0,95 m <sup>2</sup>	BSt 500
①	10 Stk. Ø12	$\frac{5180}{10}$	l = 5,18 m	nomc = 2,0 cm
②	14 Stk. Ø8	$\frac{750}{14}$	l = 1,66 m	

Figure E - 4 Slab Reinforcement used for the Experimental and FEM structure